Impact of Dark Matter and Modified Gravity on Compact Binary Systems

Dissertation
zur Erlangung des Doktorgrades
der Naturwissenschaften

vorgelegt beim Fachbereich 13
der Johann Wolfgang Goethe-Universität
in Frankfurt am Main

von
Robin Fynn Diedrichs
aus Hann.-Münden

Frankfurt (2025)

(D30)

Vom Fachbereich 13 der

Johann Wolfang Goethe-Universität als Dissertation angenommen

Dekan: Prof. Dr. Roger Erb

Gutachter: Prof. Dr. Laura Sagunski, Prof. Dr. Jürgen Schaffner-Bielich

Datum der Disputation:

“The more the universe seems comprehensible, the more it also seems pointless.”

— **Steven Weinberg**

“[...] if there is no point in the universe that we discover by the methods of science, there is a point that we can give the universe by the way we live, by loving each other, by discovering things about nature, by creating works of art. And that — in a way, although we are not the stars in a cosmic drama, if the only drama we’re starring in is one that we are making up as we go along, it is not entirely ignoble that faced with this unloving, impersonal universe we make a little island of warmth and love and science and art for ourselves.”

— **Steven Weinberg**, elaborating on whether he sees no overall point to the universe

Abstract

While current gravitational wave observatories already provide the possibility to constrain new physics, upcoming detectors, such as the Einstein Telescope, will allow for high-precision tests of General Relativity. This thesis explores how new physics would enter the gravitational wave signal produced by compact binary systems by explicitly calculating observables for concrete scenarios. We here mainly consider the impact of an additional scalar degree of freedom and thus investigate three scenarios. Firstly, a real massive scalar field that mediates an additional force between the two compact objects. For this scenario, we calculate the next-to-leading order gravitational wave phase and present it in a ready-to-use form. Secondly, we consider a complex massive scalar field that can form bound states (i.e., Boson stars), which can combine with Neutron stars to form so-called Fermion-Boson stars. We analytically derive the linear static perturbation equations and numerically solve these in order to obtain the object's quadrupolar Love number. Thirdly, we consider Horndeski theories, which cover all scalar-tensor theories with at most second-order equations of motion. We show that the extraction of the quadrupolar Love numbers is more complicated than in the pure General Relativity case when considering massless scalar fields due to additional terms in the asymptotic expansion of the perturbation fields that mimic a tidal response. We provide a detailed discussion of this ambiguity and further resolve it by leveraging effective field theory methods.

Acknowledgements

I want to thank my supervisors, Prof. Laura Sagunski and Prof. Jürgen Schaffner-Bielich, for giving me the opportunity to write this thesis under their guidance and for their continuous support throughout my time at the ITP in Frankfurt.

I am grateful to my family for always supporting me along this journey and always enabling me to push forward. Thank you for always having my back, Marla, Falk, Tim, Susanne, Günter, and Ute!

I thank the entire DMGW group and everyone else at the ITP for making the time at the ITP so enjoyable. Particularly, I want to thank Niklas, Daniel, Edwin, Jannis, Yannik, Tamara, Konrad, Sarah, Selina, Jan-Erik, Philipp, and Ishfaq. Studying and working in Frankfurt would not have been nearly as enjoyable without you.

I am grateful to all of my friends who have either directly or indirectly supported me through these many years of my physics studies. Especially, Felix, Sven, Hendrik, Ji, Fabio, Debbie, Man-Son, Edoardo, Jenny, Viktor, Ayuri, Ayaka, Kanne, Julia, and Blues, thank you so much! Even if I can't meet you regularly, I always cherish the contact we have. Special thanks go to all the members of the *4t9t* group for all the fun sessions we had!

Most importantly, I want to thank Stephan for the time we shared in Frankfurt: for making every bouldering session fun, for every movie night, for always having an open ear for my struggles, and for his unconditional support. I wouldn't have completed this without you, but now you are no longer here to read these lines.

Publications relevant to this dissertation

[1] R. F. Diedrichs, N. Becker, C. Jockel, J.-E. Christian, L. Sagunski and J. Schaffner-Bielich, *Tidal deformability of fermion-boson stars: Neutron stars admixed with ultralight dark matter*, *Phys. Rev. D* **108** (2023) 064009, [2303.04089]

The author derived the analytic expression for the perturbation equations, designed various algorithms for the efficient construction of Fermion-Boson stars, and had the primary responsibility to prepare data evaluation scripts. The C code was mainly developed by N. Becker in collaboration with C. Jockel. The author generated all figures in the final version of the manuscript. All co-authors contributed to the manuscript. Chapter 4 is based on this publication.

[2] R. F. Diedrichs, D. Schmitt and L. Sagunski, *Binary systems in massive scalar-tensor theories: Next-to-leading order gravitational wave phase from effective field theory*, *Phys. Rev. D* **110** (2024) 104073, [2311.04274]

All analytic results were derived by the author in collaboration with D. Schmitt. All figures were created by D. Schmitt. All co-authors contributed to the manuscript. Chapter 3 is based on this publication.

[3] R. F. Diedrichs, S. Tsujikawa and K. Yagi, *Tidal Love numbers of neutron stars in Horndeski theories*, *Phys. Rev. D* **112** (2025) 044023, [2501.07998]

The author obtained analytic and numerical results under the guidance of S. Tsujikawa. K. Yagi and S. Tsujikawa independently verified large portions of the analytic calculations. The author generated all figures. All co-authors contributed to the conceptualisation of this project and the writing of the manuscript. Chapter 5 is based on this publication.

Summary

Gravitational waves (GWs), predicted by Albert Einstein in 1916 [4] as a fundamental consequence of General Relativity (GR), were for decades regarded as a purely theoretical curiosity. Their extremely weak interaction with matter made them seem inaccessible to direct measurement. This changed dramatically in 2015, when the LIGO detectors observed the first GW signal from a binary black hole merger [5]. This event not only confirmed the century-old prediction but also launched a new era of astronomy.

Unlike electromagnetic radiation, which can be absorbed, scattered, or obscured, gravitational waves travel essentially unhindered through spacetime and carry insightful information about the systems that generate them. The most luminous sources in the GW spectrum are compact binary mergers involving black holes and neutron stars. These violent events produce signals that encode the masses, spins, orbital dynamics, and even the internal structure of the participating objects.

To date, all observed GW signals have been consistent with GR to high precision (see, e.g., [6–16]). Yet it remains possible, and in many ways expected, that future observations may reveal small but significant deviations. The need for extensions of GR arises from multiple fronts: its incompatibility with quantum mechanics, the absence of a mechanism for cosmic inflation, and the lack of explanation for dark matter and dark energy. Many proposed modifications of gravity introduce additional degrees of freedom, most often in the form of scalar fields [17–23].

This thesis focuses on how scalar fields, whether as mediators of new interactions, as dark matter candidates, or as components of scalar-tensor theories, can modify GW signals in measurable ways. Three complementary research directions are explored:

1. A massive real scalar mediating a fifth force in compact binary inspirals.
2. Complex scalar fields forming stable bosonic configurations that combine with neutron stars into hybrid fermion-boson stars.
3. Scalar-tensor theories in the Horndeski class, where tidal deformability is more subtle to define.

Together, these studies connect theoretical models of modified gravity and DM to observational signatures that next-generation detectors such as the Einstein Telescope and Cosmic Explorer will be able to probe.

Gravitational Waves and Scalar-Tensor Theories. Waves are ubiquitous in physics: sound waves in air, electromagnetic waves in Maxwells theory, and matter waves in quantum mechanics. Gravitational waves occupy a special place, as they represent oscillations of spacetime itself rather than a field living within it. Their existence was one of the most striking predictions of GR, and their eventual detection has transformed how we test gravity.

From an observational perspective, GWs provide access to dynamical strong-field regimes that are otherwise unreachable. Binary mergers, for instance, probe spacetime curvatures vastly exceeding those of the Solar System, where traditional tests of GR such as planetary orbits or light deflection have been performed. Thus, GW astronomy allows us to test GR in qualitatively new situations [2, 12, 24–33].

From a theoretical perspective, scalar fields are especially compelling. They arise naturally in high-energy physics: the Higgs boson is one example, while moduli fields, dilatons, and axions appear in string theory. Scalar-tensor theories extend GR by coupling such fields to, e.g., curvature invariants. Depending on the form of the coupling, these theories can generate long-range fifth forces, allow neutron stars to spontaneously develop scalar hair, or screen scalar interactions in high-density regions [34–38].

The importance of scalar-tensor theories lies not only in their elegance but also in their testability. Scalar fields can alter inspiral dynamics, affect the way compact stars deform under tidal forces, and contribute additional modes of radiation. Each of these phenomena leaves a characteristic imprint on the GW waveform, meaning they can be constrained, or potentially discovered, through precision measurements of GWs.

Post-Newtonian Framework and Effective Field Theory. To interpret GW signals, theoretical predictions must be accurate and under analytic control. During the inspiral phase of a compact binary, the orbital velocity is small compared to the speed of light, and this motivates the use of the *post-Newtonian* (PN) expansion, which expresses the equations of motion as corrections to Newtonian gravity in powers of v/c and Newton's constant G [16, 39–53].

During the last two decades, the Effective Field Theory (EFT) approach to binary dynamics introduced by Goldberger and Rothstein [54] has become a powerful framework for PN calculations. In this method, compact objects are treated as point particles with effective worldline actions, and interactions are calculated using Feynman diagrams, much like in quantum field theory. The EFT formalism is particularly suited to systematically including additional degrees of freedom, such as scalar fields, in a controlled expansion.

In this thesis, the EFT framework is extended to include a massive real scalar coupled to compact objects, where we build upon previous research in this direction [55,56]. Conservative dynamics and radiation are computed at next-to-leading order, corresponding to the 1PN correction to the conservative sector and the dissipative effect. These corrections directly influence the phase of the GW signal, which is the primary observable for detectors. Because phase can be tracked over thousands of cycles, even tiny corrections accumulate and can become measurable.

We further provide ready-to-use templates for data analysis pipelines. By comparing observed waveforms to these predictions, constraints can be placed on the scalar mass and coupling constants. In this way, EFT acts as a bridge between fundamental theory and astrophysical observation.

Dark Matter and Fermion-Boson Stars. Dark matter, which constitutes about 27% of the energy density of the Universe, remains one of the greatest mysteries of modern physics. While it has been inferred through its gravitational effects on galaxies and cosmological structure formation, its microscopic nature is still unknown. Among the many candidates, ultra-light bosonic dark matter has gained considerable interest [57,58].

A complex scalar field with a global U(1) symmetry can form stable, self-gravitating objects known as boson stars [59, 60]. These stars differ fundamentally from neutron stars and black holes: their matter content is purely scalar, and their properties depend sensitively on the scalar mass and self-interaction strength.

If BSs coexist with neutron stars, hybrid configurations can form. These so-called *fermion-boson stars* (FBSs) contain both nuclear matter and scalar field distribution. Depending on how the scalar field is distributed, two qualitatively different scenarios arise:

- **Cloud-like FBSs**, where the scalar field extends beyond the neutron star surface, typically increasing the mass, radius, and tidal deformability.
- **Core-like FBSs**, where the scalar field is concentrated at the center, generically reducing these observables.

The thesis computes the quadrupolar Love numbers of such objects by solving the linear perturbation equations for spherically symmetric and static backgrounds. These Love numbers quantify the tidal deformability, which is a key quantity encoded in the

GW signal during the inspiral phase [61].

The analysis shows that even small scalar fractions can substantially alter the tidal response, especially in the cloud-like case. This opens the exciting possibility of probing dark matter indirectly through GW observations of neutron star mergers. While current pulsar timing and binary observations are insufficiently precise to detect such effects, the sensitivity of future detectors will allow constraints to be placed on the scalar field fraction at the percent level.

Horndeski Theory and Tidal Deformability Ambiguities. The Horndeski class of theories represents the most general scalar-tensor framework with second-order field equations, avoiding the Ostrogradsky instability [62]. Horndeski theory includes many popular modified gravity models as special cases, making it a natural setting for systematic study.

A key observational probe of compact stars in this context is their tidal deformability. In GR, the extraction of Love numbers is straightforward: they are defined via the asymptotic expansion of perturbations at large radii, and the coefficients directly encode the tidal response. In scalar-tensor theories, however, the situation is more subtle. The asymptotic expansion includes additional terms from the scalar field, which can mimic tidal effects. This leads to an ambiguity in distinguishing genuine response coefficients from spurious contamination.

The thesis resolves this issue using EFT techniques. By carefully separating physical response parameters from scalar-induced terms, the definition of tidal deformability is clarified. Applied to the DamourEsposito-Farèse (DEF) model, this yields corrected Love numbers that differ by up to $\mathcal{O}(10\%)$ in some regions of parameter space, though deviations are generally within a few percent.

While such deviations are marginal for current detectors, they will become crucial for the precision era of GW astronomy. Next-generation observatories will measure Love numbers with sub-percent accuracy [63], meaning that even minor corrections can make the difference between confirming GR and discovering new physics. The analysis also outlines future directions for scalar GaussBonnet gravity [36–38], where similar contamination issues arise but require further detailed study.

Results, Outlook, and Future Directions. The thesis contributes in three major areas:

1. Extending EFT calculations of compact binary dynamics with an additional scalar field to next-to-leading order, providing precise predictions for GW phases.

2. Deriving the tidal deformability of fermion-boson stars, highlighting how even small DM mass fractions can noticeably change neutron star observables.

3. Identifying and resolving ambiguities in defining Love numbers within scalar-tensor theories, ensuring that future high-precision GW data can be consistently interpreted.

Looking forward, there are several promising avenues:

- Higher-order PN corrections, eccentric orbits, and spin effects could be incorporated into the EFT framework, enhancing waveform accuracy for scalar-tensor theories.

- Tail effects, nonlinear perturbations, and strong-field scalarization phenomena remain largely unexplored and may lead to qualitatively new predictions.

- Systematic studies of Love numbers in odd-parity and higher-multipole sectors within scalar-tensor gravity could uncover further subtleties.

Gravitational-wave astronomy has transformed our ability to test the fundamental nature of gravity. By combining effective field theory techniques with astrophysical modeling of compact stars, this thesis demonstrates how scalar fields can leave measurable imprints on GW signals.

The overarching conclusion is that scalar fields, whether real or complex, whether mediating fifth forces or constituting dark matter, can significantly influence binary dynamics, tidal deformability, and phase evolution. These effects, though subtle, accumulate in ways that are accessible via precision measurements of GWs.

As the field advances toward third-generation detectors, the potential for discovery is immense. Gravitational waves may not only confirm Einsteins theory in new regimes but also point the way toward the next, more fundamental, theory of gravity.

Contents

Chapter 1

Introduction

The story so far: In the beginning the Universe was created. This has made a lot of people very angry and been widely regarded as a bad move.

— **Douglas Adams**, The Restaurant at the End of the Universe

Waves are an ubiquitous feature of nature: from electromagnetic waves that describe, e.g., visible light, to water waves that can be observed as propagating ripples on any surface of water. Many physical phenomena can be described, at least to leading order, as being of a wave-like nature. Einstein showed in 1916 that even gravity—or, more accurately, spacetime itself—allows for the propagation of so-called gravitational waves, which are generically produced by moving matter and induce motion in objects when passing by. While GWs have been a robust prediction since 1916 [4], it was long thought that they are too elusive to be detected in practice; Kip Thorne, who was awarded the Nobel Prize in physics in 2017 for his work on GWs, labeled the concept of GW interferometers at first as "not promising" [64]. In order for GWs to be detectable, they need to be sufficiently strong, and at the moment, only a few sources are known to produce GWs with sufficient intensity. The most prominent of such sources are compact binary systems, which consist of two compact objects orbiting each other, such as two black holes. The gravitational signal of such a system has been shown to carry important information about the behavior of gravity in the strong-field regime, and current detections have thus allowed us to verify general relativity in such regimes to high accuracy.

While direct observational tests of GR have not yet revealed any discrepancy, there are strong indications that it breaks down in sufficiently strong curvature regimes, where quantum gravity effects are expected to become non-negligible. At the same time, the elusive nature of Dark Matter and Dark Energy can also be addressed as being due to modifications of GR. Attempts to construct a quantum theory of gravity, such as string theory, typically result in additional scalar degrees of freedom being present when taking the low-energy limit of such theories. Therefore, generic theories that contain not only tensorial, but also scalar degrees of freedom—so-called scalar-tensor theories—have been a well-motivated modification of GR. The additional scalar degree of freedom generically leads to a range of testable phenomena, such as spontaneous scalarization, screening mechanisms, and fifth forces, among others. These phenomena are observationally testable using GW signals from binary systems, and we will explore several of them in this thesis.

While GWs from compact binaries allow us to test deviations from GR, they also encode information about the source system, such as properties of the compact bodies and their environment. As such, they are a useful tool to investigate the internal structure of neutron stars and to thus place constraints on the nuclear equation of state. At the same time, if DM is present in or around NSs, then it also have an impact on the NS properties and thus also the emitted GW signal, and it is hence possible to also constrain DM models [65–85]. In general, one finds that DM may exhibit two qualitatively different morphological distributions. Its distribution may extend beyond the surface of the NS and thus form a *cloud*, or, if its distribution is mainly confined within the neutron star, it is considered to be a DM *core*. Cloud-like configurations typically enlarge NS observables, such as their masses and radii, while core-like configurations usually reduce them [86–88]. Most recent studies have focused on DM candidates that can be described as a perfect fluid, however, we here consider ultra-light DM in regimes where the classical field approximation is appropriate. Particularly, we consider DM to be described by a complex scalar field featuring a global U(1) symmetry. This global symmetry results in number conservation of the bosons and hence allows for the formation of stable bound objects, dubbed boson stars [59,60,89]. It is further possible to construct solutions of NSs and BSs coexisting in the same physical location, which are called Fermion-Boson stars (FBSs). These were first investigated by Henrique et al. [90,91] and their stability properties were investigated subsequently [92–95]. We will here expand upon previous results by first deriving the equations describing static linear perturbations of a isolated FBS, and then utilizing these to obtain the quadrupolar Love numbers.

In order to properly identify and extract meaningful information from GW signals, it is paramount to have firm analytical control over the expected signal. To establish such control, it is important to carefully set up a framework that allows for calculating the GW signal to a given order in certain smallness parameters. During the inspiral phase, one finds that the orbital velocity together with Newton's constant provide natural small parameter that can be used to systematically construct a series expansion in said parameters. This expansion is called the *post Newtonian* (PN) expansion as it systematically captures deviations from Newtonian gravity. We can classify PN effects as being conservative, such as Mercury's perihelion shift, or dissipative, such as energy loss due to the emission of GWs. The first conservative PN order was calculated by Einstein, Infeld, and Hoffmann in 1938 [96] and is known as the Einstein-Infeld-Hoffmann Lagrangian. During the last decades several frameworks were setup in order to systematically compute the higher PN orders and we here focus mainly on the effective field theoretical approach that was originally laid out by Goldberger and Rothstein in 2004 [54]. This framework has been extensively applied to calculate higher PN order in pure GR [40–48], as well as modified gravity scenarios [49, 50, 52]. Especially, in [55, 56] it was utilized to compute the LO modifications to the binary dynamics due to an additional massive scalar field and we will here build upon these results by extending them to the next PN order, which thus extents previously available results [97–111]. This additional scalar degree of freedom does not necessarily arise from modifications to GR and can instead also arise from standard model extensions [56, 112–114].

This thesis is outlined as follows: We begin by reviewing the essential theoretical background in Chapter 2, where important concepts, such as GWs and compact objects, are introduced. In Chapter 3, we will begin by introducing the effective field theory approach to systematically calculate the GW signal from a compact binary system. We will begin by reviewing the established approach in pure GR and next present the necessary modifications to accommodate a massive scalar degree of freedom. We will conclude this section with the calculation of the NLO GW phase in the presence of said scalar field. Chapter 4 will turn toward the impact of DM on NSs by studying how the mass, radius, and tidal deformability change when one admixes ultra-light DM onto a NS. Next, Chapter 5 is dedicated to the study of the tidal deformability in scalar-tensor theories. We discuss how the presence of the additional field increases the number of Love numbers that are necessary to describe the multipoles of an object and further show how these can be extracted from numerical data. Finally, Chapter 6 will conclude this thesis and list possible future directions.

Throughout this thesis, Roman indices run from 1 through 3, while Greek indices run from 0 through 3. We employ the Einstein sum convention and natural units, such that $\hbar = c = 1$. The reduced Planck mass is introduced as $M_{\rm pl}^2 = 1/(8\pi G)$ and we mainly adhere to the mostly positive metric signature such that the Minkowski metric is given by $\eta_{\mu\nu} = \mathrm{diag}(-1, +1, +1, +1)$. An exception to this is chapter 3, where we instead use $M_{\rm pl}^2 = 1/(32\pi G)$ and $\eta_{\mu\nu} = \mathrm{diag}(+1, -1, -1, -1)$ in order to stay consistent with the publication this chapter is based on.

Chapter 2

Theoretical Background

"So schreitet in dem engen Bretterhaus
Den ganzen Kreis der Schöpfung aus
Und wandelt mit bedächt'ger Schnelle
Vom Himmel durch die Welt zur Hölle."
— **Johann Wolfgang Goethe**, Faust I

2.1 Dark Matter

2.1.1 Evidence

In 1933, it was Fritz Zwicky who published the first work indicating that there is missing mass in the Coma galaxy cluster [115]. In his work, he measured the velocity dispersion, which gives an approximation of the total gravitational mass of a system via the virial theorem, which he noted to differ from the luminous mass. Since this missing mass has to be non-luminous, he named it *dark matter*. Almost 40 years later, in 1970, two separately conducted studies on the rotation curves of galaxies were published, the first one being by Rubin and Ford [116] and the second by Freeman [117]. Both studies concluded that there has to be additional matter present in a substantial amount to explain the observed galactic rotation curves. This has further been shown to be a general feature of disk galaxies [118].

More evidence can be found on the scale of galaxy clusters. For example, in 2006, Clowe et al. [119] utilized weak lensing techniques to investigate the distribution of gravitational mass in a system of two colliding galaxy clusters. They found that weak lensing indicates that the bulk of the gravitational mass has moved further than the luminous mass after the collision (see Fig. 2.1), exactly what one would expect for the DM components.

Moving on to cosmological scales, the dark matter density impacts the position of the peaks in the power spectrum of baryon acoustic oscillations. This power spectrum can be obtained by measuring temperature fluctuations in the cosmic microwave background. This was done by, e.g., the Planck satellite [120], which gave a high-accuracy measurement

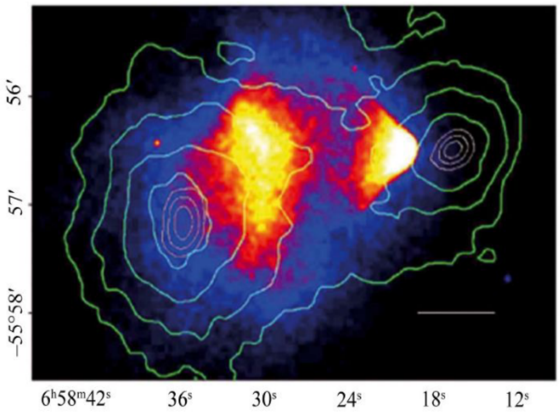

Figure 2.1: Shown is the inferred mass distributions of the bullet cluster (green contour lines) together with the distribution of luminous matter (color scale). Taken from [119].

of the DM density.

2.1.2 Candidates

Since DM evidence is based on its gravitational interaction with other matter and only constrains the DM density, there is a plethora of candidates that span a mass range of more than 80 orders of magnitude. Figure 2.2 summarizes typical candidates for various regions in the mass range, and we briefly summarize some of their properties.

- **Primordial BHs**: If a sufficient amount of BHs formed in the early universe, then these could fulfill various of the desired DM properties [121]. While this seems to be an attractive approach to explain DM, as it is not necessary to postulate any additional particle content in this way, the elusive nature of BHs complicates observational tests of this hypothesis.
- **Composite DM**: Heavy bound states of SM particles could explain DM [122], thus also eliminating the need to introduce additional particle species. However, no such bound state is currently known within the SM.
- **WIMPs**: A new particle that interacts with the SM via the weak force (or a new force that also lies on the weak scale) would match the observed DM abundance if it were thermally produced in the early universe [123]. This so-called *WIMP miracle* has been a strong motivation for this candidate.
- **Ultra-light DM**: A DM particle with masses of less than $\approx 0.1\,\mathrm{keV}$ has to be bosonic and exhibits wave-like behavior since the occupation numbers have to be larger than one. As such, one typically models ULDM as classical fields. One prominent example is the Axion, which was originally introduced to solve the strong CP problem.

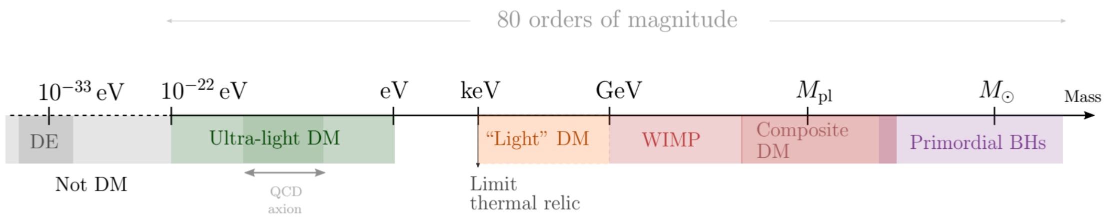

Figure 2.2: Taken from [58].

2.2 General Relativity and Modified Gravity

2.2.1 General Relativity

While Newtonian gravity was highly successful in describing planetary orbits, in 1859 Le Verrier showed that Mercury exhibits an anomalous perihelion shift that can not be accounted for when only considering Newtonian gravity and the known planets. At first, researchers attempted to explain this anomaly by introducing an additional, up to that point unobserved planet, dubbed *Vulcan*. Since this hypothetical planet remained elusive toward the end of the 19th century, some researchers have instead turned toward attempting to modify the Newtonian laws of gravitation in order to explain Mercury's perihelion shift. Motivation for this was the success of electromagnetism, which was formulated as a local field theory with propagating degrees of freedom, i.e., photons. Various attempts were made by, e.g., Lévi in 1890 and Gerber in 1898, but were insufficient to explain the perihelion shift adequately.

In 1915, Einstein showed that the anomalous perihelion shift can be explained within the framework of his previously published theory of General Relativity [124]. This theory generalizes special relativity to curved spacetimes and thus makes heavy use of differential geometry. One of the central underlying concepts is to consider spacetime to be curved in such a way that matter moves on geodesics. More precisely, the curvature of spacetime is described via the metric $g_{\mu\nu}$ from which one can build any other desired geometrical invariant, such as the Ricci tensor $R_{\mu\nu}$ and the Ricci scalar R. These objects have to further fulfill the Einstein field equations

$$R_{\mu\nu} - \frac{1}{2} g_{\mu\nu} R = \frac{1}{M_{\rm pl}^2} T_{\mu\nu} \,, \tag{2.2.1}$$

where $T_{\mu\nu}$ is the energy-momentum tensor of matter.

2.2.2 Motivation to go beyond General Relativity

One of the first pushes toward the exploration of beyond GR effects was done by Kaluza [125] and Klein [126] in the 1920s, where they separately explored the consequences of a five-dimensional spacetime, where one of the spatial dimensions is compactified. As a result, they found that in the low-energy limit, the theory behaves effectively as GR with additional scalar and vector degrees of freedom, which motivates the attempt to unify gravity with electromagnetism.

While the original approach by Kaluza and Klein was not fruitful, the general idea of having compactified spatial dimensions is an important aspect in modern approaches to quantum theories of gravity, such as string theory. As such, the low-energy limit of a given string theory generically contains scalar fields, thus strongly motivating studying the general impact of such additional degrees of freedom.

Apart from quantum gravity aspects, there are additional compelling theoretical and observational aspects that motivate going beyond GR. As summarized in [127], the observed cosmological constant is unnatural and remains one of the biggest modern mysteries in cosmology. Further, as explained above, DM has yet to be observed and might not need to be of particle nature, as modified gravity can also mimic observed effects. The BH information paradox generically also requires to go beyond GR.

2.2.3 Modified Gravity Candidates

With a lack of observational constraints, one finds oneself in a position that allows for the construction of arbitrarily complex models and the task of narrowing down this theory space seems daunting. However, there are a number of important theorems that greatly reduce the allowed theory space. For example, Deser established in 1970 that any theory describing a massless spin-2 field that couples to other matters needs to be described by the Einstein-Hilbert action [128]. In the same year, Lovelock published a proof showing that a four-dimensional spacetime needs to be described by the EFE if one imposes the conditions that gravity is described by a metric field which obeys second-order equations of motion [129, 130]. In order to go beyond GR, one of the assumptions of Lovelock's theorem has to be broken, i.e., one needs to either consider higher-dimensional spacetimes, allow for higher than second-order equations of motion, or introduce additional degrees of freedom.

While there is a plethora of such possible modifications, as mentioned in the previous section, additional scalar degrees of freedom generically appear and studying their general properties is thus of interest. Brans-Dicke theory is a prominent of such a scalar-tensor theory, which Brans and Dicke originally proposed in 1961 [131] with the intent of extending GR to obey Mach's principle. While the initially envisioned theory by Brans and Dicke has been ruled out by observations, it still serves as a prototypical scalar-tensor theory. Another example is $f(R)$ gravity [18], where one replaces the Ricci scalar in the EH action with an arbitrary function that depends on the Ricci scalar. While the resulting field equations are higher than second-order, one can show that they are generally equivalent to a scalar-tensor theory that does have second-order field equations by performing a conformal rescaling of the metric.

2.2.4 Compact Objects

General Characteristics

At the lowest order, we can characterize any object according to a few macroscopic quantities such as its mass M, radius R, etc. We define the compactness $\mathcal{C}$ of an object as the ratio of its mass to its radius, so that $\mathcal{C} = M/R$ and denote an object as *compact* if its compactness approaches the maximum value of 1/2, which is realized for black holes. As such, compactness is a convenient indicator for the relevance of relativistic effects.

If we wish to describe the dynamics of an object in a curved spacetime, then this can be achieved using it geodesic equation that derives from the point particle action

$$\mathcal{S}_{\rm pp} = -M \int \mathrm{d}\tau \,, \tag{2.2.2}$$

where $\mathrm{d}\tau$ is the proper time interval along the object's geodesic.

Due to the effacement principle, we know that information about the internal structure of an object is strongly suppressed compared to the LO effect due to an object's mass. Nonetheless, we know that finite-sized objects deform under the influence of external gravitational fields. The most prominent example for these deformations are perhaps the tides in Earths oceans that result from the Moon's gravitational field. Love was the first one to quantitatively describe this phenomenon and introduced the so-called *Love numbers* that allow to calculate the gravitating response of a body due to a given multiple moment of an external field.

While a relativistic study of an object's deformability due to external fields is much more involved, especially since an object's response is not as easily identified due to the non-linear nature of the EFE, it is possible to extent the concept of Love numbers to a fully relativistic treatment. This was first done by Hinderer in 2007 [61].

Black Holes

The modern history of BHs began with Schwarzschild when he published the first exact solution of the Einstein field equations in 1916 [132]. Schwarzschild here successfully constructed a spherically symmetric and static vacuum solution, which he considered to describe a spacetime containing one point mass. The line element of this solution can be expressed as

$$\mathrm{d}s^2 = -\left(1 - \frac{2M}{r}\right)\mathrm{d}t^2 + \left(1 - \frac{2M}{r}\right)^{-1}\mathrm{d}r^2 + \mathrm{d}\Omega^2 \,, \tag{2.2.3}$$

where M denotes the object's mass. While being a non-trivial exact solution to the EFE, it does seem to have various problems: The metric has singularities at $r = 2M$ and $r = 0$, and the time direction becomes space-like for radii $r < 2M$, while space directions become time-like. The singularity at $r = 2M$ can be understood as a mere coordinate singularity that arises due to the particular choice of used coordinate systems, but the singularity at $r = 0$ is indeed a physical one. While Einstein argued in 1939 [133] that the singularity could not be realized in nature, Oppenheimer and Snyder showed in the same year [134] that gravitational collapse of a spherical gas distribution naturally leads to black hole formation. Regge and Wheeler further proved in 1957 [135] that black holes are stable under linear perturbations, and Penrose showed in 1965 that the formation of singularities is inevitable [136] under generic assumptions, thus establishing that black holes *should* exist in nature.

While isolated BHs are fully characterized by their mass, charge, and spin, one generally expects that a set of Love numbers are required to also describe the gravitational response of a BH submerged in an external field. Somewhat surprisingly, it can be shown that all Love numbers vanish for Schwarzschild BHs in GR, which can be traced to the presence of a non-trivial symmetry in the perturbation equations [137, 138].

Neutron Stars

In 1939, Tolman [139] and Oppenheimer & Volkoff [140] derived the necessary equations to describe a star in a spherically symmetric and static background. To this end, they employed Schwarzschild coordinates, so that the line element is given by

$$\mathrm{d}s^2 = -f(r)\mathrm{d}t^2 + \frac{1}{h(r)}\mathrm{d}r^2 + \mathrm{d}\Omega^2 \tag{2.2.4}$$

and considered an ideal fluid EMT. From this, they derived an equation that allows to determine the pressure profile that we may express as [141]

$$P'(r) = -\frac{m_r\,\varepsilon}{r^2}\left(1 + \frac{P}{\varepsilon}\right)\left(1 + \frac{4\pi r^3 P}{m_r}\right)\left(1 - \frac{2m_r}{r}\right)^{-1}, \tag{2.2.5}$$

which is known as the the Tolman–Oppenheimer–Volkoff (TOV) equation and we have introduced

$$m_r = 4\pi \int_0^r \mathrm{d}r' r'^2\, \varepsilon(r')\,. \tag{2.2.6}$$

In order to close the system of equations, it is still necessary to provide an EOS that links the pressure to the energy density of the fluid. Oppenheimer and Volkoff in their 1939 paper [140] studied the resulting configurations when employing the EOS for a free Fermi gas that they used in order to describe nuclear matter. In this way, they found that the resulting stellar configurations have a maximum mass of around $M_{\mathrm{max}} \approx 0.7\, M_{\odot}$ and radii of around $\mathcal{O}(10)$ km. While these calculations showed that such object are allowed solutions to the Einstein field equations, it was unclear whether they also exist in nature.

The first evidence for a NS was published by Hewish et al. in 1968 [142].A few years later, in 1974, Hulse and Taylor published evidence for the first known binary pulsar system [143], which was subsequently employed for tests of GR [144]. Neutron stars are nowadays not only of great interest to the GR community, but also the QCD community, as they allow to derive constraints on the nuclear matter EOS.

Boson Stars and Fermion-Boson Stars

Kaup in 1968 [89] and one year later in 1969, Ruffini and Bonazzola [60] were the first ones to construct Boson star configurations by solving the Einstein-Klein-Gordon system of equations. In their studies, they have focused on non-self-interacting particles and found that for such systems, the resulting objects are greatly extended in space. Colpi, Shapiro, and Wasserman expanded on these initial efforts in 1986 [59]: They introduced a quartic self-interaction in the bosonic field and noticed that even a small self-interaction strength is sufficient to produce compact objects with solar masses and radii on the order of 10 km. They also coined the name *Boson star* in their seminal work.

Compact Objects in Scalar-Tensor Theories

Adding additional matter fields, or modifying the EFE typically also modifies the Schwarzschild metric, and there is thus a rich literature of solutions for such models. In general, however, such models do not possess analytic closed form solutions and one typically has to resort either to numerical or approximate solutions. Since we are most interested in additional scalar fields, we briefly summarize additional phenomena that can arise due to its presence:

- **Scalar charge:** Spacetimes of an isolated object at rest generally require an additional parameter to be fully specified that is denoted as the *scalar charge*, which is typically given by the r^{-1} coefficient in the asymptotic expansion of the scalar field. We will define the scalar charge more rigorously in Chap. 3.

- **Additional Love numbers:** The additional field allow for additional deformation possibilities since now there are four possible scenarios where the scalar or gravitational field of an object is deformed due to externally applied scalar or gravitational fields. We will study these Love numbers in detail later in Chap. 5.

- **Spontaneous scalarization:** For a number of models where the scalar field is sourced by either the trace of the EMT of matter or a non-vanishing geometric scalar (such as the Gauss-Bonnet invariant), the resulting compact objects might be either exactly equal or similar to the GR solutions and only significantly differ from GR in certain density or curvature regimes. A prominent model for this phenomenon is the Damour-Esposito-Farèse (DEF) model, which we will study more closely in Sec. 5.5.

2.3 Gravitational Waves

The idea of moving bodies producing GWs already arose in the 19th century, with, e.g., Heaviside promoting Newton's law of gravitation to be analogous to Maxwell's laws of electrodynamics and thus also finding propagating degrees of freedom [145]. Our modern understanding, however, began with Einstein's seminal paper in 1916 [4], where Einstein linearized his previously obtained field equations to find that GWs exist and can be generated by moving masses. Also, Einstein already realized in this publication that, in contrast to electromagnetic waves, GWs require a non-vanishing quadrupole moment to be generated.

2.3.1 Linearizing the Einstein Field Equations

We briefly review the derivation of GWs and will follow [146] throughout this section for this purpose. We begin with the Einstein field equations,

$$R_{\mu\nu} - \frac{1}{2}g_{\mu\nu}R = \frac{1}{M_{\rm pl}^2}T_{\mu\nu}, \tag{2.3.1}$$

and consider the metric to consist of small perturbations around flat space, such that $g_{\mu\nu} = \eta_{\mu\nu} + h_{\mu\nu}$, where $h_{\mu\nu}$ denotes the perturbations. Expanding the EFE to linear order in $h_{\mu\nu}$ we obtain

$$\Box\bar{h}_{\mu\nu} + \eta_{\mu\nu}\partial^\rho\partial^\sigma\bar{h}_{\rho\sigma} - \partial^\rho\partial_\nu\bar{h}_{\mu\rho} - \partial^\rho\partial_\mu\bar{h}_{\nu\rho} = -\frac{2}{M_{\rm pl}^2}T_{\mu\nu}\,, \tag{2.3.2}$$

where $\Box = \partial_\mu\partial^\mu$ and we introduced the trace-reversed metric perturbations $\bar{h}_{\mu\nu}$ in order to express the linearized equations more compactly. This quantity is defined as

$$\bar{h}_{\mu\nu} = h_{\mu\nu} - \frac{1}{2}\eta_{\mu\nu}h \tag{2.3.3}$$

with $h = \eta^{\mu\nu}h_{\mu\nu}$. In the linearized limit, we have that the usual diffeomorphism invariance reduces to a gauge invariance of the form

$$h_{\mu\nu} \to h_{\mu\nu} - \partial_\mu\xi_\nu - \partial_\nu\xi_\mu \tag{2.3.4}$$

and we can use this fact to choose the so-called *Lorentz gauge*, which is defined as

$$\partial^\nu\bar{h}_{\mu\nu} = 0\,. \tag{2.3.5}$$

This now simplifies the linearized field equations to

$$\Box\bar{h}_{\mu\nu} = -\frac{2}{M_{\rm pl}^2}T_{\mu\nu}\,, \tag{2.3.6}$$

which we recognize as a wave equation for $\bar{h}_{\mu\nu}$ with a source term given by $T_{\mu\nu}$ and can thus already deduce that matter sources GWs that propagate at the speed of light. We can further understand the behavior of GWs by specializing the linearized equations to vacuum, so that the equations simplify to

$$\Box \bar{h}_{\mu\nu} = 0\,, \tag{2.3.7}$$

which has plane wave solutions of the form

$$\bar{h}_{\mu\nu} = \bar{e}_{\mu\nu}\, e^{ik_\alpha x^\alpha}\,, \tag{2.3.8}$$

where $\bar{e}_{\mu\nu}$ is the so-called *polarization tensor*. Also, the Lorentz gauge condition in Eq. (2.3.5) further implies that the polarization tensor has to fulfill

$$k^\nu \bar{e}_{\mu\nu} = 0\,. \tag{2.3.9}$$

We can now reconstruct the metric perturbations $h_{\mu\nu}$ that we originally introduced by using

$$h_{\mu\nu} = \bar{h}_{\mu\nu} - \frac{1}{2}\eta_{\mu\nu}\bar{h} \tag{2.3.10}$$

and thus find for the plane wave solutions that

$$h_{\mu\nu} = e_{\mu\nu}\, e^{ik_\alpha x^\alpha}, \tag{2.3.11}$$

where we have introduced $e_{\mu\nu}$ to denote the polarization tensor for $h_{\mu\nu}$. We further note that the Lorentz gauge does not completely fix the gauge freedom for the source-free equations (2.3.7) and we can perform an additional gauge transformation to arrive at the *transverse-traceless gauge* that is characterized by

$$h^{0\mu} = 0\,, \quad h^i{}_i = 0\,, \quad \text{and} \quad \partial^j h_{ij} = 0\,. \tag{2.3.12}$$

Applying these constraints to the plane wave solutions in Eq. (2.3.11), we find that the polarization tensor has to obey

$$e^{0\mu} = 0\,, \quad e^i{}_i = 0\,, \quad \text{and} \quad k^j e_{ij} = 0\,. \tag{2.3.13}$$

Considering a wave that propagates in the z direction, we find that the polarization tensor has to take the form of

$$e_{\mu\nu} = \begin{pmatrix} 0 & 0 & 0 & 0 \\ 0 & h_+ & h_\times & 0 \\ 0 & h_\times & -h_+ & 0 \\ 0 & 0 & 0 & 0 \end{pmatrix}, \tag{2.3.14}$$

where we used h_+ and $h_\times$ to denote the two remaining free components of $e_{\mu\nu}$. In other words, we find that any GW can be expressed a linear combination of two polarization modes that we denote as $e^+_{\mu\nu}$ and $e^\times_{\mu\nu}$.

2.3.2 Generating Gravitational Waves

The wave equation that describes linearized GWs (2.3.6) including the source term can be straightforwardly solved by employing the wave equation's Green's function G, given by

$$G(x - x') = -\frac{1}{4\pi|\boldsymbol{x} - \boldsymbol{x}'|}\delta(t_{\mathrm{ret}} - t), \tag{2.3.15}$$

where $t_{\mathrm{ret}} = t - |\boldsymbol{x} - \boldsymbol{x}'|$. The solution for $\bar{h}_{\mu\nu}$ is then directly given by

$$\begin{aligned} \bar{h}_{\mu\nu}(x) &= -\frac{2}{M_{\mathrm{pl}}^2}\int \mathrm{d}^4x'\, G(x - x')T_{\mu\nu}(x - x') \\ &= 4\int \mathrm{d}^3\boldsymbol{x}' \frac{1}{|\boldsymbol{x} - \boldsymbol{x}'|}T_{\mu\nu}(t_{\mathrm{ret}}, \boldsymbol{x}')\,. \end{aligned} \tag{2.3.16}$$

Expanding $T_{\mu\nu}$ in multipole moments, one finds that at lowest order and far away from the source, the solution simplifies to

$$\bar{h}_{ij}(t, \boldsymbol{x}) = \frac{2}{r}\Lambda_{ij,kl}\,\ddot{Q}_{kl}(t_{\mathrm{ret}})\,, \tag{2.3.17}$$

where Q_{ij} denotes the *quadrupole moment*, which is defined as

$$Q_{ij}(t) = \int \mathrm{d}^3\boldsymbol{x}\, T^{00}(t, \boldsymbol{x})\left(\boldsymbol{x}^i\boldsymbol{x}^j - \frac{1}{3}r^2\delta^{ij}\right) \tag{2.3.18}$$

and $\Lambda_{ij,kl}$ projects onto the transverse and traceless gauge. Explicitely, this projector is given by

$$\Lambda_{ij,kl}(\hat{\boldsymbol{n}}) = P_{ik}P_{jl} - \frac{1}{2}P_{ij}P_{kl}\,, \quad \text{where} \quad P_{ij}(\hat{\boldsymbol{n}}) = \delta_{ij} - \hat{\boldsymbol{n}}_i\hat{\boldsymbol{n}}_j\,. \tag{2.3.19}$$

In order to efficiently source GWs, we thus deduce that it is crucial to have time-varying and inhomogeneous matter sources present.

Since GWs carry energy and angular momentum away from the binary systems, we have that a binary system can not remain at a fixed orbital separation. More explicitly,

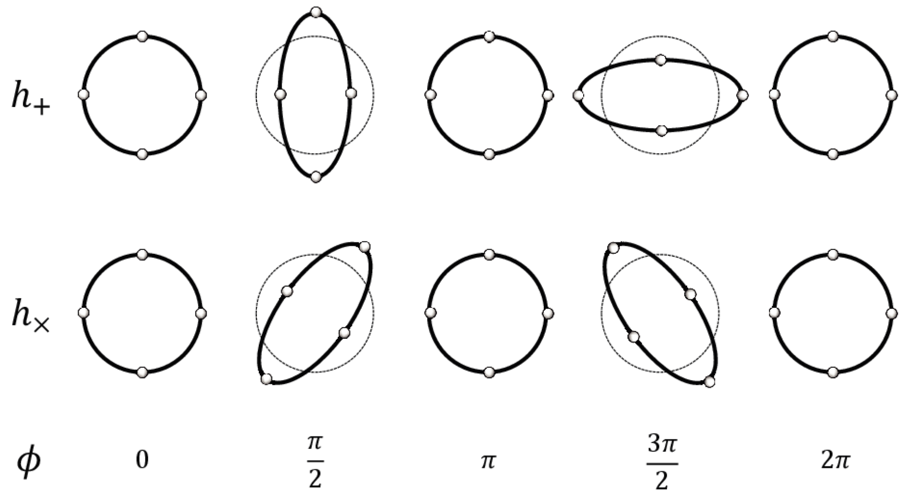

Figure 2.3: The motion of a ring of test particles under the influence of a GW is illustrated. Image from [147].

one can show that the energy loss due to quadrupolar radiation is given by

$$P_{\rm LO} = \frac{32}{5}\left(\mathcal{M}_c\,\omega_s\right)^{\frac{10}{3}}, \tag{2.3.20}$$

where ω_s is the angular frequency of the binary system and

$$\mathcal{M}_c = \frac{(m_1 m_2)^{\frac{5}{3}}}{(m_1+m_2)^{\frac{1}{5}}} \tag{2.3.21}$$

is the *chirp mass* of the system with m_1 and m_2 being the individual masses of each object. If the energy loss is small compared to the total energy of the system, so that it only impacts the system after sufficiently many orbits have occurred, then we can approximate the orbit at any given time to be Keplerian and determine its dynamical evolution via energy balance considerations, such that

$$\frac{\mathrm{d}}{\mathrm{d}t}E_{\rm tot} = -P_{\rm LO}\,. \tag{2.3.22}$$

In general, one finds that the orbital velocity will thus increase during the inspiral, which also increases the frequency of the emitted GWs.

Apart from binary systems, there are a plethora of other production mechanisms, such as supernovae explosions, superradiance, and head-on collisions of compact objects. Non-local sources, such as phase transitions and cosmic inflation are also viable sources of GWs.

2.3.3 Gravitational Wave Detectors

One can show that GWs can locally be treated as a Newtonian force so that a particle of mass m experiences a force of

$$F_i = \frac{m}{2}\ddot{h}_{ij}^{\mathrm{TT}} x^j \,, \tag{2.3.23}$$

where x^j are the particles' coordinates in a local inertial frame. Using this equation, it is now straightforward to compute the impact of a GW on particles. Considering a ring made out of test masses that lie in the (x, y) plane and a GW that propagates in the z direction, we find that this ring deforms as shown in Fig. 2.3. We most importantly note that while the GW periodically stretches and squeezes the ring made out of test particles.

Similarly, when considering the trajectory of photons, one finds that their travel distance also gets modified by a passing GW in the same fashion. Modern GW detectors leverage this phenomenon by considering two separate beams of photons, so that each beam will pick up a different phase when a GW passes through and thus leads to an interference pattern when recombining both beams, and therefore allows for the reconstruction of the gravitational wave strain. In practice, detector noise is larger than the actual GW strain and thus one has to resort to matched filtering techniques that require knowing the GW signal at very high precision, i.e., order in the PN expansion. To this end, one most commonly employs the TaylorF2 approximant that is constructed in Fourier space.

All modern GW observatories are built on this approach. Currently, there are five observatories actively in operation for observation purposes: GEO600 in Germany, LIGO Hanford and LIGO Livingston in the USA, Virgo in Italy, and KAGRA in Japan. All of these observatories are interferometry-based. Additionally, there are several planned additional interferometry-based observatories, expected to be built within the next two decades: LIGO-India, Cosmic Explorer, Einstein Telescope, LISA, Taiji, TianQin, and DECIGO.

Figure 2.4 presents all currently observed coalescences of compact binary systems together with mass measurements of BHs and NSs from electromagnetic observations.

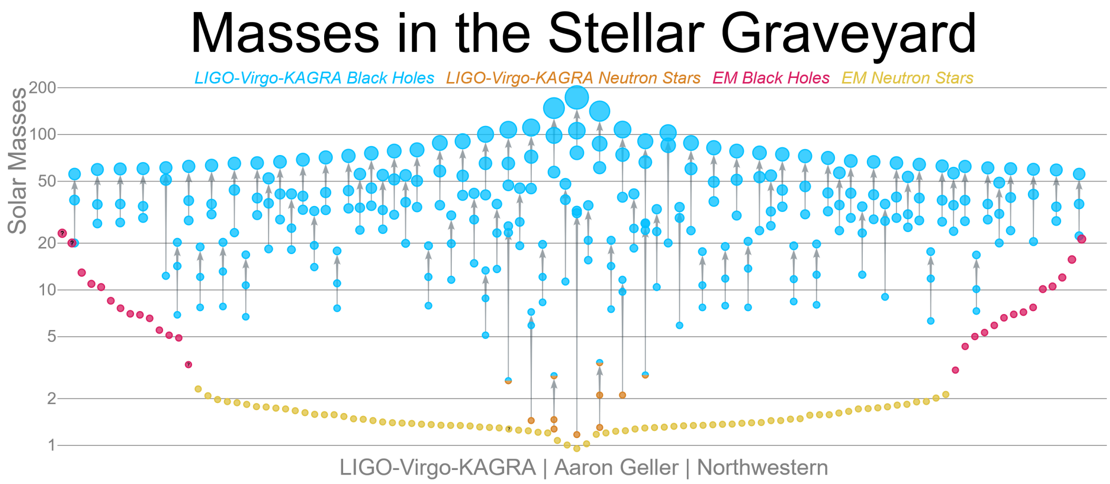

Figure 2.4: A collection of compact objects that have either been observed electromagnetically, or via GWs. Taken from [148].

Chapter 3

Binary Systems in Scalar-Tensor Theories

"When we contemplate the enormous revolution in our understanding of the universe that has come from electromagnetic astronomy over the four centuries since Galileo, we are led to wonder what revolution will come from gravitational astronomy, and from its multi-messenger partnerships, over the coming four centuries."

— **Kip Thorne**, [64]

In order to highlight the modifications due to the additional scalar degree of freedom more efficiently, we will first review the EFT construction process in pure GR and then afterward go into details on the case of scalar-tensor theories.

3.1 EFT Approach in Pure GR

3.1.1 Setting up the Binary EFT

The pure GR construction was originally laid out by Goldberger and Rothstein in [54], and we will closely follow this reference throughout this section. We start with the Einstein-Hilbert action, which is given by[1]

$$\mathcal{S}_{\text{EH}} = -2M_{\text{pl}}^2 \int \mathrm{d}x^4 \sqrt{-g} R \,. \tag{3.1.1}$$

We further add a gauge fixing term to impose the harmonic gauge, which results in

$$\mathcal{S}_{\text{GF}} = M_{\text{pl}}^2 \int \mathrm{d}x^4 \sqrt{-g}\, \Gamma^\mu \, \Gamma^\nu g_{\mu\nu} \,. \tag{3.1.2}$$

The total action thus takes the form of

$$\mathcal{S}_{\text{total}} = \mathcal{S}_{\text{EH}} + \mathcal{S}_{\text{GF}} + \mathcal{S}_{\text{matter}}, \tag{3.1.3}$$

[1] We remind the reader that we are working in units with $\hbar = c = G = 1$ and define $M_{\text{pl}}^2 = 1/(32\pi)$. Further, we use the metric signature $(+1, -1, -1, -1)$.

where $\mathcal{S}_{\text{matter}}$ denotes the matter action, typically assumed to be that of a perfect fluid. In principle, one could directly vary the total action with respect to all involved degrees of freedom and then attempt to find an analytic solution that describes the dynamics of a binary system. However, this is—in practice—not feasible since it would be necessary to model not only the gravitational dynamics but also the matter dynamics simultaneously. Due to the highly non-linear nature of the equations, this seems like a hopeless endeavor. While numerical simulations do provide a way of directly solving the equations, these simulations are quite time demanding and are thus not efficiently utilizable to study the inspiral phase of compact objects for many different binary configurations. During the inspiral phase, however, there are three length scales present that show a clear separation hierarchy: The size of an individual object R_s, the separation distance between the two objects r, and the wavelength of the emitted gravitational radiation λ_{GW}. Having these separated scales now allows us to construct an analytic expansion that allows for perturbative control. More explicitely, we have

$$R_s \sim 2M\,, \tag{3.1.4}$$

$$r \sim \frac{M}{v^2} = \frac{R_s}{2v^2}\,, \tag{3.1.5}$$

$$\lambda_{\text{GW}} \sim \frac{r}{v} = \frac{R_s}{2v^3}\,, \tag{3.1.6}$$

where we assumed that the compact object's sizes are close to their Schwarzschild radius and that the virial theorem is Newtonian at leading order. From the above relations, we can infer that the hierarchy $R_s \ll r \ll \lambda_{\text{GW}}$ is manifest as long as the orbital velocity v is small, which is given during the inspiral. The general strategy is now thus to *integrate out* energy scales that live on the scales of the size of the objects R_s and afterward further integrate out the scale r, thus arriving at a theory that describes the gravitational radiation.

Point-particle action

As a first step toward constructing the binary EFT, we will thus *integrate out* the internal matter degrees of freedom in a bottom-up approach by replacing the matter action with a world-line action in a way that allows to systematically capture finite-size effects, which appear in the world-line action as couplings of the worldline to higher-order operators. In general, one has to include all operators that fulfill all necessary symmetries, which in our case is reparametrization and diffeomorphism invariance. We thus deduce that the world-line action needs to take the following form

$$\mathcal{S}_{\text{matter}} \to \mathcal{S}_{\text{pp}} = -\sum_{n=1,2} \int \mathrm{d}\tau \Big(M_n + c_{n,R} R + \dots \Big), \tag{3.1.7}$$

where M_n denotes the gravitational mass of the nth object, $c_{n,R}$ denote the Wilsonian coefficients to the operator R and the ellipses denote higher-order operators which can be built from contractions of the Riemann tensor, its derivatives and the objects 4-velocity. In general, one can remove all operators from the effective action that are zero on-shell, which in our case means that we can drop all operators from the world-line action that vanish in vacuum [149]. As an example, as shown in [54], defining a new metric $\bar{g}$ with

$$g_{\mu\nu}(x) = \bar{g}_{\mu\nu}(x)\left[1 + \frac{\xi}{2M_{\rm pl}^2}\int \mathrm{d}\tau \frac{\delta^4(x - x(\tau))}{\sqrt{\bar{g}}}\right], \tag{3.1.8}$$

where ξ is an arbitrary parameter, will transform the Einstein-Hilbert action such that

$$-2M_{\rm pl}^2 \int \mathrm{d}^4x\sqrt{-g}\, R[g] = -2M_{\rm pl}^2 \int \mathrm{d}^4x\sqrt{-\bar{g}}\, R[\bar{g}] + \xi \int \mathrm{d}\tau\, R[\bar{g}] + \mathcal{O}(\xi^2). \tag{3.1.9}$$

Choosing $\xi = c_{1,R}$ will thus eliminate the term proportional to R in the PP action of object $n = 1$. We can likewise remove any other operator that vanishes on-shell from both worldlines. Since we have $R = 0$ and $R_{\mu\nu} = 0$ on-shell, we thus find that the first non-redundant operator must be constructed from the Riemann tensor. Including this operator, we find that the PP action reads at NLO

$$\mathcal{S}_{\rm pp} = -\sum_{n=1,2}\int \mathrm{d}\tau\left(M_n + \frac{\lambda_{n,hh}}{4}E_{\mu\nu}E^{\mu\nu} + c_{n,B}B_{\mu\nu}B^{\mu\nu} + \dots\right), \tag{3.1.10}$$

where $E_{\mu\nu}$ and $B_{\mu\nu}$ are electric and magnetic type projections of the Riemann tensor, respectively. They are defined as

$$E_{\mu\nu} = u^\alpha u^\beta R_{\mu\alpha\nu\beta}\,, \quad \text{and} \quad B_{\mu\nu} = \frac{1}{2}\epsilon_{\mu\alpha\rho\sigma}u^\alpha u^\beta R^{\rho\sigma}{}_{\beta\nu}\,. \tag{3.1.11}$$

The corresponding Wilsonian coefficients, $\lambda_{n,hh}$ and $c_{n,B}$, are denoted as the even-parity and odd-parity quadrupolar Love numbers, respectively. For the remainder of this section, we will not further investigate the role of these Love numbers, but will investigate them more closely in Chapter 5 and 4.

Orbital scale

We next turn to the orbital separation scale r. Gravitational interactions that bind the binary system live on this scale. In order to separate this scale from the radiation scale, it is first necessary to expand the Einstein-Hilbert action around vacuum. To this end, we introduce the metric perturbations $h_{\mu\nu}$, such that $g_{\mu\nu} = \eta_{\mu\nu} + h_{\mu\nu}/M_{\rm pl}$ and then further separate $h_{\mu\nu}$ into an off-shell component $H_{\mu\nu}$, which we are aiming to integrate out, and an on-shell component $\bar{h}_{\mu\nu}$, which represents the gravitational radiation. This distinction is now useful since we can mathematically separate them by how their derivatives scale, since we have that

$$\text{On-shell modes:} \quad \partial_\alpha \bar{h}_{\mu\nu} \sim \frac{v}{r}\bar{h}_{\mu\nu}\,, \tag{3.1.12}$$

$$\text{Off-shell modes:} \quad \partial_0 H_{\mu\nu} \sim \frac{v}{r}H_{\mu\nu}\,, \quad \partial_i H_{\mu\nu} \sim \frac{1}{r}H_{\mu\nu}\,. \tag{3.1.13}$$

Put differently, we have that the components of the four-momentum each scale as

$$\text{On-shell modes:} \quad k^0 \sim \frac{v}{r}\,, \quad \boldsymbol{k} \sim \frac{v}{r}\,, \tag{3.1.14}$$

$$\text{Off-shell modes:} \quad k^0 \sim \frac{v}{r}\,, \quad \boldsymbol{k} \sim \frac{1}{r}\,. \tag{3.1.15}$$

Now, inserting this metric decomposition into the Einstein-Hilbert action together with the gauge-fixing term results in

$$\mathcal{S}_{\text{EH}} + \mathcal{S}_{\text{GF}} = \int \mathrm{d}^4x \Big(\mathcal{L}^{(\bar{h}^2)} + \mathcal{L}^{(H^2)} + \mathcal{L}^{(H^2\bar{h})} + \ldots \Big), \tag{3.1.16}$$

where, e.g., $\mathcal{L}^{(\bar{h}^2)}$ denotes all terms that are quadratic in $\bar{h}_{\mu\nu}$ and the ellipses denote higher-order interactions terms. Explicitly we have for the lowest order terms

$$\mathcal{L}^{(\bar{h}^2)} = \int \mathrm{d}^4x\, \frac{1}{2}\partial_\alpha \bar{h}_{\rho\sigma}\Big(\eta^{\mu\rho}\eta^{\nu\sigma} - \frac{1}{2}\eta^{\mu\nu}\eta^{\rho\sigma}\Big)\partial^\alpha \bar{h}_{\mu\nu}\,, \tag{3.1.17}$$

$$\mathcal{L}^{(H^2)} = \int \mathrm{d}^4x\, \frac{1}{2}\partial_\alpha H_{\rho\sigma}\Big(\eta^{\mu\rho}\eta^{\nu\sigma} - \frac{1}{2}\eta^{\mu\nu}\eta^{\rho\sigma}\Big)\partial^\alpha H_{\mu\nu}\,. \tag{3.1.18}$$

These two expressions enable us to define the propagator for both on-shell and off-shell gravitons. We find that the on-shell propagator is given by

$$\langle \bar{h}_{\mu\nu}(x)\bar{h}_{\alpha\beta}(y)\rangle = P_{\mu\nu;\alpha\beta}\int \frac{\mathrm{d}^4k}{(2\pi)^4}\frac{ie^{-ik(x-y)}}{k^2 + i\epsilon}\,, \tag{3.1.19}$$

where

$$P_{\mu\nu;\alpha\beta} = \frac{1}{2}\big(\eta_{\mu\alpha}\eta_{\nu\beta} + \eta_{\nu\alpha}\eta_{\mu\beta} - \eta_{\mu\nu}\eta_{\alpha\beta}\big) \tag{3.1.20}$$

and we will diagrammatically represent the on-shell propagator as

$$\text{On-shell:} \quad \langle \bar{h}_{\mu\nu}(x)\bar{h}_{\alpha\beta}(y)\rangle \quad \longrightarrow \quad \mu\nu \overset{\xrightarrow{k}}{\rightsquigarrow} \alpha\beta \tag{3.1.21}$$

The terms in the Action that are quadratic in $H_{\mu\nu}$, as shown in Eq. (3.1.18), are formally the same as those of the radiation field $\bar{h}_{\mu\nu}$ (given in Eq. (3.1.17)) and thus one might be tempted to use the same propagator we just defined for the radiation gravitons also for the potential gravitons. However, note that the Fourier space propagator takes the form of

$$\frac{1}{k^2 + i\epsilon} = \frac{1}{(k^0)^2 - \boldsymbol{k}^2 + i\epsilon} \tag{3.1.22}$$

and we have discussed around Eq. (3.1.13) that k^0 and $\boldsymbol{k}$ scale differently for potential gravitons. More explicitly, we have that k^0 is suppressed by v relative to $\boldsymbol{k}$, which allows us to expand Eq. (3.1.22) in powers of $(k^0)^2/|\boldsymbol{k}|^2$, such that

$$\frac{1}{k^2 + i\epsilon} = -\frac{1}{|\boldsymbol{k}|^2}\left(1 + \frac{(k^0)^2}{|\boldsymbol{k}|^2} + \dots\right), \tag{3.1.23}$$

where we dropped the ϵ since it becomes irrelevant for the off-shell propagator. We define the potential graviton propagator to be given by the leading-order term in this expansion and treat the higher-order corrections as propagator insertions. The off-shell propagator is thus explicitly given by

$$\langle H_{\mu\nu}(x) H_{\alpha\beta}(y)\rangle = -P_{\mu\nu;\alpha\beta} \int \frac{\mathrm{d}^4 k}{(2\pi)^4} \frac{i e^{-ik(x-y)}}{|\boldsymbol{k}|^2} \tag{3.1.24}$$

and we will use double squiqqly lines to represent this propagator in Feynman diagrams, such that

Off-shell: $\langle H_{\mu\nu}(x) H_{\alpha\beta}(y)\rangle \longrightarrow \mu\nu$ 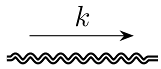

$\alpha\beta\,.$ (3.1.25)

We can alternatively understand this choice for the off-shell propagator as constructing it by only using the terms in Eq. (3.1.18) containing spatial derivatives, and we thus have to treat the remaining term containing temporal derivatives of $H_{\mu\nu}$ as perturbations. This term is given by

$$\mathcal{L}^{(H^2)} \supset \int \mathrm{d}^4 x \, \frac{1}{2} \partial_0 H_{\rho\sigma} \left(\eta^{\mu\rho}\eta^{\nu\sigma} - \frac{1}{2}\eta^{\mu\nu}\eta^{\rho\sigma}\right) \partial^0 H_{\mu\nu} \tag{3.1.26}$$

and we will diagrammatically represent this interaction as insertions of crossed circles in the off-shell propagator, so that at LO we have

LO propagator correction: 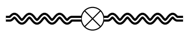 (3.1.27)

Having obtained the propagators for the potential and radiation gravitons as well as their interaction terms, we next have to identify how these modes couple to the worldline of each point-particle. To this end, we first expand the point-particle action in terms of the metric perturbations $h_{\mu\nu}$, such that

$$\mathcal{S}_{\rm pp} = \int \mathrm{d}t \left(\mathcal{L}^{(0)} + \mathcal{L}^{(1)} + \mathcal{L}^{(2)} + \dots\right), \tag{3.1.28}$$

where $\mathcal{L}^{(n)}$ denotes all terms that contain n powers of $h_{\mu\nu}$ and we explicitly have

$$\mathcal{L}^{(0)} = -M\left(1 - \frac{1}{2}\boldsymbol{v}^2 - \frac{1}{8}\boldsymbol{v}^4 + \mathcal{O}\big(\boldsymbol{v}^6\big)\right), \tag{3.1.29}$$

$$\begin{aligned}\mathcal{L}^{(1)} = -\frac{M}{2M_{\mathrm{pl}}}\bigg(&h_{00} + 2h_{0i}\boldsymbol{v}^i + h_{ij}\boldsymbol{v}^i\boldsymbol{v}^j + \frac{h_{00}}{2}\boldsymbol{v}^2 + h_{0i}\boldsymbol{v}^i\boldsymbol{v}^2 \\ &+ \frac{h_{ij}}{2}\boldsymbol{v}^i\boldsymbol{v}^j\boldsymbol{v}^2 + \frac{3}{8}h_{00}\boldsymbol{v}^4 + \mathcal{O}\big(\boldsymbol{v}^6\big)\bigg),\end{aligned} \tag{3.1.30}$$

$$\begin{aligned}\mathcal{L}^{(2)} = \frac{M}{8M_{\mathrm{pl}}^2}\bigg(&h_{00}^2 + 4h_{00}h_{0i}\boldsymbol{v}^i + \big(h_{0i}\boldsymbol{v}^i\big)^2 + 2h_{00}h_{ij}\boldsymbol{v}^i\boldsymbol{v}^j + \frac{3}{2}h_{00}^2\boldsymbol{v}^2 \\ &+ 4h_{0i}h_{jk}\boldsymbol{v}^i\boldsymbol{v}^j\boldsymbol{v}^k + 6h_{00}h_{0i}\boldsymbol{v}^i\boldsymbol{v}^2 + \big(h_{ij}\boldsymbol{v}^i\boldsymbol{v}^j\big)^2 \\ &+ 6\big(h_{0i}\boldsymbol{v}^i\big)^2\boldsymbol{v}^2 + 3h_{00}h_{ij}\boldsymbol{v}^i\boldsymbol{v}^j\boldsymbol{v}^2 + \frac{15}{8}h_{00}\boldsymbol{v}^4 + \mathcal{O}\big(\boldsymbol{v}^6\big)\bigg).\end{aligned} \tag{3.1.31}$$

Power counting

While we now have all the necessary ingredients to perform calculations, it is still necessary to introduce *power counting* rules that allow us to systematically organize all resulting diagrams in a fashion that allows us to clearly identify which diagrams are necessary at which order in the post-Newtonian expansion.

First, we again utilize the virial theorem to note that

$$v^2 \sim \frac{M}{rM_{\mathrm{pl}}^2}\,. \tag{3.1.32}$$

At this point it is convenient to introduce the angular momentum L of the system, which is defined via $L = M v\, r$. Combined with the virial theorem we thus find

$$\frac{M}{M_{\mathrm{pl}}} \sim L^{\frac{1}{2}} v^{\frac{1}{2}}\,. \tag{3.1.33}$$

Next, we find that the radiation and potential graviton propagator, defined in Eq. (3.1.19) and Eq. (3.1.24), scale as

$$\text{On-shell:}\quad \mu\nu \;\overset{k}{\rightsquigarrow}\; \alpha\beta \;\sim\; \left(\frac{v}{r}\right)^4\left(\frac{v}{r}\right)^{-2} = \left(\frac{v}{r}\right)^2, \tag{3.1.34}$$

$$\text{Off-shell:}\quad \mu\nu \;\overset{k}{\rightsquigarrow}\; \alpha\beta \;\sim\; \left(\frac{v}{r}\right)\left(\frac{1}{r}\right)^3 r^2 = \frac{v}{r^2}\,. \tag{3.1.35}$$

From this, we can now infer that

$$\bar{h}_{\mu\nu} \sim \frac{v}{r}\,, \tag{3.1.36}$$

$$H_{\mu\nu} \sim \frac{v^{\frac{1}{2}}}{r}\,. \tag{3.1.37}$$

Next, for the propagator insertions, defined in Eq. (3.1.26), we find that

$\mu\nu$ 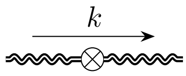 $\alpha\beta$

$$\sim \left(\frac{v}{r}\right)\left(\frac{1}{r}\right)^3 r^2 v^2 = \frac{v^3}{r^2}\,. \tag{3.1.38}$$

It is straightforward to analyze the scalings of arbitrarily many insertions and one finds that generally, n insertions carry along a scaling of v^{2n} relative to the potential graviton propagator.

With this, we have now all ingredients to lay out the general recipe for obtaining the power scaling of a given diagram:

$$\textbf{Virial theorem:} \qquad M/M_{\rm pl} \longrightarrow L^{\frac{1}{2}} v^{\frac{1}{2}} \tag{3.1.39}$$

Insertions: 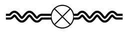

$$\longrightarrow v^2 \tag{3.1.40}$$

$$\textbf{Graviton factors:} \qquad \bar{h}_{\mu\nu} \longrightarrow \frac{v}{r} \tag{3.1.41}$$

$$H_{\mu\nu} \longrightarrow \frac{v^{\frac{1}{2}}}{r} \tag{3.1.42}$$

$$\textbf{Integrals:} \qquad \int \mathrm{d}t \longrightarrow \frac{r}{v} \tag{3.1.43}$$

$$\int \mathrm{d}^3x \longrightarrow r^3 \tag{3.1.44}$$

While the above-presented recipe requires fully writing out the mathematical expression that corresponds to a given diagram, it is also possible to derive scalings for the individual components of a diagram. For example, we find that the first term in Eq. (3.1.30) corresponds to a single potential graviton coupling to the worldline. Applying the obtained power counting rules, we get

$$-\frac{M}{2M_{\rm pl}}\int \mathrm{d}t H_{00} \longrightarrow$$

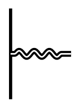

$$\sim L^{\frac{1}{2}}\,. \tag{3.1.45}$$

Similarly, we can investigate the power counting rules for graviton self-interactions. Considering a 3-point vertex of potential gravitons, we find that

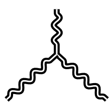

$$\sim L^{-\frac{1}{2}} v^2 \tag{3.1.46}$$

In App. 3.B we summarize the scalings for various couplings and self-interactions. As a specific example, consider the exchange of a single potential graviton, which couples to

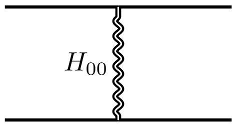

(a) The LO interaction diagram that scales with Lv^0 and hence contributes to the 0PN order.

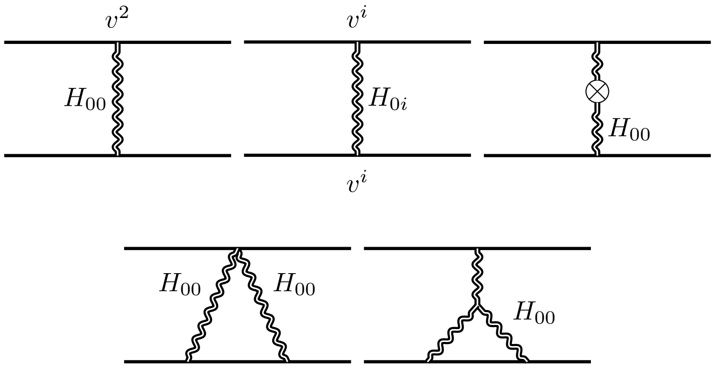

(b) The five interaction diagrams that scale with Lv^2 and thus contribute at 1PN order.

Figure 3.1: All diagrams diagrams in pure GR that contribute to the binding Energy up to 1PN order. Diagrams were created by D. Schmitt.

H_{00} at both worldlines and features one propagator insertion:

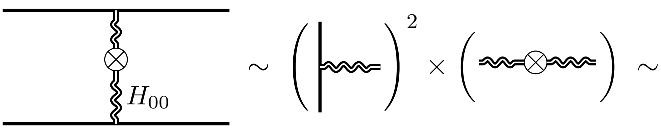

$$\sim \; Lv^2 \, . \tag{3.1.47}$$

In general one finds that all conservative diagrams scale with Lv^{2n} for some integer n and we therefore identify n to be counting the post-Newtonian orders, i.e., the above diagram would contribute at the first post-Newtonian order, while a diagram that scales with Lv^0 contributes at the zeroth post-Newtonian order.

3.1.2 Conservative Dynamics

Having the power counting rules in our hands now, we are ready to categorize the Feynman diagrams depending on which PN order they contribute to. We will illustrate this in the following by computing the LO contribution to the binding energy, i.e., the Newtonian potential. We find that at the lowest order in the expansion, i.e., at 0PN order, we only have one interaction diagram, which is shown in Fig. 3.1a. Writing out this diagram's contribution to the effective action explicitly, we find that

$$i\,\mathcal{S}_{\text{eff}}\Big|_{\text{Fig. 3.1a}} = iP_{00;00}\frac{M_1 M_2}{4M_{\text{pl}}^2}\int \mathrm{d}t_1 \int \mathrm{d}t_2\, \delta(t_2 - t_1) \int \frac{\mathrm{d}^3\boldsymbol{k}}{(2\pi)^3}\frac{e^{-i\boldsymbol{k}(\boldsymbol{x}(t_1)-\boldsymbol{y}(t_2))}}{|\boldsymbol{k}|^2}\, . \tag{3.1.48}$$

While the integral over t_2 is easily evaluated thanks to the Dirac delta function, the momentum integral—albeit a standard calculation in every QFT book—requires a bit more care, and we will go over it for instructive purposes. Also, we will introduce the orbital separation vector $\boldsymbol{r}(t) = \boldsymbol{x}(t) - \boldsymbol{y}(t)$ and denote its length by $|\boldsymbol{r}(t)| = r(t)$. Next, focusing on the momentum integral and introducing spherical coordinates, we find that

$$\begin{aligned}\int \frac{\mathrm{d}^3\boldsymbol{k}}{(2\pi)^3}\frac{e^{-i\boldsymbol{k}\boldsymbol{r}}}{|\boldsymbol{k}|^2} &= \frac{1}{(2\pi)^2}\int_{-1}^{1}\mathrm{d}u\int_0^\infty \mathrm{d}|\boldsymbol{k}|\, e^{-iu|\boldsymbol{k}|r} \\ &= \frac{1}{r}\frac{i}{(2\pi)^2}\int_0^\infty \mathrm{d}|\boldsymbol{k}|\frac{1}{|\boldsymbol{k}|}\left(e^{-i|\boldsymbol{k}|r} - e^{i|\boldsymbol{k}|r}\right) ,\end{aligned} \tag{3.1.49}$$

where in the second line, we have solved the angle integrals such that only the radial integral remains. By substituting $|\boldsymbol{k}| \to -|\boldsymbol{k}|$ in the first term of the above integral, we can extent the integration limits to $(-\infty, \infty)$, so that we obtain

$$\begin{aligned}\int \frac{\mathrm{d}^3\boldsymbol{k}}{(2\pi)^3}\frac{e^{-i\boldsymbol{k}\boldsymbol{r}}}{|\boldsymbol{k}|^2} &= \frac{1}{r}\frac{-i}{(2\pi)^2}\int_{-\infty}^{\infty}\mathrm{d}|\boldsymbol{k}|\frac{e^{i|\boldsymbol{k}|r}}{|\boldsymbol{k}|} \\ &= \frac{1}{4\pi r} .\end{aligned} \tag{3.1.50}$$

Putting this result back into Eq. (3.1.48) we find

$$i\,\mathcal{S}_{\text{eff}}\big|_{\text{Fig. } 3.1a} = iP_{00;00}\frac{M_1M_2}{4M_{\text{pl}}^2}\int \mathrm{d}t\frac{1}{4\pi r} = iGM_1M_2\int \mathrm{d}t\,\frac{1}{r} , \tag{3.1.51}$$

where in the last step we have used the definition of the Planck mass and reinserted powers of G. At this point, we can already recognize the well-known Newtonian potential. However, we also still need to find the diagrams that contribute the kinetic terms to the effective action. We find that these diagrams are given by just the worldline of each object without any interactions happening between them. Looking at the corresponding terms in Eq. (3.1.29), we find that these diagrams contribute with

$$i\mathcal{S}_{\text{eff}} \supset i\int \mathrm{d}t\left(\frac{1}{2}M_1\boldsymbol{v}_1^2 + \frac{1}{2}M_2\boldsymbol{v}_2^2\right) . \tag{3.1.52}$$

Putting these results together, we find at 0PN order

$$\mathcal{S}_{\text{eff}}^{\text{con}} = \int \mathrm{d}t\underbrace{\left(\frac{1}{2}M_1\boldsymbol{v}_1^2 + \frac{1}{2}M_2\boldsymbol{v}_2^2 - G\frac{M_1M_2}{r}\right)}_{\equiv\mathcal{L}_{\text{0PN}}} + \int \mathrm{d}t\,\mathcal{L}_{\text{1PN}} + \mathcal{O}(\text{2PN}) . \tag{3.1.53}$$

Thus, we successfully derived Newtonian gravity to be the LO approximation to GR.

Going to 1PN order is now straightforward, and the necessary diagrams are already presented in Fig. 3.1b. Without calculating each diagram explicitly, we note that the final result is given by

$$\begin{aligned}\mathcal{L}_{\rm EIH} =& \frac{1}{8}M_1\boldsymbol{v}_1^4 + \frac{1}{8}M_2\boldsymbol{v}_2^4 + G\frac{M_1M_2}{2r}\left[3(\boldsymbol{v}_1^2+\boldsymbol{v}_2^2) - 7(\boldsymbol{v}_1\cdot\boldsymbol{v}_2) + \frac{(\boldsymbol{v}_1\cdot\boldsymbol{r})(\boldsymbol{v}_2\cdot\boldsymbol{r})}{r^2}\right] \\ &- G^2\frac{M_1M_2(M_1+M_2)}{2r^2}\,.\end{aligned} \tag{3.1.54}$$

The effective Lagrangian up to 1PN order was first derived in 1938 by Einstein, Infeld, and Hoffmann [96] and is thus also known as the Einstein-Infeld-Hoffman (EIH) Lagrangian.

Having obtained the 1PN conservative Lagrangian, we are now in a position to study the 1PN corrections to, e.g., the Kepler relations. To do this, we will now specialize to circular orbits and parameterize the worldlines as

$$\boldsymbol{x}_1(t) = r_1\begin{pmatrix}\cos(\omega t)\\ \sin(\omega t)\\ 0\end{pmatrix}\,, \quad \text{and} \quad \boldsymbol{x}_2(t) = r_2\begin{pmatrix}\cos(\omega t+\pi)\\ \sin(\omega t+\pi)\\ 0\end{pmatrix}\,. \tag{3.1.55}$$

Substituting this parametrization into the conservative action, we find that only the parameters r_1, r_2, and ω remain as degrees of freedom. Since each one is time-independent, we find that the Euler-Lagrange equations simplify to

$$\begin{aligned}0 &= \frac{\partial\mathcal{L}^{\rm cons}_{\rm 1PN}}{\partial r_1} = 2\,r\,r_1 + r\,r_1^3\omega^2 + 6GM_2r + GM_2r_2\,,\\ 0 &= \frac{\partial\mathcal{L}}{\partial r_2} = 2\,r\,r_2 + r\,r_2^3\omega^2 + 6GM_1r + GM_1r_1\,.\end{aligned} \tag{3.1.56}$$

Combining these equations we can solve for r_2 in terms of $r = r_1 + r_2$:

$$r_2 = \frac{M_1}{M}r + \frac{\nu\delta M}{2}\left(G - \frac{r^3\omega^2}{M}\right) + \mathcal{O}(2\text{PN})\,, \tag{3.1.57}$$

where we have introduced $\nu = M_1M_2/M^2$ and $\delta M = M_1 - M_2$. The first term simply reproduces the Newtonian result and the second term introduces corrections due to the 1PN effects. Likewise, we use the Euler-Lagrange equations to obtain a relation between ω and r:

$$\omega^2 = \frac{GM}{r} + \frac{G^2M^2}{r^2}(\nu-3) + \mathcal{O}(2\,\text{PN})\,. \tag{3.1.58}$$

For future convenience it is useful to express ω and r in dimensionless quantities. For this purpose we introduce

$$x = (GM\omega)^{\frac{2}{3}}, \quad \text{and} \quad \gamma = \frac{GM}{r}\,. \tag{3.1.59}$$

Expressed in these quantities, we find that the Kepler relation takes the form of

$$x^3 = \gamma^3 + (\nu-3)\gamma^4 + \mathcal{O}(2\,\text{PN})\,. \tag{3.1.60}$$

It will later become relevant to also have an expression for γ in terms of x, which we obtain by inverting the above expression:

$$\gamma = x + \left(1 - \frac{\nu}{3}\right) x^2 + \mathcal{O}(2\,\mathrm{PN})\,. \tag{3.1.61}$$

The final quantity of interest is the system's binding energy E, which is readily obtained from the Lagrangian via

$$E = \sum_{n=1,2} \frac{\partial \mathcal{L}}{\partial \dot{\boldsymbol{x}}_n^k} \dot{\boldsymbol{x}}_n^k - \mathcal{L}\,. \tag{3.1.62}$$

For the circular orbits considered here, we find that

$$\frac{E}{\mu} = -\frac{1}{2}\gamma - \frac{1}{8}\gamma^2(\nu - 7) + \mathcal{O}(2\,\mathrm{PN})\,, \tag{3.1.63}$$

where we have used the previously obtained Kepler relations to express the result in terms of γ. Equivalently, we can express the binding energy in terms of x, such that

$$\frac{E}{\mu} = -\frac{1}{2}x + \left(\frac{\nu}{24} + \frac{3}{8}\right) x^2 + \mathcal{O}(2\,\mathrm{PN})\,. \tag{3.1.64}$$

The steps presented here can now be readily generalized to go beyond the EIH Lagrangian by first identifying all necessary diagrams for the 2 PN order and then evaluating them. However, at 1.5 PN order the procedure becomes more complicated since tail effects become relevant. We will not discuss these effects here since they will not be relevant to the 1PN dynamics in scalar-tensor theories that we will derive later on. Instead, we refer the reader to [41] for more information on these effects.

3.1.3 Radiation

In order to investigate the radiation produced by the binary system, we again start out by collecting all diagrams that are relevant up to 1PN order. We find that at lowest order the diagram given in Fig. 3.2a and it is straightforward to show that this diagram scales with $L^{\frac{1}{2}}v^{\frac{1}{2}}$. Going to NLO, we find that there appear two additional diagrams, shown in Fig. 3.2b. The left diagram of this figure has an unambiguous scaling of $L^{\frac{1}{2}}v^{\frac{5}{2}}$, however, it is not clear how to assign a scaling to the right diagram right away. The problem here lies in the interaction vertex of two potential gravitons coupling to the radiation graviton. Making the momentum flow explicit, we find that

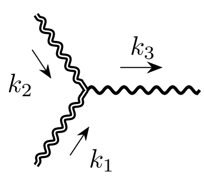

(3.1.65)

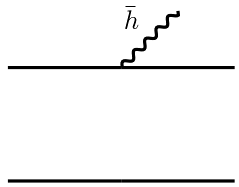

(a) The LO radiation diagram that scales with $L^{\frac{1}{2}} v^{\frac{1}{2}}$.

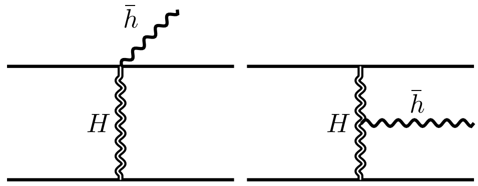

(b) Next-to-leading order diagrams that scale with $L^{\frac{1}{2}} v^{\frac{3}{2}}$

Figure 3.2: All diagrams in pure GR that contribute to graviton radiation at 1 PN order. Diagrams were created by D. Schmitt.

so that the outgoing onshell graviton will have a momentum space propagator given by

$$\frac{1}{k_3^2} = \frac{1}{(k_1^0 + k_2^0)^2 - (\boldsymbol{k}_1 + \boldsymbol{k}_2)^2} \,. \tag{3.1.66}$$

While the first term in the denominator scales as $(k_1^0 + k_2^0)^2 \sim v^2/r^2$ we have that the second term in the denominator scales with $(\boldsymbol{k}_1 + \boldsymbol{k}_2)^2 \sim 1/r^2$ and it is thus not possible to assign an overall scaling to the above-presented vertex. In order to remedy the situation we wish to expand the problematic propagator in powers of $|\boldsymbol{k}_1 + \boldsymbol{k}_2|/|k_1^0 + k_2^0|$, which we can achieve by performing a multipole expansion of $\bar{h}_{\mu\nu}$ at the level of the action.

Multipole expansion. Before introducing the multipole expansion formally, it is worth to first take a look at what we ultimately wish to compute. In order to calculate the emitted radiation, it is necessary to identify the terms in the effective action that sources the radiation gravitons. These terms can generically be expressed by

$$\mathcal{S}_{\text{eff}} \supset \mathcal{S}_{\text{src}} = -\frac{1}{2M_{\text{pl}}} \int \mathrm{d}^4x \, T_{\text{eff}}^{\mu\nu}(x) \, \bar{h}_{\mu\nu}(x) \,, \tag{3.1.67}$$

where we have introduced the effective energy-momentum tensor $T_{\text{eff}}^{\mu\nu}$, which we can determine from the Feynman diagrams. From this it becomes clear that the above-described problem—that the given radiation diagram has no clear scaling—arises for any diagram in which $T_{\text{eff}}^{\mu\nu}$ has non-local contributions. To resolve this situation, we can expand $\bar{h}(x)$ in its spatial coordinates locally, such that

$$\bar{h}_{\mu\nu}(x^0, \boldsymbol{x}) = \bar{h}_{\mu\nu}(x^0, \boldsymbol{X}) + \delta \boldsymbol{x}^i \partial_i \bar{h}_{\mu\nu}(x^0, \boldsymbol{X}) + \frac{1}{2} \delta \boldsymbol{x}^i \delta \boldsymbol{x}^j \partial_i \partial_j \bar{h}_{\mu\nu}(x^0, \boldsymbol{X}) + \mathcal{O}(\delta \boldsymbol{x}^3) \,. \tag{3.1.68}$$

We have here introduced $\delta \boldsymbol{x} = \boldsymbol{x} - \boldsymbol{X}$, which denotes the distance to the expansion point $\boldsymbol{X}$, which we will set to the origin from now on such that $\boldsymbol{X} = 0$. For future convenience, we will also introduce the multi-index L that is defined via $\boldsymbol{x}^L = \boldsymbol{x}^{i_1}\boldsymbol{x}^{i_2}\cdots\boldsymbol{x}^{i_l}$. Leveraging this notation we can write the expansion more compactly as

$$\bar{h}_{\mu\nu}(x^0, \boldsymbol{x}) = \sum_{l=0}^{\infty} \frac{1}{l!} \boldsymbol{x}^L \partial_L \bar{h}_{\mu\nu} \,, \tag{3.1.69}$$

with the derivatives evaluated at $(t, \boldsymbol{x} = 0)$. From this, we now have the great advantage that the scaling of each multipole moment is unambiguous.

As an example, we will calculate the LO power loss due to graviton emission. At LO, the quadrupole moment reads

$$I^{ij} = \sum_{n=1,2} M_n \left[\boldsymbol{r}_n^i \boldsymbol{r}_n^j\right]^{\mathrm{STF}} . \tag{3.1.70}$$

Using the obtained expansion for $\boldsymbol{r}_i$ we get

$$I^{ij} = \mu \left[\boldsymbol{r}^i \boldsymbol{r}^j\right]^{\mathrm{STF}} . \tag{3.1.71}$$

The energy loss is now given by

$$P_{\mathrm{LO}} = \frac{G}{5} \left\langle \left(\partial_t^3 I^{ij}\right)^2 \right\rangle = \frac{32G}{5} M^2 \nu^2 r^4 \omega^6 = \frac{32}{5G} \nu^2 x^5 \,, \tag{3.1.72}$$

where in the last equation we have utilized the Kepler relations to eliminate r in favor of x. This is the famous quadropolar power loss, which was first derived in 1918 by Einstein [150].

As shown in [54] we have that the power loss at 1PN order is given by

$$P_{\mathrm{1PN}} = \frac{32}{5} \nu^2 x^5 \left[1 - \left(\frac{1247}{336} + \frac{35}{12}\nu\right) x\right] . \tag{3.1.73}$$

3.1.4 Gravitational Wave Signal

In order to calculate the gravitational wave signal, we will work in the adiabatic regime, where the momentary orbit can always be assumed to be Keplerian. We will here focus on the gravitational wave phase, which the ground based detectors are most sensitive to.

TaylorF2 Phase. In the time domain we can generally express the gravitational wave $h(t)$ as

$$h(t) = A(t) \cos \varphi(t), \tag{3.1.74}$$

with A and φ being, respectively, the time-dependent amplitude and phase. Applying the stationary phase approximation we can rewrite h in Fourier space, such that

$$\tilde{h}(f) = \mathcal{A}(f)e^{i\Psi(f)}\,. \tag{3.1.75}$$

Further, Ψ needs to fulfill the following differential equations

$$0 = \frac{\mathrm{d}t}{\mathrm{d}f} + \frac{G\pi M}{3v^2}\frac{E'(f)}{P(f)}\,, \tag{3.1.76}$$
$$0 = \frac{\mathrm{d}\Psi}{\mathrm{d}f} - 2\pi t(f)\,, \tag{3.1.77}$$

where primes denote differentiation with respect to v. In order to obtain the GW phase, we thus first need to calculate $E'(f)/P(f)$.

It is useful to restate the differential equations in terms of the expansion parameter x, which is straightforwardly done to yield

$$0 = \frac{\mathrm{d}t}{\mathrm{d}x} + \frac{1}{P}\frac{\mathrm{d}E}{\mathrm{d}x}\,, \tag{3.1.78}$$
$$0 = \frac{\mathrm{d}\Psi}{\mathrm{d}x} - \frac{3x^{\frac{1}{2}}}{GM}t\,. \tag{3.1.79}$$

Focusing only on the LO effects by using Eq. (3.1.64) for the binding energy and Eq. (3.1.72) for the powerloss, we first obtain

$$\frac{1}{P}\frac{\mathrm{d}E}{\mathrm{d}x} = -\frac{5MG}{64\nu}x^{-5}\,. \tag{3.1.80}$$

Solving for $t(x)$ we thus find

$$t(x) = \frac{5MG}{64\nu}\int_{x_0}^{x}\mathrm{d}\tilde{x}\,\tilde{x}^{-5} = -\frac{5MG}{256\nu}\left(x^{-4} - x_0^{-4}\right). \tag{3.1.81}$$

Inserting this result into Eq. (3.2.103) and solving for Ψ we find that

$$\begin{aligned}\Psi(x) &= -\frac{15}{256\nu}\int_{x_0}^{x}\mathrm{d}\tilde{x}\left(\tilde{x}^{-\frac{7}{2}} - x_0^{-4}\tilde{x}^{\frac{1}{2}}\right) = \frac{3}{128\nu}\left(x^{-\frac{5}{2}} - x_0^{-\frac{5}{2}}\right) + \frac{5}{128\nu}x_0^{-4}x^{\frac{3}{2}} - \frac{5}{128\nu}x_0^{-\frac{5}{2}}\\ &= 2\pi f_{\mathrm{gw}}t_c - \phi_c - \frac{\pi}{4} + \frac{3}{128\nu}x^{-\frac{5}{2}} + \mathcal{O}(1\mathrm{PN})\,,\end{aligned} \tag{3.1.82}$$

where in the second line we have introduced ϕ_c and t_c to write the constant term and the term linear in f_{gw} more compactly. In total, we thus found that at LO the GW phase is given by a term proportional to $x^{-5/2}$. Going to higher orders in the PN expansion will add terms with increasingly higher powers in x to the GW phase, such that

$$\Psi(x) = 2\pi f_{\rm gw} t_c - \phi_c - \frac{\pi}{4} + \frac{3}{128\nu} x^{-\frac{5}{2}} \sum_{n=0}^{\infty} c_n x^{\frac{n}{2}} , \tag{3.1.83}$$

for some real coefficients c_n and terms proportional to powers $n = 2i$ of x are denoted as the iPN order. Suppose we want to calculate the GW phase up to order iPN, then how do we know how many PN orders we need for the binding energy and power loss? Working through the integrals backward, we can see that one would need to determine E'/P up to order x^{i-5}. Expanding the binding energy and power loss in a similar fashion, such that

$$P = \frac{32}{5}\nu^2 x^5 \sum_{n=0}^{\infty} a_n x^{\frac{n}{2}} , \quad \text{and} \quad E = -\frac{\mu}{2} x \sum_{m=0}^{\infty} b_m x^{\frac{m}{2}} , \tag{3.1.84}$$

then we find

$$\frac{1}{P} = \frac{5}{32\nu^2} x^{-5} \sum_{n=0}^{\infty} \tilde{a}_n x^{\frac{n}{2}} , \quad \text{and} \quad E' = -\frac{\mu}{2} \sum_{m=0}^{\infty} b_m \left(\frac{m}{2} + 1\right) x^{\frac{m}{2}} . \tag{3.1.85}$$

Hence we have that

$$\frac{E'}{P} \propto x^{-5} \left(\sum_{n=0}^{\infty} \tilde{a}_n x^{\frac{n}{2}} \right) \left(\sum_{m=0}^{\infty} b_n \left(\frac{m}{2} + 1\right) x^{\frac{m}{2}} \right) . \tag{3.1.86}$$

From this we can conclude that in order to know E'/P at order x^{i-5} we need to know E and P up to iPN order. In other words, upon obtaining the binding energy and power loss at order iPN, one can also calculate the TaylorF2 GW phase at the same PN order. Since we presented the necessary 1PN results above, we are thus in a position to determine the 1PN GW phase, which reads

$$\Psi(x) = 2\pi f_{\rm gw} t_c - \phi_c - \frac{\pi}{4} + \frac{3}{128\nu} x^{-\frac{5}{2}} \left[1 + \frac{20}{9} \left(\frac{743}{336} + \frac{11}{4}\nu \right) x + \mathcal{O}\left(x^{\frac{3}{2}}\right) \right] . \tag{3.1.87}$$

3.2 EFT Approach in Scalar-Tensor Theories

Having reviewed the EFT construction and its applications in the pure GR case, we are now well-prepared to tackle scalar-tensor theories. In the following, we will first go over how the construction is modified and then calculate the modifications to the conservative dynamics, the radiation, and the GW phase at NLO in the scalar parameters.

3.2.1 Setting up the EFT

We mainly focus on scalar-tensor theories whose total action can be written as

$$\mathcal{S}_{\rm total} = \mathcal{S}_{\rm EH} + \mathcal{S}_{\rm GF} + \mathcal{S}_{\phi} + \mathcal{S}_{\rm matter} , \tag{3.2.1}$$

where we assume that all interactions between ϕ and the other fields can be absorbed into $\mathcal{S}_{\text{matter}}$ (we will come back to this point later in this section). The scalar field action is thus of the form

$$\mathcal{S}_\phi = \int \mathrm{d}^4x\sqrt{-g}\left[\frac{1}{2}\partial_\mu\phi\partial^\mu\phi - V(\phi)\right]. \tag{3.2.2}$$

Here, $V(\phi)$ denotes an arbitrary potential that we expand around $\phi = 0$ with

$$V(\phi) = \frac{m_s^2}{2}\phi^2 + M_{\text{pl}}\frac{c_3}{3!}\phi^3 + \frac{\lambda}{4!}\phi^4 + \dots, \tag{3.2.3}$$

where m_s is the scalar field mass. We also introduced c_3 and λ as self-interaction coefficients and will later discuss the role they play during the inspiral. Also, note that we have introduced a factor of M_{pl} in the cubic interaction term so that c_3 itself is dimensionless. Choosing M_{pl} to normalize c_3 is at this point arbitrary, and one can always change to another normalization, say M, by substituting $c_3 \to c_3\, M/M_{\text{pl}}$. Only when introducing the power-counting rules later on, the normalization will indeed become relevant, and we will discuss it in more detail at that time.

Relevant scales

Before going on to construct the PP action, it is useful to discuss the new scales that enter the system due to the additional dimensionful parameters we have introduced along with the scalar field. Most notably, due to the mass m_s of the scalar field, we have introduced a new length scale: the Compton wavelength $\lambda_c = 1/m_s$. In general, we expect that the scalar field will have at LO a Yukawa-type falloff, such that

$$\phi(r) = Q\frac{e^{-m_s r}}{r} + \dots \tag{3.2.4}$$

at large distances for some constant Q. From this, we can see that at radii larger than the Compton wavelength, the exponential function will rapidly suppress the scalar field. On the other hand, for radii smaller than the Compton wavelength, we have that the scalar field behaves essentially massless, i.e., expanding around $m_s r = 0$, we have

$$\phi(r) = \frac{Q}{r} + \dots. \tag{3.2.5}$$

This leads us to conclude that λ_c sets the length scale at which the scalar field can effectively act. In general, one would need to decide how the scale λ_c relates to the other scales in the system *before* constructing the EFT. More explicitly, suppose that $\lambda_c \approx R_s$, then the scalar field would effectively be confined to solely act within the object under consideration. If one now constructs the PP action for such an object, then one would completely integrate out the scalar field at this step so that its impact would only lie in modifying the PP action's Wilsonian coefficients, such as the mass of the object. Similarly, if $\lambda_c \lessapprox r$, then one would integrate out the scalar field's dynamics completely when constructing the radiation EFT. Throughout this section, we will assume that $\lambda_c > R_s$ but will not impose any additional hierarchy between neither λ_c and r, nor between λ_c and $\lambda_{\rm gw}$. We will see that this will inhibit us from assigning unambiguous power-counting rules that are valid for each step in the calculations, with the upshot that the results will be valid for a broader range of scalar masses m_s. We will highlight this issue whenever it arises during the EFT calculations.

Further, we will treat all other coefficients that appear in the expansion of $V(\phi)$ perturbatively. Since these coefficients carry along an additional dimensionful parameter (apart from λ), they potentially introduce additional length scales that we have to consider. Their discussion is not as straightforward as the one concerning the scalar mass m_s and so we will postpone the discussion for later when we can diagrammatically investigate their behavior.

Point-particle action

Analogous to the pure GR case, we will construct the PP action from the bottom up. In pure GR this meant that we will couple any operator that is invariant under diffeomorphisms to the worldline of the point-particles. In our current setup we do not introduce any additional symmetries that would need to be respected[2], meaning that any operator that was allowed in pure GR is still allowed in the current setup. In general, we can split the PP action into three sub-actions with

$$\mathcal{S}_{\rm pp} = \mathcal{S}_{{\rm pp},h} + \mathcal{S}_{{\rm pp},\phi} + \mathcal{S}_{{\rm pp},h\phi}\,, \tag{3.2.6}$$

where $\mathcal{S}_{{\rm pp},h}$ captures all terms that are purely built from geometric invariants, $\mathcal{S}_{{\rm pp},\phi}$ contains all terms build from ϕ, and $\mathcal{S}_{{\rm pp},h\phi}$ contains couplings of ϕ to geometric invariants. More explicitly, we have

$$\mathcal{S}_{{\rm pp},h} = -\sum_{n=1,2}\int {\rm d}\tau \left(M_n + c_{n,R} R + \dots \right), \tag{3.2.7}$$

$$\mathcal{S}_{{\rm pp},\phi} = -\sum_{n=1,2}\int {\rm d}\tau \left(q_n \frac{\phi}{M_{\rm pl}} + p_n \frac{\phi^2}{M_{\rm pl}^2} + \dots \right), \tag{3.2.8}$$

$$\mathcal{S}_{{\rm pp},h\phi} = -\sum_{n=1,2}\int {\rm d}\tau \left(d_n \phi R + \dots \right), \tag{3.2.9}$$

where we introduced the coefficients q_n, p_n, and d_n. For reasons that will become obvious later, we will denote q_n as the *scalar charge* and p_n as the *induced charge*. Also, we have

[2] If one was to only consider even-powers in the scalar field potential, then the total action would be invariant under $\phi \to -\phi$. One might wonder whether this would inhibit a linear coupling in the PP action, but instead, this would rather imply that the scalar charge transforms as $q \to -q$ under such a transformation.

normalized powers of ϕ in $\mathcal{S}_{\mathrm{pp},\phi}$ so that each accompanying coefficient has mass units. Choosing M_{pl} here is again at this point—just as discussed above for c_3—arbitrary, and we will discuss the consequences regarding the power-counting rules later in this section. In pure GR, we argued that we can drop any operator from the PP action that vanishes by virtue of the vacuum field equations, which turned out to be the Ricci scalar R and Ricci tensor $R_{\mu\nu}$. In the present case, however, we have that these quantities do not vanish identically in vacuum. Instead, we have that the vacuum field equations now are

$$\Box\phi = -\frac{\partial V}{\partial \phi} \tag{3.2.10}$$

$$-R_{\mu\nu} + \frac{1}{2}Rg_{\mu\nu} = g_{\mu\nu}\bigg(-\frac{1}{2}\partial_\alpha\phi\partial^\alpha\phi + V(\phi)\bigg) + \partial_\mu\phi\partial_\nu\phi \equiv T^{\phi}_{\mu\nu}\,, \tag{3.2.11}$$

where we have defined the scalar field's energy-momentum tensor $T^{\phi}_{\mu\nu}$. Tracing over $\mu\nu$ results in

$$R = -\partial_\alpha\phi\partial^\alpha\phi + V(\phi)\,. \tag{3.2.12}$$

Inserting this back into the field equations, we obtain

$$R_{\mu\nu} = -\frac{1}{2}g_{\mu\nu}V(\phi) - \partial_\mu\phi\partial_\nu\phi\,. \tag{3.2.13}$$

Next, we wish to perform field redefinitions that allow us to transform away *redundant* operators. In order to illustrate this procedure, suppose that we had an action that only depended on a single field Ψ, then we have

$$\mathcal{S}[\Psi + \epsilon\, I(\Psi)] = \mathcal{S}[\Psi] + \epsilon\, I(\Psi)\frac{\delta\mathcal{S}}{\delta\Psi} + \mathcal{O}(\epsilon^2) \tag{3.2.14}$$

Thus, consider changing from the metric $g_{\mu\nu}$ to the new metric $\bar{g}_{\mu\nu}$ such that

$$\bar{g}_{\mu\nu} = g_{\mu\nu}\bigg[1 + \xi\frac{1}{2M_{\mathrm{pl}}}\int \mathrm{d}\tau\frac{\delta^4(x - x(\tau))}{\sqrt{-g}}\bigg]\,, \tag{3.2.15}$$

then

$$\mathcal{S}_{\mathrm{tot}}[\bar{g}] = \mathcal{S}_{\mathrm{tot}}[g] + \xi\int \mathrm{d}\tau\Big[R + \partial_\alpha\phi\partial^\alpha\phi - V(\phi)\Big]\,. \tag{3.2.16}$$

Hence, we can eliminate the term proportional to R in the PP action in favor of terms involving $\partial_a\phi\partial^\alpha\phi$ and $V(\phi)$. We thus use these relations to again remove all occurrences of R and $R_{\mu\nu}$ in the bulk action, however, in contrast to the GR case, this will generate corresponding terms in the ϕ part of the action. More explicitly, we can simplify the above-presented PP action decomposition to

$$\mathcal{S}_{\mathrm{pp},h} = -\sum_{n=1,2}\int \mathrm{d}\tau\Big(M_n + (\mathrm{tidal}) + \dots\Big)\,, \tag{3.2.17}$$

$$\mathcal{S}_{\mathrm{pp},\phi} = -\sum_{n=1,2}\int \mathrm{d}\tau\Big(q_n\frac{\phi}{M_{\mathrm{pl}}} + p_n\frac{\phi^2}{M_{\mathrm{pl}}^2} + d_n\partial_\alpha\phi\partial^\alpha\phi + \dots\Big)\,, \tag{3.2.18}$$

$$\mathcal{S}_{\mathrm{pp},h\phi} = -\sum_{n=1,2}\int \mathrm{d}\tau\Big((\mathrm{tidal}) + \dots\Big)\,. \tag{3.2.19}$$

Orbital scale

In order to separate out the orbital scale, we again split the fields into *on-shell* and *off-shell* components. We hence decompose $h_{\mu\nu}$ in the same fashion as in pure GR and apply the same treatment to ϕ, so that we write $\phi = \Phi + \bar{\phi}$, with Φ the off-shell and $\bar{\phi}$ the on-shell components, which have the following scaling behavior:

$$\text{On-shell modes:}\quad \partial_\alpha\bar{\phi}_{\mu\nu} \sim \frac{v}{r}\bar{\phi}_{\mu\nu}\,, \tag{3.2.20}$$

$$\text{Off-shell modes:}\quad \partial_0\Phi_{\mu\nu} \sim \frac{v}{r}\Phi_{\mu\nu},\ \partial_i\Phi_{\mu\nu} \sim \frac{1}{r}\Phi_{\mu\nu}\,. \tag{3.2.21}$$

Inserting this split into the bulk action, we can decompose the resulting scalar field part in the bulk action such that

$$\mathcal{S}_\phi = \int \mathrm{d}^4x\Big(\mathcal{L}^{(\Phi^2)} + \mathcal{L}^{(\bar{\phi}^2)} + \mathcal{L}^{(\Phi h)} + \mathcal{L}^{(\Phi^2 h)} + \mathcal{L}^{(\Phi^3)} + \dots\Big)\,. \tag{3.2.22}$$

Note that all terms in $\mathcal{L}^{(\Phi h)}$ vanish by performing a field redefinition involving the LO EOM of $\bar{\phi}$. We can now directly read off the propagators for Φ and $\bar{\phi}$:

$$\langle\bar{\phi}(x)\bar{\phi}(y)\rangle = \int\frac{\mathrm{d}^4k}{(2\pi)^4}\frac{ie^{-ik(x-y)}}{k^2 - m_s^2 + i\epsilon}\,, \tag{3.2.23}$$

$$\langle\Phi(x)\Phi(y)\rangle = -\int\frac{\mathrm{d}^4k}{(2\pi)^4}\frac{ie^{-ik(x-y)}}{|\boldsymbol{k}|^2 + m_s^2}\,, \tag{3.2.24}$$

where we only used the spatial momenta to define the off-shell propagator and treat the time derivatives as propagator insertions, just as in the pure GR case.

We next turn to the PP action, which we decompose as

$$\mathcal{S}_{\mathrm{pp}} = \int \mathrm{d}t\Big(\mathcal{L}_{\mathrm{pp}}^{(0)} + \mathcal{L}_{\mathrm{pp}}^{(h)} + \mathcal{L}_{\mathrm{pp}}^{(\phi)} + \mathcal{L}_{\mathrm{pp}}^{(h\phi)} + \mathcal{L}_{\mathrm{pp}}^{(h\phi^2)} + \dots\Big)\,, \tag{3.2.25}$$

with, e.g., $\mathcal{L}_{\mathrm{pp}}^{(h\phi)}$ denoting all terms that are linear in h and ϕ. We note that $\mathcal{L}_{\mathrm{pp}}^{(0)}$ is already given in Eq. (3.1.29) and $\mathcal{L}_{\mathrm{pp}}^{(h)}$ in Eq. (3.1.30). The other relevant terms are explicitly given by

$$\mathcal{L}_{\mathrm{pp}}^{(\phi)} = -\phi \frac{q_n}{M_{\mathrm{pl}}} \left[1 - \frac{1}{2}\boldsymbol{v}^2 - \frac{1}{8}\boldsymbol{v}^4 + \mathcal{O}(\boldsymbol{v}^6) \right] , \tag{3.2.26}$$

$$\mathcal{L}_{\mathrm{pp}}^{(\phi^2)} = -\phi^2 \frac{p_n}{M_{\mathrm{pl}}^2} \left[1 - \frac{1}{2}\boldsymbol{v}^2 - \frac{1}{8}\boldsymbol{v}^4 + \mathcal{O}(\boldsymbol{v}^6) \right] , \tag{3.2.27}$$

$$\mathcal{L}_{\mathrm{pp}}^{(\phi h)} = -\phi \frac{q_n}{2M_{\mathrm{pl}}} \left[h_{00} + 2h_{0i}\boldsymbol{v}^i + h_{ij}\boldsymbol{v}^i\boldsymbol{v}^j + \frac{h_{00}}{2}\boldsymbol{v}^2 + h_{0i}\boldsymbol{v}^i\boldsymbol{v}^2 \right. \\ \left. + \frac{h_{ij}}{2}\boldsymbol{v}^i\boldsymbol{v}^j\boldsymbol{v}^2 + \frac{3}{8}h_{00}\boldsymbol{v}^4 + \mathcal{O}(\boldsymbol{v}^6) \right] . \tag{3.2.28}$$

Power counting

We impose that the corrections due to the scalar field are small enough, so that the Newtonian virial theorem still holds at LO, so that

$$v^2 \sim \frac{M}{rM_{\mathrm{pl}}^2} , \tag{3.2.29}$$

which together with the definition of the angular momentum $L = Mvr$ again implies

$$\frac{M}{M_{\mathrm{pl}}} \sim L^{\frac{1}{2}} v^{\frac{1}{2}} . \tag{3.2.30}$$

Next, we will investigate the scalar propagators. While the procedure so far was completely analogous to the GR case, we now arrive at the first conceptual difference, arising due to the scalar field mass m_s, which we already alluded to earlier. Simply applying the scaling we have obtained so far, we note that

$$\text{On-shell:} \quad \mu\nu \overset{k}{\dashrightarrow} \alpha\beta \;\sim\; \left(\frac{v}{r}\right)^4 \frac{1}{\left(\frac{v}{r}\right)^2 + m_s^2} \tag{3.2.31}$$

$$\text{Off-shell:} \quad \mu\nu \overset{k}{\dashrightarrow} \alpha\beta \;\sim\; \left(\frac{v}{r}\right)\left(\frac{1}{r}\right)^3 \frac{1}{\left(\frac{1}{r}\right)^2 + m_s^2} . \tag{3.2.32}$$

In order to obtain unambiguous power counting rules, we would now need to define a scaling for m_s. Since we already assumed that $1/m_s \gg R_s$, we have essentially two choices if we do not want to introduce an additional scale:

1. $m_s \sim \frac{1}{r}$: The Compton wavelength is on the order of the binary separation, and we can expand the on-shell propagator in powers of k^2/m_s^2, treating the higher-order terms as insertions. The off-shell propagator would not need any additional treatment.

2. $m_s \sim \frac{v}{r}$: The Compton wavelength now is much larger than the binary separation and thus the scalar field seems effectively massless to the binary constituents. While

the power counting is now manifest in the on-shell propagator, we find that the off-shell propagator can be expanded in powers of $m_s r$.

If we were to assign such a scale, then we would arrive at results that are also only valid if the mass lies on the specified scale. This is quite inconvenient for us since the orbital separation will scan over several orders of magnitude during the inspiral, and we do not know the size of m_s apriori. We will instead proceed by introducing *worst case scalings*: Any time that we have to assign a scale to m_s, we will assign the most conservative scale in order to arrive at results that are applicable during the entire inspiral. This ultimately implies keeping the scalar propagators presented in Eq. (3.2.24) as is without performing an additional expansion. To see why this is sensible, consider the case where initially $m_s \sim \frac{1}{r}$. If we were to impose strict power counting rules, then we would expand the on-shell propagator in powers of k^2/m_s^2 and carry on with the calculations. At some point during the inspiral, however, we will find that the orbital separation has decreased and $1/m_s$ approaches the radiation scale, such that $m_s \sim v/r$. In this regime, we would now expand the off-shell propagator in powers of $m_s^2/|\boldsymbol{k}|^2$ and only consider the necessary amount of insertions. If we don't expand the off-shell propagator, then we would essentially end up with a result that contains higher-order terms of the PN expansion that would not be necessary anymore at this stage. This does not invalidate the result itself since it still is accurate to *at least* the desired PN order during the entire inspiral.

We next turn to the scaling of the worldline coefficients. We find that for the LO coupling of the potential scalar field to the worldline is given by the scalar charge with

$$-\frac{q}{M_{\rm pl}} \int \mathrm{d}t\, \phi \quad \longrightarrow$$

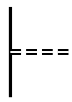

$$\sim \frac{q}{M} L^{\frac{1}{2}} \,. \qquad (3.2.33)$$

We thus see that couplings to the scalar charge are suppressed by q/M relative to couplings to the object's mass. In order for Newtonian gravity and hence the Newtonian Virial theorem to describe the binary dynamics at LO, we thus impose that $|q|/M < 1$ and will again work with a worst-case scaling, which here assigns $|q|/M \sim 1$. The PP action also contains terms quadratic in ϕ, which scale as

$$-\frac{p}{M_{\rm pl}^2} \int \mathrm{d}t\, \phi^2 \quad \longrightarrow$$

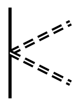

$$\sim \frac{p}{M} v^2 \,. \qquad (3.2.34)$$

In order to treat this coupling perturbatively, we impose $|p|/M < 1$ and thus a worst case scaling of $|p|/M \sim 1$.

Turning to the interaction vertices in the bulk action, we first note that the cubic scalar self-interaction scales as

$$-M_{\rm pl}\frac{c_3}{3!}\int \mathrm{d}^4x\,\phi^3 \quad \longrightarrow$$ 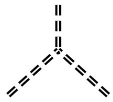 $$\sim\; c_3 M_{\rm pl}^2 r^2 L^{-\frac{1}{2}} v^2 \tag{3.2.35}$$

and we thus impose $|c_3|M_{\rm pl}^2 r^2 < 1$ in order to maintain perturbative control. Note that this constraint explicitly depends on the orbital separation of the binary system, while the previous constraints on q and p did not explicitly depend on quantities that change during the inspiral. Restating the constraint on c_3, we have

$$|c_3|\frac{M^2}{M_{\rm pl}^2} < \gamma^2 < 1\,, \tag{3.2.36}$$

so that $|c_3|M^2/M_{\rm pl}^2 < 1$ in order for the inspiral to allow for perturbative control during some stage of the inspiral. For a system with $M \approx M_\odot$ this implies $|c_3| < 10^{-80}$, which was also noted in [151], where it was argued that this implies the need for unnatural fine-tuning on c_3. However, we need to keep in mind that this constraint on c_3 is conservative in the sense that it was derived assuming the scalar field acts massless, and hence that $m_s r < 1$. The scalar field mass will introduce additional exponential suppression on any quantity calculated from the cubic interaction vertex, which will restore perturbative control (as we will see more explicitly further below). Also, in certain scalar-tensor theories, such as $f(R)$ gravity, the derived bound on c_3 is naturally fulfilled since in this case $c_3 \sim m_s^2/M_{\rm pl}^2$ and thus only requiring $m_s < 10^{-13}\,$eV, which is the mass range that is most relevant to the inspiral. Lastly, we have the $\phi^2 - h$ interaction vertex, which scales as

$$-\frac{m_s^2}{4M_{\rm pl}^2}\int \mathrm{d}^4x\, h_{\mu\nu}\eta^{\mu\nu}\phi^2 \quad \longrightarrow$$ 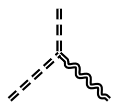 $$\sim\; m_s^2 r^2 L^{-\frac{1}{2}} v^2\,, \tag{3.2.37}$$

implying that $m_s r \lesssim 1$, which is, however, naturally fulfilled as per our initial construction we have $m_s r \approx 1$.

With this we have established all necessary power counting rules, which we also summarized in App. 3.B. We are thus now ready to the collection of the necessary diagrams for the conservative dynamics.

3.2.2 Conservative Dynamics

We are now ready to investigate the conservative dynamics. Figure 3.3 presents all diagrams that are necessary to calculate the 1PN conservative Lagrangian[3], where we identify the diagrams in Fig. 3.3a and Fig. 3.3b being the 0PN and 1PN pure GR contributions, respectively, that we already calculated in Eq. (3.1.51). Since we have to linearly add

[3]We have not presented mirror diagrams, as well as diagrams that result by couplings to the worldline that carry powers of the object's velocity.

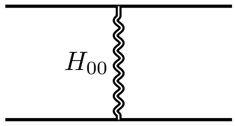

(a) Binding energy diagrams at 1PN order in pure GR.

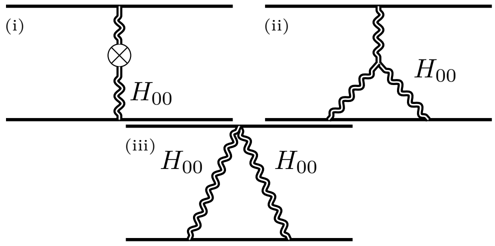

(b) 1PN diagrams in pure GR.

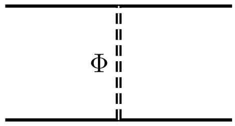

(c) Binding energy diagrams at 1PN order in pure GR.

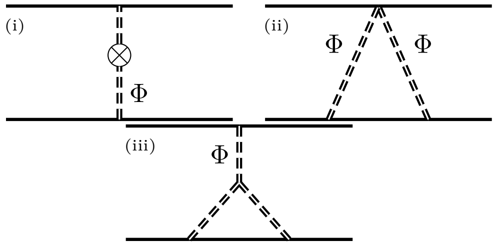

(d) 1PN pure scalar diagrams.

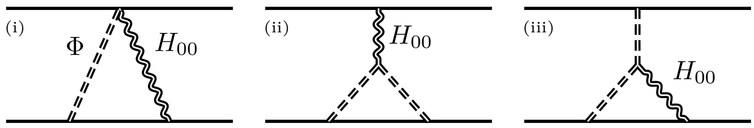

(e) Mixed contributions to the binding energy.

Figure 3.3: All diagrams contributing to the binding energy at 1PN order. Diagrams were created by D. Schmitt.

the diagrams in order to obtain the effective action, we can simply reuse the previously obtained 1 PN results in pure GR and add all diagrams that arise due to the additional scalar couplings. Before going over the 1PN results, it is instructive to only consider the 0PN sector.

0PN

In order to obtain the 0PN dynamics, we have to calculate the diagrams given in Fig. 3.3a and Fig. 3.3c. While the former diagram simply reproduces the Newtonian potential, the latter diagram results in

$$
i\mathcal{S}_{\text{eff}}\big|_{\text{Fig. 3.3c}} = \left(\frac{-i\,q_1}{M_{\text{pl}}}\right)\left(\frac{-i\,q_2}{M_{\text{pl}}}\right)\int \mathrm{d}t \int \frac{\mathrm{d}\boldsymbol{k}^3}{(2\pi)^3}\,\frac{-i\,e^{-i\boldsymbol{k}(\boldsymbol{x}-\boldsymbol{y})}}{\boldsymbol{k}^2+m_s^2} \tag{3.2.38}
$$

$$
\overset{3.A.3}{=} i8Gq_1q_2 \int \mathrm{d}t \frac{e^{-m_s r}}{r}\,. \tag{3.2.39}
$$

Combining this result with the kinetic terms we obtain

$$
\mathcal{L}_{0\text{PN}} = \frac{1}{2}M_1\boldsymbol{v}_1^2 + \frac{1}{2}M_2\boldsymbol{v}_2^2 + G\frac{M_1M_2}{r} + 8G\frac{q_1q_2}{r}e^{-m_s r}\,. \tag{3.2.40}
$$

Introducing circular orbits and using the Euler-Lagrange equations, we find a relation between r_2 and r:

$$r_2 = \frac{M_1}{M} r + G\frac{\nu\delta M}{2}\left(8\overline{Q}e^{-m_s r}+1\right) + \mathcal{O}(1\mathrm{PN})\,, \tag{3.2.41}$$

where we have introduced $\overline{Q} \equiv q_1 q_2/(M_1 M_2)$. We further also obtain a modified version of the Kepler relations, such that

$$\omega^2 = \frac{GM}{r^3}\left[1+8\overline{Q}(1+m_s r)e^{-m_s r}\right] + \mathcal{O}(1\mathrm{PN})\,. \tag{3.2.42}$$

Introducing the same PN expansion parameters as before, $x = (GM\omega)^{\frac{2}{3}}$ and $\gamma = GM/r$, we can rewrite this expression as

$$x^3 = \gamma^3\left[1+8\overline{Q}\left(1+\frac{\overline{m}_s}{\gamma}\right)e^{-\overline{m}_s/\gamma}\right] + \mathcal{O}(1\mathrm{PN})\,. \tag{3.2.43}$$

Inverting this expression for γ we find

$$\gamma = x - \overline{Q}\frac{8}{3}(\overline{m}_s + x)e^{-m_s/x} + \mathcal{O}(1\mathrm{PN})\,. \tag{3.2.44}$$

1PN

We now turn to the 1PN calculations and begin with the pure scalar contributions, which are depicted in Fig. 3.3d. The first two diagrams are straightforwardly evaluated using standard techniques. We find that

$$\begin{aligned} i\mathcal{S}_{3.3\mathrm{d(i)}} &= \left(\frac{-iq_1}{M_{\mathrm{pl}}}\right)\left(\frac{-iq_2}{M_{\mathrm{pl}}}\right)\int_{t_1}\int_{t_2}\delta(t_1-t_2)\int_{\boldsymbol{k}}\frac{-i}{(\boldsymbol{k}^2+m_s^2)^2}\frac{\partial^2}{\partial t_1\partial t_2}e^{-i\boldsymbol{k}(\boldsymbol{x}_1-\boldsymbol{x}_2)} \\ &= -i\frac{q_1q_2}{M_{\mathrm{pl}}^2}\int_t\int_{\boldsymbol{k}}\boldsymbol{v}_1^i\boldsymbol{v}_2^j\frac{\boldsymbol{k}_i\boldsymbol{k}_j}{(\boldsymbol{k}^2+m_s^2)^2}e^{-i\boldsymbol{k}(\boldsymbol{x}_1-\boldsymbol{x}_2)} \\ &\overset{3.A.4}{=} i4Gq_1q_2\int_t\frac{e^{-m_s r}}{r}\left(\boldsymbol{v}_1\cdot\boldsymbol{v}_2-\frac{(\boldsymbol{v}_1\cdot\boldsymbol{r})(\boldsymbol{v}_2\cdot\boldsymbol{r})}{r^2}(1+m_s r)\right) \end{aligned} \tag{3.2.45}$$

$$\begin{aligned} i\mathcal{S}_{3.3\mathrm{d(ii)}} &= \sum_{1\leftrightarrow 2}\left(\frac{-ip_1}{M_{\mathrm{pl}}^2}\right)\left(\frac{-iq_2}{M_{\mathrm{pl}}}\right)\left(\frac{-iq_2}{M_{\mathrm{pl}}}\right)\int_t\int_{\boldsymbol{k}_1}\frac{-ie^{-i\boldsymbol{k}_1(\boldsymbol{x}_1-\boldsymbol{x}_2)}}{\boldsymbol{k}_1^2+m_s^2}\int_{\boldsymbol{k}_2}\frac{-ie^{-i\boldsymbol{k}_2(\boldsymbol{x}_1-\boldsymbol{x}_2)}}{\boldsymbol{k}_2^2+m_s^2} \\ &\overset{3.A.3}{=}\sum_{1\leftrightarrow 2}\frac{-ip_1q_2^2}{16\pi^2M_{\mathrm{pl}}^4}\int_t\frac{e^{-2m_s r}}{r^2} \\ &= -i64G^2(p_1q_2^2+p_2q_1^2)\int_t\frac{e^{-2m_s r}}{r^2} \end{aligned} \tag{3.2.46}$$

Figure 3.3d(iii) is more tedious to evaluate due to the cubic self-interaction. We here find that

$$
\begin{aligned}
i\mathcal{S}_{3.3\mathrm{d(iii)}} &= \sum_{1\leftrightarrow 2} \frac{3!}{2}\left(\frac{-iq_2}{M_{\rm pl}}\right)^2\left(\frac{-iq_1}{M_{\rm pl}}\right)\left(\frac{-ic_3M_{\rm pl}}{3!}\right)\int_t\int_{\boldsymbol{r}_v}\int_{\boldsymbol{k}_1}\int_{\boldsymbol{k}_2}\int_{\boldsymbol{k}_3} \\
&\qquad\qquad \times \frac{-ie^{-i\boldsymbol{k}_1(\boldsymbol{r}_1-\boldsymbol{r}_v)}}{\boldsymbol{k}_1^2+m_s^2}\frac{-ie^{-i\boldsymbol{k}_2(\boldsymbol{r}_1-\boldsymbol{r}_v)}}{\boldsymbol{k}_2^2+m_s^2}\frac{-ie^{-i\boldsymbol{k}_3(\boldsymbol{r}_v-\boldsymbol{r}_2)}}{\boldsymbol{k}_3^2+m_s^2} \\
&\overset{3.A.18}{=} i\frac{G}{2\pi}\frac{q_1q_2(q_1+q_2)c_3}{m_s}\int_t\frac{e^{-m_sr}}{r}\Big[-\mathrm{Ei}(-3m_sr)e^{2m_sr}+\mathrm{Ei}(-m_sr)+\ln(3)\Big]\,.
\end{aligned}
\tag{3.2.47}
$$

Before continuing with the remaining diagrams, it is worth investigating the massless ($m_sr \ll 1$) and super-massive ($m_sr \gg 1$) limits. While the contributions from Fig. 3.3d(i)&(ii) simply reduce to a polynomial in r, just as is the case for the graviton contributions, we find that Fig. 3.3d(iii) diverges in this limit. This can be seen by first noting that we can expand the exponential integral around $x = 0$ and $x = \infty$ as

$$
\mathrm{Ei}(-x) = \gamma_{\rm E} + \log(x) - x + \mathcal{O}(x^2)\,, \tag{3.2.48}
$$

$$
\mathrm{Ei}(-x) = e^{-x}\Big(-\frac{1}{x}+\mathcal{O}(x^{-2})\Big)\,. \tag{3.2.49}
$$

Hence

$$
i\mathcal{S}_{3.3\mathrm{d(iii)}} \propto c_3\Big(\log(3m_sr)+\gamma_{\rm E}-1\Big)+\mathcal{O}(m_sr)\,. \tag{3.2.50}
$$

The cause of this divergent behavior can be traced back to the discussion surrounding the power-counting rules of the cubic scalar self-interaction, which begins at Eq. (3.2.35). The resolution is that the higher-order contributions due to c_3 generically become non-perturbative in the massless limit. As previously noted, c_3 itself is often not a free parameter, but also depends on the scalar mass in a way that the limit is well-defined.

Continuing with the mixed contributions, we find that the first diagram in Fig. 3.3e easily factors to give

$$
\begin{aligned}
i\mathcal{S}_{3.3\mathrm{e(i)}} &= \sum_{1\leftrightarrow 2} P_{00;00}\left(\frac{-iq_1}{2M_{\rm pl}^2}\right)\left(\frac{-iq_2}{M_{\rm pl}}\right)\left(\frac{-iM_2}{2M_{\rm pl}}\right)\int_t\int_{\boldsymbol{k}_1}\frac{-ie^{-i\boldsymbol{k}_1\boldsymbol{r}}}{\boldsymbol{k}_1^2}\int_{\boldsymbol{k}_2}\frac{-ie^{-i\boldsymbol{k}_2\boldsymbol{r}}}{\boldsymbol{k}_2^2+m_s^2} \\
&\overset{3.A.3}{=} \sum_{1\leftrightarrow 2} -i\frac{q_1q_2M_2}{128\pi^2M_{\rm pl}^4}\int_t\frac{e^{-m_sr}}{r^2} \\
&= -i8G^2q_1q_2(M_1+M_2)\int_t\frac{e^{-m_sr}}{r^2}
\end{aligned}
\tag{3.2.51}
$$

The diagrams in Fig. 3.3e(ii) and (iii) are again more tedious due to the cubic interactions.

Starting with (ii), we find

$$\begin{aligned}
i\mathcal{S}_{3.3\mathrm{e(ii)}} =& \sum_{1\leftrightarrow 2} \overbrace{\eta^{\mu\nu}P_{00;\mu\nu}}^{=-1} \left(\frac{-iq_2}{M_{\mathrm{pl}}}\right)^2 \left(\frac{-iM_1}{2M_{\mathrm{pl}}}\right)\left(\frac{-im_s^2}{4M_{\mathrm{pl}}}\right) \int_t \int_{\boldsymbol{r}_v} \int_{\boldsymbol{k}_1} \int_{\boldsymbol{k}_2} \int_{\boldsymbol{k}_3} \\
&\times \frac{-ie^{-i\boldsymbol{k}_1(\boldsymbol{r}_1-\boldsymbol{r}_v)}}{\boldsymbol{k}_1^2+m_s^2} \frac{-ie^{-i\boldsymbol{k}_2(\boldsymbol{r}_1-\boldsymbol{r}_v)}}{\boldsymbol{k}_2^2+m_s^2} \frac{-ie^{-i\boldsymbol{k}_3(\boldsymbol{r}_v-\boldsymbol{r}_2)}}{\boldsymbol{k}_3^2} \\
\overset{3.A.16}{=}& -i4G^2(q_2^2M_1+q_1^2M_2)\int_t \frac{m_s}{r}\left[1-2m_s r\,\mathrm{Ei}(-2m_s r)-e^{-2m_s r}\right]. \qquad (3.2.52)
\end{aligned}$$

The last necessary diagram is given by Fig. 3.3e(iii) and we find

$$\begin{aligned}
i\mathcal{S}_{3.3\mathrm{e(iii)}} =& \sum_{1\leftrightarrow 2} \eta^{\mu\nu}P_{00;\mu\nu} \left(\frac{-iq_2}{M_{\mathrm{pl}}}\right)\left(\frac{-iq_1}{M_{\mathrm{pl}}}\right)\left(\frac{-iM_2}{2M_{\mathrm{pl}}}\right)\left(\frac{-im_s^2}{4M_{\mathrm{pl}}}\right) \int_t \int_{\boldsymbol{r}_v} \int_{\boldsymbol{k}_1} \int_{\boldsymbol{k}_2} \int_{\boldsymbol{k}_3} \\
&\times \frac{-ie^{-i\boldsymbol{k}_1(\boldsymbol{r}_1-\boldsymbol{r}_v)}}{\boldsymbol{k}_1^2+m_s^2} \frac{-ie^{-i\boldsymbol{k}_2(\boldsymbol{r}_1-\boldsymbol{r}_v)}}{\boldsymbol{k}_2^2} \frac{-ie^{-i\boldsymbol{k}_3(\boldsymbol{r}_v-\boldsymbol{r}_2)}}{\boldsymbol{k}_3^2+m_s^2} \qquad (3.2.53)\\
\overset{3.A.17}{=}& -i8G^2q_1q_2(M_1+M_2)m_s\int_t \frac{e^{-m_s r}}{r}\left[\gamma_E+\log(2m_s r)-\mathrm{Ei}(-2m_s r)e^{2m_s r}\right].
\end{aligned}$$

It is worth noting that the mixed diagrams all behave well in the massless limit, so that no divergence appears, as was the case for the diagram containing c_3. Also, one can easily see that taking the super-massive limit will eliminate all diagrams that contain scalar contributions.

Shifting the worldline coefficients

Before writing out the complete 1PN result, we want to note that several terms in the effective action can be eliminated by shifting the scalar charges. More explicitly if we only consider all terms in the Lagrangian whose functional dependency is given by $e^{-m_s r}/r$ we obtain

$$\mathcal{L}^{\phi}_{1\mathrm{PN}} = \left[8Gq_1q_2 + \frac{G}{2\pi}\frac{q_1q_2(q_1+q_2)c_3}{m_s}\ln(3) - 8G^2q_1q_2(M_1+M_2)m_s\gamma_E\right]\frac{e^{-m_s r}}{r} + \dots \qquad (3.2.54)$$

and it is easy to see that these terms can be removed—at the 1PN order—by shifting q_i according to

$$q_i \to q_i - q_i\frac{G}{2\pi}\frac{q_ic_3}{m_s}\ln(3) + 8G^2q_iM_im_s\gamma_E\,. \qquad (3.2.55)$$

Further, we have again omitted all diagrams that contain pure-self force sub-diagrams, such as the ones shown in Fig. 3.4, whose effect can also be trivially shifted away by performing a shift in the scalar charges and masses of the objects.

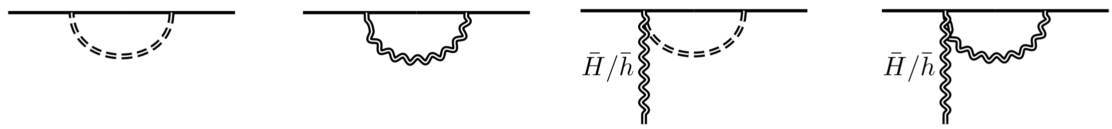

(a) Diagrams contributing to the renormalization of the mass with no external vertices.

(b) Diagrams contributing to the renormalization of the mass vertex with one external graviton.

Figure 3.4: Diagrams that contribute to a shift in the object's mass.

The 1PN Lagrangian

Collecting the obtained results and dropping all terms that are trivially removed by redefinitions of the q_i's and M_i's, we find that the 1PN Lagrangian can be expressed as

$$\mathcal{L}_{\rm 1PN} = \mathcal{L}_{\rm EIH} + \mathcal{L}^{\phi}_{\rm 1PN}\,, \tag{3.2.56}$$

with $\mathcal{L}_{\rm EIH}$ given in Eq. (3.1.54) and

$$\begin{aligned}
\mathcal{L}^{\phi}_{\rm 1PN} =& 8Gq_1q_2\frac{e^{-m_s r}}{r}\left[1 - G\frac{M_1+M_2}{r} - \frac{\boldsymbol{v}_1^2+\boldsymbol{v}_2^2}{2} - \frac{(\boldsymbol{v}_1\cdot\boldsymbol{r}_1)(\boldsymbol{v}_2\cdot\boldsymbol{r}_2)}{2\,r^2}(1+m_s r) + \frac{\boldsymbol{v}_1\cdot\boldsymbol{v}_2}{2}\right] \\
&- 64G^2(p_1q_2^2+p_2q_1^2)\frac{e^{-2m_s r}}{r^2} + 4m_sG^2\frac{M_1q_2^2+M_2q_1^2}{r}\left[e^{-2m_s r} + 2m_s r\,\mathrm{Ei}(-2m_s r)\right] \\
&- 8m_sG^2q_1q_2\,\frac{M}{r}\left[\log(2m_s r)e^{-m_s r} - \mathrm{Ei}(-2m_s r)e^{m_s r}\right] \\
&+ Gc_3q_1q_2\frac{q_1+q_2}{2\pi m_s r}\left[\mathrm{Ei}(-m_s r)e^{-m_s r} - \mathrm{Ei}(-3m_s r)e^{m_s r}\right].
\end{aligned} \tag{3.2.57}$$

Circular Orbits

Following the same procedure we applied in the 0PN case it is now straightforward to obtain the modified Kepler relations at LO in the scalar field parameter, so that

$$\begin{aligned}
x^3 =& \frac{\gamma^2\bar{c}_3}{2\pi\overline{m}_s}\left[e^{\frac{\overline{m}_s}{\gamma}}\left(\overline{m}_s-\gamma\right)\mathrm{Ei}\left(-\frac{3\overline{m}_s}{\gamma}\right) + e^{-\frac{\overline{m}_s}{\gamma}}\left(\overline{m}_s+\gamma\right)\mathrm{Ei}\left(-\frac{\overline{m}_s}{\gamma}\right)\right] - 128\gamma^3\xi_p e^{-\frac{2\overline{m}_s}{\gamma}}\left(\overline{m}_s+\gamma\right) \\
&+ 4\gamma^3\xi_q\overline{m}_s e^{-\frac{2\overline{m}_s}{\gamma}} + 8\gamma^2\overline{Q}e^{-\frac{\overline{m}_s}{\gamma}}\left[-\overline{m}_s e^{\frac{2\overline{m}_s}{\gamma}}\left(\overline{m}_s-\gamma\right)\mathrm{Ei}\left(-\frac{2\overline{m}_s}{\gamma}\right) + \gamma(3\nu-4)\overline{m}_s\right. \\
&\left. - \overline{m}_s\left(\overline{m}_s+\gamma\right)\log\left(\frac{2\overline{m}_s}{\gamma}\right) + \overline{m}_s + 2\gamma^2(\nu-2)+\gamma\right] + \underbrace{\gamma^3(\gamma(\nu-3)+1)}_{\equiv x_{\rm GR}}\,.
\end{aligned} \tag{3.2.58}$$

Similarly, we can invert this expression to obtain γ in terms of x at 1PN, such that

$$\begin{aligned}\gamma =&\frac{\bar{c}_3}{6\pi\overline{m}_s}\left[-e^{\frac{\overline{m}_s}{x}}\left(\overline{m}_s-x\right)\mathrm{Ei}\left(-\frac{3\overline{m}_s}{x}\right)-e^{-\frac{\overline{m}_s}{x}}\left(\overline{m}_s+x\right)\mathrm{Ei}\left(-\frac{\overline{m}_s}{x}\right)\right]+\frac{128}{3}x\xi_p e^{-\frac{2\overline{m}_s}{x}}\left(\overline{m}_s+x\right)\\&-\frac{4}{3}x\xi_q\overline{m}_s e^{-\frac{2\overline{m}_s}{x}}+\frac{8}{9}\bar{Q}e^{-\frac{\overline{m}_s}{x}}\Bigg[3\overline{m}_s e^{\frac{2\overline{m}_s}{x}}\left(\overline{m}_s-x\right)\mathrm{Ei}\left(-\frac{2\overline{m}_s}{x}\right)+\nu\left(-4x\overline{m}_s+\overline{m}_s^2-x^2\right)\\&-3\left(x\overline{m}_s+\overline{m}_s^2+\overline{m}_s+x^2+x\right)+3\overline{m}_s\left(\overline{m}_s+x\right)\log\left(\frac{2\overline{m}_s}{x}\right)\Bigg]\underbrace{-\frac{1}{3}(\nu-3)x^2+x}_{\equiv\gamma_{\mathrm{GR}}}\ .\end{aligned}\tag{3.2.59}$$

Likewise, the binding energy can now be expressed in terms of x as

$$\begin{aligned}\frac{E}{\mu}=&\frac{\bar{c}_3}{6\pi\overline{m}_s}e^{-\frac{\overline{m}_s}{x}}\left[(2\overline{m}_s-x)\mathrm{Ei}\left(-\frac{\overline{m}_s}{x}\right)+e^{\frac{2\overline{m}_s}{x}}\left(2\overline{m}_s+x\right)\mathrm{Ei}\left(-\frac{3\overline{m}_s}{x}\right)\right]-\frac{64}{3}x\xi_p e^{-\frac{2\overline{m}_s}{x}}\left(4\overline{m}_s+x\right)\\&+\frac{4}{3}\xi_q\overline{m}_s\left[x\left(-e^{-\frac{2\overline{m}_s}{x}}\right)-6\overline{m}_s\mathrm{Ei}\left(-\frac{2\overline{m}_s}{x}\right)\right]+\frac{4}{9}\bar{Q}e^{-\frac{\overline{m}_s}{x}}\Bigg[-6\overline{m}_s e^{\frac{2\overline{m}_s}{x}}\left(2\overline{m}_s+x\right)\mathrm{Ei}\left(-\frac{2\overline{m}_s}{x}\right)\\&-4(\nu-3)\overline{m}_s^2+4((\nu-3)x+3)\overline{m}_s+6\overline{m}_s\left(x-2\overline{m}_s\right)\log\left(\frac{2\overline{m}_s}{x}\right)+x((\nu-3)x-6)\Bigg]\end{aligned}\tag{3.2.60}$$

$$+\frac{\nu x^2}{24}+\frac{3x^2}{8}-\frac{x}{2}$$

and in terms of γ as

$$\begin{aligned}\frac{E}{\mu}=&\frac{\bar{c}_3}{4\pi\overline{m}_s}\left[e^{-\frac{\overline{m}_s}{\gamma}}\left(\overline{m}_s-\gamma\right)\mathrm{Ei}\left(-\frac{\overline{m}_s}{\gamma}\right)+e^{\frac{\overline{m}_s}{\gamma}}\left(\overline{m}_s+\gamma\right)\mathrm{Ei}\left(-\frac{3\overline{m}_s}{\gamma}\right)\right]-64\gamma\xi_p\overline{m}_s e^{-\frac{2\overline{m}_s}{\gamma}}\\&+\xi_q\left[-8\overline{m}_s^2\mathrm{Ei}\left(-\frac{2\overline{m}_s}{\gamma}\right)-2\gamma\overline{m}_s e^{-\frac{2\overline{m}_s}{\gamma}}\right]+\bar{Q}e^{-\frac{\overline{m}_s}{\gamma}}\Bigg[-4\overline{m}_s e^{\frac{2\overline{m}_s}{\gamma}}\left(\overline{m}_s+\gamma\right)\mathrm{Ei}\left(-\frac{2\overline{m}_s}{\gamma}\right)\\&+2(-\nu\gamma+\gamma+2)\overline{m}_s+4\overline{m}_s\left(\gamma-\overline{m}_s\right)\log\left(\frac{2\overline{m}_s}{\gamma}\right)-2\gamma(\gamma(\nu-3)+2)\Bigg]-\frac{1}{8}\gamma(\gamma(\nu-7)+4)\ .\end{aligned}\tag{3.2.61}$$

3.2.3 Scalar Radiation

Having obtained the binding energy of the binary system, the next objective is to determine the power loss. Due to the additional scalar degree of freedom, there is now an additional channel through which energy can leave the system. In the following, we will only consider linear emission diagrams, allowing us to classify each diagram by whether a graviton or a scalar is being emitted. We will begin by investigating the scalar radiation.

Scalar Radiation

Starting out with the scalar radiation, we first have to identify the linear source term, which is defined via

$$S_{\mathrm{eff}}\supset S_{\mathrm{src},\bar{\phi}}=\frac{1}{M_{\mathrm{pl}}}\int\mathrm{d}^4xJ(x)\bar{\phi}(x)\ .\tag{3.2.62}$$

Similarly to the pure GR case, it is necessary to perform a multipole expansion of $\bar{\phi}$ in order to obtain clear power counting rules. The multipole expansion for massless scalar and non-interacting scalar fields was done in [152], which found that the source term can be rewritten as

$$S_{\text{src}} = \frac{1}{M_{\text{pl}}} \int \text{d}t \sum_{l=0}^{\infty} \frac{1}{l!} \mathcal{I}^L \partial_L \bar{\phi} \,, \tag{3.2.63}$$

where the $\partial_L \bar{\phi}$ are evaluated at $(t, \boldsymbol{x} = 0)$ and the $\mathcal{I}^L$ are denoted as the *multipole moments*. For the massless and non-interacting case that was considered in [152], the authors find the following expression for the multipole moments

$$\mathcal{I}^L = \sum_{p=0}^{\infty} \frac{(2l+1)!!}{(2p)!!(2l+2p+1)!!} \int d^3\mathbf{x}\, r^{2p} \mathbf{x}^L_{\text{STF}}\, \partial_t^{2p} J \,, \tag{3.2.64}$$

however, as was also noted in [114], this expression is not valid in the massive and self-interacting case. In order to see more closely why this is the case, we can follow the derivation of [152] until the point where the equations of motion become relevant. First, expanding $\bar{\phi}$ in the spatial coordinates around the origin we have

$$\bar{\phi}(x) = \sum_n \frac{1}{n!} \boldsymbol{x}^L \partial_L \bar{\phi} \,. \tag{3.2.65}$$

Inserting this expression into Eq. (3.2.63) and expressing the result in STF representations of SO(3), we have

$$S_{\text{src}} = \frac{1}{M_{\text{pl}}} \int dt \sum_{l=0}^{\infty} \frac{1}{l!} \sum_{p=0}^{\infty} \frac{(2l+1)!!}{(2p)!!(2l+2p+1)!!} \int d^3\boldsymbol{x} J r^{2p} \boldsymbol{x}^L_{\text{STF}} (\nabla^2)^p \partial_L \bar{\phi} \,. \tag{3.2.66}$$

Next, outside the source, we can use the LO equations of motion to replace the gradients acting on $\bar{\phi}$. We have at LO

$$\Box\bar{\phi} \equiv \partial_t^2 \bar{\phi} - \nabla^2 \bar{\phi} = -V'(\bar{\phi}) = -m_s^2 \bar{\phi} \tag{3.2.67}$$

and therefore

$$\nabla^2 \bar{\phi} = \left(\partial_t^2 + m_s^2\right) \bar{\phi} \,. \tag{3.2.68}$$

Inserting this relation into Eq. (3.2.66) and performing partial integration to move the time derivatives acting on $\bar{\phi}$ to J we arrive at a modified version of the multipole moments

$$\mathcal{I}^L = \sum_{p=0}^{\infty} \frac{(2l+1)!!}{(2p)!!(2l+2p+1)!!} \int d^3\boldsymbol{x}\, r^{2p} \boldsymbol{x}^L_{\text{STF}}\, (\partial_t^2 + m_s^2)^p J \,. \tag{3.2.69}$$

Power Loss From Multipoles

Having expressed the source term in a multipole expansion, it is now straightforward to calculate the power loss in each multipole. To this end, we consider the diagram shown

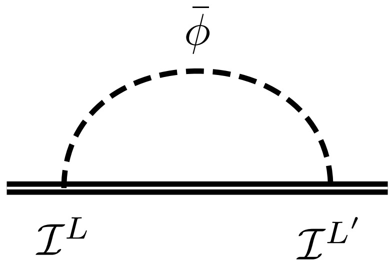

Figure 3.5: Leading-order self-force diagram that contributes to the scalar radiation starting at −1PN order.

in Fig. 3.5, which evaluates to

$$\begin{aligned} i\mathcal{S}_{\text{fig}} &= -i\frac{1}{M_{\text{pl}}^2}\frac{1}{l!\,\tilde{l}!}\int \mathrm{d}t_1 \int \mathrm{d}t_2\, \mathcal{I}^L(t_1)\mathcal{I}^{\tilde{L}}(t_2) \int \frac{\mathrm{d}^4k}{(2\pi)^4}\frac{e^{ik_0(t_1-t_2)}}{k^2-m^2+i\epsilon}\boldsymbol{k}^L\boldsymbol{k}^{\tilde{L}} \\ &= -i\frac{1}{M_{\text{pl}}^2}\frac{1}{l!\,\tilde{l}!}\int \frac{\mathrm{d}^4k}{(2\pi)^4}\frac{1}{k^2-m^2+i\epsilon}\mathcal{I}^L(k_0)\mathcal{I}^{\tilde{L}}(k_0)^*\boldsymbol{k}^L\boldsymbol{k}^{\tilde{L}} \\ &= -i\frac{1}{M_{\text{pl}}^2}\frac{1}{l!\,\tilde{l}!}\int \frac{\mathrm{d}k_0}{2\pi}\int \mathrm{d}\Omega \int_0^\infty \frac{\mathrm{d}|\boldsymbol{k}|}{(2\pi)^3}|\boldsymbol{k}|^{2+l+\tilde{l}}\boldsymbol{n}^L\boldsymbol{n}^{\tilde{L}}\frac{1}{k_0^2-|\boldsymbol{k}|^2-m^2+i\epsilon}\mathcal{I}^L(k_0)\mathcal{I}^{\tilde{L}}(k_0)^* , \end{aligned} \tag{3.2.70}$$

where we introduced $\boldsymbol{n} = \boldsymbol{k}/|\boldsymbol{k}|$. Also, we used the time integrals to express $\mathcal{I}^L(t)$ in terms of their Fourier transform $\mathcal{I}^L(k)$. In the last line we have switched to spherical coordinates. The $\mathrm{d}\Omega$ integral can be evaluated to give

$$\int \mathrm{d}\Omega\, \boldsymbol{n}^L\boldsymbol{n}^{\tilde{L}} = \delta^{l\tilde{l}}\frac{4\pi}{(2l+1)!!}l! \,. \tag{3.2.71}$$

Inserting this back into Eq. (3.2.70) we obtain

$$i\mathcal{S}_{\text{fig}} = -i\frac{1}{M_{\text{pl}}^2}\frac{1}{l!(2l+1)!!}\frac{1}{4\pi^3}\int \mathrm{d}k_0 \int_0^\infty \mathrm{d}|\boldsymbol{k}|\,|\boldsymbol{k}|^{2l+2}\left|\mathcal{I}^L(k_0)\right|^2\frac{1}{k_0^2-|\boldsymbol{k}|^2-m^2+i\epsilon} . \tag{3.2.72}$$

We can solve the dk integral by closing the contour in the upper complex plane. We first extend the integration limits to $(-\infty,\infty)$ and then pick up the residue at $|\boldsymbol{k}| = \sqrt{k_0^2-m_s^2-i\epsilon}$. This results in

$$i\mathcal{S}_{\text{fig}} = -\frac{1}{M_{\text{pl}}^2}\frac{1}{l!(2l+1)!!}\frac{1}{8\pi^2}\int \mathrm{d}k_0\,(k_0^2-m^2)^{l+1/2}\left|\mathcal{I}^L(k_0)\right|^2 \,. \tag{3.2.73}$$

Leveraging the optical theorem we thus obtain the power loss as

$$P_l = \frac{1}{l!(2l+1)!!}\frac{1}{4\pi^2M_{\text{pl}}^2T}\int_{m_s}^\infty \mathrm{d}\omega\left(1-\frac{m_s^2}{\omega^2}\right)^{l+1/2}\omega^{2l+2}\left|\mathcal{I}^L(\omega)\right|^2 , \tag{3.2.74}$$

where we have replaced $k_0 \to \omega$ and introduced $T \equiv 2\pi\delta(0)$. An important remark is in order. When going from Eq. (3.2.73) to Eq. (3.2.74) we only keep the imaginary part of the effective action and we see that only frequencies with $\omega^2 \geq m_s^2$ thus contribute to the power loss. All frequencies with $\omega^2 < m_s^2$ instead contribute to the conservative part of the effective action. However, since this contribution only enters at a PN order higher than what is considered here, we will not investigate it further.

Power Counting Rules

Before calculating the diagrams, it is useful to review the power counting rules in the current context, which will make it easier to identify the relevant contributions. From Eq. (3.2.69) we find that a general multipole scales with

$$\mathcal{I}^L(t) \sim r^{2p+l+3}\left(\frac{v^2}{r^2} + m_s^2\right)^p J \tag{3.2.75}$$

and its Fourier transform hence scales with

$$\mathcal{I}^L(\omega) \sim r^{2p+l+4}\frac{1}{v}\left(\frac{v^2}{r^2} + m_s^2\,.\right)^p J \tag{3.2.76}$$

A diagram contributing to the effective action will thus scale as

$$\begin{aligned}\mathcal{S} &\sim r^{2p_1+2p_2+6}v^{2l+1}\left(\frac{v^2}{r^2} + m_s^2\right)^{p_1+p_2} J_1 J_2 \\ &\sim r^6 v^{2l+1}\left(v^2 + m_s^2 r^2\right)^{p_1+p_2} J_1 J_2\,.\end{aligned} \tag{3.2.77}$$

We thus only need to determine the scaling of J for a given diagram. Also, in Eq. (3.2.74) we can see that scalar radiation at a frequency ω can only occur if $\omega > m_s$. We will later see that a general multipole l will have a frequency of $\omega_l = l\,\omega$ and hence it only radiates if $l\,\omega > m_s$. Hence, if we only consider low multipolar numbers l, then we can apply the scaling $m_s \sim \omega = v/r$ in the current calculations.

As an example, consider the diagram shown in Fig. 3.6a(i). We find that $J \sim r^{-3}$ and thus this diagram contributes at lowest order with

$$\mathcal{S}_{3.6a(i)} \sim L\, v^{2l+2p+2}\,. \tag{3.2.78}$$

We will see in the next section that the $l = 0$ mode does not radiate on circular orbits, so that the lowest order contribution arises due to dipolar radiation and scales with $L\, v^4$, which corresponds to -1PN order.

Collecting the Diagrams

From the previous discussion, we find that at order $L\, v^4$ we need to calculate the $(l,p) = (1,0)$ contribution from the LO scalar emission shown in Fig. 3.6a(i). At order $L\, v^5$, we

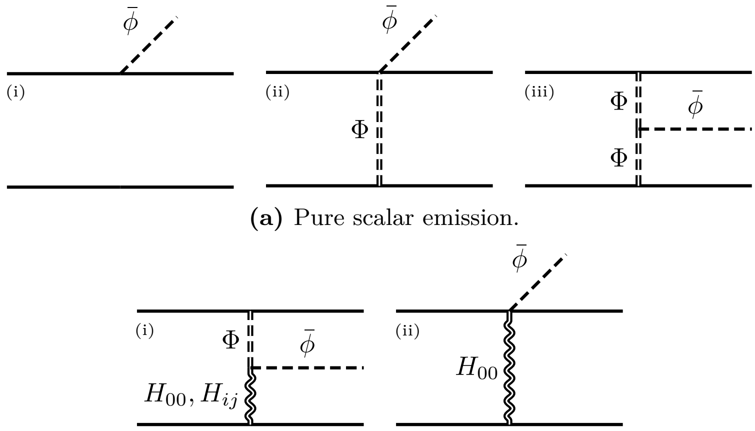

(a) Pure scalar emission.

(b) Modified scalar emission.

Figure 3.6: All emission diagrams appearing at 1PN, except for the last diagram in Fig. 3.6b. Figure 3.7a shows all emission diagrams appearing in pure GR, while Fig. 3.7b displays the new graviton emission diagrams appearing due to couplings with the scalar field. Similarly, Fig. 3.6a shows pure scalar emission diagrams. Fig. 3.6b shows all scalar emission diagrams that also contain graviton interactions. Diagrams were created by D. Schmitt.

need to additionally calculate the $(l,p) = (1,0)$ for the diagrams in Fig. 3.6a(ii-iii) and Fig. 3.6b, together with the $(l,p) = (2,0)$ component of the LO emission in Fig. 3.6a(i).

Starting out with the LO emission diagram in Fig. 3.6a(i), we have

$$i\mathcal{S}_{3.6a(i)} = -\sum_{1\leftrightarrow 2} \frac{iq_1}{M_{\rm pl}} \int \mathrm{d}t \left(1 - \frac{1}{2}\boldsymbol{v}_1^2\right)\bar{\phi}\,. \tag{3.2.79}$$

We thus find that the source term is given by

$$J_{3.6a(i)} = -q_1\left(1 - \frac{1}{2}\boldsymbol{v}_1^2\right)\delta^3(\boldsymbol{x}-\boldsymbol{x}_1) - q_2\left(1 - \frac{1}{2}\boldsymbol{v}_2^2\right)\delta^3(\boldsymbol{x}-\boldsymbol{x}_2)\,. \tag{3.2.80}$$

Inserting this into Eq. (3.2.74), we find for the dipole moment

$$\mathcal{I}^i_{3.6a(i)} = -\sum_{1\leftrightarrow 2} q_1\left[\left(1-\frac{1}{2}\boldsymbol{v}_1^2\right)\boldsymbol{x}_1^i + \frac{1}{10}(m_s^2+\partial_t^2)\left\{\left(1-\frac{1}{2}\boldsymbol{v}_1^2\right)\boldsymbol{x}_1^2\boldsymbol{x}_1^i\right\} + \mathcal{O}(p>1)\right], \tag{3.2.81}$$

where we use $\mathcal{O}(p > 1)$ to denote the $p \geq 2$ terms. The quadrupole moment is given by

$$\mathcal{I}^{ij}_{3.6a(i)} = -\sum_{1\leftrightarrow 2} q_1\left[\boldsymbol{x}_1^i\boldsymbol{x}_1^j\right]^{\rm STF} = -\sum_{1\leftrightarrow 2} q_1\left(\boldsymbol{x}_1^i\boldsymbol{x}_1^j - \frac{1}{3}\boldsymbol{x}_1^2\right). \tag{3.2.82}$$

The diagrams in Fig. 3.6a(ii) and Fig. 3.6b(ii) are similarly evaluated in a straightforward manner, yielding

$$\mathcal{I}^i_{3.6a(ii)} = \sum_{1\leftrightarrow 2} \frac{p_1 q_2}{2\pi M_{\rm pl}^2}\frac{e^{-m_s r}}{r}\boldsymbol{x}_1^i + \mathcal{O}(p>0) \tag{3.2.83}$$

and

$$\mathcal{I}^i_{3.6b(ii)} = \sum_{1\leftrightarrow 2} \frac{p_1 M_2}{32\pi M_{\rm pl}^2} \frac{1}{r} \boldsymbol{x}_1^i + \mathcal{O}(p>0)\,. \tag{3.2.84}$$

The 3-point vertices in Fig. 3.6a(iii) and Fig. 3.6b(ii) require a bit more care. We start out by noting that the full diagram in Fig. 3.6a(iii) contributes to the effective action with

$$i\mathcal{S}_{3.6a(iii)} = -iq_1 q_2 c_3 \int dt \int_{\boldsymbol{r}_v} \int_{\boldsymbol{k}_1} \frac{e^{i\boldsymbol{k}_1(\boldsymbol{r}_1-\boldsymbol{r}_v)}}{\boldsymbol{k}_1^2+m_s^2} \int_{\boldsymbol{k}_2} \frac{e^{i\boldsymbol{k}_2(\boldsymbol{r}_2-\boldsymbol{r}_v)}}{\boldsymbol{k}_2^2+m_s^2} \frac{\bar{\phi}}{M_{\rm pl}} \tag{3.2.85}$$

and thus contributes to the source with

$$J_{3.6a(iii)}(\boldsymbol{x}) = -q_1 q_2 c_3 \int_{\boldsymbol{k}_1} \frac{e^{i\boldsymbol{k}_1(\boldsymbol{r}_1-\boldsymbol{x})}}{\boldsymbol{k}_1^2+m_s^2} \int_{\boldsymbol{k}_2} \frac{e^{i\boldsymbol{k}_2(\boldsymbol{r}_2-\boldsymbol{x})}}{\boldsymbol{k}_2^2+m_s^2}\,. \tag{3.2.86}$$

The $(l,p)=(1,0)$ contribution to the multipole moments is thus

$$\begin{aligned}\mathcal{I}^i_{3.6a(iii)} &= -q_1 q_2 c_3 \int_{\boldsymbol{x}} \int_{\boldsymbol{k}_1} \frac{e^{i\boldsymbol{k}_1(\boldsymbol{r}_1-\boldsymbol{x})}}{\boldsymbol{k}_1^2+m_s^2} \int_{\boldsymbol{k}_2} \frac{e^{i\boldsymbol{k}_2(\boldsymbol{r}_2-\boldsymbol{x})}}{\boldsymbol{k}_2^2+m_s^2} \boldsymbol{x}^i \\ &= -\frac{q_1 q_2 c_3}{16 m_s \pi} e^{-m_s r} (\boldsymbol{r}_1^i + \boldsymbol{r}_2^i)\,.\end{aligned} \tag{3.2.87}$$

Likewise, we find for Fig. 3.6b(ii)

$$\mathcal{I}^i_{3.6b(ii)} = \sum_{1\leftrightarrow 2} \frac{q_1 M_2}{4 M_{\rm pl}^2} \left[\boldsymbol{r}^i \frac{(m_s^2 r^2 - 2) + 2e^{-m_s r}(m_s r + 1)}{4\pi m_s^2 r^3} + \boldsymbol{r}_2^i \frac{1-e^{-m_s r}}{4\pi r} \right]\,. \tag{3.2.88}$$

Leading-Order Power Loss

Having collected all necessary multipole moments to calculate the power loss up to NLO, we start out by investigating its LO behavior. The lowest order dipole moment can be read off from Eq. (3.2.81), so that

$$\mathcal{I}^i = -\left(q_1 \boldsymbol{x}_1^i + q_2 \boldsymbol{x}_2^i \right) + \dots\,. \tag{3.2.89}$$

We next introduce circular orbits with

$$\boldsymbol{x}_1(t) = r_1 \begin{pmatrix} \cos(\omega_{\rm b} t) \\ \sin(\omega_{\rm b} t) \\ 0 \end{pmatrix}\,, \quad \text{and} \quad \boldsymbol{x}_2(t) = r_2 \begin{pmatrix} \cos(\omega_{\rm b} t + \pi) \\ \sin(\omega_{\rm b} t + \pi) \\ 0 \end{pmatrix}\,. \tag{3.2.90}$$

Going to Fourier space, we now find

$$\mathcal{I}^i(\omega) = \pi(q_2 r_2 - q_1 r_1) \begin{pmatrix} \delta(\omega-\omega_b) + \delta(\omega+\omega_b) \\ i\delta(\omega-\omega_b) - i\delta(\omega+\omega_b) \\ 0 \end{pmatrix}\,. \tag{3.2.91}$$

M	x	γ	μ	ν	Q	$\bar{Q}$	$\overline{m}_s$	$\bar{c}_3$	ξ_q	ξ_p
M_1+M_2	$(GM\omega)^{\frac{2}{3}}$	$\frac{GM}{r}$	$\frac{M_1M_2}{M}$	$\frac{\mu}{M}$	$\frac{q_1+q_2}{M}$	$\frac{q_1q_2}{M_1M_2}$	GMm_s	$c_3GM^2Q\overline{Q}$	$\frac{q_1^2M_2+q_2^2M_1}{MM_1M_2}$	$\frac{p_1q_2^2+p_2q_1^2}{MM_1M_2}$

v	δq	δM	Ξ_p	Ξ_c	Ξ_q	g_1	g_2
$(GM\omega)^{\frac{1}{3}}$	$\frac{M_2q_1-M_1q_2}{M^2}$	M_1-M_2	$\frac{M_1p_2q_1-M_2p_1q_2}{M^3}\delta q$	$\frac{c_3\overline{Q}\delta M\delta q}{M}$	$\frac{M_2^2q_1+M_1^2q_2}{M^3}$	$\frac{M_2^2q_1-M_1^2q_2}{M^3}$	$\frac{M_2^3q_1-M_1^3q_2}{M^4}$

Table 3.1: Overview of the parameters introduced in our work. Besides the typical PN expansion variables, we rescale the EFT parameters for convenience.

We therefore have

$$\begin{aligned}|\mathcal{I}^i(\omega)|^2 &= \pi^2(q_2r_2-q_1r_1)^2\left[\Big(\delta(\omega-\omega_b)+\delta(\omega+\omega_b)\Big)^2+\Big(\delta(\omega-\omega_b)-\delta(\omega+\omega_b)\Big)^2\right]\\ &= 2\pi^2(q_2r_2-q_1r_1)^2\left[\delta(\omega-\omega_b)^2+\delta(\omega+\omega_b)^2\right].\end{aligned} \tag{3.2.92}$$

Due to the delta functions, we have that the integral in Eq. (3.2.74) is straightforward to evaluate, giving

$$P_{l=1} = \frac{(q_2r_2-q_1r_1)^2}{6\pi M_{\text{pl}}^2}\left(1-\frac{m_s^2}{\omega_b^2}\right)^{3/2}\omega_b^4\,. \tag{3.2.93}$$

At LO, we have that

$$r_1 = \frac{M_1}{M}r\,, \quad \text{and} \quad r_2 = \frac{M_2}{M}r\,, \tag{3.2.94}$$

which we can insert into Eq. (3.2.93) to obtain

$$P_{l=1} = \frac{\big(q_2M_1-q_1M_2\big)^2}{12\pi M^2M_{\text{pl}}^2}\left(1-\frac{m_s^2}{\omega_b^2}\right)^{3/2}r^2\omega_b^4\,\Theta(\omega_b-m_s)\,. \tag{3.2.95}$$

Higher-Order Power Loss

The generalization to higher-order diagrams and multipoles is now straightforward. We have already obtained the necessary multipole moments in Eqs. (3.2.81), (3.2.82), (3.2.83), (3.2.84), and (3.2.87). Inserting them into Eq. (3.2.74) and expanding up to NLO, we obtain for the dipole radiation

$$P_{\bar{\phi}}^{l=1,\mathrm{LO}} = \frac{8}{3}GM^2\delta q^2 r^2\omega^4\left(1-\frac{m_s^2}{\omega_b^2}\right)^{3/2}, \tag{3.2.96a}$$

$$P_{\bar{\phi}}^{l=1,p_1,p_2} = \frac{256}{3}G^2M^3\Xi_p\, r\,\omega^4\left(1-\frac{m_s^2}{\omega_b^2}\right)^{3/2}, \tag{3.2.96b}$$

$$P_{\bar{\phi}}^{l=1,c_3} = \frac{GM_1M_2M}{3\pi m_s}\Xi_c(m_s r-1)r^2\omega^4\left(1-\frac{m_s^2}{\omega_b^2}\right)^{3/2}, \tag{3.2.96c}$$

$$P_{\bar{\phi}}^{l=1,\mathrm{NLO}} = \frac{8GM^2}{15}\delta q\Big[-10g_1GM+g_2r^3(m_s^2-6\omega^2)\Big]r\omega^4\left(1-\frac{m_s^2}{\omega_b^2}\right)^{3/2}, \tag{3.2.96d}$$

and the single quadrupolar contribution is given by

$$P_{\bar{\phi}}^{l=2} = \frac{128}{15}GM^2\Xi_q^2 r^4\omega^6\left(1-\frac{m_s^2}{4\,\omega^2}\right)^{5/2}. \tag{3.2.97}$$

Using the Kepler relations, we can eliminate r in favor of ω and then express the result in terms of the dimensionless PN parameter x, which results in

$$P_{\bar{\phi}}^{l=1,\mathrm{LO}} = \frac{8}{3G}\delta q^2 x^4\left(1-\frac{\overline{m}_s^2}{x^3}\right)^{3/2}, \tag{3.2.98a}$$

$$P_{\bar{\phi}}^{l=1,p_1,p_2} = \frac{256}{3G}\Xi_p\, x^5\left(1-\frac{\overline{m}_s^2}{x^3}\right)^{3/2}, \tag{3.2.98b}$$

$$P_{\bar{\phi}}^{l=1,c_3} = \frac{M_1M_2}{3\pi}\frac{\overline{m}_s-x}{\overline{m}_s}\Xi_c\, x^3\left(1-\frac{\overline{m}_s^2}{x^3}\right)^{3/2}, \tag{3.2.98c}$$

$$\begin{aligned}P_{\bar{\phi}}^{l=1,\mathrm{NLO}} = &\bigg[\frac{16}{9G}(-3+\nu)\delta q^2\, x^5+\frac{8}{15G}\overline{m}_s^2\, g_2\,\delta q\, x^2\\ &-\frac{16}{15G}(5g_1+3g_2)\delta q\, x^5\bigg]\left(1-\frac{\overline{m}_s^2}{x^3}\right)^{3/2},\end{aligned} \tag{3.2.98d}$$

and for the quadrupolar contribution

$$P_{\bar{\phi}}^{l=2} = \frac{128}{15G}\Xi_q^2\, x^5\left(1-\frac{\overline{m}_s^2}{4\,x^3}\right)^{5/2}. \tag{3.2.99}$$

3.2.4 Gravitational Radiation

The necessary diagrams to calculate the gravitational radiation at 1PN order are shown in Fig. 3.7, and we note that the diagrams in Fig. 3.7b provide additional graviton emission diagrams due to the coupling of gravitons to the scalar field. However, as was noted in

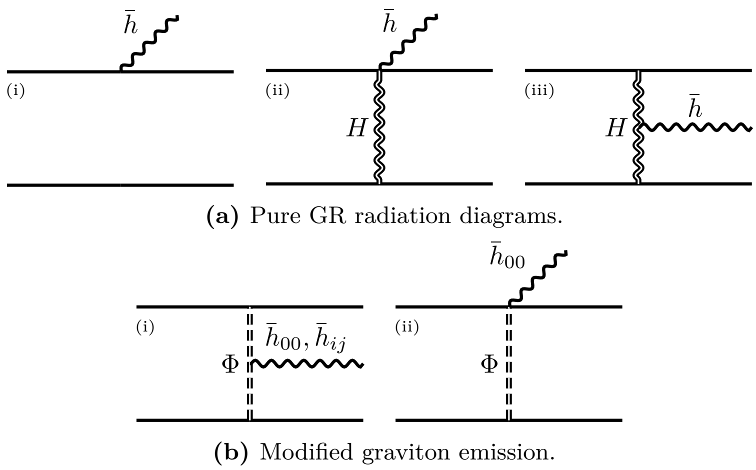

Figure 3.7: All emission diagrams appearing at 1PN, except for the last diagram in Fig. 3.6b. Figure 3.7a shows all emission diagrams appearing in pure GR, while Fig. 3.7b displays the new graviton emission diagrams appearing due to couplings with the scalar field. Similarly, Fig. 3.6a shows pure scalar emission diagrams. Fig. 3.6b shows all scalar emission diagrams that also contain graviton interactions. Diagrams were created by D. Schmitt.

the previous section, we found that scalar emission already begins at -1PN order, and it is thus sufficient for our purposes to calculate the power loss due to graviton emission at 0PN order. In Sec. 3.1.3 we have noted that this LO power loss is given by

$$P_{\mathrm{LO}} = \frac{G}{5}\left\langle \left(\partial_t^3 I^{ij}\right)^2 \right\rangle = \frac{32G}{5} M^2 \nu^2 r^4 \omega^6 \,. \tag{3.2.100}$$

Inserting the modified Kepler relations and expanding up to LO in the scalar field couplings, we arrive at

$$P_{\mathrm{LO}} = \frac{32}{5G}\nu^2 x^5 + \frac{1024}{15G}\nu^2 \overline{Q} e^{-\overline{m}_s/x}(\overline{m}_s + x)x^4 \,. \tag{3.2.101}$$

In Fig. 3.8, we are displaying all obtained components of the power loss as a function of x for two scenarios. In the first scenario, we have a binary system in which both objects carry a (differing) scalar charge and induced charge, thus finding that all computed components contribute to the power loss. In the second scenario, only one object has non-vanishing scalar couplings to its worldline. We therefore have that, for example, the lowest-order contribution due to the modified Kepler relations (as seen in Eq. (3.2.101)) vanishes since it depends on the product of both scalar charges.

	m_s [eV]	M_1 [$M_\odot$]	M_2 [$M_\odot$]	q_1 [M_1]	q_2 [M_2]	p_1 [q_1]	p_2 [q_2]	c_3
Left	10^{-15}	1.8	2.0	1.8×10^{-3}	2×10^{-3}	5×10^{-2}	5×10^{-2}	$m_s^2/M_{\rm pl}^2$
Right	10^{-15}	1.8	2.0	1.8×10^{-4}	0	5×10^{-3}	0	$m_s^2/M_{\rm pl}^2$

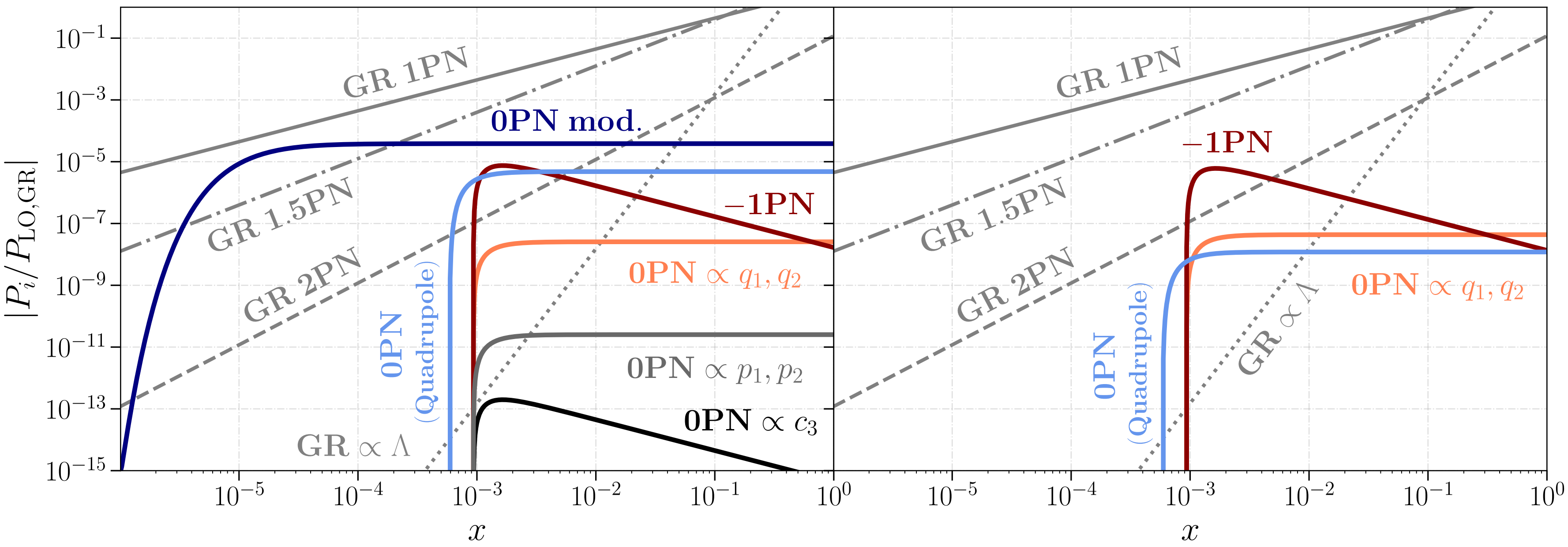

Figure 3.8: Power loss of an inspiraling binary system in massive scalar-tensor gravity, relative to the LO power loss in pure GR. Different colors indicate different contributions. We display the power loss arising due to scalar effects on the Kepler relation (dark blue, Eq. (3.2.101)), LO scalar dipole radiation (dark red, Eq. (3.2.98a)), dipole effects due to the induced scalar charges (dark gray, Eq. (3.2.98b)) and cubic self-coupling (black, Eq. (3.2.98c)), NLO scalar dipole radiation (orange, Eq. (3.2.98d)), as well as scalar quadrupole radiation (light blue, Eq. (3.2.99)). The light gray curves indicate higher-order pure GR corrections up to 2PN order. In addition, we show typical pure GR finite-size contributions, where for the NS tidal deformability we choose a benchmark value of $\Lambda = 100$. All other involved parameter are shown in the table above the figure. The left panel depicts a system where both objects carry a scalar charge, while the right panel only one object carries a charge. As a consequence, at the here considered order, the scalar degree of freedom has no effect on the modified Kepler relation in the right panel. In addition, the contributions from the induced scalar charges p_1, p_2 and the self-coupling c_3 vanish. Plot created by D. Schmitt.

3.2.5 Gravitational Wave Phase

We now turn to the calculation of the GW phase. In Sec. 3.1.4, we already noted that the phase can be calculated via

$$0 = \frac{\mathrm{d}t}{\mathrm{d}x} + \frac{1}{P}\frac{\mathrm{d}E}{\mathrm{d}x}\,, \tag{3.2.102}$$

$$0 = \frac{\mathrm{d}\Psi}{\mathrm{d}x} - \frac{3x^{\frac{1}{2}}}{GM}t\,, \tag{3.2.103}$$

where we can now directly insert the obtained results for the modified power loss and binding energy. When calculating the phase, we first expand in the small scalar quantities, such as $\overline{Q}$, $\bar{c}_3$, etc., before expanding in the PN parameter x. In this way we treat the modifications due to the scalar sector as perturbations around the LO GR effects and the quadrupolar GR emission is therefore assumed to be the dominant channel for energy loss[4]. In this way, we find that the resulting GW phase can be separated, such that

$$\Psi_{\text{tot}} = \Psi_{\text{GR}} + \Psi_{\text{ST}}, \tag{3.2.104}$$

where Ψ_{GR} denotes the usual GW phase in GR, and Ψ_{ST} denote the corrections due to the scalar degree of freedom. Next, we can further decompose Ψ_{ST} into components that arise due to the emitted scalar radiation in a given multipole mode l, Ψ_l, and due to modifications of the binding energy, Ψ_E. We thus write

$$\Psi_{\text{ST}} = \Psi_E + \theta\left(\frac{v^3}{\overline{m}_s} - 1\right)\Psi_{l=1} + \theta\left(\frac{v^3}{\overline{m}_s} - \frac{1}{2}\right)\Psi_{l=2} \tag{3.2.105}$$

and have here made explicit that dipolar scalar radiation only occurs for $v^3 > \overline{m}_s$ and quadrupolar scalar radiation for $v^3 > \overline{m}_s/2$ by using the Heaviside step function θ.

We find that the phase contributions due to the modified binding energy begins to contribute at 0PN order, while the phase contributions due to dipolar scalar radiation enter at -1PN order. The explicit contributions are given by

$$\begin{aligned}\Psi_E^{0\text{PN}} = {}& \frac{5\overline{Q}}{6\nu\overline{m}_s^{5/2}}\left[\Gamma\left(\frac{5}{2},\frac{\overline{m}_s}{v^2}\right) + \Gamma\left(\frac{7}{2},\frac{\overline{m}_s}{v^2}\right) + 2\,\Gamma\left(\frac{9}{2},\frac{\overline{m}_s}{v^2}\right)\right] \\ & - v^3\frac{5\overline{Q}}{6\nu\overline{m}_s^4}\left[\Gamma\left(4,\frac{\overline{m}_s}{v^2}\right) + \Gamma\left(5,\frac{\overline{m}_s}{v^2}\right) + 2\,\Gamma\left(6,\frac{\overline{m}_s}{v^2}\right)\right],\end{aligned} \tag{3.2.106a}$$

$$\Psi_{l=1}^{-1\text{PN}} = \delta q^2\frac{5}{896\nu^3}\left[-\frac{1}{v^7}\,{}_3F_2\left(-\frac{3}{2},\frac{5}{3},\frac{7}{6};\frac{8}{3},\frac{13}{6};\frac{\overline{m}_s^2}{v^6}\right) - \frac{90\cdot 2^{1/3}3^{1/2}v^3\Gamma\left(\frac{2}{3}\right)^3}{247\pi\overline{m}_s^{10/3}} + \frac{63\,\Gamma\left(\frac{1}{3}\right)^3}{256\cdot 2^{1/3}\pi\overline{m}_s^{7/3}}\right]. \tag{3.2.106b}$$

We have here expressed the results by using the generalized hypergeometric function ${}_3F_2$

[4] In [109], the authors also consider a regime where the scalar dipole radiation is the LO energy loss.

and the *upper* incomplete gamma function, which is defined as $\Gamma(a,x) = \int_x^\infty t^{a-1}e^{-t}\mathrm{d}t$. Note that these LO contributions only depend on the scalar charges q_1 and q_2. Corrections due to the induced charges p_1 and p_2, as well as the self-interaction parameter c_3, arise at NLO (0PN) with respect to the scalar radiation. Explicitly, these terms are given by

$$\begin{aligned}\Psi^{0\mathrm{PN},q}_{l=1} = &-\frac{5g_2\delta q\overline{m}_s^2}{9856\nu^3v^{11}}\,{}_3F_2\left(-\frac{3}{2},\frac{7}{3},\frac{11}{6};\frac{10}{3},\frac{17}{6};\frac{\overline{m}_s^2}{v^6}\right)\\ &+\frac{45\,\Gamma\left(\frac{2}{3}\right)^3\delta q\left(-1680g_1-966g_2+5(1064\nu+659)\delta q\right)}{1605632\;2^{2/3}\pi\nu^3\overline{m}_s^{5/3}}\\ &+\frac{\delta q\left(1680g_1+1008g_2-5(1064\nu+659)\delta q\right)}{86016\nu^3v^5}\,{}_3F_2\left(-\frac{3}{2},\frac{4}{3},\frac{5}{6};\frac{7}{3},\frac{11}{6};\frac{\overline{m}_s^2}{v^6}\right)\\ &+\frac{5\sqrt{3}v^3\Gamma\left(\frac{1}{3}\right)^3\delta q\left(7728g_1+4368g_2-23(1064\nu+659)\delta q\right)}{30829568\sqrt[3]{2}\pi\nu^3\overline{m}_s^{8/3}}\,,\end{aligned} \tag{3.2.107a}$$

$$\Psi^{0\mathrm{PN},p}_{l=1} = \Xi_p\frac{5}{16\nu^3}\left[-\frac{1}{v^5}\,{}_3F_2\left(-\frac{3}{2},\frac{4}{3},\frac{5}{6};\frac{7}{3},\frac{11}{6};\frac{\overline{m}_s^2}{v^6}\right)-\frac{6\cdot 2^{2/3}3^{1/2}v^3\Gamma\left(\frac{1}{3}\right)^3}{187\pi\overline{m}_s^{8/3}}+\frac{135\,\Gamma\left(\frac{2}{3}\right)^3}{56\cdot 2^{2/3}\pi\overline{m}_s^{5/3}}\right], \tag{3.2.107b}$$

$$\begin{aligned}\Psi^{0\mathrm{PN},c_3}_{l=1} = &\,\Xi_c\frac{5GM_1M_2}{7168\pi\overline{m}_s\nu^3}\left[\frac{1}{v^7}\,{}_3F_2\left(-\frac{3}{2},\frac{5}{3},\frac{7}{6};\frac{8}{3},\frac{13}{6};\frac{\overline{m}_s^2}{v^6}\right)+\frac{90\cdot 2^{1/3}3^{1/2}v^3\Gamma\left(\frac{2}{3}\right)^3}{247\pi\overline{m}_s^{10/3}}-\frac{63\,\Gamma\left(\frac{1}{3}\right)^3}{256\cdot 2^{1/3}\pi\overline{m}_s^{7/3}}\right]\\ &+\Xi_c\frac{25GM_1M_2}{55296\pi\nu^3}\left[-\frac{1}{v^9}\,{}_3F_2\left(-\frac{3}{2},2,\frac{3}{2};3,\frac{5}{2};\frac{\overline{m}_s^2}{v^6}\right)-\frac{24v^3}{35\overline{m}_s^4}+\frac{3\pi}{8\overline{m}_s^3}\right],\end{aligned} \tag{3.2.107c}$$

$$\Psi^{0\mathrm{PN}}_{l=2} = \Xi_q^2\frac{1}{32\nu^3}\left[-\frac{1}{v^5}\,{}_3F_2\left(-\frac{5}{2},\frac{4}{3},\frac{5}{6};\frac{7}{3},\frac{11}{6};\frac{\overline{m}_s^2}{4v^6}\right)-\frac{720\cdot 2^{1/3}3^{1/2}v^3\Gamma\left(\frac{1}{3}\right)^3}{4301\pi\overline{m}_s^{8/3}}+\frac{405\,\Gamma\left(\frac{2}{3}\right)^3}{112\pi\overline{m}_s^{5/3}}\right]. \tag{3.2.107d}$$

We here denote the contribution to the phase that arises due to a certain coupling parameter with a corresponding superscript, such that, e.g., the contributions that arise at LO due to p_1 and p_2 are denoted as $\Psi^{0\mathrm{PN},p}_{l=1}$.

We further note here that we have checked that our results properly reproduce the known results for massless BD theory. More explicitly, our expressions for the binding energy, power loss, and GW phase match those given in [100, 109] when taking the limit $m_s \to 0$ and setting $c_3 = 0$. Also, the LO massive case was also considered in [56], and we have verified that our LO results are identical.

The obtained phase corrections can now readily be combined with the already known GR phase at any desired order. To utilize our results more easily, we have prepared a repository [153] that contains a Python implementation of the phase corrections given in Eq. (3.2.106) and Eq. (3.2.107).

3.3 Conclusion

We have leveraged the PP EFT formalism to obtain the conservative and dissipative dynamics of a compact binary system. In this way, we have obtained the conservative Lagrangian and power loss at NLO, i.e., 1PN for the conservative Lagrangian and 0PN for the power loss. We have further utilized these results to obtain the TaylorF2 phase of the emitted gravitational wave signal at NLO and presented it in a format that is ready to use to perform, e.g., Bayesian inferences. In the EFT framework, it is straightforward to generalize and expand upon our calculations by introducing additional operators into the PP and bulk actions, or by pushing the calculations to higher orders in the PN expansion.

In our approach using the PP action, we have kept the setup largely model-independent by choosing a generic polynomial potential for the scalar field, and we have kept the necessary worldline couplings up to the desired order. This allows us now to apply the obtained results to a multitude of models.

As the next steps, the goal is to utilize the TaylorF2 template by performing Bayesian inferences, which will allow us to put general constraints on the model parameters. Also, by matching the worldline coefficients to a specific model—such as $f(R)$ gravity—it is possible to obtain more refined constraints from the inferences. Also, it would be interesting to extend the calculations to non-circular orbits, which would also allow us to utilize binary pulsar data.

3.A Integral Identities

The most commonly encountered integral is given by (see App. B of [41])

$$\int \frac{\mathrm{d}^{d-1}\boldsymbol{k}}{(2\pi)^{d-1}} \frac{e^{i\boldsymbol{k}\boldsymbol{r}}}{\left(\boldsymbol{k}^2\right)^{\alpha}} = \frac{1}{(4\pi)^{\frac{d-1}{2}}} \frac{\Gamma\left(\frac{d-1}{2}-\alpha\right)}{\Gamma(\alpha)} \left(\frac{\boldsymbol{r}^2}{4}\right)^{\alpha-\frac{d-1}{2}} . \tag{3.A.1}$$

It is straightforward to derive further solutions of related integrals by taking spatial derivatives, so that

$$\begin{aligned} \int \frac{\mathrm{d}^{d-1}\boldsymbol{k}}{(2\pi)^{d-1}} \frac{\boldsymbol{k}^m\boldsymbol{k}^n e^{i\boldsymbol{k}\boldsymbol{r}}}{\left(\boldsymbol{k}^2\right)^{\alpha}} &= -\partial_m\partial_n \int \frac{\mathrm{d}^{d-1}\boldsymbol{k}}{(2\pi)^{d-1}} \frac{e^{i\boldsymbol{k}\boldsymbol{r}}}{\left(\boldsymbol{k}^2\right)^{\alpha}} \\ &= \frac{1}{(4\pi)^{\frac{d-1}{2}}} \frac{\Gamma\left(\frac{d+1}{2}-\alpha\right)}{2\,\Gamma(\alpha)} \left(\frac{\boldsymbol{r}^2}{4}\right)^{\alpha-\frac{d+1}{2}} \left[\delta^{mn} + 2\left(\alpha - \frac{d+1}{2}\right)\frac{\boldsymbol{r}^m\boldsymbol{r}^n}{\boldsymbol{r}^2}\right]. \end{aligned} \tag{3.A.2}$$

Integrals that are regularized by the scalar field mass typically do not need to be evaluated using dimensional regularization and we thus present their result directly in three spatial dimensions. We have

$$\int \frac{\mathrm{d}^3\boldsymbol{k}}{(2\pi)^3} \frac{e^{i\boldsymbol{k}\boldsymbol{r}}}{\left(\boldsymbol{k}^2+m_s^2\right)^{\alpha}} = \frac{1}{(4\pi)^{\frac{3}{2}}} \frac{2\,\mathbf{K}_{\alpha-\frac{3}{2}}\left(m_s r\right)}{\Gamma(\alpha)} \left(\frac{r}{2m_s}\right)^{\alpha-\frac{3}{2}} , \tag{3.A.3}$$

where $r = |\boldsymbol{r}|$ and $\mathbf{K}$ denotes the modified Bessel function of the second kind. We further find that

$$\int \frac{\mathrm{d}^3\boldsymbol{k}}{(2\pi)^3} \frac{\boldsymbol{k}^m\boldsymbol{k}^n e^{i\boldsymbol{k}\boldsymbol{r}}}{\left(\boldsymbol{k}^2+m_s^2\right)^2} = \frac{1}{8\pi r} e^{-m_s r}\left[\delta^{ij} - (1+m_s r)\frac{\boldsymbol{r}^m\boldsymbol{r}^n}{\boldsymbol{r}^2}\right]. \tag{3.A.4}$$

Diagrams involving cubic self-interactions further require solving integrals consisting of three propagators, and we will thus solve the integral that generically appears, which has the form of

$$\mathcal{I}(m_1,m_2,m_3) = \int \mathrm{d}^3\boldsymbol{r}_v \int \frac{\mathrm{d}^3\boldsymbol{k}_1}{(2\pi)^3} \int \frac{\mathrm{d}^3\boldsymbol{k}_2}{(2\pi)^3} \int \frac{\mathrm{d}^3\boldsymbol{k}_3}{(2\pi)^3} \frac{e^{i\boldsymbol{k}_1(\boldsymbol{r}_1-\boldsymbol{r}_v)}}{\boldsymbol{k}_1^2+m_1^2} \frac{e^{i\boldsymbol{k}_2(\boldsymbol{r}_1-\boldsymbol{r}_v)}}{\boldsymbol{k}_2^2+m_2^2} \frac{e^{i\boldsymbol{k}_3(\boldsymbol{r}_v-\boldsymbol{r}_2)}}{\boldsymbol{k}_3^2+m_3^2} . \tag{3.A.5}$$

Since the calculation is more involved than the integrals presented above, we will present a step-by-step calculation here. We begin by noting

$$\mathcal{I}(m_1,m_2,m_3) = \int_{\boldsymbol{k}_1}\int_{\boldsymbol{k}_3} \frac{1}{\boldsymbol{k}_1^2+m_1^2} \frac{1}{(\boldsymbol{k}_3-\boldsymbol{k}_1)^2+m_2^2} \frac{e^{i\boldsymbol{k}_3\boldsymbol{r}}}{\boldsymbol{k}_3^2+m_3^2} , \tag{3.A.6}$$

where we have first integrated over $\boldsymbol{r}_v$ to obtain a delta function of the form $\delta^3(\boldsymbol{k}_1+\boldsymbol{k}_2-\boldsymbol{k}_3)$ and then integrated over $\boldsymbol{k}_2$. We first focus on the $\boldsymbol{k}_1$ integral and denote it by

$$\mathcal{I}_1 \equiv \int_{\boldsymbol{k}_1} \frac{1}{\boldsymbol{k}_1^2+m_1^2} \frac{1}{(\boldsymbol{k}_3-\boldsymbol{k}_1)^2+m_2^2} . \tag{3.A.7}$$

Using Feynman parametrization, we can rewrite the integral as

$$\mathcal{I}_1 = \int_{\boldsymbol{k}_1} \int_0^1 \mathrm{d}a \int_0^1 \mathrm{d}b \frac{\delta(a+b-1)}{\left[a\left(\boldsymbol{k}_1^2 + m_1^2\right) + b\left(\boldsymbol{k}_3 - \boldsymbol{k}_1\right)^2 + b\, m_2^2\right]^2} \,.$$

Next, we carry out the integration over b and complete the square in the denominator to find

$$\mathcal{I}_1 = \int_{\boldsymbol{k}_1} \int_0^1 \mathrm{d}a \frac{1}{\left[\left(\boldsymbol{k}_1 - (1-a)\boldsymbol{k}_3\right)^2 + a(1-a)\boldsymbol{k}_3^2 + a\, m_1^2 + (1-a)m_2^2\right]^2} \,. \tag{3.A.8}$$

We can simplify the integral by shifting $\boldsymbol{k}_1 \to \boldsymbol{k} + (1-a)\boldsymbol{k}_3$ and thus have

$$\mathcal{I}_1 = \int_{\boldsymbol{k}_1} \int_0^1 \mathrm{d}a \frac{1}{\left[\boldsymbol{k}_1^2 + a(1-a)\boldsymbol{k}_3^2 + a\, m_1^2 + (1-a)m_2^2\right]^2} \,. \tag{3.A.9}$$

It is now straightforward to evaluate the integral over $\boldsymbol{k}_1$ and we find

$$\mathcal{I}_1 = \frac{1}{8\pi} \int_0^1 \mathrm{d}a \frac{1}{\sqrt{a(1-a)\boldsymbol{k}_3^2 + a\, m_1^2 + (1-a)m_2^2}} \,. \tag{3.A.10}$$

We can solve the da integral exactly to obtain

$$\mathcal{I}_1 = \frac{1}{4\pi|\boldsymbol{k}_3|}\left[\operatorname{atan}\left(\frac{|\boldsymbol{k}_3|}{m_1 - m_2}\right) - \operatorname{atan}\left(\frac{2|\boldsymbol{k}_3|m_2}{\boldsymbol{k}_3^2 + m_1^2 - m_2^2}\right)\right] . \tag{3.A.11}$$

Inserting this back into Eq. (3.A.6), we arrive at

$$\begin{aligned}\mathcal{I}(m_1, m_2, m_3) = &-\frac{i}{16\pi^3 r} \underbrace{\int_{\mathbb{R}} \mathrm{d}k \, \operatorname{atan}\left(\frac{k}{m_1 - m_2}\right) \frac{e^{ikr}}{k^2 + m_3^2}}_{\mathcal{I}_2 \equiv} \\ &+ \frac{i}{16\pi^3 r} \underbrace{\int_{\mathbb{R}} \mathrm{d}k \, \operatorname{atan}\left(\frac{2k\, m_2}{k^2 + m_1^2 - m_2^2}\right) \frac{e^{ikr}}{k^2 + m_3^2}}_{\mathcal{I}_3 \equiv} \,.\end{aligned} \tag{3.A.12}$$

We have here defined $\mathcal{I}_2$ and $\mathcal{I}_3$, which we will next evaluate separately.

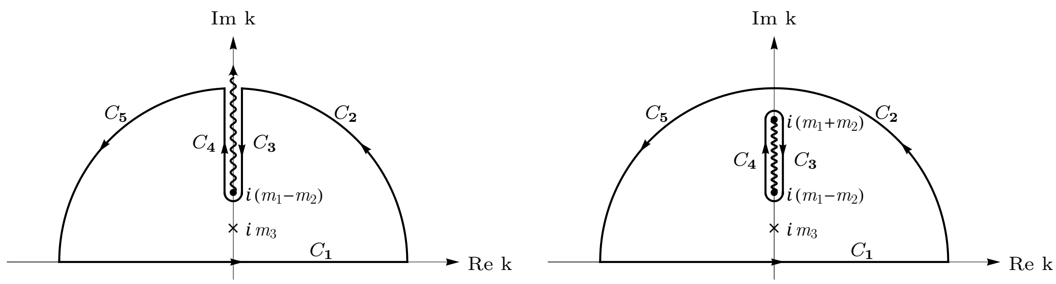

Figure 3.10: Contours used for calculation of the integrals $\mathcal{I}_2$ and $\mathcal{I}_3$, which are defined in Eq. (3.A.12).

We continue wth the first integral and use the contour given in the left panel of Fig. 3.10. For the further calculations we will assume that $m_1 > m_2 + m_3$. We note that the contours C_2 and C_5 give a vanishing contribution to the integral, so that only C_3, C_4, and the pole at $k = im_3$ contribute. Next, arctan jumps by a shift of π when going across the branch cut, so that it is straightforward to find that the integral is given by

$$\begin{aligned}\mathcal{I}_2 &= i\pi \int_{m_1-m_2}^{\infty} \mathrm{d}k \frac{e^{-kr}}{m_3^2 - k^2} + \frac{i\pi}{m_3} e^{-m_3 r} \mathrm{arctanh}\left(\frac{m_3}{m_1 - m_2}\right) \\ &= -\frac{i\pi}{2m_3} e^{m_3 r} \mathrm{Ei}\big(-(m_1 - m_2 + m_3)r\big) + \frac{i\pi}{2m_3} e^{-m_3 r} \mathrm{Ei}\big((-m_1 + m_2 + m_3)r\big) \\ &\quad + \frac{i\pi}{m_3} e^{-m_3 r} \mathrm{arctanh}\left(\frac{m_3}{m_1 - m_2}\right).\end{aligned} \tag{3.A.13}$$

The second integral in Eq. (3.A.12) uses the contour presented in the right panel of Fig. 3.10. We here find by the same arguments that

$$\begin{aligned}\mathcal{I}_3 &= i\pi \int_{m_1-m_2}^{m_1+m_2} \frac{e^{-kr}}{m_3^2 - k^2} \\ &= -\frac{i\pi}{2m_3} e^{-m_3 r} \mathrm{Ei}\big(-(m_1 + m_2 - m_3)r\big) - \frac{i\pi}{2m_3} e^{m_3 r} \mathrm{Ei}\big(-(m_1 - m_2 + m_3)r\big) \\ &\quad + \frac{i\pi}{2m_3} e^{-m_3 r} \mathrm{Ei}\big((-m_1 + m_2 + m_3)r\big) + \frac{i\pi}{2m_3} e^{m_3 r} \mathrm{Ei}\big(-(m_1 + m_2 + m_3)r\big) \\ &\quad - \frac{i\pi}{m_3} e^{-m_3 r} \mathrm{arctanh}\left(\frac{2m_2 m_3}{-m_1^2 + m_2^2 + m_3^2}\right).\end{aligned} \tag{3.A.14}$$

Combining these results, we hence find

$$\begin{aligned}\mathcal{I}(m_1, m_2, m_3) = \frac{1}{32\pi^2} \frac{1}{m_3 r} e^{-m_3 r} \Bigg[&\mathrm{Ei}\big(-(m_1 + m_2 - m_3)r\big) + \log\left(\frac{m_1 + m_2 + m_3}{m_1 + m_2 - m_3}\right) \\ &- e^{2m_3 r} \mathrm{Ei}\big(-(m_1 + m_2 + m_3)r\big) \Bigg].\end{aligned} \tag{3.A.15}$$

From this, it is now straightforward to derive the following limiting cases:

$$\mathcal{I}(m_s, m_s, 0) = \frac{1}{32\pi^2}\frac{1}{m_s r}\left[1 - e^{-2m_s r} - 2m_s r \mathrm{Ei}\big(-2m_s r\big)\right], \tag{3.A.16}$$

$$\mathcal{I}(m_s, 0, m_s) = \frac{1}{32\pi^2}\frac{1}{m_s r}e^{-m_s r}\left[\gamma_{\mathrm{E}} + \log(2m_s r) - e^{2m_s r}\mathrm{Ei}\big(-2m_s r\big)\right], \tag{3.A.17}$$

$$\mathcal{I}(m_s, m_s, m_s) = \frac{1}{32\pi^2}\frac{1}{m_s r}e^{-m_s r}\left[\log(3) + \mathrm{Ei}\big(-m_s r\big) - e^{2m_s r}\mathrm{Ei}\big(-3m_s r\big)\right]. \tag{3.A.18}$$

3.B Feynman Rules

Diagram	Scaling	Expression
	$\sim L$	$i\int dt \frac{M}{2}\boldsymbol{v}^2$
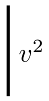	$\sim Lv^2$	$i\int dt \frac{M}{8}\boldsymbol{v}^4$
	~ 1	$-(2\pi)^3 \frac{i}{\lvert\boldsymbol{k}\rvert^2}\delta^{(3)}(\boldsymbol{k}+\boldsymbol{q})\delta(t_1-t_2)P_{\mu\nu;\alpha\beta}$
	~ 1	$-(2\pi)^3 \frac{i}{\lvert\boldsymbol{k}\rvert^2+m^2}\delta^{(3)}(\boldsymbol{k}+\boldsymbol{q})\delta(t_1-t_2)$
	$\sim v^2$	$-(2\pi)^3 \frac{i}{\lvert\boldsymbol{k}\rvert^4}\delta^{(3)}(\boldsymbol{k}+\boldsymbol{q})\frac{\partial^2}{\partial t_1 \partial t_2}\delta(t_1-t_2)P_{\mu\nu;\alpha\beta}$
	$\sim v^2$	$-(2\pi)^3 \frac{i}{(\lvert\boldsymbol{k}\rvert^2+m^2)^2}\delta^{(3)}(\boldsymbol{k}+\boldsymbol{q})\frac{\partial^2}{\partial t_1 \partial t_2}\delta(t_1-t_2)$
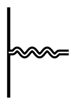	$\sim L^{\frac{1}{2}}$	$-i\frac{M}{2M_{\mathrm{pl}}}\int dt \int_{\boldsymbol{k}} \exp(i\boldsymbol{k}\boldsymbol{x})\,\eta^{0\mu}\eta^{0\nu}$
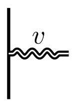	$\sim L^{\frac{1}{2}}v$	$-i\frac{M}{M_{\mathrm{pl}}}\int dt \int_{\boldsymbol{k}} \exp(i\boldsymbol{k}\boldsymbol{x})\,\boldsymbol{v}^i\eta^{0(\mu}\eta_i^{\nu)}$
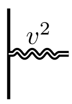	$\sim L^{\frac{1}{2}}v^2$	$-i\frac{M}{2M_{\mathrm{pl}}}\int dt \int_{\boldsymbol{k}} \exp(i\boldsymbol{k}\boldsymbol{x})\left(\eta_i^{\mu}\eta_j^{\mu}\boldsymbol{v}^i\boldsymbol{v}^j+\frac{1}{2}\eta^{0\mu}\eta^{0\nu}\boldsymbol{v}^2\right)$
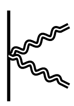	$\sim v^2$	$i\frac{M}{8M_{\mathrm{pl}}^2}\int dt \int_{\boldsymbol{k},\boldsymbol{q}} \exp(i(\boldsymbol{k}+\boldsymbol{q})\boldsymbol{x})\,\eta^{0\mu}\eta^{0\nu}\eta^{0\lambda}\eta^{0\sigma}$
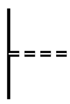	$\sim \frac{q}{M}L^{\frac{1}{2}}$	$-i\frac{q}{M_{\mathrm{pl}}}\int dt \int_{\boldsymbol{k}} \exp(i\boldsymbol{k}\boldsymbol{x})$
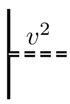	$\sim \frac{q}{M}L^{\frac{1}{2}}v^2$	$i\frac{q}{2M_{\mathrm{pl}}}\int dt \int_{\boldsymbol{k}} \exp(i\boldsymbol{k}\boldsymbol{x})\,\boldsymbol{v}^2$

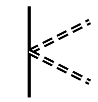	$\sim \frac{p}{M} v^2$	$-i\frac{p}{M_{\text{pl}}^2}\int dt \int_{\boldsymbol{k},\boldsymbol{q}} \exp\left(i(\boldsymbol{k}+\boldsymbol{q})\boldsymbol{x}\right)$
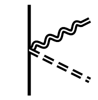	$\sim \frac{q}{M} v^2$	$-i\frac{q}{2M_{\text{pl}}^2}\int dt \int_{\boldsymbol{k},\boldsymbol{q}} \exp\left(i(\boldsymbol{k}+\boldsymbol{q})\boldsymbol{x}\right)$
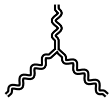	$\sim L^{-\frac{1}{2}} v^2$	$-\frac{i}{4M_{\text{pl}}}\delta(t_1-t_2)\delta(t_1-t_3)(2\pi)^3\delta^{(3)}\left(\sum_r \boldsymbol{k}_r\right)\prod_r \frac{i}{\boldsymbol{k}_r^2}\sum_r \boldsymbol{k}_r^2$
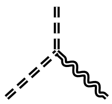	$\sim m_s^2 r^2 \frac{v^2}{L^{\frac{1}{2}}}$	$-i\frac{m_s^2}{4M_{\text{pl}}}\delta(t_1-t_2)\delta(t_1-t_3)(2\pi)^3\delta^{(3)}\left(\sum_r \boldsymbol{k}_r\right)\left(\prod_{r=1,2}\frac{i}{\boldsymbol{k}_r^2+m^2}\right)\frac{i}{\boldsymbol{k}_3^2}\eta^{\mu\nu}P_{00;\mu\nu}$
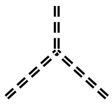	$\sim c_3 \frac{M_{\text{pl}}^2 r^2}{L^{\frac{1}{2}}} v^2$	$-i\frac{c_3}{3!}\delta(t_1-t_2)\delta(t_1-t_3)(2\pi)^3\delta^{(3)}\left(\sum_r \boldsymbol{k}_r\right)\prod_r \frac{i}{\boldsymbol{k}_r^2+m^2}$

Table 3.2: Feynman rules necessary to compute the binding energy diagrams at 1PN order. Tables were prepared by D. Schmitt.

Diagram	Scaling	Expression
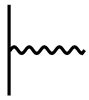	$\sim L^{\frac{1}{2}} v^{\frac{1}{2}}$	$-i\dfrac{M}{2M_{\rm pl}}\int dt\,\bar{h}_{00}$
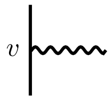	$\sim L^{\frac{1}{2}} v^{\frac{3}{2}}$	$-i\dfrac{M}{M_{\rm pl}}\int dt\,\bar{h}_{0i}\boldsymbol{v}^i$
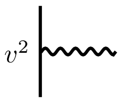	$\sim L^{\frac{1}{2}} v^{\frac{5}{2}}$	$-i\dfrac{M}{2M_{\rm pl}}\int dt\left(\bar{h}_{ij}\boldsymbol{v}^i\boldsymbol{v}^j + \dfrac{\bar{h}_{00}}{2}\boldsymbol{v}^2\right)$
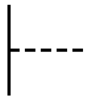	$\sim \dfrac{q}{M} L^{\frac{1}{2}} v^{\frac{1}{2}}$	$-i\dfrac{q}{M_{\rm pl}}\int dt\,\bar{\phi}$
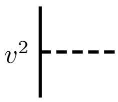	$\sim \dfrac{q}{M} L^{\frac{1}{2}} v^{\frac{5}{2}}$	$-i\dfrac{q}{2M_{\rm pl}}\int dt\,\boldsymbol{v}^2\bar{\phi}$
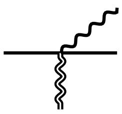	$\sim v^{\frac{5}{2}}$	$-i\dfrac{M}{4M_{\rm pl}^2}\int dt\int_{\boldsymbol{k}}\exp\left(i\boldsymbol{k}\boldsymbol{x}\right)\eta^{0\mu}\eta^{0\nu}\bar{h}_{00}$
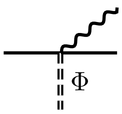	$\sim \dfrac{q}{M} v^{\frac{5}{2}}$	$-i\dfrac{q}{2M_{\rm pl}^2}\int dt\int_{\boldsymbol{k}}\exp\left(i\boldsymbol{k}\boldsymbol{x}\right)\bar{h}_{00}$
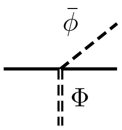	$\sim \dfrac{p}{M} v^{\frac{5}{2}}$	$-i\dfrac{2p}{M_{\rm pl}}\int dt\int_{\boldsymbol{k}}\exp\left(i\boldsymbol{k}\boldsymbol{x}\right)\bar{\phi}$
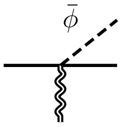	$\sim \dfrac{q}{M} v^{\frac{5}{2}}$	$-i\dfrac{q}{2M_{\rm pl}^2}\int dt\int_{\boldsymbol{k}}\exp\left(i\boldsymbol{k}\boldsymbol{x}\right)\eta^{0\mu}\eta^{0\nu}\bar{\phi}$
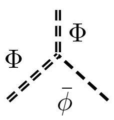	$\sim c_3\dfrac{Mrv^{\frac{1}{2}}}{L^{\frac{1}{2}}}$	$-iM_{\rm pl}\dfrac{3c_3}{3!}\delta(t-t_1)\delta(t-t_2)(2\pi)^3\dfrac{i}{\boldsymbol{k}_1^2+m^2}\dfrac{i}{\boldsymbol{k}_2^2+m^2}\bar{\phi}$
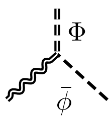	$\sim \overline{m}_s^2\dfrac{1}{L^{\frac{1}{2}}v^{\frac{3}{2}}}$	$-i\dfrac{2m_s^2}{4M_{\rm pl}}\delta(t-t_1)\delta(t-t_2)(2\pi)^3\dfrac{i}{\boldsymbol{k}_1^2+m^2}\dfrac{i}{\boldsymbol{k}_2^2}\eta^{\mu\nu}P_{00;\mu\nu}\bar{\phi}$

Table 3.3: Feynman rules involving the radiation modes, up to 1PN order. Tables were prepared by D. Schmitt.

Chapter 4

Dark Matter Impact on Binary Systems

We begin by constructing isolated systems of FBSs in spherical equilibrium and then move on to the construction of their quadrupolar Love numbers.

4.1 Constructing Isolated Systems

We consider a system consisting of a minimally coupled complex scalar field and additional—also minimally coupled—matter fields that describe nuclear matter. The total action for this system is thus given by

$$\mathcal{S} = \int d^4x\sqrt{-g}\left[\frac{M_{\rm pl}^2}{2}R - \nabla_\alpha\bar{\Phi}\nabla^\alpha\Phi - V(\bar{\Phi}\Phi) + \mathcal{L}_m\right], \tag{4.1.1}$$

where R is the Ricci scalar, $\mathcal{L}_m$ is the Lagrangian describing nuclear matter, and $V(\bar{\Phi}\Phi)$ is the scalar field's potential. We note that the action is invariant under a global U(1) transformation of the form $\Phi \to \Phi\, e^{i\alpha}$, with α a real constant. Applying Noether's theorem, we thus find an associated Noether current

$$j_\mu = i\big(\bar{\Phi}\nabla_\mu\Phi - \Phi\nabla_\mu\bar{\Phi}\big)\,. \tag{4.1.2}$$

Since by construction $\nabla^\mu j_\mu = 0$, we can use it to define the Noether charge on a given spatial hypersurface Σ

$$M_{\rm b} \equiv \int_\Sigma d^3x\sqrt{-g}\, g^{0\mu} j_\mu\,, \tag{4.1.3}$$

where we have denoted the Noether charge with $M_{\rm b}$ and identify it as the total rest mass of the bosonic subsystem[1]. Varying the action with respect to the scalar field results in the Klein-Gordon equation

$$\nabla_\mu\nabla^\mu\Phi = \Phi V'(\bar{\Phi}\Phi), \quad \text{with} \quad V'(\bar{\Phi}\Phi) \equiv \frac{dV}{d|\Phi|^2}\,. \tag{4.1.4}$$

[1]One can also define the total number of bosons $N_{\rm b} = M_{\rm b}/m$. However, this quantity is not relevant for the further disccusion.

Varying the action with respect to $g_{\mu\nu}$ we retrieve the usual Einstein field equations

$$R_{\mu\nu} - \frac{1}{2} g_{\mu\nu} R = \frac{1}{M_{\rm pl}^2} \left[T^{(\Phi)}_{\mu\nu} + T^{(\rm NS)}_{\mu\nu} \right] , \tag{4.1.5}$$

where $R_{\mu\nu}$ is the Ricci tensor, $T^{(\Phi)}_{\mu\nu}$ the scalar field's EMT, and $T^{(\rm NS)}_{\mu\nu}$ the matter EMT. We explicitly obtain the scalar field's EMT as

$$T^{(\Phi)}_{\mu\nu} = -g_{\mu\nu} \Big[\partial_\alpha \bar{\Phi} \partial^\alpha \Phi + V(\bar{\Phi}\Phi) \Big] + \partial_\mu \bar{\Phi} \partial_\nu \Phi + \partial_\mu \Phi \partial_\nu \bar{\Phi} \, . \tag{4.1.6}$$

Note that the Klein-Gordon directly implies that the scalar field's EMT is conserved by itself

$$\nabla^\mu T^{(\Phi)}_{\mu\nu} = 0 \tag{4.1.7}$$

and we can thus deduce that the matter EMT is also conserved individually

$$\nabla^\mu T^{(\rm NS)}_{\mu\nu} = 0 \, . \tag{4.1.8}$$

For the matter sector we assume an ideal fluid, which is characterized by its EMT

$$T^{(\rm NS)}_{\mu\nu} = \big[e + P \big] u_\mu u_\nu + P g_{\mu\nu} \, , \tag{4.1.9}$$

where e is the local energy density, P the pressure and u_μ the fluid's four-velocity. We can further decompose the energy density by expressing it in terms of the rest-mass energy density ρ and the internal energy per particle ϵ, such that $e = \rho(1+\epsilon)$. Particle number conservation of the perfect fluid is then expressed as

$$\nabla_\mu \big(\rho u^\mu \big) = 0 \, , \tag{4.1.10}$$

which allows to calculate the baryonic restmass on a given spatial hypersurface as

$$M_{\rm f} = \int_\Sigma {\rm d}^3 x \sqrt{-g} \, \rho \, u^0 \, . \tag{4.1.11}$$

Spherically Symmetrical Systems

We now specialize to spherical coordinates by adopting Schwarzschild coordinates with the line element given by

$${\rm d}s^2 = -f(r){\rm d}t^2 + h(r)^{-1}{\rm d}r^2 + r^2 {\rm d}\theta^2 + r^2 \sin(\theta)^2 {\rm d}\varphi^2 \tag{4.1.12}$$

and further also impose an ansatz on Φ that respects the spherical symmetry

$$\Phi = \phi(r)e^{-i\omega t}\,. \tag{4.1.13}$$

The matter fluid's four-velocity is expressed as $u_\mu = (\sqrt{f}, 0, 0, 0)$ and we thus find that the matter EMT is simply expressed as

$$T^{\mu}_{\ \nu}{}^{(\mathrm{NS})} = \begin{pmatrix} -e & 0 & 0 & 0 \\ 0 & P & 0 & 0 \\ 0 & 0 & P & 0 \\ 0 & 0 & 0 & P \end{pmatrix}\,. \tag{4.1.14}$$

We insert the metric, matter EMT, and scalar field ansatz into the Einstein field equations and use their tt and rr components to arrive at differential equations for f and h:

$$f'(r) = -\frac{f(h-1)}{r\,h} + \frac{r\,f}{M_{\mathrm{pl}}^2 h}P + \frac{r}{M_{\mathrm{pl}}^2 h}\left[\omega^2\phi^2 + f\,h\phi'^2 - f\,V(\phi^2)\right] \tag{4.1.15}$$

$$h'(r) = \frac{1-h}{r} - \frac{r}{M_{\mathrm{pl}}^2}e - \frac{r}{M_{\mathrm{pl}}^2 f}\left[\omega^2\phi^2 + f\,h\,\phi'^2 + f\,V(\phi^2)\right]\,. \tag{4.1.16}$$

We further obtain a differential equation for ϕ'' by utilizing the Klein-Gordon equation

$$\phi''(r) = -\left[\frac{2}{r} + \frac{f'}{2f} + \frac{h'}{2h}\right]\phi' + \frac{1}{f\,h}\left[f\,V'(\phi^2) - \omega^2\right]\phi\,. \tag{4.1.17}$$

Finally, the matter continuity equation gives us an equation for P:

$$P'(r) = -\frac{f'}{2f}(e+P)\,. \tag{4.1.18}$$

We thus arrived at a system of four coupled partial differential equations for the five unknown quantities P, e, f, h, and ϕ. In order to close this set of differential equations, it is still necessary to provide a fifth equation, which links P and e. This is the equation of state (EoS) which arises from microphysical considerations and is, for our purpose, expressed as $e = e(P)$.

Numerical Solutions

We solve the given system of differential equations by integrating from the spacetime's center outward. To this end it is necessary to specify ω together with the behavior of all involved functions around the origin, i.e., it is necessary to specify ω, $P(0)$, $f(0)$, $h(0)$, $\phi(0)$, and $\phi'(0)$. Additionally, these initial conditions have to be chosen such that the spacetime is asymptotically flat, i.e., we require

$$\lim_{r\to\infty}\phi(r)=0,\quad \lim_{r\to\infty}f(r)=1,\quad \text{and}\quad \lim_{r\to\infty}h(r)=1\,. \tag{4.1.19}$$

In order to simplify the initial conditions, we first note that by imposing regularity at the origin, we automatically find that $\phi'(0)=0$. Further, the differential equation system is invariant under

$$f\to\alpha^2 f,\quad \omega\to\alpha\,\omega, \tag{4.1.20}$$

where α is a real constant. We can leverage this symmetry by shifting $f\to\tilde{f}=f/f(0)$, so that we automatically have $\tilde{f}(0)=1$, thus fixing one more initial condition. One has to keep in mind that this rescaling also changes ω and the spacetime does not seem asymptotically flat anymore since we now have $\lim_{r\to\infty}\tilde{f}(r)=1/f(0)$. However, we can always retrieve f together with the physical value of ω by first extracting $f(0)$ from the asymptotic behavior of $\tilde{f}$ and then using it to reconstruct f and ω. Lastly, we note that $h'(0)=0$ in order to ensure that the spacetime is regular at the origin and combining this fact with Eq. (4.1.16) we thus find that also $h(0)=0$. In total, we thus find that there are three remaining free parameters—ω, $\phi(0)$, and $P(0)$—that have to be chosen in such a way that asymptotic flatness is achieved.

In practice, one is free to specify $P(0)$ and $\phi(0)$ and then has to fix ω in order to ensure asymptotic flatness. As discussed in [90,154], this condition indeed allows for a countably infinite family of possible values ω_n, which can be labeled by how often the corresponding function $\phi(r)$ changes its sign in the interval $r\in(0,\infty)$, such that for ω_0 we have $\phi(r)>0$ everywhere. The $n=0$ solution is also referred to as the *ground state* and solutions with $n>0$ as radially *excited states*. If one expands the here-presented setup to non-spherical systems, then one also finds that the angular directions similarly admit discrete solutions that fulfill the same boundary conditions. These excited states are generically unstable to perturbations (aspects of stability will be reviewed in the next section) and we thus limit our analysis here to the ground state of the system.

It remains to establish a procedure that allows for the efficient determination of ω_0 for a given choice of ϕ_c and P_c. If one solves the differential equations by choosing an arbitrary value for ω that does not result in an asymptotically flat spacetime, then $\phi(r)$ will generically diverge either to $+\infty$ or $-\infty$ at large radii. Crucially, this divergent part in ϕ experiences a sign flip whenever $\omega\in\{\omega_0,\omega_1,\dots\}$. In other words, if one constructs a solution for ϕ—denoted as $\phi_<$—by choosing a value $\omega<\omega_0$ and another solution—denoted as $\phi_>$—by choosing a value $\omega_0<\omega<\omega_1$, then one finds that either $\phi_>$ or $\phi_<$ has to diverge to $+\infty$ at large radii, while the other diverges to $-\infty$. This particular behavior provides a convenient binary criterion that we use to perform a bisection search for ω_n.

While the above-described bisection method allows for the construction of approximations of ω_0 efficiently, one will find that the resulting scalar field profiles will always diverge at sufficiently large radii. The radial onset of divergence depends on how close the numerically constructed approximation is to the physical value of ω_0, so that—due to the limited numerical accuracy—one finds that the divergence is inevitable. For pure BS systems, this is not typically a hindrance, since one always finds that there is a region in spacetime that is sufficiently well converged to the desired solution, and one can extract all desired information, such as the total mass of the system, from this particular region. For FBS systems, however, one finds that the scalar field might already start to diverge inside the neutron star since ω_0 can not be determined accurately enough for particular configurations. In order to mitigate this problem, we truncate the scalar field profile to zero for radii $r > r_B^*$, where r_B^* is determined by the condition $\phi(r_B^*)/\phi_c = \phi^*$ with ϕ^* a positive constant and choose $\phi^* = 10^{-4}$ for all subsequent results. This truncation is motivated by the fact that $\phi(r)$ will decrease faster than exponentially at large radii, thus rapidly approaching zero. Also, we have verified that choosing smaller values for ϕ^*, i.e., larger truncation radii, has an insignificant impact on the derived observables.

Stability

In the previous section, we have established that the solution space for FBSs in the ground state is two-dimensional, with each solution being characterized by ϕ_c, P_c, and have also presented the general procedure that allows us to find ω_0. While we are thus able to now numerically construct FBS solutions, we have to note that not all possible configurations are generally stable against small perturbations and do thus not present viable solutions. In order to discriminate stable from unstable configurations, it is generally necessary to perform a perturbative analysis: for an unstable solution, at least one of the oscillation eigenmodes will present exponential growth. If all perturbation modes are of an oscillatory nature, then we can call the configuration stable. In general it is not feasible to investigate each oscillation mode separately and typically only radial oscillation modes are relevant to study the stability of an object. In what follows, we will thus focus on radial oscillation modes.

In [91], the authors outlined a general argument that allows one to determine regions in the ϕ_c-ρ_c plane that are potentially stable without having to calculate the eigenfrequencies explicitly. We will briefly review their arguments here. Suppose one introduces linear perturbations, such that we schematically have

$$\xi(r,t) \to \xi_{\rm bg}(r) + \delta\xi(r,t) \tag{4.1.21}$$

with

$$\delta\xi(r,t) = \sum_{n=0}^{\infty} A_n \sin(\nu_n t)\, \delta\xi_n(r)\,. \tag{4.1.22}$$

We have here introduced ξ as a placeholder for any background quantity, such as ϕ, and have decomposed its perturbations $\delta\xi$ into its eigenmodes $\delta\xi_n$ that are labeled by n. Since we are working in linear perturbation theory, we must have that such perturbations do not change the total gravitational mass M_{tot}, the baryon rest mass M_{b}, and the fermion rest mass M_{f}. Also, one generally finds that the squared eigenfrequencies ν_n^2 are real-valued numbers and we can thus infer from Eq. (4.1.22) that if $\nu^2 < 0$ for a particular value n, then the corresponding mode exhibits exponential growth, while $\nu_n^2 > 0$ results in a purely oscillatory behavior. Suppose we perturb the system by adding only one pure eigenmode to it. We could then determine the onset of instability for that particular mode by determining the line of $\nu_n^2 = 0$ in the ϕ_c-ρ_c plane. These particular perturbations are neither oscillatory nor growing and are instead static perturbations that only shift the background quantities ξ. As such we find that $\xi + \delta\xi$ has to again fulfill the background field equations and is such also to be found in the ϕ_c-ρ_c plane, but with a different pair of values, which we denote by $(\phi_{c,1} + \delta\phi_{c,1}, \rho_{c,1} + \delta\rho_{c,1})$. As previously mentioned, the perturbation has to conserve M_{tot}, M_{b}, and M_{f}, meaning that taking the directional derivative of any of these quantities in the direction of $(\delta\phi_{c,1}, \delta\rho_{c,1})$ has to vanish. For practical purposes, it is easiest to determine the direction in which M_{tot} remains constant and then calculate the directional derivatives of M_{f} and M_{b} in the same direction. We thus arrive at the condition

$$\frac{\mathrm{d}N_f}{\mathrm{d}\sigma} = \frac{\mathrm{d}N_b}{\mathrm{d}\sigma} = 0, \tag{4.1.23}$$

where $\mathrm{d}/\mathrm{d}\sigma$ denotes the derivative in the direction of constant gravitational mass. We can write out this directional derivative explicitly, such that, e.g.,

$$\frac{\mathrm{d}N_f}{\mathrm{d}\sigma} \propto -\frac{\partial M_{\text{tot}}}{\partial \rho_c}\frac{\partial M_{\text{f}}}{\partial \phi_c} + \frac{\partial M_{\text{tot}}}{\partial \phi_c}\frac{\partial M_{\text{f}}}{\partial \rho_c}\,. \tag{4.1.24}$$

Before continuing with our exploration of FBSs, it is important to stress a few points about this approach to the stability analysis:

1. Any line that is found in this way is not necessary a point at which an eigenmode actually becomes unstable.

2. All points within a given stability region have to be either stable or unstable. As such it is sufficient to explicitly check the stability of a single point in the region in order to conclude that all points in the given region are stable.

3. While we have argued that stability borders can be found by using Eq. (4.1.23), the reverse implication is also true: Every point in the ϕ_c-ρ_c plane that fulfills Eq. (4.1.23) has to be part of a stability border. This is easy to see since Eq. (4.1.23) directly implies the existence of a static perturbation and is therefore an exhaustive criterion to identify stability borders.

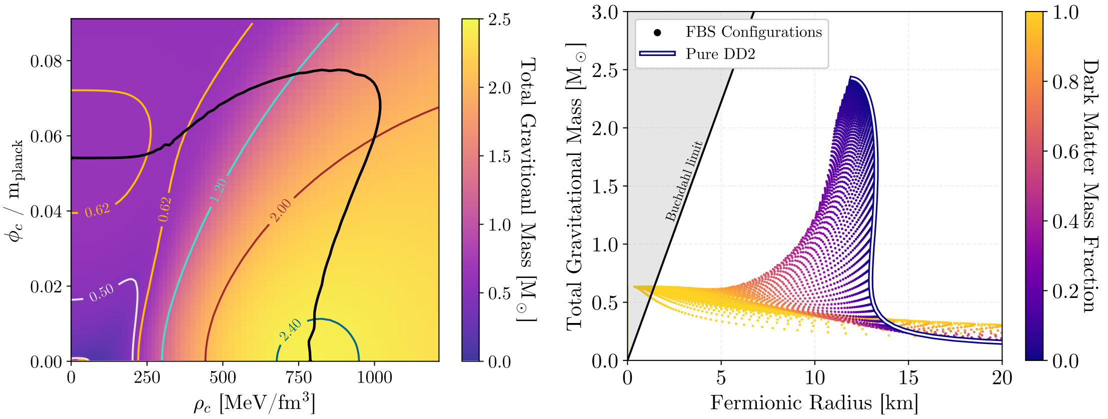

Figure 4.1: Left panel: Density plot that displays the total gravitational mass as a function of the central rest-mass density (ρ_c) and central value of the scalar field (ϕ_c). Additionally, it displays the stability curve as the solid black line calculated using Eq. (4.1.23), i.e., all configurations that lie within the bottom left parameter region that is bordered by the black line are stable against linear radial perturbations. **Right panel:** Mass-radius diagram displaying the fermionic radius vs. the total gravitational mass for configurations that are within the stable region displayed in the left panel. Each point corresponds to a single configuration and is color-coded according to the rest mass fraction of the dark matter component. The solid black line shows the mass-radius curve for pure fermionic matter. For both plots a massive scalar field with no self-interactions and the mass set to $m = 1.3 \times 10^{-10}$ eV was considered in addition to the DD2 EoS.

4. It is important to keep in mind that the presented argument only works for linear perturbations. Indeed, one finds that the $n = 1$ excited BS are generally unstable, while they seem to be stable according to the here presented argument.

The last point highlights the necessity to investigate found configurations non-perturbatively, in order to ensure that higher-order effects do not spoil the configuration's stability. This is done by utilizing the full Einstein field equations to dynamically evolve a background solution in time. This was done in, e.g., [155], where it was shown that the above-described stability argument is appropriate to identify stable ground state configurations.

4.1.1 Background Solutions

Figure 4.1 presents a density plot of the the gravitational mass in the ϕ_c-ρ_c plane for the case of $m = 1.34 \times 10^{-10}$ and $\Lambda_{\text{int}} = 0$. Additionally, the stability curve was calculated using Eq. (4.1.23) and is shown a the black solid line, so that all solutions within, i.e., the bottom left, are stable[2]. We note that the stability line reproduces the expected results for pure NS in the limit $\phi_c \to 0$ and pure BS in the limit $\rho_c \to 0$. Also, we note that ϕ_c and ρ_c can exceed the maximum allowed value one would expect from pure BS and pure NS, respectively, without destabilizing the FBS. The right panel of the same figure presents the resulting masses and radii as a scatter plot, such that each individual point corresponds to one FBS configuration. Also, each point is colored according to the dark

[2]We have to keep in mind that there are additional stability lines that delimit, e.g., unstable white dwarf configurations. These lines appear for rather small values of ρ_c and are thus not shown.

matter mass fraction of that configuration. We here note that larger dark matter fractions typically decrease the overall gravitational mass and fermionic radius.

In order to further study the impact of varying the scalar field mass and self-interaction strength, we present the mass-radius scatter plots for the cases $m \in \{1.34 \times 10^{-11}, 1.34 \times 10^{-10}, 1.34 \times 10^{-9}\}$ and $\Lambda_{\rm int} \in \{0, 10, 100\}$ in Fig. 4.2, where we again only plot stable configurations. We generally observe that larger scalar field masses typically result in a smaller impact on the gravitational mass and fermionic radius, while smaller masses lead to greater variation. More specifically, we note that smaller masses seem to generally decrease the mass and radius, while larger masses generally increase these observables. We further observe a similar trend with the self-interaction strength, such that larger values of $\Lambda_{\rm int}$ generally lead to larger masses and radii, when compared to the $\Lambda_{\rm int} = 0$ case. We can understand this phenomenon qualitatively by also considering the *effective gravitational radius*, which we define to be the radius within 99 % of the total mass lies. We present the scatter plots that compare the total gravitational mass to the effective gravitational radius in Fig. 4.3. By comparing it to Fig. 4.2, we note that the smaller scalar field masses typically lead to configurations with effective gravitational radii that are larger than the fermionic radii, meaning that a significant portion of the DM exists within the so-called cloud configuration around the NS.

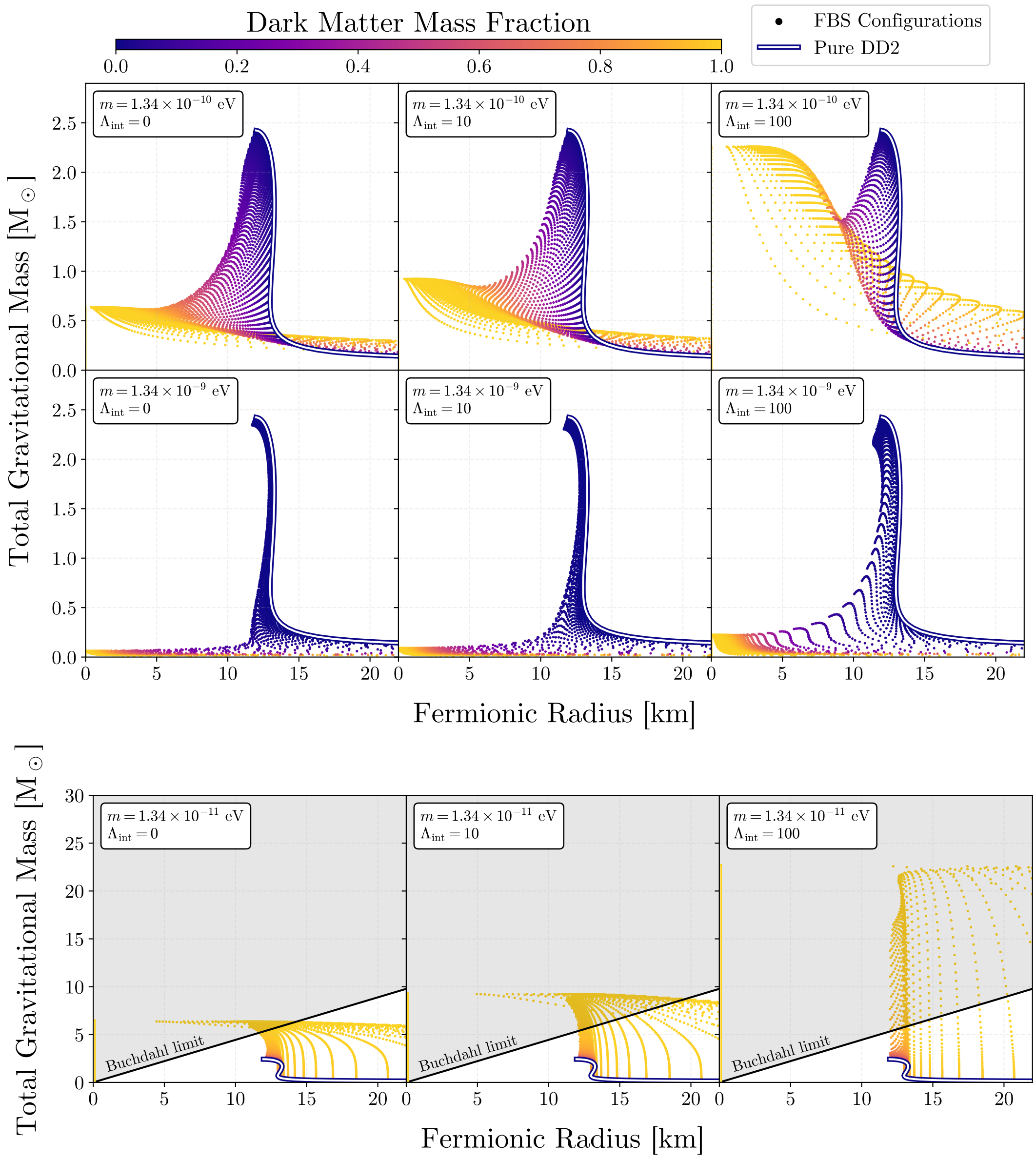

Figure 4.2: The relation between total gravitational mass M and the fermionic radius R_f for the FBSs with different DD2 forms mass fractions. The rows correspond to three different bosonic masses $m = \{1, 10, 0.1\} \cdot 1.34 \times 10^{-10}$ eV, while the columns correspond to three different $\Lambda_{\text{int}} = \{0, 10, 100\}$. The EoS we employ for the fermionic part is the DD2. Notice the different scale of the bottom plots. Observing only the fermionic radius of these systems would appear to violate the Buchdahl limit, even though the whole FBS does not.

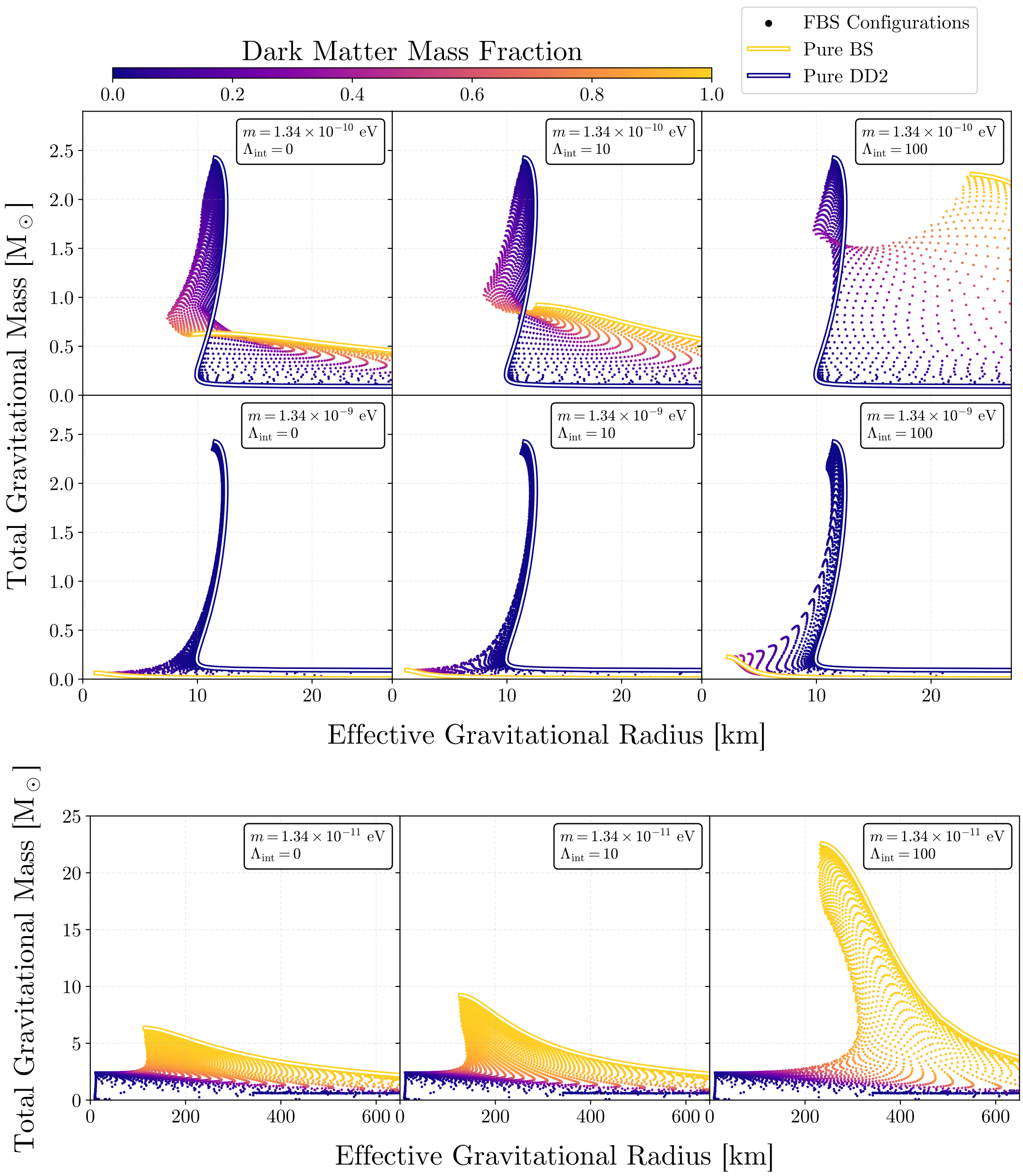

Figure 4.3: The relation between total gravitational mass M and the effective gravitational radius R_g for the FBSs with different DD2 forms mass fractions. The effective gravitational radius is the radius at which 99% of the rest mass is contained. The rows correspond to three different bosonic masses $m = \{1, 10, 0.1\} \cdot 1.34 \times 10^{-10}$ eV, while the columns correspond to three different $\Lambda_{\text{int}} = \{0, 10, 100\}$. The EoS we employ for the fermionic part is the DD2. In the case of pure neutron stars, the crust has comparatively low density, which makes this effective gravitational radius significantly smaller than the fermionic one. Notice the different scales of the bottom plots. For low masses, the bosonic component forms a core and the total compactness of the object increases. For higher masses, the bosonic component forms a cloud and can significantly decrease the compactness of the object.

4.2 Quadrupolar Love Numbers

The Love numbers are defined via the asymptotic behavior of linear perturbations around the background solutions. As a first step, we will therefore introduce metric and scalar field perturbations. Starting out with the metric perturbations, it was shown in [135] that the most general even-parity metric perturbations can be written in the form

$$h_{\mu\nu} = \sum_{\ell,m} \begin{pmatrix} fH_0 & H_1 & h_0\nabla_a \\ H_1 & h^{-1}H_2 & h_1\nabla_a \\ h_0\nabla_a & h_1\nabla_a & Kg_{ab} + r^2 G\,\nabla_a\nabla_b \end{pmatrix} Y_{\ell m}(\theta,\varphi)\,, \tag{4.2.1}$$

where H_0, H_1, h_0, h_1, K, and G are functions that depend on the radial coordinate and the numbers ℓ and m. Further, ∇_a with $a \in \{\theta, \phi\}$ denotes the covariant derivative on the 2-sphere. In order to simplify calculations, one typically exploits the gauge invariance to choose the Regge-Wheeler gauge, which is characterized by

$$h_0 = 0, \quad h_1 = 0, \quad G = 0\,. \tag{4.2.2}$$

In this way, the metric perturbations are simplified to

$$h_{\mu\nu} = \sum_{\ell,m} \begin{pmatrix} fH_0 & H_1 & 0 & 0 \\ H_1 & h^{-1}H_2 & 0 & 0 \\ 0 & 0 & Kr^2 & 0 \\ 0 & 0 & 0 & Kr^2\sin^2(\theta) \end{pmatrix} Y_{\ell m}(\theta,\varphi)\,. \tag{4.2.3}$$

Next, we introduce scalar field perturbations and also decompose them into spherical harmonics with

$$\delta\Phi = \sum_{\ell,m} \phi_1 \frac{e^{-i\omega t}}{r} Y_{\ell m}(\theta,\varphi), \tag{4.2.4}$$

where ϕ_1 depends on the radial coordinate and (ℓ, m). Finally, we are introducing matter perturbations as

$$\delta T^{\mu}{}_{\nu} = \sum_{\ell,m} \begin{pmatrix} -\delta e & 0 & 0 & 0 \\ 0 & \delta P & 0 & 0 \\ 0 & 0 & \delta P & 0 \\ 0 & 0 & 0 & \delta P \end{pmatrix} Y_{\ell m}(\theta,\varphi)\,, \tag{4.2.5}$$

where, again, δe and δP are radial functions that depend on (ℓ, m). In what follows, we will—without loss of generality—focus on the $(\ell, m) = (2, 0)$ case. This is justified by noting that, at linear order in the perturbations, the different multipole moments decouple and can thus be treated individually. Since each $\ell = 2$ moment will carry the same information about the quadrupolar Love number, we choose to set $m = 0$ for convenience.

Also, we generally note that, due to the linear nature of the perturbation equations, we will find that an externally applied quadrupolar field $\mathcal{E}_{ij}$ will result in a linear response $Q_{ij} = -\lambda_{\rm tidal}\mathcal{E}_{ij}$ with the quadrupolar Love number $\lambda_{\rm tidal}$ being the proportionality constant. As discussed in [156], these quadrupolar moments enter the g_{00} component of the metric at large radii as

$$g_{00} = -1 + \frac{2M_{\rm tot}}{r} - \mathcal{E}_{ij}x^i x^j \left(1 + \frac{3\lambda_{\rm tidal}}{r^5}\right) + \dots . \tag{4.2.6}$$

Before tending to the calculation of the FBS's quadrupolar Love numbers, we first briefly review their calculation for a pure NS, which will allow us to highlight the similarities and differences in the procedure more efficiently.

Pure Neutron Stars

The perturbation equations are now obtained by inserting the perturbed metric together with the metric perturbations into the Einstein equations and the continuity equation. The procedure is as follows:

1. From the tr component we deduce that $H_1 \equiv 0$.
2. Substracting the $\varphi\varphi$ from the $\theta\theta$ component reveals $H_0 \equiv H_2$.
3. The $r\theta$ component allows to solve for K':
$$K'(r) = H_0'(r) + H_0(r)\frac{f'(r)}{f(r)} . \tag{4.2.7}$$
4. The θ component of the continuity equation reveals that
$$\delta P(r) = \frac{1}{2}H_0(r)\Big(P(r) + e(r)\Big) \tag{4.2.8}$$
5. Substracting the rr from the tt component now results in a differential equation for H_0:
$$H_0'' + \left[\frac{2}{r} + \frac{f'}{2f} + \frac{h'}{2h}\right]H_0' - \left[\frac{c_s^2 - 1}{2M_{\rm pl}^2 h c_s^2}(e+P) + \frac{8+3rh'}{r^2 h} + \frac{rf'(rf'-5f)}{r^2 f^2} - \frac{2}{r^2}\right]H_0 = 0 \tag{4.2.9}$$

From the and we further note that the $\theta\theta$ and $\phi\phi$ components reveal that $H_2 \equiv -H_0$. Next, adding the $\theta\theta$ component to the $\phi\phi$ component allows to obtain an expression for δP. We utilize this expression to obtain a differential equation for H_0, which reads

$$H_0'' + \frac{h+1}{rh}H_0' - \frac{4(1+h^2+4h)M_{\rm pl}^4}{4M_{\rm pl}^4 r^2 h^2}H_0 = 0 . \tag{4.2.10}$$

Inserting $h = 1 - 2M/r$ we further obtain

$$r^2\left(1-\frac{2M}{r}\right)H_0''+2r\left(1-\frac{M}{r}\right)H_0'-2\left(3-\frac{6M}{r}+\frac{2M^2}{r^2}\right)\left(1-\frac{2M}{r}\right)^{-1}H_0=0\,. \tag{4.2.11}$$

As discussed in [61], there exists an exact solution to this differential equation in terms of associated Legendre polynomials, such that

$$H_0(r) = c_1 Q_2^2\left(\frac{r}{M}-1\right) + c_2 P_2^2\left(\frac{r}{M}-1\right), \tag{4.2.12}$$

with c_1 and c_2 being real constants. Expanding this solution for large radii, we then find

$$H_0(r) = 3\,c_2\left(\frac{r}{M}\right)^2\left(1-\frac{2M}{r}\right) + c_1\frac{8}{5}\left(\frac{M}{r}\right)^3 + c_1\mathcal{O}\left(r^{-4}\right). \tag{4.2.13}$$

Comparing with Eq. (4.2.6) we can identify

$$c_1 = \frac{15}{8}\frac{1}{M^3}\lambda\,\mathcal{E}\,, \quad \text{and} \quad c_2 = \frac{1}{3}M^2\mathcal{E}\,. \tag{4.2.14}$$

Since Eq. (4.2.12) is valid for the entire vacuum spacetime, i.e., the star's exterior, we can use it to match H_0 and H_0' at the star's surface in order to obtain an exact expression for λ. Doing so results in

$$\begin{aligned}\lambda =& \frac{16}{15}M^5(1-2C)^2\left[2+2C(y-1)-y\right]\Big\{2C\left[6-3y+3C(5y-8)\right]\\ &+4C^3\left[13-11y+C(3y-2)+2C^2(1+y)\right]\\ &+3(1-2C)^2\left[2-y+2C(y-1)\right]\log(1-2C)\Big\}^{-1},\end{aligned} \tag{4.2.15}$$

where $y = RH_0'(R)/H_0(R)$ and $C = M/R$, with R denoting the star's surface radius. In order to obtain the desired Love number it is thus necessary to integrate the obtained differential equation H_0 from the center of the spacetime up to the star's surface, where then Eq. (4.2.15) is used to calculate λ. Having reviewed the calculation of λ for a pure NS, we will next turn to the case of FBSs.

Fermion-Boson Stars

We use the same ansatz for the perturbed metric and matter perturbations and additionally obtain the perturbed energy momentum tensor of the scalar field by utilizing Eq. (4.2.4). Due to the involved nature of these equations, we refrain from explicitly presenting them here, but note that the construction is straightforward. Similarly to the outlined procedure above for pure NS, we next perform the following steps:

1. From the tr component we deduce that $H_1 \equiv 0$.
2. Substracting the $\varphi\varphi$ from the $\theta\theta$ component reveals $H_0 \equiv H_2$.

3. The $r\theta$ component allows to solve for K':

$$K' = H_0' + H_0 \frac{f'}{f} - 4\phi_1 \frac{\phi'}{r} \,. \tag{4.2.16}$$

4. The θ component of the continuity equation reveals that

$$\delta P = \frac{1}{2} H_0 \Big(P + e \Big) \,. \tag{4.2.17}$$

5. Substracting the rr from the tt component now results in a differential equation for H_0:

$$\begin{aligned} H_0'' + \left[\frac{2}{r} + \frac{f'}{2f} + \frac{h'}{2h} \right] H_0' - \left[\frac{c_s^2 - 1}{2M_{\rm pl}^2 h c_s^2} (e+P) + \frac{8\phi'^2}{M_{\rm pl}^2} + \frac{8+3rh'}{r^2 h} + \frac{rf'(rf'-5f)}{r^2 f^2} - \frac{2}{r^2} \right] H_0 \\ = \left[\phi \frac{4fV'(\phi^2) - 8\omega^2}{M_{\rm pl}^2 rfh} - \frac{4f'\phi'}{M_{\rm pl}^2 rf} \right] \phi_1 \,. \end{aligned} \tag{4.2.18}$$

6. Expanding the Klein-Gordon equation to linear order in the perturbation, we also obtain a differential equation for ϕ_1:

$$\begin{aligned} \phi_1'' + \left[\frac{f'}{2f} + \frac{h'}{2h} \right] \phi_1' - \left[\frac{4\phi'^2}{M_{\rm pl}^2} + \frac{2\phi^2 V''(\phi^2)}{h} + \frac{V'(\phi^2) f - \omega^2}{f\,h} + \frac{12f + r(fh' + f'h)}{2r^2 fh} \right] \phi_1 \\ = \left[\frac{r\,\phi}{f\,h} \Big(fV'(\phi^2) - 2\omega^2 \Big) - \frac{rf'\phi'}{f} \right] H_0 \,. \end{aligned} \tag{4.2.19}$$

While in the pure NS case we were able to construct an exact solution for H_0 in the exterior spacetime, this is no longer the case for the FBS system, and we can thus not apply the previously obtained expression for λ that was presented in Eq. (4.2.15). Instead, since the bosonic field decays exponentially at large radii, we find that at the exterior spacetime rapidly approaches a pure vacuum spacetime, meaning that Eq. (4.2.12) still describes the behavior of H_0, but only for asymptotically large radii. We now leverage this knowledge by matching Eq. (4.2.12) to H_0 and H_0' at what we denote as the *extraction radius* $r_{\rm ext}$, so that the obtained λ is again given by

$$\begin{aligned} \lambda = & \frac{16}{15} M^5 (1-2C_{\rm ext})^2 \big[2 + 2C_{\rm ext}(y_{\rm ext} - 1) - y_{\rm ext} \big] \Big\{ 2C_{\rm ext} \big[6 - 3y_{\rm ext} + 3C_{\rm ext}(5y_{\rm ext} - 8) \big] \\ & + 4C_{\rm ext}^3 \big[13 - 11y_{\rm ext} + C_{\rm ext}(3y_{\rm ext} - 2) + 2C_{\rm ext}^2 (1 + y_{\rm ext}) \big] \\ & + 3(1-2C_{\rm ext})^2 \big[2 - y_{\rm ext} + 2C_{\rm ext}(y_{\rm ext} - 1) \big] \log(1 - 2C_{\rm ext}) \Big\}^{-1} , \end{aligned}$$

but with $y_{\rm ext} = r_{\rm ext} H_0'(r_{\rm ext})/H_0(r_{\rm ext})$ and $C_{\rm ext} = M/r_{\rm ext}$. For sufficiently large $r_{\rm ext}$ we will thus have that the above equation converges to the desired Love number.

We obtain the necessary profile of H_0 by first preparing a background solution and then integrating Eq. (4.2.18) and Eq. (4.2.19) radially outward. To do so, we need to specify the boundary conditions of H_0 and ϕ_1 at the origin. We obtain the behavior of the fields by expanding H_0 and ϕ_1 in a power series around the origin with

$$H_0 = \sum_{i=0}^{\infty} H_{0,i}\, r^i, \quad \text{and} \quad \phi_1 = \sum_{i=0}^{\infty} \phi_{1,i}\, r^i \tag{4.2.20}$$

and then insert this expansion into Eqs. (4.2.18) and (4.2.19) in order to determine the coefficients $\phi_{1,i}$ and $H_{0,i}$. Doing so, we find that that

$$\phi_1 = \phi_{1,3}\, r^3 + \mathcal{O}\big(r^4\big), \quad \text{and} \quad H_0 = H_{0,2}\, r^2 + \mathcal{O}\big(r^3\big)\,. \tag{4.2.21}$$

Next, we note that the perturbation equations ((4.2.18) and (4.2.19)) are invariant under a rescaling of the form

$$\phi_1 \to \alpha\, \phi_1, \quad H_0 \to \alpha\, H_0\,, \tag{4.2.22}$$

with α a real constant. We leverage this symmetry in order to set $H_{0,2} = 1$ and we thus find that the perturbations are entirely determined by $\phi_{1,3}$. Further, we also define appropriate boundary conditions at asymptotic large radii as

$$H_0 \xrightarrow{r\to\infty} \mathcal{O}\big(r^2\big), \quad \phi_1 \xrightarrow{r\to\infty} \mathcal{O}\big(r^{-1}\big)\,. \tag{4.2.23}$$

We find that these boundary conditions now uniquely fix $\phi_{1,3}$. Similar to the discussion on ω, choosing a value for $\phi_{1,3}$ that slightly deviates from the one that would fulfill the conditions in Eq. (4.2.23), we obtain a profile for ϕ_1 that will either diverge to $+\infty$ or $-\infty$ and changes its direction of divergence when $\phi_{1,3}$ passes the desired value. We use this fact to again perform a bisection search that allows us to efficiently determine $\phi_{1,3}$.

4.2.1 Numerical Results

While the discussion up to this point was done for a general scalar field potential V, we now specialize to a potential that is quartic in the field and explicitly given by

$$V(\bar{\Phi}\Phi) = m^2\bar{\Phi}\Phi + \frac{\lambda}{2}(\bar{\Phi}\Phi)^2, \tag{4.2.24}$$

where m is the scalar field mass and λ the quartic self-interaction strength. As was shown in [59], it is convenient to introduce the effective self-interaction strength $\Lambda_{\text{int}} = \lambda\, M_{\text{pl}}^2/m^2$. In general, one finds that for $\Lambda_{\text{int}} \ll 1$ the gravitational mass of the boson star scales as $M \propto M_{\text{pl}}^2/m$, while for $\Lambda_{\text{int}} \gg 1$ it scales as $M \propto M_{\text{pl}}^3/m^2$.

Further, in order to ensure that the self-interaction strength does not violate constraints from, e.g., the bullet cluster, we impose [157, 158]

$$\frac{\sigma}{m} < 1\,\frac{\text{cm}^2}{\text{g}} \tag{4.2.25}$$

and since $\sigma = \lambda^2/(64\pi m^3)$, we can directly follow that

$$\Lambda_{\text{int}} < 10^{50}\sqrt{\frac{1.34 \cdot 10^{-10}\,\text{eV}}{m}}\,. \tag{4.2.26}$$

This constrain is readily satisfied for the self-interaction strengths we consider here, which are in the range of $\Lambda_{\text{int}} \leq 100$.

In Figure 4.4 we present the extracted dimensionless Love number $\Lambda = \lambda/M^5$ for the cases of $m \in \{1.34 \times 10^{-11}, 1.34 \times 10^{-10}, 1.34 \times 10^{-9}\}$ and $\Lambda_{\text{int}} \in \{0, 10, 100\}$. We first generally observe that the obtained Love numbers smoothly transition between pure NS and pure BS configurations when varying the dark matter mass fraction. We next note that the impact on the Love numbers generally diminishes when the scalar field mass increases, as can be seen in the $m = 1.34 \times 10^{-9}\,\text{eV}$ case, such that the deviations from a pure NS only become pronounced when the dark matter mass fraction is close to 100 %. Contrarily, light scalar field masses, as is the case with $m = 1.34 \times 10^{-11}\,\text{eV}$, typically impact the deformability quite significantly by increasing the Love numbers multiple orders of magnitude. We can qualitatively understand this behavior being due to the scalar field arranging itself in a core configuration for large scalar field masses and cloud configuration for lighter scalar field masses. Since a DM cloud extents far beyond the NS, it is typically only weakly bound and thus more easily deformed. The core configuration, on the other hand, is more tightly bound, harder to deform, and hence only marginally modifies the deformability.

Increasing the self-interaction strength has a similar qualitative impact as decreasing the scalar field mass. We can understand this influence with the same reasoning, as larger self-interaction strengths lead to greater extended DM configurations, which then are more easily deformed.

4.2.2 Comparison to Observational Data

The left panel of Fig. 4.5 compares the masses and radii of obtained configurations with fixed scalar mass and self-interaction to observational data on masses and radii of pulsars. For this purpose, we have chose one scalar mass that results in a core configuration and one that results in a cloud configuration and plotted lines of constant dark matter mass fractions with the percentages denoting each used value. The object HESS J1731-347 typically requires DM core configurations in order to reach the required radius. On the other hand, pulsar mass measurements favor DM cloud configurations in order to reach the observed gravitational masses.

Further, the right panel of Fig. 4.5 similarly presents the tidal deformability and compares it to the constraint obtained from GW170817 [164]. We observe that light scalar field masses can enhance the deformability by multiple order of magnitude, even if the dark matter fraction is only 0.5 %. This is in contrast to the left panel of the same figure,

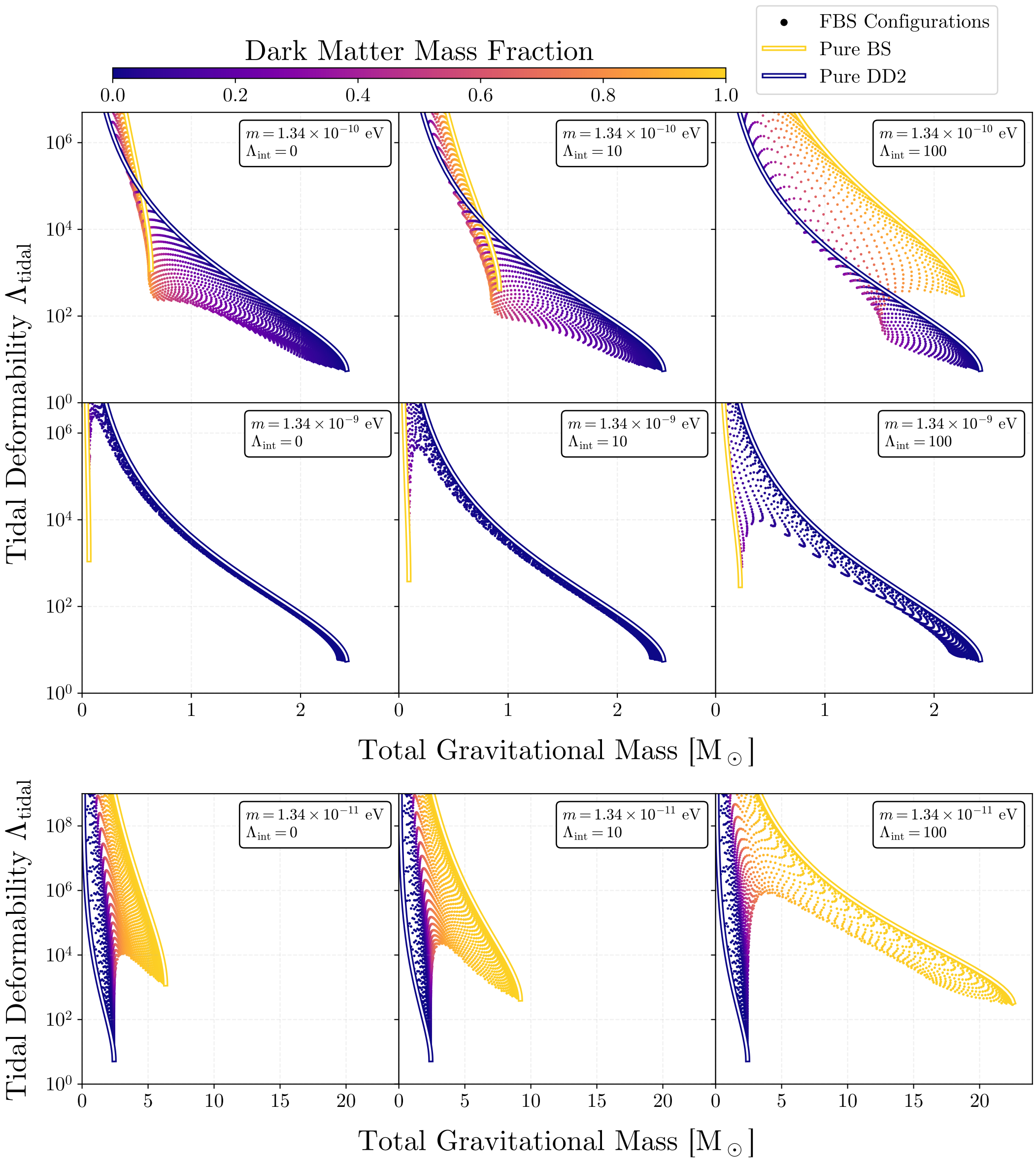

Figure 4.4: The relation between dimensionless tidal deformability $\Lambda_{\text{tidal}} = \lambda_{\text{tidal}}/M^5$ and total gravitational mass M for the FBSs with different DM mass fraction. The rows correspond to three different bosonic masses $m = \{1, 10, 0.1\} \cdot 1.34 \times 10^{-10}$ eV, while the columns correspond to three different interactions strengths $\Lambda_{\text{int}} = \{0, 10, 100\}$. For the fermionic part, we employ the DD2 EoS.

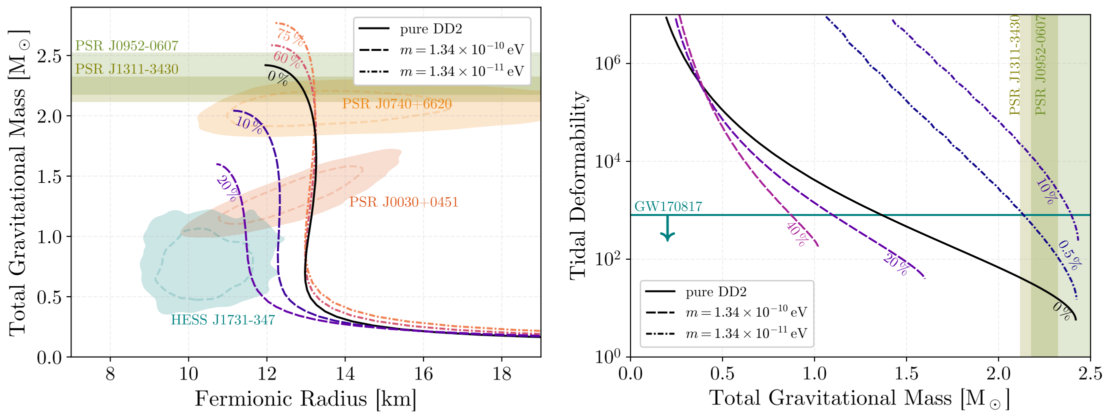

Figure 4.5: Left panel: Resulting mass and radii of FBS for the two cases of $m = 1.34\times10^{-10}$ eV and $m = 1.34 \times 10^{-11}$ eV shown together with constraints from HESS J1731-347 [159], PSR J0030+0451 [160], PSR J0740+6620 [161], PSR J1311-3430 [162] and J0952-0607 [163]. In both cases, the self-interaction was set to zero and the percentage number denotes the DM mass fraction. For the NICER and HESS measurements, dashed lines display the 1σ, while straight lines show the 2σ regions. **Right panel:** Dimensionless tidal deformability for the same set of parameters shown together with the constraint coming from the GW170817 event [164].

where a mass fraction of 60 % was necessary to impact the mass-radius curve significantly. At the same time, the core configuration also requires much higher DM fractions to impact the deformability. We find this to be a strong indicator that measurements of the tidal deformability can put significant constraints on the presence of light DM clouds around neutron stars.

4.2.3 Effective Equation of State

It was noted in [59] that the energy momentum tensor becomes isotropic in the limit $\Lambda_{\text{int}} \gg 1$ and one can hence construct an effective EOS that is given by

$$P = \frac{2m^4}{9\lambda}\left[\left(1 + \frac{3\lambda}{2m^4}\,e\right)^{1/2} - 1\right]^2 . \tag{4.2.27}$$

This effective EOS was used in [165] to investigate the tidal deformability of DM admixed NS using a two fluid approach. We here follow their construction and compare the resulting Love numbers to those we obtained by solving the full system.

In order to compare both approaches, we calculate the resulting FBS configurations for various values of Λ_{int} and then consider the relative differences in the obtained masses and tidal deformabilities. From this, we further obtain the relative differences of the bottom 50 %, 68 %, and 95 % of configurations, which we plot in Fig. 4.6. As an example, the straight line shows what fraction of obtained configurations has a relative error of less than 50 %. We generally observe that increasing Λ_{int} overall improves the accuracy of the effective EOS, but generally find that even for $\Lambda_{\text{int}} = 300$ there remain configurations that deviate by more than 1000 %, indicating that one has to be cautious when employing

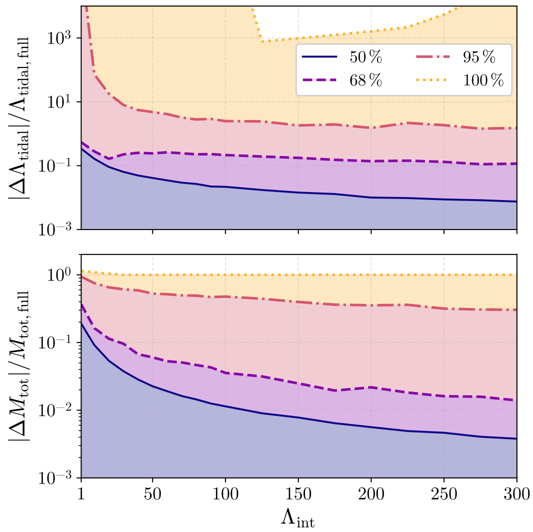

Figure 4.6: Relative difference between the full and effective systems for the dimensionless tidal deformability Λ_{tidal} (upper panel) and total mass M_{tot} (lower panel) as a function of Λ_{int}. The lines show the relative difference for a given fraction of configurations. For example, 50 % of obtained configurations have a relative difference that falls below the straight line. Only stable FBS were considered for the relative error at a given Λ_{int} and computations were performed for $m = 6.7 \times 10^{-11}$ eV.

this effective EOS.

4.3 Conclusion

We derived the quadrupolar perturbation equations of a system that consists of a minimally coupled complex scalar field and nuclear matter in a spherically symmetric and static system. We were further able to numerically construct solutions to these perturbation equations and relate their behavior for asymptotically large radii to the quadrupolar Love numbers. We then numerically constructed background and perturbation profiles for FBS configurations and analyzed their behavior. We here found that core-like configurations typically decrease the value of observables, such as the mass, radii, and tidal deformability, while cloud-like configurations increases them.

Having obtained the Love numbers, we next compared them to observational data of pulsars, where we noticed that observational uncertainties are too large to make conclusive statements about the presence or nature of DM. We noted, however, that already small fractions of DM in cloud-like configurations can significantly enhance the tidal deformability and thus be a potential smoking-gun signature for DM clouds. Additional observations of NS-NS inspiral events will here help to bring more clarity, especially by testing EOS-insensitive relations that can give strong hints on the presence of DM in NS.

In addition to our analysis of the Love numbers resulting from the full system, we also studied the deviations that arise when utilizing an effective EOS together with a two-fluid approach. This approach is expected to be valid in the limit where $\Lambda_{\text{int}} \gg 1$ since the EMT of the scalar field becomes isotropic in this limit and can thus be described by an ideal fluid. We found that the tidal deformabilities obtained from both approaches indeed typically agree for $\Lambda_{\text{int}} \gg 1$. However, certain configurations still result in significantly different values, with a relative difference of $\approx 100\,\%$ in the tidal deformability at $\Lambda_{\text{int}} = 300$, which signals the need for caution when using the effective EOS.

Chapter 5

Quadrupolar Love Numbers in Horndeski Theory

"We wondered who would be crazy enough to work with such equations. Then crazy showed up! And is still here today."

— **Gregory W. Horndeski**, 50 years after discovering Horndeski's Theory

The previous chapter introduced the PP action that encodes finite-size effects via Wilsonian coefficients. While we were able to connect the Wilsonian coefficients to observable quantities, such as the power loss and the GW phase, it remains to establish a procedure that allows us to derive the Wilsonian coefficients themselves for a given theory. While this is most easily done for the gravitational mass, which can be extracted from the asymptotic behavior of the metric fields in a gauge-invariant way, the procedure is not as trivial for, e.g., the Love numbers, which quantify the deformability of the gravitational field due to an external gravitational field.

The aim of this section is to outline the general matching procedure for Horndeski Theory, which is the most general scalar-tensor theory that has at most second-order equations of motion. The total action can be written as

$$\mathcal{S} = \int \mathrm{d}^4x\sqrt{-g}\,\mathcal{L}_\mathrm{H} + \mathcal{S}_m(g_{\mu\nu})\,, \tag{5.0.1}$$

where $g_{\mu\nu}$ is the spacetime metric, g its determinant, $\mathcal{L}_\mathrm{H}$ the Horndeski Lagrangian, and $\mathcal{S}_m$ the matter action, which is minimally coupled. The Horndeski Lagrangian can be expressed as

$$\begin{aligned}\mathcal{L}_\mathrm{H} = G_2 - G_3\Box\phi + G_4R + G_5G_{\mu\nu}\nabla^\mu\nabla^\nu\phi + G_{4,X}\Big[(\Box\phi)^2 - (\nabla_\mu\nabla_\nu\phi)(\nabla^\mu\nabla^\nu\phi)\Big] \\ - \frac{1}{6}G_{5,X}\Big[(\Box\phi)^3 - 3(\Box\phi)(\nabla_\mu\nabla_\nu\phi)(\nabla^\mu\nabla^\nu\phi) + 2(\nabla^\mu\nabla_\alpha\phi)(\nabla^\alpha\nabla_\beta\phi)(\nabla^\beta\nabla_\mu\phi)\Big]\,.\end{aligned} \tag{5.0.2}$$

where G_2, G_3, G_4, and G_5 are functions that only depend on the scalar field ϕ and its kinetic term $X \equiv \partial_\mu\phi\partial^\mu\phi/2$. Further, R denotes the Ricci scalar, $G_{\mu\nu}$ the Einstein tensor, and $\Box \equiv \nabla_\mu\nabla^\mu$ the d'Alambert operator. Also, in order to simplify notation, we denote partial derivatives with respect to X with a comma in the subscript, such that, e.g., $G_{4,X} \equiv \partial_X G_4$.

We model the matter sector as a perfect fluid that is minimally coupled to the gravitational sector, such that its action can be described by the Schutz-Sorkin action

$$\mathcal{S}_m = -\int \mathrm{d}^4x \Big[\sqrt{-g}\, e(n) + J^\mu(\partial_\mu\ell + \mathcal{A}_i\partial_\mu\mathcal{B}^i)\Big] , \tag{5.0.3}$$

where e denotes the total energy density, J^μ is related to the fluid's four velocity via

$$u^\mu = \frac{J^\mu}{n\sqrt{-g}} \tag{5.0.4}$$

and the remaining quantities — ℓ, $\mathcal{A}_i$, and $\mathcal{B}^i$ — are Lagrange multiplier. It is straightforward to see that varying the Schutz-Sorkin action with respect to the metric $g_{\mu\nu}$, one obtains the usual EMT of a perfect fluid

$$T_{\mu\nu} = (e + P)\, u_\mu u_\nu + P g_{\mu\nu} , \tag{5.0.5}$$

where $P = ne_{,p} - e$ denotes the fluid's pressure. As usual, we have that the fluid's EMT is covariantly conserved with

$$\nabla_\mu T^\mu{}_\nu = 0 . \tag{5.0.6}$$

5.1 Background Equations

In order to construct spherically symmetric and static background configurations, we consider the usual Schwarzschild coordinates, so that the line element is given by

$$\mathrm{d}s^2 = -f(r)\mathrm{d}t^2 + h^{-1}(r)\mathrm{d}r^2 + r^2\mathrm{d}\Omega^2 , \tag{5.1.1}$$

where f and h are functions of the radial coordinate r only. Also $\mathrm{d}\Omega = \mathrm{d}\theta^2 + \sin(\theta)^2\mathrm{d}\varphi^2$ is the usual line element on the two-sphere. In order to derive the background equations, we now vary the total action first with respect to the metric, which results in

$$\mathcal{E}_{00} \equiv \left(A_1 + \frac{A_2}{r} + \frac{A_3}{r^2}\right)\phi'' + \left(\frac{\phi'}{2h}A_1 + \frac{A_4}{r} + \frac{A_5}{r^2}\right)h' + A_6 + \frac{A_7}{r} + \frac{A_8}{r^2} = \rho\,, \tag{5.1.2a}$$

$$\mathcal{E}_{11} \equiv -\left(\frac{\phi'}{2h}A_1 + \frac{A_4}{r} + \frac{A_5}{r^2}\right)\frac{hf'}{f} + A_9 - \frac{2\phi'}{r}A_1 - \frac{1}{r^2}\left[\frac{\phi'}{2h}A_2 + (h-1)A_4\right] = P\,, \tag{5.1.2b}$$

$$\begin{aligned}\mathcal{E}_{22} \equiv{}& \left[\left\{A_2 + \frac{(2h-1)\phi' A_3 + 2hA_5}{h\phi' r}\right\}\frac{f'}{4f} + A_1 + \frac{A_2}{2r}\right]\phi'' \\ &+ \frac{1}{4f}\left(2hA_4 - \phi' A_2 + \frac{2hA_5 - \phi' A_3}{r}\right)\left(f'' - \frac{f'^2}{2f}\right) \\ &+ \left[A_4 + \frac{2h(2h+1)A_5 - \phi' A_3}{2h^2 r}\right]\frac{f'h'}{4f} + \left(\frac{A_7}{4} + \frac{A_{10}}{r}\right)\frac{f'}{f} \\ &+ \left(\frac{\phi'}{h}A_1 + \frac{A_4}{r}\right)\frac{h'}{2} + A_6 + \frac{A_7}{2r} = -P\,,\end{aligned} \tag{5.1.2c}$$

where A_1 to A_{10} denote functions that depend on f, h, ϕ, and X. Their explicit expressions are given in App. 5.A. The continuity equation further provides a differential equation for P

$$\mathcal{E}_P \equiv P' + \frac{f'}{2f}(\rho + P) = 0\,. \tag{5.1.3}$$

Lastly, varying the action with respect to the scalar field ϕ we obtain the scalar field's equation of motion that we can conveniently express as

$$\mathcal{E}_\phi \equiv -\frac{2}{\phi'}\left[\frac{f'}{2f}\mathcal{E}_{00} + \mathcal{E}'_{11} + \left(\frac{f'}{2f} + \frac{2}{r}\right)\mathcal{E}_{11} + \frac{2}{r}\mathcal{E}_{22} + \mathcal{E}_P\right] = 0\,. \tag{5.1.4}$$

Upon specifying an equation of state together with boundary conditions at the origin, we can integrate the above-presented set of equations outward in order to solve for the fluid's density profile, the scalar field, and the metric functions.

5.2 Perturbation Equations

The general equations describing perturbations were presented in [166] and we will here briefly review the most important steps that the authors took. We start out by introducing metric perturbations by splitting the metric $g_{\mu\nu} = \bar{g}_{\mu\nu} + h_{\mu\nu}$, so that $\bar{g}_{\mu\nu}$ denotes the background metric—with the line element given in Eq. (5.1.1)—while $h_{\mu\nu}$ denotes the perturbations. As was discussed in [135], $h_{\mu\nu}$ can generally be decomposed into

$$h_{\mu\nu} = \sum_{\ell,m}\begin{pmatrix} fH_0 & H_1 & h_0\nabla_a \\ H_1 & h^{-1}H_2 & h_1\nabla_a \\ h_0\nabla_a & h_1\nabla_a & Kg_{ab} + r^2 G\nabla_a\nabla_b\end{pmatrix} Y_{\ell m}(\theta,\varphi)\,, \tag{5.2.1}$$

where H_0, H_1, h_0, h_1, K, and G are functions that only depend on the radial coordinate and the numbers (ℓ, m), which characterize the spherical harmonic $Y_{\ell m}$. We similarly split the scalar field into

$$\phi = \bar{\phi}(r) + \sum_{\ell,m} \delta\phi(r) Y_{\ell m}(\theta,\varphi)\,, \tag{5.2.2}$$

where $\bar{\phi}$ denotes the background solution and $\delta\phi$ the perturbations, which we also decomposed into spherical harmonics. We also introduce perturbations into the number density and four velocity of the fluid via

$$\delta n = \sum_{l,m} \frac{\delta\rho(r)}{\rho_{,n}(r)} Y_{lm}(\theta,\varphi)\,, \tag{5.2.3}$$

$$u_r = \sum_{l,m} \delta u_r(r) Y_{lm}(\theta,\varphi)\,, \tag{5.2.4}$$

$$u_a = \sum_{l,m} v(r) \nabla_a Y_{lm}(\theta,\varphi)\,. \tag{5.2.5}$$

The authors of [166] next inserted the perturbed quantities into the action in Eq. (5.0.1) and expanded it up to second order in the perturbations. In this way, they arrive at an action that describes the linear perturbations, and they obtain their equations of motion by varying said action with respect to the perturbed quantities. While the authors performed these calculations without specializing the perturbations to a gauge, we find it most convenient to choose the Regge-Wheeler gauge in order to simplify the equations. This gauge is characterized by

$$h_0 = 0\,, \qquad h_1 = 0\,, \qquad G = 0\,. \tag{5.2.6}$$

Also, we can make one further simplification before presenting the full set of equations. Varying the second-order action with respect to H_1, we obtain

$$\left[2Lb_1 - \frac{r^2(\rho+P)\sqrt{h}}{\sqrt{f}}\right] H_1 + r^2(\rho+P)\sqrt{h}\,\delta u_r = 0\,, \tag{5.2.7}$$

where $L = \ell(\ell+1)$ and the definition of b_1 is given in App. 5.B. Varying $\mathcal{S}^{(2)}$ with respect to $\delta\mathcal{A}_1$, we further obtain

$$H_1 = \sqrt{f}\,\delta u_r\,. \tag{5.2.8}$$

Combining these two equations we deduce that

$$2L\,b_1\,H_1 = 0 \tag{5.2.9}$$

and since generally $b_1 \neq 0$, we must have that $H_1 \equiv 0$.

The general perturbation equations of motion that result from varying $\mathcal{S}^{(2)}$ with respect to the metric and scalar field perturbations are given in Eqs. (4.30) to (4.37) in [166]. In our gauge choice together with $H_1 \equiv 0$ and specializing to static perturbations we find that

$$
\begin{aligned}
0 &= a_1\delta\phi'' + a_2\delta\phi' + a_3H_2' + (a_5 + La_6)\delta\phi + (a_7 + La_8)H_2 \\
&\quad + \frac{r^2\sqrt{f}}{2\sqrt{h}}\delta\rho - 2g_2K'' - 2g_{13}K' + (L-2)k_1K\,,
\end{aligned}
\tag{5.2.10a}
$$

$$
\begin{aligned}
0 &= c_2\delta\phi' + (c_3 + Lc_4)\delta\phi + 2c_6H_2 - a_3H_0' + (La_8 + a_7 - a_3')H_0 \\
&\quad - 2g_{14}K' + k_2(L-2)K\,,
\end{aligned}
\tag{5.2.10b}
$$

$$
0 = d_2\delta\phi' + d_3\delta\phi - a_4H_0' + (a_9 - a_4')H_0 + c_5H_2 - g_{16}K'\,,
\tag{5.2.10c}
$$

$$
\begin{aligned}
0 &= -2g_2H_0'' - 4g_4K'' - 4g_4'K' + 2g_{12}\delta\phi'' + 2(g_{13} - 2g_2')H_0' + 2g_{14}H_2' \\
&\quad + 2(g_{15} + g_{12}')\delta\phi' + \left[(L-2)k_3 + 2g_{15}'\right]\delta\phi \\
&\quad + \left[(L-2)k_1 - 2g_2'' + 2g_{13}'\right]H_0 + \left[(L-2)k_2 + 2g_{14}'\right]H_2\,,
\end{aligned}
\tag{5.2.10d}
$$

$$
0 = (L-2)\left(k_1H_0 + k_2H_2 + k_3\delta\phi\right)\,,
\tag{5.2.10e}
$$

$$
\begin{aligned}
0 &= -2e_2\delta\phi'' + 2(e_3 + Le_4)\delta\phi + a_1H_0'' + (2a_1' - a_2)H_0' \\
&\quad + (a_1'' - a_2' + a_5 + La_6)H_0 - c_2H_2' - (c_2' - c_3 - Lc_4)H_2 \\
&\quad - 2e_2'\delta\phi' + 2g_{12}K'' - 2(g_{15} - g_{12}')K' + k_3(L-2)K\,,
\end{aligned}
\tag{5.2.10f}
$$

where the functions a_1, a_2, etc., are defined in App. 5.B. Also, varying $\mathcal{S}^{(2)}$ with respect to δe we find

$$
\delta\rho = \frac{\rho + P}{2c_s^2}H_0\,,
\tag{5.2.11}
$$

where c_s is the matter fluid's sound speed, which is defined via $c_s^2 = \partial P/\partial e$.

In order to numerically solve the above-presented system of differential equations, we find it convenient to rearrange them by eliminating K, H_2, and δe and thus reducing the system to only two coupled differential equations for H_0 and $\delta\phi$. The procedure is as follows:

1. We use Eq. (5.2.11) to eliminate all occurrences of δe.

2. According to Eq. (5.2.10e), we find that for $\ell > 1$

$$
H_2 = -\frac{k_1}{k_2}H_0 - \frac{k_3}{k_2}\delta\phi\,,
\tag{5.2.12}
$$

   which allows us to eliminate H_2 in favor of H_0 and $\delta\phi$.

3. Next, Eq. (5.2.10c) and Eq. (5.2.10b) provides us with expressions for K and K' in terms of H_0 and $\delta\phi$. From these expressions, it is straightforward to also obtain K'' in terms of H_0 and $\delta\phi$.

4. Inserting the expressions of K, K', and K'' into Eq. (5.2.10a) and Eq. (5.2.10f) we obtain two coupled differential equations that we can solve for H_0 and $\delta\phi$.

Since the resulting differential equations are quite lengthy for the general case, we will refrain from presenting them here. We will instead study them more closely upon specializing to specific models later. Before continuing on with our discussion on the perturbation equations, we will take a moment to review the point particle action approach and construct the relevant worldline operators that will describe quadrupolar perturbations.

5.3 Point Particle Action

While the PP action was already extensively discussed in Sec. 3.2.1, we will here briefly review the most essential parts. When constructing the PP action in pure GR, we are free to add any curvature invariant quantity to the action, such that we may write, e.g.,

$$\mathcal{S}_{\rm pp} = -\int \mathrm{d}\tau \left(M + c_R R + d_R u^\mu u^\nu R_{\mu\nu} + \dots\right) , \tag{5.3.1}$$

where we have added the Ricci scalar R and Ricci tensor $R_{\mu\nu}$. When considering an additional scalar degree of freedom, then we may further consider couplings of the scalar field to the PP worldline, so that the PP action becomes

$$\mathcal{S}_{\rm pp} = -\int \mathrm{d}\tau \left(M + Q\frac{\phi}{M_{\rm pl}} + p\frac{\phi^2}{M_{\rm pl}^2} + \dots\right) , \tag{5.3.2}$$

where Q and p are denoted as the *scalar charge* and *induced charge*, respectively. In order to incorporate quadrupolar tidal effects, we need to introduce curvature invariants that contain second derivatives of the metric and scalar field at quadratic order. For example, in pure GR we know that the even-partiy quadrupolar tidal deformability is captured by

$$\mathcal{S}_{\rm pp} \supset \int \mathrm{d}\tau \,\frac{\lambda_{hh}}{4} E_{\mu\nu}E^{\mu\nu} , \tag{5.3.3}$$

where

$$E_{\mu\nu} = u^\alpha u^\beta R_{\mu\alpha\nu\beta} \tag{5.3.4}$$

is a even-parity projection of the Riemann tensor. From these considerations it is now straightforward to introduce the additional operators that appear due to the presence of the scalar field. We find that there are in total three possible terms given by

$$\mathcal{S}_{\rm pp} \supset \mathcal{S}_{\rm pp}^{\lambda} = \int \mathrm{d}\tau \left(\frac{\lambda_{hh}}{4} E_{\mu\nu}E^{\mu\nu} + \frac{\lambda_{h\phi}}{2M_{\rm pl}} E^{\mu\nu}\nabla_\mu\nabla_\nu\phi + \frac{\lambda_{\phi\phi}}{4M_{\rm pl}^2}\nabla_\mu\nabla_\nu\phi\nabla^\mu\nabla^\nu\phi\right) , \tag{5.3.5}$$

where we have introduced $\lambda_{h\phi}$ and $\lambda_{\phi\phi}$ that are the Wilsonian coefficients of the two additional operators. Also, we use $\mathcal{S}_{\rm pp}^{\lambda}$ to denote all operators in $\mathcal{S}_{\rm pp}$ that encode information about the quadrupolar and even-parity Love numbers.

While we will later see exactly how the Love numbers impact the asymptotic behavior of the perturbations, we can intuitively understand their role as follows: Suppose one applies an external gravitational field to the PP, then the PP's own fields will deform as a consequence and λ_{hh} and $\lambda_{h\phi}$ quantify the strength of the quadrupolar deformation in the metric and scalar field, respectively. Note that this means that an external gravitational field will thus generally source a scalar field perturbation, even if the background scalar field vanishes. Instead of an external gravitational field, one may apply an external scalar field, which will then, again, source a quadrupolar reaction in the metric and scalar field, quantified by $\lambda_{h\phi}$ and $\lambda_{\phi\phi}$, respectively. One important note is that a scalar field response due an external gravitational field and a gravitational response due to an external scalar field are both quantified by the same parameter $\lambda_{h\phi}$.

5.4 Minimally Coupled Scalar Field

As a first case study to apply the so-far outlined methods, we will study the behavior of a minimally coupled and massless scalar field combined with the usual Einstein-Hilbert action. The total action is thus given by

$$\mathcal{S}_{\text{bulk}} = \mathcal{S}_{\text{EH}} + \mathcal{S}_{\phi} = \int \mathrm{d}^4x\sqrt{-g}\left(\frac{M_{\text{pl}}^2}{2}R - \frac{1}{2}\nabla_\mu\phi\nabla^\mu\phi\right) . \tag{5.4.1}$$

We can arrive at the same action by setting

$$G_2 = X\,, \quad G_3 = 0\,, \quad G_4 = \frac{M_{\text{pl}}^2}{2}\,, \quad G_5 = 0 \tag{5.4.2}$$

in the Horndeski action and can hence apply the previously presented perturbation equations.

While this setup seems overly simplistic at first glance, it is important to note that the asymptotic behavior that we derive for this model will be identical to any model that reduces to Eq. (5.4.1) in vacuum and is thus directly applicable to any such model. As a specific example, one may consider a model in which the scalar field couples to the trace of the EMT. Also, the background field equations can be solved in an analytic closed form by using Just coordinates with the solution known as the Janis-Newman-Winicour spacetime. However, since there is no general closed-form solution for Horndeski theory, we will only work with asymptotic expansions that we construct in powers of the radial coordinate. In this way, we can present how one would perform the analysis for an arbitrary model.

5.4.1 Asymptotic Expansion

We begin by deriving the asymptotic expansion of the background fields using the in Eqs. (5.1.2a) – (5.1.3) presented background equations. By inserting the expressions for the G_i functions of Eq. (5.4.2), we find that the background equations simplify to

$$h' = \frac{1-h}{r} - \frac{rh\phi'^2}{2M_{\rm pl}^2}\,, \quad \frac{f'}{f} - \frac{h'}{h} = \frac{r\phi'^2}{M_{\rm pl}^2}\,, \quad \phi'' + \frac{h+1}{rh}\phi' = 0\,. \tag{5.4.3}$$

Next, we use the following ansatz for the asymptotic behavior

$$f = \sum_{i=0}^{\infty} f_i\, r^{-i}\,, \quad h = \sum_{i=0}^{\infty} h_i\, r^{-i}\,, \quad \phi = \sum_{i=0}^{\infty} \phi_i\, r^{-i}\,, \tag{5.4.4}$$

where the f_i, h_i, and ϕ_i are real coefficients. Note that we require $f_0 = h_0 = 1$ in order to arrive at an asymptotically flat spacetime. We insert this ansatz into the background equations and then solve these order by order in r. Up to to order r^{-4} we obtain

$$f = 1 - \frac{2M}{r} + \frac{M\phi_1^2}{6M_{\rm pl}^2 r^3} + \frac{M^2\phi_1^2}{3M_{\rm pl}^2 r^4} + \mathcal{O}(r^{-5})\,, \tag{5.4.5a}$$

$$h = 1 - \frac{2M}{r} + \frac{\phi_1^2}{2M_{\rm pl}^2 r^2} + \frac{M\phi_1^2}{2M_{\rm pl}^2 r^3} + \frac{2M^2\phi_1^2}{3M_{\rm pl}^2 r^4} + \mathcal{O}(r^{-5})\,, \tag{5.4.5b}$$

$$\phi = \phi_0 + \frac{\phi_1}{r} + \frac{M\phi_1}{r^2} + \frac{\phi_1(16M^2M_{\rm pl}^2 - \phi_1^2)}{12M_{\rm pl}^2 r^3} + \frac{M\phi_1(6M^2M_{\rm pl}^2 - \phi_1^2)}{3M_{\rm pl}^2 r^4} + \mathcal{O}(r^{-5})\,, \tag{5.4.5c}$$

where we have identified $h_1 = -2M$. In general, we find that every coefficient is completely determined in terms of M and ϕ_1. We will later see that we can identify (up to a constant factor) ϕ_1 with the scalar charge that appears in the PP action. Also, even though ϕ_0 appears as a free parameter in the expansion, we note that it can not have any impact on observables since the total action is symmetric under shifts of the form $\phi \to \phi + \alpha$ for any real α and we may thus set $\phi_0 = 0$ for convenience. We have in total derived the background expansion up to order r^{-9} and present the obtained coefficients explicitly in App. 5.C.1.

Having obtained the background expansion, we can now similarly construct an asymptotic expansion of the perturbation fields. We first note that the perturbation equations simplify to

$$0 = H_0'' + \frac{h+1}{rh}H_0' - \frac{4[1+h^2+(L-2)h]M_{\rm pl}^4 - 4hr^2\phi'^2(h-1)M_{\rm pl}^2 + r^4h^2\phi'^4}{4M_{\rm pl}^4 r^2h^2}H_0 \tag{5.4.6a}$$
$$- \frac{\phi'[2M_{\rm pl}^2(h-1) - r^2h\phi'^2]}{M_{\rm pl}^4 rh}\delta\phi\,,$$

$$0 = \delta\phi'' + \frac{h+1}{rh}\delta\phi' - \frac{2r^2h\phi'^2 + LM_{\rm pl}^2}{M_{\rm pl}^2 r^2 h}\delta\phi + \frac{\phi'[2(1-h)M_{\rm pl}^2 + r^2h\phi'^2]}{2M_{\rm pl}^2 rh}H_0\,. \tag{5.4.6b}$$

We now use the following ansatz for the asymptotic behavior of the perturbation fields

$$H_0 = \sum_{i=-2}^{\infty} H_{0,i} r^{-i} \,, \quad \delta\phi = \sum_{i=-2}^{\infty} \delta\phi_i r^{-i} \,, \tag{5.4.7}$$

where the $H_{0,i}$ and $\delta\phi_i$ are real coefficients. We insert this ansatz into the perturbation equations together with the previously obtained expansion of the background fields and again solve them order by order in r. Up to order r^{-3} we find that

$$\begin{aligned} H_0(r) &= H_{0,-2} r^2 - 2H_{0,-2} M r + \frac{\phi_1 (H_{0,-2}\phi_1 - 2\delta\phi_{-2} M)}{3M_{\mathrm{pl}}^2} \\ &\quad + \frac{H_{0,-2} M \phi_1^2}{6M_{\mathrm{pl}}^2 r} + \frac{H_{0,-2} M^2 \phi_1^2}{3M_{\mathrm{pl}}^2 r^2} + \frac{H_{0,3}}{r^3} + \mathcal{O}\left(r^{-4}\right) \,, \end{aligned} \tag{5.4.8a}$$

$$\begin{aligned} \delta\phi(r) &= \delta\phi_{-2} r^2 - 2\delta\phi_{-2} M r + \frac{M(2M\delta\phi_{-2} - H_{0,-2}\phi_1)}{3} \\ &\quad + \frac{\delta\phi_{-2} M \phi_1^2}{6M_{\mathrm{pl}}^2 r} + \frac{\delta\phi_{-2} M^2 \phi_1^2}{3M_{\mathrm{pl}}^2 r^2} + \frac{\delta\phi_3}{r^3} + \mathcal{O}\left(r^{-4}\right) \,. \end{aligned} \tag{5.4.8b}$$

In total, we have derived the expansion up to order r^{-8} and present the obtained coefficients in App. 5.C.1. We note that the asymptotic series is completely determined by $H_{0,-2}$, $H_{0,3}$, $\delta\phi_{-2}$, and $\delta\phi_3$. Intuitively we can expect $H_{0,-2}$ and $\delta\phi_{-2}$ to quantify the strength of the externally applied quadrupolar field, while $H_{0,3}$ together with $\delta\phi_3$ quantify the object's response due to the external fields. At this point, we do not have the means to make this separation between external and response field rigorous and will instead leverage the PP EFT approach in the section for this purpose. However, due to the linear nature of the perturbation equations, we can already deduce that it is possible to express $H_{0,3}$ and $\delta\phi_3$ as

$$H_{0,3} = c_{hh} H_{0,-2} + c_{h\phi}\delta\phi_{-2} \,, \quad \delta\phi_3 = c_{\phi\phi}\delta\phi_{-2} + c_{\phi h} H_{0,-2} \,, \tag{5.4.9}$$

where c_{hh}, $c_{h\phi}$, $c_{\phi h}$, and $c_{\phi\phi}$ are real coefficients that we will later relate to the Love numbers.

5.4.2 EFT Side

We now wish to investigate how exactly the Love numbers impact the asymptotic spacetime and will, in this way, understand how exactly we can extract the numerical values for a given spacetime. We will use the PP EFT approach as it was originally laid out by Kol and Smolkin in [167]. The general idea in this approach is to directly calculate the asymptotic behavior of the metric and scalar field by evaluating the path integral of the bulk and PP action at the classical level in terms of Feynman diagrams. In this way, we can directly relate the asymptotic expansion to the Wilsonian coefficients that appear in the PP action and thus can identify their impact more easily. Since these calculations are most conveniently performed in isotropic coordinates, we will follow [167] and decompose the metric as

$$\hat{g}_{00} = -e^{\sqrt{2}\hat{\varphi}(\hat{x}^i)/M_{\rm pl}}\,, \tag{5.4.10a}$$

$$\hat{g}_{0i} = 0\,, \tag{5.4.10b}$$

$$\hat{g}_{ij} = e^{-\sqrt{2}\hat{\varphi}(\hat{x}^i)/M_{\rm pl}}\,\hat{\psi}(\hat{x}^i)\,\delta_{ij}\,, \tag{5.4.10c}$$

where have introduced the metric fields $\hat{\varphi}$ and $\hat{\psi}$. Also, we use overhead hats in order to distinguish all quantities that are obtained in isotropic coordinates from those in Schwarzschild coordinates. Inserting this metric decomposition into the bulk action we find that

$$\mathcal{S}_{\rm bulk} = \int {\rm d}^4x \left[\frac{M_{\rm pl}^2}{4}\hat{\psi}^{-3/2}(\partial\hat{\psi})^2 - \frac{1}{2}\hat{\psi}^{1/2}(\partial\hat{\varphi})^2 - \frac{1}{2}\hat{\psi}^{1/2}(\partial\hat{\phi})^2\right]. \tag{5.4.11}$$

We now wish to expand the bulk action around flat spacetime, which corresponds to $\hat{\varphi} = 0$ and $\hat{\psi} = 1$. To this end it is convenient to introduce $\hat{\sigma}$, such that

$$\hat{\psi} = 1 + \frac{\sqrt{2}}{M_{\rm pl}}\hat{\sigma} \tag{5.4.12}$$

and flat spacetime now corresponds to $\hat{\sigma} = 0$. Using $\hat{\sigma}$, we can express the bulk action as

$$\mathcal{S}_{\rm bulk} = \int {\rm d}^4x \left[\frac{1}{2}\hat{\psi}^{-3/2}(\partial\hat{\sigma})^2 - \frac{1}{2}\hat{\psi}^{1/2}(\partial\hat{\varphi})^2 - \frac{1}{2}\hat{\psi}^{1/2}(\partial\hat{\phi})^2\right]. \tag{5.4.13}$$

Expanding the bulk action around $\hat{\varphi} = 0 = \hat{\sigma}$ now results in

$$\mathcal{S}_{\rm bulk} = \int {\rm d}^4x \left[\frac{1}{2}\partial_i\hat{\sigma}\partial^i\hat{\sigma} - \frac{1}{2}\partial_i\hat{\varphi}\partial^i\hat{\varphi} - \frac{1}{2}\partial_i\hat{\phi}\partial^i\hat{\phi} + \dots\right], \tag{5.4.14}$$

where the ellipses denote higher-order operators. From this it is now straightforward to read off the propagators, such that

$$\langle\hat{\varphi}(x)\hat{\varphi}(y)\rangle = -i\int_k \frac{e^{ik(x-y)}}{k^2 + i\epsilon}\,, \tag{5.4.15a}$$

$$\langle\hat{\psi}(x)\hat{\psi}(y)\rangle = +i\int_k \frac{e^{ik(x-y)}}{k^2 + i\epsilon}\,, \tag{5.4.15b}$$

$$\langle\hat{\phi}(x)\hat{\phi}(y)\rangle = -i\int_k \frac{e^{ik(x-y)}}{k^2 + i\epsilon}\,. \tag{5.4.15c}$$

We next turn to the background action. Inserting the metric decomposition results in

$$\mathcal{S}_{\rm pp}^{\rm (bg)} = -\int {\rm d}t\, e^{\sqrt{2}\hat{\varphi}/(2M_{\rm pl})}\left(M + Q\frac{\hat{\phi}}{M_{\rm pl}}\right). \tag{5.4.16}$$

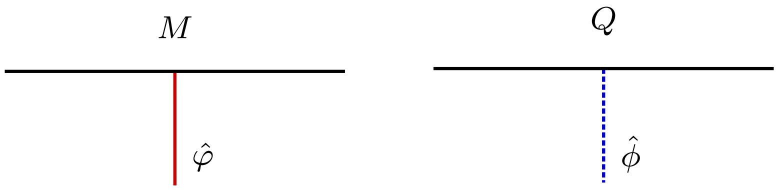

Figure 5.1: Leading-order contribution to the asymptotic expansions of $\hat{\varphi}$ (left) and $\hat{\phi}$ (right).

Expanding the action around flat space, we find

$$\mathcal{S}_{\rm pp}^{(\rm bg)} = -\int {\rm d}t \left(M\frac{\hat{\varphi}}{\sqrt{2}M_{\rm pl}} + Q\frac{\hat{\phi}}{M_{\rm pl}} + \dots \right) , \tag{5.4.17}$$

with the ellipses denoting higher-order operators that contain higher powers of $\hat{\varphi}$. These operators are not relevant for the problem at hand since it can be shown that their effect falls in one of three classes: (1) generating a monopolar perturbation as a response to an external field, (2) generating a quantum loop diagram that will contain powers of $\hbar$ and is thus not relevant to classical physics, or (3) generating a scale-less divergent integral that vanishes in dimensional regularization. We will therefore only consider the linear-order operators in the background PP action.

Background

Having prepared the bulk and PP actions, we are now ready to utilize these in order to calculate the background field expansions. While we are mainly interested in the perturbations, it is instructive to showcase the procedure by calculating the LO correction to flat space due to the presence of the PP. The necessary diagrams are shown in Fig. 5.1 and we will start out by calculating $\hat{\phi}$ at linear order in Q. We find that

$$\begin{aligned}
\langle\hat{\phi}(x)\rangle_{\text{Fig. 5.1}} &= -i\frac{Q}{M_{\rm pl}}\int_{\mathbb{R}} {\rm d}t\, \langle\hat{\phi}(x)\hat{\phi}(0)\rangle \\
&= -\frac{Q}{M_{\rm pl}}\int_{\mathbb{R}} {\rm d}t \int_{\mathbb{R}^4} \frac{{\rm d}^4 k}{(2\pi)^4}\frac{e^{ikx}}{k^2+i\epsilon} \\
&= -\frac{Q}{M_{\rm pl}}\int_{\mathbb{R}^3} \frac{{\rm d}^3 \boldsymbol{k}}{(2\pi)^3}\frac{e^{i\boldsymbol{k}\cdot\boldsymbol{x}}}{\boldsymbol{k}^2+i\epsilon} ,
\end{aligned} \tag{5.4.18}$$

where we have carried out the ${\rm d}t$ and ${\rm d}k_0$ integrals in the last line. Changing to spherical coordinates and extending the integration range to $(-\infty, +\infty)$ we obtain

$$\langle\hat{\phi}(x)\rangle_{\text{Fig. 5.1}} = \frac{i\,Q}{4\pi^2 M_{\rm pl}\hat{r}}\int_{\mathbb{R}} {\rm d}\hat{k}\,\hat{k}\frac{e^{i\hat{k}\hat{r}}}{\hat{k}^2+i\epsilon} . \tag{5.4.19}$$

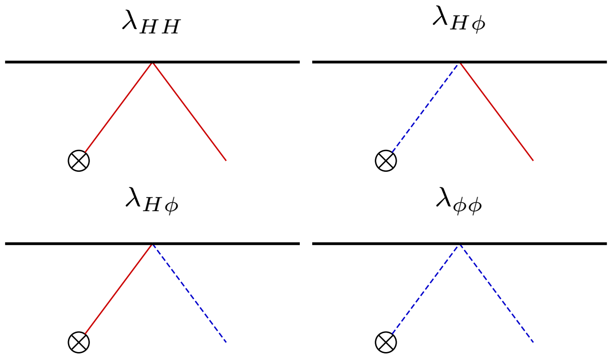

Figure 5.2: Leading-order contributions of tidal Love numbers to the asymptotic expansion of the perturbation fields. The crossed circle denotes the external field.

This integral is now easily carried out using the residue theorem, which results in

$$\langle \hat{\phi}(x) \rangle_{\text{Fig. 5.1}} = -\frac{Q}{4\pi M_{\text{pl}} \hat{r}} \,. \tag{5.4.20}$$

Turning to the left diagram of Fig. 5.1, we can similarly calculate $\hat{\varphi}$ at linear order in M, which results in

$$\langle \hat{\varphi}(x) \rangle_{\text{Fig. 5.1}} = -\frac{\sqrt{2}M}{8\pi M_{\text{pl}} \hat{r}} \,. \tag{5.4.21}$$

As a consistence check we can plug this result into the metric decomposition to find for the 00 component

$$\langle \hat{g}_{00}(x) \rangle_{\text{Fig. 5.1}} = -1 + \frac{2M}{8\pi M_{\text{pl}}^2 \hat{r}} = -1 + \frac{2M}{\hat{r}} \,, \tag{5.4.22}$$

which agrees with the expected result at this order in M.

Perturbations

We now turn to the tidal parts of the PP action. Inserting the metric decomposition into Eq. (5.3.5), we find that

$$\mathcal{S}_{\text{pp}}^{\lambda} = \int \mathrm{d}t \left[\frac{\lambda_{hh}}{8M_{\text{pl}}^2} \partial_i \partial_j \hat{\varphi} \partial^i \partial^j \hat{\varphi} + \frac{\lambda_{h\phi}}{2\sqrt{2}M_{\text{pl}}^2} \partial_i \partial_j \hat{\varphi} \partial^i \partial^j \hat{\phi} + \frac{\lambda_{\phi\phi}}{4M_{\text{pl}}^2} \partial_i \partial_j \hat{\phi} \partial^i \partial^j \hat{\phi} + \dots \right] , \tag{5.4.23}$$

with the ellipses denoting higher-order operators. These operators are negligible for the here-considered effects by the same argument that was provided for the background PP action, and we will thus not consider them further here. We introduce perturbations by splitting the fields $\hat{\varphi}$ and $\hat{\phi}$ according to

$$\hat{\varphi} \to \hat{\varphi} + \delta\hat{\varphi} + \delta\hat{\varphi}_{\text{ext}} \,, \qquad \delta\hat{\varphi}_{\text{ext}} = \hat{\varphi}_{ij}\hat{x}^i\hat{x}^j \,, \tag{5.4.24}$$

$$\hat{\phi} \to \hat{\phi} + \delta\hat{\phi} + \delta\hat{\phi}_{\text{ext}} \,, \qquad \delta\hat{\phi}_{\text{ext}} = \hat{\phi}_{ij}\hat{x}^i\hat{x}^j \,, \tag{5.4.25}$$

where $\hat{\varphi}_{\text{ext}}$ denote the externally applied quadrupolar perturbations, $\delta\hat{\varphi}$ the response, and $\hat{\varphi}_{ij}$ a symmetric and traceless tensor. The decomposition for $\hat{\phi}$ is analogous. Inserting this split into the tidal PP action we arrive at

$$\mathcal{S}^{\lambda}_{\text{pp}} = \int \text{d}t \left[\frac{\lambda_{hh}}{2M_{\text{pl}}^2}\hat{\varphi}_{ij}\partial^i\partial^j\delta\hat{\varphi} + \frac{\lambda_{h\phi}}{\sqrt{2}M_{\text{pl}}^2}\hat{\varphi}_{ij}\partial^i\partial^j\delta\hat{\phi} + \frac{\lambda_{h\phi}}{\sqrt{2}M_{\text{pl}}^2}\hat{\phi}_{ij}\partial^i\partial^j\delta\hat{\varphi} + \frac{\lambda_{\phi\phi}}{M_{\text{pl}}^2}\hat{\phi}_{ij}\partial^i\partial^j\delta\hat{\phi}\right]. \tag{5.4.26}$$

At leading order, these operators will generate the four diagrams shown in Fig. 5.2. It is straightforward to evaluate these diagrams and find that they have the following contribution to $\delta\hat{\varphi}$ and $\delta\hat{\phi}$

$$\delta\hat{\varphi} \supset \left(\frac{3\lambda_{hh}}{8\pi M_{\text{pl}}^2}\hat{\varphi}_{ij} + \frac{3\lambda_{h\phi}}{4\sqrt{2}\pi M_{\text{pl}}^2}\hat{\phi}_{ij}\right)\frac{\hat{x}^i\hat{x}^j}{\hat{r}^5}, \tag{5.4.27}$$

$$\delta\hat{\phi} \supset \left(\frac{3\lambda_{h\phi}}{4\sqrt{2}\pi M_{\text{pl}}^2}\hat{\varphi}_{ij} + \frac{3\lambda_{\phi\phi}}{4\pi M_{\text{pl}}^2}\hat{\phi}_{ij}\right)\frac{\hat{x}^i\hat{x}^j}{\hat{r}^5}\,. \tag{5.4.28}$$

In order to express these contributions in terms of spherical harmonics, we follow [168] and first rewrite $\hat{\varphi}_{ij}$ and $\hat{\phi}_{ij}$ as

$$\hat{\varphi}_{ij} = \sum_{m=-2}^{2}\hat{\varphi}_m\mathcal{Y}^{2,m}_{ij}, \qquad \hat{\phi}_{ij} = \sum_{m=-2}^{2}\hat{\phi}_m\mathcal{Y}^{2,m}_{ij}, \tag{5.4.29}$$

where $\mathcal{Y}^{2,m}_{ij}$ is related to the usual spherical harmonics via

$$Y_{2,m}(\theta,\varphi) = \mathcal{Y}^{2,m}_{ij}\frac{\hat{x}^i\hat{x}^j}{\hat{r}^2}\,. \tag{5.4.30}$$

With this decomposition it is now straightforward to identify

$$\hat{\varphi}_{ij}\hat{x}^i\hat{x}^j = \sum_{m=-2}^{2}\hat{\varphi}_m\hat{r}^2Y_{2,m}(\theta,\varphi)\,, \tag{5.4.31}$$

$$\hat{\phi}_{ij}\hat{x}^i\hat{x}^j = \sum_{m=-2}^{2}\hat{\phi}_m\hat{r}^2Y_{2,m}(\theta,\varphi)\,. \tag{5.4.32}$$

Without loss of generality, we will from now on focus on the $m = 0$ mode and absorb $Y_{2,m}$ into a redefinition of $\hat{\phi}_m$. We can justify only considering this mode since the different modes decouple at linear order in perturbation theory and since every mode carries the same information about the tidal Love numbers, we are free to choose the most convenient one[1]. Also, we will relabel $\hat{\varphi}_{m=0}$ as $\hat{\varphi}_{-2}$ and $\hat{\phi}_{m=0}$ as $\hat{\phi}_{-2}$, which will allow us to compare this expansion more easily to the previously obtained expansion in Sec. 5.4.1. We thus find that the contribution in Eq. (5.4.27) and Eq. (5.4.28) are expressed as

$$\delta\hat{\varphi} \supset \left(\frac{3\lambda_{hh}}{8\pi M_{\rm pl}^2}\delta\hat{\varphi}_{-2} + \frac{3\lambda_{h\phi}}{4\sqrt{2}\pi M_{\rm pl}^2}\delta\hat{\phi}_{-2}\right)\frac{1}{\hat{r}^3}, \tag{5.4.33}$$

$$\delta\hat{\phi} \supset \left(\frac{3\lambda_{h\phi}}{4\sqrt{2}\pi M_{\rm pl}^2}\delta\hat{\varphi}_{-2} + \frac{3\lambda_{\phi\phi}}{4\pi M_{\rm pl}^2}\delta\hat{\phi}_{-2}\right)\frac{1}{\hat{r}^3}\,. \tag{5.4.34}$$

Together with the externally applied quadrupolar perturbation, we thus find that the total perturbation contains

$$\delta\hat{\varphi} + \delta\hat{\varphi}_{\rm ext} \supset \delta\hat{\varphi}_{-2}\hat{r}^2 + \left(\frac{3\lambda_{hh}}{8\pi M_{\rm pl}^2}\delta\hat{\varphi}_{-2} + \frac{3\lambda_{h\phi}}{4\sqrt{2}\pi M_{\rm pl}^2}\delta\hat{\phi}_{-2}\right)\frac{1}{\hat{r}^3}\,, \tag{5.4.35}$$

$$\delta\hat{\phi} + \delta\hat{\phi}_{\rm ext} \supset \delta\hat{\phi}_{-2}\hat{r}^2 + \left(\frac{3\lambda_{h\phi}}{4\sqrt{2}\pi M_{\rm pl}^2}\delta\hat{\varphi}_{-2} + \frac{3\lambda_{\phi\phi}}{4\pi M_{\rm pl}^2}\delta\hat{\phi}_{-2}\right)\frac{1}{\hat{r}^3}\,. \tag{5.4.36}$$

Contamination

With the above given equations, it now appears to be straightforward to obtain the Love numbers for a given Model. In order to do so, we would numerically construct a perturbation profile and then first extract the coefficients of the $\hat{r}^2$ and $\hat{r}^{-3}$ terms. From these coefficients, it is then straightforward to obtain the Love numbers. However, in order to properly apply this procedure we have to be sure that there are no additional contributions to the $\hat{r}^{-3}$ term in the form of terms that are independent of the Love numbers. More explicitly, due to the interaction vertices in the bulk action, we find that there are diagrams that do not involve the Love numbers (i.e., no coupling to the Love operators is present) but would still produce a contribution to the $\hat{r}^{-3}$ coefficient. From dimensional analysis, we find that such a diagram would require five couplings to the worldline and thus needs to be of the form presented in Fig. 5.3.

To determine whether such a contribution is present, we can now calculate each diagram individually. However, it turns out that there is a certain symmetry present in the system that will help us to simplify the problem at hand.

A Neat Symmetry

We know that any term that may contaminate the $\hat{r}^{-3}$ term in the expansions of $\delta\hat{\phi}$ and $\delta\hat{\varphi}$ can not contain the Love numbers and must thus be generated from interaction

[1]We may also imagine starting with a perturbation $\hat{\phi}_{ij}$ that is already constructed in such a way that only $\hat{\phi}_{m=0}$ is non-vanishing.

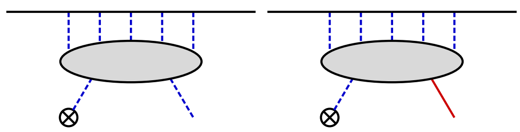

Figure 5.3: Two exemplary diagrams that would also contribute to the asymptotic perturbation field with the same radial dependency as the Love numbers, i.e., the diagrams in Fig. (b). The gray shaded area is a placeholder for any allowed interactions between the perturbations and the five couplings to the worldline.

vertices that are contained in the bulk and background PP action. We will thus consider a system where the total action is given by

$$\mathcal{S} = \mathcal{S}_{\text{bulk}} + \mathcal{S}_{\text{pp}}^{(\text{bg})} \,. \tag{5.4.37}$$

We now note that this action is invariant under the symmetry

$$\begin{aligned} \hat{\varphi} &\to -\hat{\varphi}\,, \quad & \hat{\phi} &\to -\hat{\phi}\,, \\ Q &\to -Q\,, \quad & M &\to -M\,. \end{aligned} \tag{5.4.38}$$

Due to this symmetry, we find that the expansions of $\delta\hat{\phi}_{\text{tot}}$ and $\delta\hat{\varphi}_{\text{tot}}$ can only contain terms where the combined powers of M and Q have to be even. Since each power of M and Q results from a coupling to the worldline of the PP, we thus have that only diagrams with an even number of such couplings are allowed, so that the expansion needs to take the form of

$$\delta\hat{\varphi} = \sum_{i=-1}^{\infty} \delta\hat{\varphi}_{2i}\,\hat{r}^{-2i}\,, \quad \delta\hat{\phi} = \sum_{i=-1}^{\infty} \delta\hat{\phi}_{2i}\,\hat{r}^{-2i}\,. \tag{5.4.39}$$

Further, as already previously mentioned, a contamination would result from diagrams that feature five couplings to the worldline and we can hence conclude that there can not be any contamination in the isotropic coordinate system we used throughout this section.

5.4.3 Matching

We next want to relate the expansion ansatz we obtained in isotropic coordinates to the expansion in Schwarzschild coordinates. To this end, we will explicitly construct the necessary coordinate transformation for the background fields. We begin by expressing the spatial part of the isotropic metric in spherical coordinates, so that

$$\mathrm{d}s^2 = -\hat{f}(\hat{r})\mathrm{d}\hat{t}^2 + \hat{h}^{-1}(\hat{r})\left(\mathrm{d}\hat{r}^2 + \hat{r}^2\mathrm{d}\hat{\Omega}^2\right)\,. \tag{5.4.40}$$

Comparing this to Schwarzschild coordinates we find that

$$f(r) = \hat{f}(\hat{r})\,, \quad \hat{h}^{-1}(\hat{r})\mathrm{d}\hat{r}^2 = h^{-1}(r)\mathrm{d}r^2\,, \quad \text{and} \quad \hat{h}^{-1}(\hat{r})\,\hat{r}^2 = r^2\,. \tag{5.4.41}$$

Dividing the second by the third equation and taking the square root gives

$$\frac{1}{\hat{r}}\mathrm{d}\hat{r} = \frac{1}{r\sqrt{h}}\mathrm{d}r\,. \tag{5.4.42}$$

Integration further results in

$$\ln(\hat{r}) = \int \frac{1}{r\sqrt{h}}\mathrm{d}r \tag{5.4.43}$$

and hence

$$\hat{r} = \exp\left(\int \frac{1}{r\sqrt{h}}\mathrm{d}r\right). \tag{5.4.44}$$

When evaluating the indefinite integral, one has to be careful to choose the integration constant such that both radial coordinates—$\hat{r}$ and r—agree at radial infinity. For a Schwarzschild black hole, it is possible to carry out the integration analytically, but in the present case, we only have the asymptotic expansion of h available. Nevertheless, we can insert this expansion into the above expression and then carry out the integration order by order. Doing so and expanding the exponential function accordingly, we find that the first few terms of this transformation are given by

$$\hat{r} = r - M + \frac{1}{r}\left(\frac{\phi_1^2}{8M_{\mathrm{pl}}^2} - \frac{M^2}{4}\right) + \mathcal{O}(r^{-2})\,, \tag{5.4.45}$$

which now allows us to relate the background fields in both coordinate systems at asymptotically large radii.

Relating the perturbations is more difficult since we would first need to transform the perturbations we obtained in the isotropic coordinates to the Regge-Wheeler gauge. Instead, it is more convenient to utilize gauge-invariant quantities that allow one to relate both perturbations directly. For this purpose, we will first express the obtained metric perturbations in the standard metric decomposition. Denoting the metric perturbations in isotropic coordinates with $\hat{h}_{\mu\nu}$ we can write

$$\hat{g}_{00} = -\hat{f} + \hat{h}_{00} = -\hat{f}\left(1 - \hat{H}_0\right)\,. \tag{5.4.46}$$

At the same time, we can express $\hat{g}_{00}$ using Eq. (5.4.10a) such that

$$\hat{g}_{00} = -e^{\sqrt{2}(\hat{\varphi}+\delta\hat{\varphi})/M_{\mathrm{pl}}} = -\hat{f}e^{\sqrt{2}\delta\hat{\varphi}/M_{\mathrm{pl}}}\,. \tag{5.4.47}$$

Comparing both expansions, we deduce that

$$1 - \hat{H}_0 = e^{\sqrt{2}\delta\hat{\varphi}/M_{\mathrm{pl}}} \tag{5.4.48}$$

and since we are only interested in linear perturbations, we can safely drop all non-linear terms on the right-hand side, thus arriving at

$$\hat{H}_0(\hat{r}) = -\frac{\sqrt{2}}{M_{\rm pl}}\delta\hat{\varphi}(\hat{r})\,. \tag{5.4.49}$$

We can also decompose $\hat{H}_0$ into a power series with

$$\hat{H}_0(\hat{r}) = \sum_{i=-2}^{\infty} \hat{H}_{0,i}\,\hat{r}^{-i} \tag{5.4.50}$$

and can use Eq. (5.4.49) now to relate it to the expansion of $\delta\hat{\varphi}$. For the growing mode, we thus find

$$\hat{H}_{0,-2} = -\frac{\sqrt{2}}{M_{\rm pl}}\delta\hat{\varphi}_{-2} \tag{5.4.51}$$

and we can express the tidal contributions to $\delta\hat{\varphi}$ and $\delta\hat{\phi}$ as

$$\hat{H}_0 \supset \left(\frac{3\lambda_{hh}}{8\pi M_{\rm pl}^2}\hat{H}_{0,-2} - \frac{3\lambda_{h\phi}}{4\pi M_{\rm pl}^3}\delta\hat{\phi}_{-2}\right)\frac{1}{\hat{r}^3}\,, \tag{5.4.52}$$

$$\delta\hat{\phi} \supset \left(-\frac{3\lambda_{h\phi}}{8\pi M_{\rm pl}}\hat{H}_{0,-2} + \frac{3\lambda_{\phi\phi}}{4\pi M_{\rm pl}^2}\delta\hat{\phi}_{-2}\right)\frac{1}{\hat{r}^3}\,. \tag{5.4.53}$$

As already mentioned above, these expressions are not yet in the Regge-Wheeler gauge. In order to relate them directly to the expansion in Eqs. (5.4.8), we will utilize gauge-invariant quantities. To this end, consider a general infinitesimal coordinate transformation of the form $x_\mu \to x_\mu + \xi_\mu$ with

$$\xi_t = \sum_{l,m} \mathcal{T}(t,r)Y_{lm}(\theta,\varphi), \tag{5.4.54a}$$

$$\xi_r = \sum_{l,m} \mathcal{R}(t,r)Y_{lm}(\theta,\varphi), \tag{5.4.54b}$$

$$\xi_a = \sum_{l,m} \Theta(t,r)\nabla_a Y_{lm}(\theta,\varphi)\,, \tag{5.4.54c}$$

with $\mathcal{T}$, $\mathcal{R}$, and Θ being arbitrary functions and $a \in \{\theta,\varphi\}$. Under such a transformation, one finds that the perturbations H_0, $\delta\phi$, h_0, and G transform as

$$H_0 \to H_0 + \frac{2}{f}\dot{\mathcal{T}} - \frac{f'h}{f}\mathcal{R}\,, \tag{5.4.55a}$$

$$\delta\phi \to \delta\phi - \phi' h\mathcal{R}\,, \tag{5.4.55b}$$

$$h_0 \to h_0 + \mathcal{T} + \dot{\Theta}\,, \tag{5.4.55c}$$

$$G \to G + \frac{2}{r^2}\Theta\,. \tag{5.4.55d}$$

From this we thus find that the combination

$$\Psi \equiv H_0 - \frac{f'}{f\phi'}\delta\phi - \frac{2}{f}\dot{h}_0 + \frac{r^2}{f}\ddot{G} \tag{5.4.56}$$

is invariant under infinitesimal transformations. Since we only consider static perturbations, we can simplify this expression to

$$\Psi = H_0 - \frac{f'}{f\phi'}\delta\phi \tag{5.4.57}$$

and thus have

$$-\frac{\sqrt{2}}{M_{\rm pl}}\delta\hat{\varphi}(\hat{r}) - \frac{f'(r)}{f(r)\phi'(r)}\delta\hat{\phi}(\hat{r}) = H_0(r) - \frac{f'(r)}{f(r)\phi'(r)}\delta\phi(r)\,. \tag{5.4.58}$$

where we have used Eq. (5.4.51) to replace $\hat{H}_0$ in favor of $\delta\hat{\varphi}$. Next, we will isolate any contamination by separating $H_{0,3}$ and $\delta\phi_3$ as

$$H_{0,3} = H^{\lambda}_{0,3} + H^{0}_{0,3}\,, \tag{5.4.59}$$

$$\delta\phi_3 = \delta\phi^{\lambda}_{0,3} + \delta\phi^{0}_{0,3}\,, \tag{5.4.60}$$

where the superscript 0 denotes the contamination terms, while λ denotes the pure tidal contributions. We now first consider the case of vanishing Love numbers, which will allow us to determine the contamination in Schwarzschild coordinates. To this end, we insert the obtained background expansion together with the perturbation expansions into the matching condition above, expand it around spatial infinity, and then match it order by order. At the various orders we find

1. $\mathcal{O}(r^2)$: We solve for $\delta\hat{\varphi}_{-2}$.
2. $\mathcal{O}(r^1)$: The equation at this order is automatically satisfied if we use the above solution for $\delta\hat{\varphi}_{-2}$.
3. $\mathcal{O}(r^0)$: We can solve the equation for $\delta\hat{\varphi}_0$.
4. $\mathcal{O}(r^{-1})$: The equation at this order is automatically satisfied if we use the above solutions for $\delta\hat{\varphi}_{-2}$ and $\delta\hat{\varphi}_0$.
5. $\mathcal{O}(r^{-2})$: We solve for $\delta\hat{\varphi}_2$.
6. $\mathcal{O}(r^{-3})$: At this order, the above pattern breaks. The coefficients $\delta\hat{\varphi}_{2i}$ and $\delta\hat{\phi}_{2i}$ do not appear after using the solutions at previous orders, but we still find an equation which we can solve for $H_{0,3}$ in terms of $H_{0,-2}$, $\delta\phi_{-2}$, and $\delta\phi_3$.
7. $\mathcal{O}(r^{-4})$: We solve for $\delta\hat{\varphi}_4$.

8. $\mathcal{O}(r^{-5})$: Finally, at this order, we find an equation similar to that at $\mathcal{O}(r^{-3})$, which we can solve for $\delta\phi_3$ in terms of $\delta\phi_{-2}$. Using this solution for the equation of $H_{0,3}$ derived in step 6 above, we find that the dependence on $\delta\phi_{-2}$ cancels.

In this way, we are able to uniquely determine the coefficients $H^0_{0,3}$ and $\delta\phi^0_3$:

$$H^0_{0,3} = H_{0,-2}\left(\frac{3M^3\phi_1^2}{5M_{\rm pl}^2} - \frac{3M\phi_1^4}{80M_{\rm pl}^4}\right), \tag{5.4.61}$$

$$\delta\phi^0_3 = \delta\phi_{-2}\left(\frac{3M^3\phi_1^2}{5M_{\rm pl}^2} - \frac{3M\phi_1^4}{80M_{\rm pl}^4}\right). \tag{5.4.62}$$

In order to match the tidal contributions we consider the limit $M \to 0$ together with $Q \to 0$. In this limit we find that the coordinate transformation in Eq. (5.4.44) becomes trivial, such that $\hat{r} \equiv r$. Further, since we have $\phi \equiv 0$ and $f' \equiv 0$ in this limit, we find that $\delta\phi$ and H_0 are unaffected by the infinitesimal transformations in Eqs. (5.4.54). We can thus identify

$$\hat{H}_0(\hat{r}) = H_0(r) \quad \text{and} \quad \delta\hat{\phi}(\hat{r}) = \delta\phi(r)\,. \tag{5.4.63}$$

In this way, we directly find that the tidal contributions are

$$H^\lambda_{0,3} = \frac{3\lambda_{hh}}{8\pi M_{\rm pl}^2}H_{0,-2} - \frac{3\lambda_{h\phi}}{4\pi M_{\rm pl}^3}\delta\phi_{-2}\,, \tag{5.4.64}$$

$$\delta\phi^\lambda_3 = -\frac{3\lambda_{h\phi}}{8\pi M_{\rm pl}}H_{0,-2} + \frac{3\lambda_{\phi\phi}}{4\pi M_{\rm pl}^2}\delta\phi_{-2}\,. \tag{5.4.65}$$

In total we thus conclude that the coefficients $H_{0,3}$ and $\delta\phi_3$ are uniquely determined to be

$$H_{0,3} = H_{0,-2}\left(\frac{3M^3\phi_1^2}{5M_{\rm pl}^2} - \frac{3M\phi_1^4}{80M_{\rm pl}^4}\right) + \frac{3\lambda_{hh}}{8\pi M_{\rm pl}^2}H_{0,-2} - \frac{3\lambda_{h\phi}}{4\pi M_{\rm pl}^3}\delta\phi_{-2}\,, \tag{5.4.66}$$

$$\delta\phi_3 = \delta\phi_{-2}\left(\frac{3M^3\phi_1^2}{5M_{\rm pl}^2} - \frac{3M\phi_1^4}{80M_{\rm pl}^4}\right) - \frac{3\lambda_{h\phi}}{8\pi M_{\rm pl}}H_{0,-2} + \frac{3\lambda_{\phi\phi}}{4\pi M_{\rm pl}^2}\delta\phi_{-2}\,. \tag{5.4.67}$$

It is important to note that this result is universal for any scalar tensor theory that reduces to a minimally coupled and massless scalar field in vacuum.

5.5 Damour-Esposito-Farèse Model

To apply these results to a specific model, we now turn to the study of the Damour-Esposito-Farèse model. This model is specified by the following action in the Jordan frame

$$\mathcal{S}_{\text{DEF}} = \int \mathrm{d}^4x\sqrt{-g}\left[\frac{M_{\text{pl}}^2}{2}F(\phi)R - \frac{1}{2}\left(1 - \frac{3M_{\text{pl}}^2F_{,\phi}^2}{2F^2}\right)F(\phi)\nabla^\mu\phi\nabla_\mu\phi\right], \tag{5.5.1}$$

where

$$F = e^{-\beta\phi^2/(2M_{\text{pl}}^2)} \tag{5.5.2}$$

and β being a real constant. The same action can be obtained by choosing

$$G_2 = \left(1 - \frac{3M_{\text{pl}}^2F_{,\phi}^2}{2F^2}\right)F(\phi)X\,, \quad G_3 = 0\,, \quad G_4 = \frac{M_{\text{pl}}^2}{2}\,, \quad G_5 = 0\,. \tag{5.5.3}$$

in the Horndeski action, and we can thus apply the results of Secs. 5.1 and 5.2 here.

5.5.1 Expansion in the Jordan Frame

We begin by preparing the background expansions. For this purpose, we choose the same ansatz as in Sec. 5.1, which is given by

$$f = \sum_{i=0}^{\infty} f_i\,r^{-i}\,, \quad h = \sum_{i=0}^{\infty} h_i\,r^{-i}\,, \quad \phi = \sum_{i=0}^{\infty} \phi_i\,r^{-i}\,, \tag{5.5.4}$$

with the coefficients f_i, h_i, and ϕ_i being real constants. We insert this ansatz into Eqs. (5.1.2) and solve them order by order in r thus finding up to order r^{-2}

$$\phi(r) = \frac{\phi_1}{r} + \frac{M\phi_1}{r^2} + \mathcal{O}(r^{-3})\,, \tag{5.5.5a}$$

$$h(r) = 1 - \frac{2M}{r} + \frac{\phi_1^2(1-2\beta)}{2M_{\text{pl}}^2r^2} + \mathcal{O}(r^{-3})\,, \tag{5.5.5b}$$

$$f(r) = 1 - \frac{2M}{r} + \frac{\beta\phi_1^2}{2M_{\text{pl}}^2r^2} + \mathcal{O}(r^{-3})\,. \tag{5.5.5c}$$

In total, we have calculated the expansions up to order r^{-8} and present them in App. 5.C.2. Turning to the perturbations next, we also follow the same strategy as in Sec. 5.4.1 in order to expand the fields around asymptotic infinity and choose the following ansatz

$$H_0(r) = \sum_{i=-2}^{\infty} H_{0,i}r^{-i}\,, \qquad \delta\phi(r) = \sum_{i=-2}^{\infty} \delta\phi_i r^{-i}\,, \tag{5.5.6}$$

with $H_{0,i}$ and $\delta\phi_i$ also being real constants. We determine most of these coefficients by inserting this ansatz into Eqs. (5.2.10) and solving it order by order. Doing so, we find that, just as in Sec. 5.4.1, all coefficients are completely determined in terms of $H_{0,-2}$, $H_{0,3}$, $\delta\phi_{-2}$, and $\delta\phi_3$. We have obtained this expansion up to order r^{-8} and present the obtained coefficients in App. 5.C.2. Since the expansion is quite involved, we refrain from presenting parts of it here explicitly.

In order to obtain numeric results, we first have to determine the field behaviors around the origin. To this end, we expand all fields around the origin using the following ansatz

$$\begin{aligned} P(r) &= P_c + \sum_{i=1}^{\infty} P_i r^i\,, & \rho(r) &= \rho_c + \sum_{i=1}^{\infty} \rho_i r^i\,, \\ \phi(r) &= \phi_c + \sum_{i=1}^{\infty} \phi_i r^i\,, & h(r) &= h_c + \sum_{i=1}^{\infty} h_i r^i\,, \\ f(r) &= f_c + \sum_{i=1}^{\infty} f_i r^i\,, \end{aligned} \tag{5.5.7}$$

where P_c, P_i, ρ_c, ρ_i, ϕ_c, ϕ_i, h_c, h_i, f_c, and f_i are real constants. We insert this ansatz into Eqs. (5.1.2) and solve it order by order while also enforcing regularity at the origin. In this way, we find that at NLO order in r, the fields are given by

$$P(r) = P_c - \frac{\rho_c + P_c}{F(\phi_c)}\left[\frac{\rho_c + 3P_c}{12M_{\rm pl}^2} + \frac{\beta^2\phi_c^2(\rho_c - 3P_c)}{24M_{\rm pl}^4}\right]r^2 + \mathcal{O}(r^4)\,, \tag{5.5.8a}$$

$$\phi(r) = \phi_c + \frac{\beta\phi_c(\rho_c - 3P_c)}{12M_{\rm pl}^2 F(\phi_c)}r^2 + \mathcal{O}(r^4)\,, \tag{5.5.8b}$$

$$h(r) = 1 - \frac{2M_{\rm pl}^2\rho_c - \beta^2\phi_c^2(\rho_c - 3P_c)}{6M_{\rm pl}^4 F(\phi_c)}r^2 + \mathcal{O}(r^4)\,, \tag{5.5.8c}$$

$$f(r) = f_c + \frac{f_c}{F(\phi_c)}\left[\frac{\rho_c + 3P_c}{6M_{\rm pl}^2} + \frac{\beta^2\phi_c^2(\rho_c - 3P_c)}{12M_{\rm pl}^4}\right]r^2 + \mathcal{O}(r^4)\,. \tag{5.5.8d}$$

Overall, the expansion is entirely determined by P_c, ϕ_c, and f_c. Finally, we will expand the perturbations around the origin by using the ansatz

$$H_0(r) = H_{0,c} + \sum_{i=1}^{\infty} H_{0,i} r^i\,, \quad \delta\phi(r) = \delta\phi_c + \sum_{i=1}^{\infty} \delta\phi_i r^i\,. \tag{5.5.9}$$

Inserting this expansion into Eqs 5.2.10 together with the background expansion given in Eqs. (5.5.8), we find at NLO in r that

$$H_0(r) = H_{0,c} r^2 + \mathcal{O}(r^4)\,, \tag{5.5.10}$$

$$\delta\phi(r) = \delta\phi_c r^2 + \mathcal{O}(r^4)\,, \tag{5.5.11}$$

with $H_{0,c}$ and $\delta\phi_c$ being real coefficients.

5.5.2 Expansion in the Einstein Frame

We can recast the action in Eq. (5.5.1) to the Einstein frame by performing a rescaling of the metric with

$$\tilde{g}_{\mu\nu} = F(\phi) g_{\mu\nu}\,, \tag{5.5.12}$$

so that $\tilde{g}_{\mu\nu}$ is the new metric in the Einstein frame. In what follows we will generally use an overhead tilde to denote quantities in the Einstein frame and thus distinguish them from quantities we obtained in the Jordan frame. The action now takes the form of

$$\tilde{\mathcal{S}}_{\rm DEF} = \int \mathrm{d}^4x\sqrt{-\tilde{g}}\left[\frac{M_{\rm pl}^2}{2}\tilde{R} - \frac{1}{2}\tilde{g}^{\mu\nu}\tilde{\nabla}_\mu\phi\tilde{\nabla}_\nu\phi\right] + \mathcal{S}_m(F^{-1}(\phi)\tilde{g}_{\mu\nu}) \tag{5.5.13}$$

and we note that in vacuum it reduces to a minimally coupled and massless scalar field. This property is now crucial since it allows us to utilize all previously obtained results in Sec. 5.4, such as the background expansions and the tidal contamination. As such, it is not necessary to perform any additional expansions in this frame.

5.5.3 Matching both Expansions

In order to determine the contamination term in the Jordan frame, we next transform the asymptotic expansions from the Einstein frame, where we already know the contamination terms, to the Jordan frame. To this end, we first need to identify the transformation law for the background fields.

Background

We start out by splitting the metric and scalar field into background and perturbation modes such that

$$g_{\mu\nu} = \bar{g}_{\mu\nu} + h_{\mu\nu}\,, \quad \phi = \bar{\phi} + \delta\phi\,, \tag{5.5.14}$$

such that overhead bars denote the background fields, while $h_{\mu\nu}$ are the metric pertubrations and $\delta\phi$ the scalar field perturbations. Next, considering the metric rescaling given in Eq. (5.5.12), we find that a metric $\bar{g}_{\mu\nu}$ in Schwarzschild coordinates results in a metric $\tilde{\bar{g}}_{\mu\nu}$ given by

$$\tilde{\bar{g}}_{\mu\nu} = \mathrm{diag}\Big(- F(\phi)\, f, F(\phi)h^{-1}, F(\phi)r^2, F(\phi)r^2\sin^2\theta\Big) \tag{5.5.15}$$

and note that $\tilde{\bar{g}}_{\mu\nu}$ is not itself in Schwarzschild coordinates anymore. We therefore need to perform an additional coordinate transformation with

$$\tilde{r} = r\sqrt{F(\bar{\phi})}\,. \tag{5.5.16}$$

This coordinate transformation together with the metric rescaling in Eq. (5.5.12) now allows to directly relate the background fields in both frames to each other.

Perturbations

Turning to the perturbations, we start out by noting that the scalar field perturbations can readily be related to each other using the coordinate transformation in Eq. (5.5.16), such that

$$\delta\tilde{\phi}(\tilde{r}) = \delta\phi(r)\,. \tag{5.5.17}$$

Turning to the metric perturbations, we insert the metric splits into the rescaling law given in Eq. (5.5.12) to first find

$$\tilde{\bar{g}}_{\mu\nu} + \tilde{h}_{\mu\nu} = F(\bar{\phi} + \delta\phi)(\bar{g}_{\mu\nu} + h_{\mu\nu})\,. \tag{5.5.18}$$

We next expand this equation in powers of the perturbation fields and find at linear order that

$$\tilde{h}_{\mu\nu} = F_{,\phi}(\bar{\phi})\bar{g}_{\mu\nu}\delta\phi + F(\bar{\phi})h_{\mu\nu}\,. \tag{5.5.19}$$

From this relation we can deduce that $\tilde{h}_{\mu\nu}$ is already guaranteed to be in the Regge-Wheeler gauge. We can deduce that since $h_{\mu\nu}$ and $\bar{g}_{\mu\nu}$ only contain diagonal elements, $\tilde{h}_{\mu\nu}$ can also only contain diagonal elements and hence $\tilde{h}_0$, $\tilde{h}_1$, and $\tilde{G}$ need to vanish. While we needed to perform an additional coordinate transformation at the background level to arrive at Schwarzschild coordinates, it is thus not necessary to perform an additional gauge transformation. Further, since our goal is to identify a relation between H_0 and $\tilde{H}_0$, we now focus on the 00 component of this equation and use

$$\tilde{h}_{00} = \tilde{f}\tilde{H}_0\,, \quad \bar{g}_{00} = -f\,, \quad h_{00} = fH_0\,. \tag{5.5.20}$$

We therefore find

$$\tilde{f}\tilde{H}_0 = -F_{,\phi}(\bar{\phi})f\delta\phi + F(\bar{\phi})fH_0 \tag{5.5.21}$$

and further note that since $\tilde{f} = F(\bar{\phi})f$, we can simplify this relation to

$$\tilde{H}_0(\tilde{r}) = -\frac{F_{,\phi}(\bar{\phi}(r))}{F(\bar{\phi}(r))}\delta\phi(r) + H_0(r)\,. \tag{5.5.22}$$

Equipped with this relation for $\tilde{H}_0$ together with the relation for $\delta\tilde{\phi}$ in Eq. (5.5.17), we are now ready to match the asymptotic expansions in both frames to each other.

We find that

$$
\begin{aligned}
H_{0,3} = {} & \beta\delta\phi_{-2}\phi_1 \frac{-128M^4M_{\rm pl}^4 + M^2\phi_1^2M_{\rm pl}^2\left(1320\beta - 208\right) + \phi_1^4\left(135\beta^2 - 30\beta - 27\right)}{1440M_{\rm pl}^6} \\
& + H_{0,-2}M\beta\phi_1^2\frac{\phi_1^2\left(50 - 69\beta\right) - 152M^2M_{\rm pl}^2}{144M_{\rm pl}^4} + H_{0,-2}\left(\frac{3M^3\phi_1^2}{5M_{\rm pl}^2} - \frac{3M\phi_1^4}{80M_{\rm pl}^4}\right) \\
& + \frac{3\lambda_{hh}}{8\pi M_{\rm pl}^2}H_{0,-2} - \frac{3\lambda_{h\phi}}{4\pi M_{\rm pl}^3}\delta\phi_{-2}\,,
\end{aligned} \tag{5.5.23a}
$$

$$
\begin{aligned}
\delta\phi_3 = {} & 3\delta\phi_{-2}M\beta\phi_1^2\frac{\phi_1^2(2-3\beta) - 8M^2M_{\rm pl}^2}{16M_{\rm pl}^4} + \delta\phi_{-2}\left(\frac{3M^3\phi_1^2}{5M_{\rm pl}^2} - \frac{3M\phi_1^4}{80M_{\rm pl}^4}\right) \\
& - \frac{3\lambda_{h\phi}}{8\pi M_{\rm pl}}H_{0,-2} + \frac{3\lambda_{\phi\phi}}{4\pi M_{\rm pl}^2}\delta\phi_{-2}\,.
\end{aligned} \tag{5.5.23b}
$$

Especially, we note that we thus found additional contamination terms to be present that depend on β.

5.5.4 Numerical Analysis

We begin our numerical analysis by first constructing background solutions that we then use to build the perturbations numerically on top. We will go over the techniques used to extract the Love numbers and also comment on the numerical accuracy of our results.

Background

We integrate the background equations (5.1.2) radially outward using Eqs. (5.5.8) as the boundary conditions around the origin. We fix ϕ_c by demanding that $\phi_0 = 0$ and f_c in order to obtain asymptotic flatness. By doing so, there only remains one free parameter, the central pressure P_c, and we thus arrive at a one-parameter family of solutions, whose masses and radii we plot in the left panel of Fig. 5.4. While for most of the parameter space we find that asymptotic flatness can only be fulfilled for $\phi \equiv 0$—and the results thus reduce to pure GR—there is a finite window of values for the central pressure that allow for a scalarized branch of solutions. We also plot the mass-radius curve of the scalarized branch in the left panel of Fig. 5.4 and additionally present the resulting scalar charges in the right panel of the same figure.

Extracting the Love Numbers

Turning to the perturbations, we will first describe the general procedure for extracting them from a given perturbation profile. From Eqs. (5.4.8) we know that the perturbation profiles are fully determined in terms of $\delta\phi_{-2}$, $\delta\phi_3$, $H_{0,-2}$, and $H_{0,3}$. In order to extract these coefficients from a given perturbation profile, we perform a least-squares fit of the asymptotic expansions for H_0 and $\delta\phi$ to the numerically obtained profiles of H_0'' and $\delta\phi''$. We use the second derivative of these profiles since these converge to a constant value at

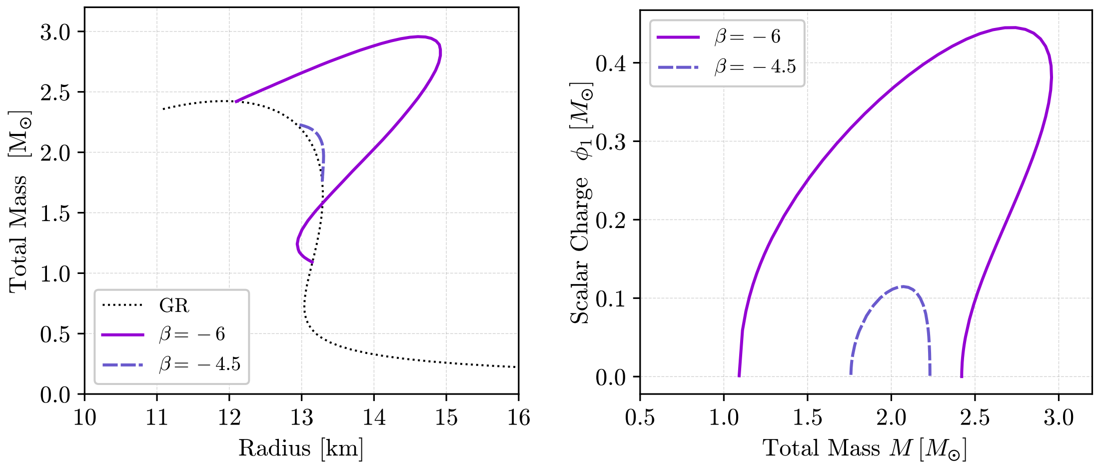

Figure 5.4: Left: The mass-radius curve for NSs in the DEF model with $\beta = -4.5$ and $\beta = -6$, where $M_\odot$ is the solar mass. We choose the DD2 equation of state for describing the property of perfect fluids inside the NS. The dotted black line shows the non-scalarized solutions, which are identical to the GR solutions, while the purple-colored lines represent the scalarized solutions. **Right:** Scalar charge ϕ_1 versus the total gravitational mass.

large radii, which is numerically more convenient to work with rather than the divergent behavior of H_0 and $\delta\phi$ themselves. To carry out the least-square fit, we then use 100 data points that are equally spaced in the radial interval of $r \approx 60\,\mathrm{km}$ up to $r_{\max} \approx 75\,\mathrm{km}$.

The Love numbers could now be obtained by, e.g., performing a shooting procedure on $H_{0,c}$ and $\delta\phi_c$ to find a profile for which either $H_{0,-2}$ or $\delta\phi_{-2}$ vanishes, so that one can easily extract the Love numbers using the Eqs. (5.5.23). However, it is numerically much more efficient to exploit the linear nature of the perturbation equations in such a way that we only need to construct two linearly independent perturbation profiles. More explicitly, consider two sets of perturbation profiles, which we denote as $H_0^{(1)}$, $\delta\phi^{(1)}$ for the first set and $H_0^{(2)}$, $\delta\phi^{(2)}$ for the second set. Focusing on the H_0 profiles, we know from Eq. (5.4.9) that we can decompose the $H_{0,3}$ coefficient for both sets as

$$H_{0,3}^{(1)} = c_{h\phi}\delta\phi_{-2}^{(1)} + c_{hh}H_{0,-2}^{(1)}\,, \tag{5.5.24}$$
$$H_{0,3}^{(2)} = c_{h\phi}\delta\phi_{-2}^{(2)} + c_{hh}H_{0,-2}^{(2)}\,. \tag{5.5.25}$$

We can restate these equations in matrix form, such that

$$\begin{pmatrix} \delta\phi_{-2}^{(1)} & H_{0,-2}^{(1)} \\ \delta\phi_{-2}^{(2)} & H_{0,-2}^{(2)} \end{pmatrix} \begin{pmatrix} c_{h\phi} \\ c_{hh} \end{pmatrix} = \begin{pmatrix} H_{0,3}^{(1)} \\ H_{0,3}^{(2)} \end{pmatrix}\,, \tag{5.5.26}$$

which can be solved for $c_{h\phi}$ and c_{hh} straightforwardly to give

$$\begin{pmatrix} c_{h\phi} \\ c_{hh} \end{pmatrix} = \begin{pmatrix} \delta\phi_{-2}^{(1)} & H_{0,-2}^{(1)} \\ \delta\phi_{-2}^{(2)} & H_{0,-2}^{(2)} \end{pmatrix}^{-1} \begin{pmatrix} H_{0,3}^{(1)} \\ H_{0,3}^{(2)} \end{pmatrix}. \tag{5.5.27}$$

Likewise, we can use the two $\delta\phi$ profiles to solve for $c_{\phi\phi}$ and $c_{\phi h}$ with

$$\begin{pmatrix} c_{\phi\phi} \\ c_{\phi h} \end{pmatrix} = \begin{pmatrix} \delta\phi^{(1)}_{0,-2} & H^{(1)}_{0,-2} \\ \delta\phi^{(2)}_{0,-2} & H^{(2)}_{0,-2} \end{pmatrix}^{-1} \begin{pmatrix} \delta\phi^{(1)}_{3} \\ \delta\phi^{(2)}_{3} \end{pmatrix}. \tag{5.5.28}$$

In order to ensure that the two sets of profiles are linearly independent we choose the initial conditions $(H^{(1)}_{0,-2}, \delta\phi^{(1)}_{-2}) = (1, 0)$ for the first set and $(H^{(2)}_{0,-2}, \delta\phi^{(2)}_{-2}) = (0, 1)$ for the second.

Having obtained the coefficients c_{hh}, $c_{h\phi}$, $c_{\phi h}$, and $c_{\phi\phi}$, we still have to relate these to the Love numbers, which we can do by using Eqs. (5.5.23). In what follows, we will differentiate between *corrected* and *non-corrected* Love numbers, such that the *non-corrected* Love numbers are obtained by neglecting the contamination terms in Eqs. (5.5.23), while the corrected ones take the contamination into account. More explicitly, we define the non-corrected Love numbers as

$$\begin{aligned} \lambda_{hh,\mathrm{nc}} &= \frac{8\pi M_{\mathrm{pl}}^2}{3} c_{hh}\,, & \lambda_{h\phi,\mathrm{nc}} &= -\frac{4\pi M_{\mathrm{pl}}^3}{3} c_{h\phi}\,, \\ \hat{\lambda}_{h\phi,\mathrm{nc}} &= -\frac{8\pi M_{\mathrm{pl}}}{3} c_{\phi h}\,, & \lambda_{\phi\phi,\mathrm{nc}} &= \frac{4\pi M_{\mathrm{pl}}^2}{3} c_{\phi\phi}\,, \end{aligned} \tag{5.5.29}$$

Where we use the subscript nc in order to distinguish them from the corrected Love numbers. Also, we have introduced $\hat{\lambda}_{h\phi}$, which we obtained by using the coefficient $c_{\phi h}$, while $\lambda_{h\phi}$ is obtained using the coefficient $c_{h\phi}$. While these two numbers should be the same when accounting for the contamination terms, the non-corrected mixed Love number should differ depending on whether one uses $c_{h\phi}$ or $c_{\phi h}$. This will later allow us to directly demonstrate that a contamination is indeed present. Further, the corrected Love numbers are obtained as

$$\lambda_{hh} = \frac{8\pi M_{\mathrm{pl}}^2}{3}\left[c_{hh} - M\beta\phi_1^2 \frac{\phi_1^2\,(50-69\beta) - 152M^2M_{\mathrm{pl}}^2}{144M_{\mathrm{pl}}^4} - \frac{3M^3\phi_1^2}{5M_{\mathrm{pl}}^2} + \frac{3M\phi_1^4}{80M_{\mathrm{pl}}^4}\right], \tag{5.5.30a}$$

$$\lambda_{h\phi} = -\frac{4\pi M_{\mathrm{pl}}^3}{3}\left[c_{h\phi} - \beta\phi_1 \frac{M^2\phi_1^2M_{\mathrm{pl}}^2\,(1320\beta-208) + \phi_1^4\left(135\beta^2 - 30\beta - 27\right) - 128M^4M_{\mathrm{pl}}^4}{1440M_{\mathrm{pl}}^6}\right], \tag{5.5.30b}$$

$$\hat{\lambda}_{h\phi} = -\frac{8\pi M_{\mathrm{pl}}}{3} c_{\phi h}\,, \tag{5.5.30c}$$

$$\lambda_{\phi\phi} = \frac{4\pi M_{\mathrm{pl}}^2}{3}\left[c_{\phi\phi} - 3M\beta\phi_1^2 \frac{\phi_1^2(2-3\beta) - 8M^2M_{\mathrm{pl}}^2}{16M_{\mathrm{pl}}^4} - \frac{3M^3\phi_1^2}{5M_{\mathrm{pl}}^2} + \frac{3M\phi_1^4}{80M_{\mathrm{pl}}^4}\right]. \tag{5.5.30d}$$

Numerical Accuracy

Before presenting our results for the tidal Love numbers, we first study the numerical accuracy of the outlined procedure. We can do this by considering stars in pure GR, where one has an exact solution for H_0 outside the star and can thus obtain λ_{hh} by matching H_0 at the star's surface to the exact solution. This procedure was first introduced by

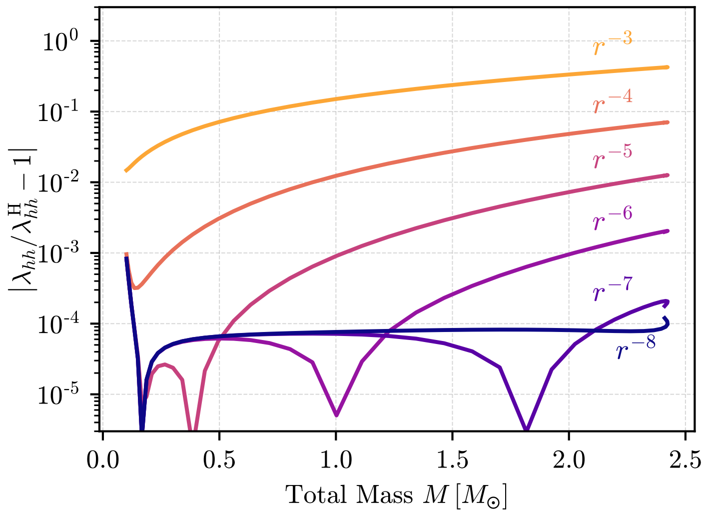

Figure 5.5: Absolute relative difference of the quadrupolar Love numbers λ_{hh} on the GR branch when extracted using the exact formula derived by Hinderer [61], to the ones obtained by the matching procedure described in the main text. The text inset denotes up to which order the asymptotic expansion is used for the matching, e.g., the dark blue curve corresponds to the expansion up to (including) order r^{-8}.

Hinderer in [61], where it was found that

$$\begin{aligned}\lambda_{hh}^{\mathrm{H}} =& \frac{16}{15} M^5 (1-2C)^2 \left[2 + 2C(y-1) - y\right] \\ &\times \left\{2C\left[6 - 3y + 3C(5y-8)\right]\right. \\ &+ 4C^3\left[13 - 11y + C(3y-2) + 2C^2(1+y)\right] \\ &\left.+ 3(1-2C)^2\left[2 - y + 2C(y-1)\right]\log(1-2C)\right\}^{-1},\end{aligned} \tag{5.5.31}$$

where $C = M/R$, $y = RH_0'(R)/H_0(R)$, R denotes the stellar radius, and we have used the superscript H to distinguish the obtained Love number from this procedure. At the same time, we can obtain λ_{hh} by performing the above-described least-square fit at large radii using the series expansion of H_0 at large radii. In Fig. 5.5 we present the relative difference between λ_{hh} and $\lambda_{hh}^{\mathrm{H}}$ for various orders of the asymptotic series expansion. We note that the relative difference first exponentially decreases for each order that is added to the asymptotic expansion, but the improvement seems to stagnate at order r^{-8}, where the relative difference plateaus for the majority of stellar configurations. We attribute this stagnation of improvement to the finite numerical accuracy and since no further improvement is to be expected by adding more orders to the asymptotic expansion of H_0, we will perform all further analysis at order r^{-8}. At this order, we find that the relative difference is $\approx 0.01\,\%$ and we will assume that the numerical errors in all further derived quantities are of similar order.

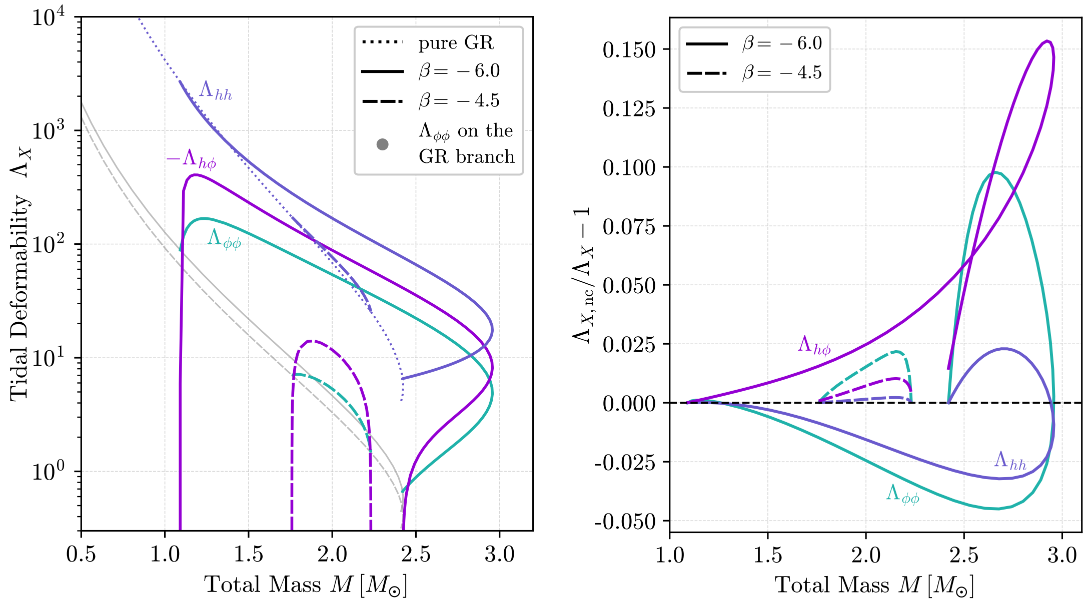

Figure 5.6: Left: The quadrupolar even-parity dimensionless Love numbers for NSs in the DEF model with $\beta \in \{-6, -4.5\}$ and the DD2 equation of state. We obtain the dimensionless Love numbers via $\Lambda_x \equiv \lambda_x/M^5$, where $x \in \{hh, h\phi, \phi\phi\}$. $\Lambda_{\phi\phi}$ is shown for both in the scalarized (colored) and GR (gray) branches. Note that $\Lambda_{h\phi}$ drops to zero on the GR branch, which is due to the parity symmetry explained at the beginning of Sec. 5.5. **Right:** The relative difference between the non-corrected ($\Lambda_{x,nc}$) and corrected (Λ_x) Love numbers.

Numerical Results

We are now ready to present our results for the corrected tidal Love numbers. The left panel in Fig. 5.6 presents the dimensionless tidal deformabilities, defined by $\Lambda_{\mathrm{x}} = \lambda_{\mathrm{x}}/M^5$, with $\mathrm{x} \in \{hh, h\phi, \phi\phi\}$. We generally observe that the Love numbers are enhanced on the scalarized branch, with this enhancement amounting up to one order of magnitude for $\beta = -6$, but being less pronounced for $\beta = -4.5$. Further, the mixed Love number, $\Lambda_{h\phi}$, is exactly zero—within numerical accuracy—on the GR branch. This is consistent with our earlier discussion, where we argued that $\Lambda_{h\phi}$ needs to vanish on the GR branch due to the $\phi \to -\phi$ symmetry. However, $\Lambda_{\phi\phi}$ does not vanish on the GR branch and is generally smaller than the other Love numbers.

Further, the right panel of Fig. 5.6 demonstrates the relative difference between the corrected and non-correct Love numbers. We observe that the relative difference is generally larger in the case of $\beta = -6$, where the largest deviation is observed in $\Lambda_{h\phi}$, which differs by up to 15 %. The case of $\beta = -4.5$ % is much less severe, with the largest deviation arising in $\Lambda_{\phi\phi}$ at about 2.5 %.

Figure 5.7 demonstrates the relative difference between $\hat{\lambda}_{h\phi}$ and $\lambda_{h\phi}$. As alluded to earlier, if the contamination is properly taking care of, then the relative difference is expected to vanish as both values need to be equal. Indeed, we find that the relative difference in the non-corrected case can be as high as 10 % for $\beta = -6$ and 1 % for

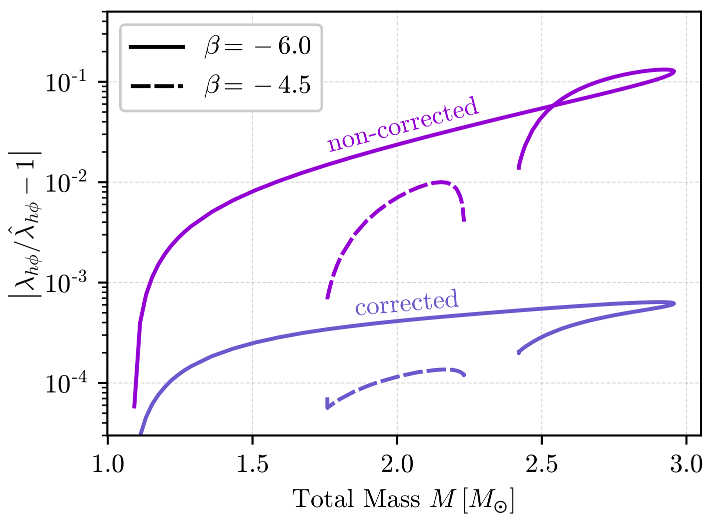

Figure 5.7: Comparison of the extracted tidal Love numbers $\lambda_{h\phi}$ when obtained via $c_{h\phi}$ from Eq. (5.5.27) to the ones obtained via $c_{\phi h}$ from Eq. (5.5.28). The blue line displays the relative difference for the *corrected* Love numbers, as defined in Eqs. (5.5.30), while the purple line demonstrates the relative difference for the *non-corrected* Love numbers, defined in Eqs. (5.5.29). If the Love numbers are correctly extracted, then the relative difference should approach zero. Notably, the curves of non-corrected Love numbers show significant deviations, with a relative difference of up to 13 %.

$\beta = -4.5$. For the corrected Love numbers we observe that this difference significantly drops to below 0.07 % for $\beta = -6$ and to around 0.01 % for $\beta = -4.5$. As discussed in the previous section on numerical accuracy, we expect the results to be accurate at the order of $\mathcal{O}(0.01\,\%)$ and we can thus deduce that—within numerical accuracy—we can confirm that $\lambda_{h\phi}$ and $\hat{\lambda}_{h\phi}$ are indeed identical when considering the corrected Love numbers.

5.6 Scalar-Gauss-Bonnet Gravity

Having successfully studied the DEF model, we now turn our attention to scalar-Gauss-Bonnet (sGB) gravity. While we will not be able to present expressions for the contamination terms, as the previously outlined method is not applicable here, it is still instructive to see precisely why this model eludes our procedure. The sGB model is characterized by a coupling of the scalar field ϕ to the Gauss-Bonnet invariant $R^2_{\rm GB}$, such that the action is given by

$$\mathcal{S}_{\rm sGB} = \int \mathrm{d}^4x\sqrt{-g}\left[\frac{M_{\rm pl}^2}{2}R - \frac{1}{2}\nabla^\mu\phi\nabla_\mu\phi + \xi(\phi)R^2_{\rm GB}\right] , \tag{5.6.1}$$

where ξ is a real function of ϕ and

$$R^2_{\rm GB} = R^2 - 4R_{\alpha\beta}R^{\alpha\beta} + R_{\alpha\beta\mu\nu}R^{\alpha\beta\mu\nu} . \tag{5.6.2}$$

This model is also captured by Horndeski's theory and can be obtained by setting

$$G_2 = X + 8\xi^{(4)}X^2(3 - \ln|X|)\,, \tag{5.6.3a}$$

$$G_3 = 4\xi^{(3)}X(7 - 3\ln|X|)\,, \tag{5.6.3b}$$

$$G_4 = \frac{M_{\rm pl}^2}{2} + 4\xi^{(2)}X(2 - \ln|X|)\,, \tag{5.6.3c}$$

$$G_5 = -4\xi^{(1)}\ln|X|\,, \tag{5.6.3d}$$

where $\xi^{(n)}(\phi) \equiv \mathrm{d}^n\xi(\phi)/\mathrm{d}\phi^n$.

5.6.1 Asymptotic Expansion

As we did for the other models, we now first prepare an asymptotic expansion for the background and perturbation fields. To do so, it is convenient to first expand $\xi(\phi)$ in powers of ϕ around the asymptotic value of ϕ, which we denote by ϕ_0. We set $\phi_0 = 0$ for convenience and can thus write

$$\xi(\phi) = \sum_{n=2}^{\infty}\frac{\xi_n}{n!}\phi^n\,, \tag{5.6.4}$$

where we have dropped the terms containing ξ_0 and ξ_1 since the former results in a surface term in the action and the latter would inhibit spontaneous scalarization [169]. The asymptotic expansions for the background fields were already presented in, e.g., [170], and we will therefore not further study them here.

The asymptotic expansions for the perturbations are given by

$$\begin{aligned} H_0(r) = {} & H_{0,-2}r^2 - 2H_{0,-2}Mr + \frac{H_{0,-2}\phi_1^2}{3M_{\rm pl}^2} + \frac{H_{0,-2}M\phi_1^2}{6M_{\rm pl}^2 r} \\ & + \frac{H_{0,-2}\phi_1^2(M^2+48\xi_2)}{3M_{\rm pl}^2 r^2} + \frac{H_{0,3}}{r^3} + \mathcal{O}\left(r^{-4}\right)\,, \end{aligned} \tag{5.6.5a}$$

$$\delta\phi(r) = -\frac{H_{0,-2}M\phi_1}{3} + \frac{12H_{0,-2}M\phi_1\xi_2}{r^2} + \frac{\delta\phi_3}{r^3} + \mathcal{O}\left(r^{-4}\right)\,, \tag{5.6.5b}$$

where we set $\delta\phi_{-2} = 0$ for convenience. Note that ξ_2 appears at order r^{-2} in the expansion and we can thus expect that ξ_2 will likely also appear within a contamination term at order r^{-3}. Indeed, from dimensional analysis it is straightforward to see that at order r^{-n} with $n \geq 2$ generally all coefficients $\xi_2, \ldots, \xi_n$ can appear.

5.6.2 EFT Side

We next turn to the EFT perspective again in an attempt to leverage it for disentangling the contamination terms. Using the same metric decomposition as before, Eq. (5.4.10),

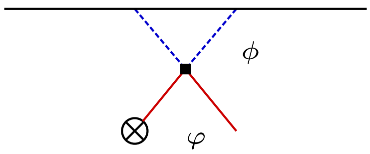

Figure 5.8: Leading-order diagram arising from the scalar field coupled to a Gauss-Bonnet term. Since we consider theories in which ξ is an even function of ϕ, the above diagram corresponds to the leading-order effect from ξ_2. We denote the corresponding operator, which is given in Eq. (5.6.7), with a black square.

we find that the Gauss-Bonnet contribution to the total action can be written as

$$\begin{aligned}\int \mathrm{d}^4x\sqrt{-g}\,\xi(\phi)R_{\mathrm{GB}}^2 = \int \mathrm{d}^4x\,\xi(\hat{\phi})\,\partial_i\Bigg[e^{\sqrt{2}\hat{\varphi}/M_{\mathrm{pl}}}\Bigg\{&2\sqrt{2}\frac{(\partial_j\partial^j\hat{\varphi})\partial^i\hat{\psi}}{M_{\mathrm{pl}}\,\hat{\psi}^{3/2}} + 2\frac{(\partial_j\hat{\varphi}\partial^j\hat{\varphi})\,\partial^i\hat{\psi}}{{M_{\mathrm{pl}}}^2\hat{\psi}^{3/2}} \\ &+ \sqrt{2}\frac{(\partial_j\hat{\psi}\partial^j\hat{\psi})\,\partial^i\hat{\varphi}}{M_{\mathrm{pl}}\hat{\psi}^{5/2}} - 6\frac{(\partial_j\hat{\varphi}\partial^j\hat{\psi})\,\partial^i\hat{\varphi}}{{M_{\mathrm{pl}}}^2\hat{\psi}^{3/2}} - 4\frac{(\partial_j\partial^j\hat{\varphi})\partial^i\hat{\varphi}}{{M_{\mathrm{pl}}}^2\,\hat{\psi}^{1/2}} \\ &+ 2\sqrt{2}\frac{(\partial_j\hat{\varphi}\partial^j\hat{\varphi})\,\partial^i\hat{\varphi}}{{M_{\mathrm{pl}}}^3\hat{\psi}^{1/2}} - 2\sqrt{2}\frac{\partial_j\partial^i\hat{\varphi}\partial^j\hat{\psi}}{M_{\mathrm{pl}}\,\hat{\psi}^{3/2}} + 4\frac{\partial^i\partial_j\hat{\varphi}\,\partial^j\hat{\varphi}}{{M_{\mathrm{pl}}}^2\hat{\psi}^{1/2}}\Bigg\}\Bigg]\,.\end{aligned} \tag{5.6.6}$$

We can here now already deduce that the symmetry that enable us to previously deduce that only even powers of $\hat{r}$ are allowed to appear in the expansions of $\delta\hat{\phi}$ and $\delta\hat{\varphi}$ is not present here anymore. In order to study the impact of the Gauss-Bonnet term more closely, we expand it around flat space and find that the LO contribution is given by

$$\mathcal{S}_{\mathrm{GB}}^{(\mathrm{LO})} = \frac{4\xi_2}{M_{\mathrm{pl}}^2}\int \mathrm{d}^4x\,\hat{\phi}\,\partial_i\hat{\phi}\Big(\partial_j\partial^j\hat{\varphi}\partial^i\hat{\varphi} - \partial^i\partial_j\hat{\varphi}\partial^j\hat{\varphi}\Big)\,. \tag{5.6.7}$$

The resulting LO diagram is shown in Fig. 5.8 and from dimensional analysis we deduce that it results in a contribution to $\delta\hat{\varphi}$ that is proportional to $\xi_2/\hat{r}^2$, consistent with what we found in the asymptotic expansion of H_0 in Eq. (5.6.5a).

While we are thus not able to determine the contamination term in sGB gravity, we were able to show that a non-trivial contamination is expected to be present, and we postpone further investigation of it to future work.

5.7 Conclusion

We have expanded upon the results of [166]—where the authors derived the general linear perturbation equations for a spherically symmetric and static system in Horndeski theory—by specializing their result to static perturbations and then presenting the general procedure that allows us to determine the perturbation profiles. We next defined the quadrupolar Love numbers by leveraging the PP EFT approach. Having finished this general setup, we turned to the study of a minimally coupled scalar field and have shown that the $1/r^3$ term in the asymptotic expansions of $\delta\phi$ and H_0 does not solely depend on the quadrupolar Love numbers, as is usually assumed. We identified the source of the additional terms that contaminate the $1/r^3$ terms and derived their exact expressions.

In order to quantitatively study our results, we chose the DEF model in the Jordan frame. Since a conformal rescaling of the metric can recast this model into the Einstein frame, where our previously obtained results for the minimally coupled scalar field are applicable, we were also able to determine the contamination terms for the DEF model. We then solved the background and perturbation equations numerically, where we used the DD2 equation of state to model nuclear matter. When comparing the corrected to the non-corrected Love numbers, we found that that the deviation can become quite noticeable—e.g., 15 % for $\beta = -6$ —but is less than $\approx 2\,\%$ for $\beta < -4.5$, which is the parameter range for β that has not yet been excluded. As such, while this difference in the Love numbers might not be observable with current observatories, next-generation detectors will be able to determine the Love numbers to sub-percent level precision [63], and it will thus be crucial to have a firm understanding of their calculation.

After studying the DEF model, we turned to the sGB model. We demonstrated that the procedure we leveraged to determine the contamination for the minimally coupled model does not apply to the sGB model in the same way. However, we were able to show that additional contamination terms most likely exist, and we postpone the study of their exact shape to future work.

5.A Background Equations

We present the definition of the functions that are used in the background equations of motion of the Horndeski action in Eq. Eq. (5.1.2).

$$
\begin{aligned}
A_1 &= -h^2(G_{3,X} - 2G_{4,\phi X})\phi'^2 - 2G_{4,\phi}h\,,\\
A_2 &= 2h^3(2G_{4,XX} - G_{5,\phi X})\phi'^3 - 4h^2(G_{4,X} - G_{5,\phi})\phi'\,,\\
A_3 &= -h^4 G_{5,XX}\phi'^4 + h^2 G_{5,X}(3h-1)\phi'^2\,,\\
A_4 &= h^2(2G_{4,XX} - G_{5,\phi X})\phi'^4 + h(3G_{5,\phi} - 4G_{4,X})\phi'^2 - 2G_4\,,\\
A_5 &= -\frac{1}{2}\left[G_{5,XX}h^3\phi'^5 - hG_{5,X}(5h-1)\phi'^3\right]\,,\\
A_6 &= h(G_{3,\phi} - 2G_{4,\phi\phi})\phi'^2 + G_2\,,\\
A_7 &= -2h^2(2G_{4,\phi X} - G_{5,\phi\phi})\phi'^3 - 4G_{4,\phi}h\phi'\,,\\
A_8 &= G_{5,\phi X}h^3\phi'^4 - h(2G_{4,X}h - G_{5,\phi}h - G_{5,\phi})\phi'^2 - 2G_4(h-1)\,,\\
A_9 &= -h(G_{2,X} - G_{3,\phi})\phi'^2 - G_2\,,\\
A_{10} &= \frac{1}{2}G_{5,\phi X}h^3\phi'^4 - \frac{1}{2}h^2(2G_{4,X} - G_{5,\phi})\phi'^2 - G_4 h\,.
\end{aligned}
$$

5.B Coefficients of perturbation equations of motion

The coefficients appearing in the perturbation equations of motion (5.2.10a)-(5.2.10f) are given by

$$
\begin{aligned}
a_1 = \sqrt{fh}\Bigg[&\left\{G_{4,\phi} + \frac{1}{2}h(G_{3,X} - 2G_{4,\phi X})\phi'^2\right\}r^2\\
&+2h\phi'\left\{G_{4,X} - G_{5,\phi} - \frac{1}{2}h(2G_{4,XX} - G_{5,\phi X})\phi'^2\right\}r\\
&+\frac{1}{2}G_{5,XX}h^3\phi'^4 - \frac{1}{2}G_{5,X}h(3h-1)\phi'^2\Bigg]\,,
\end{aligned}
$$

$$
a_2 = \sqrt{fh}\left(\frac{a_1}{\sqrt{fh}}\right)' - \left(\frac{\phi''}{\phi'} - \frac{1}{2}\frac{f'}{f}\right)a_1 + \frac{r}{\phi'}\left(\frac{f'}{f} - \frac{h'}{h}\right)a_4 - \frac{1}{2}\frac{\sqrt{f}r^2(\rho+P)}{\sqrt{h}\phi'}\,,
$$

$$
a_3 = -\frac{1}{2}\phi' a_1 - r a_4\,, \qquad a_4 = \frac{\sqrt{fh}}{2}\mathcal{H}\,, \qquad a_5 = a_2' - a_1''\,, \qquad a_6 = -\frac{\sqrt{f}}{2\sqrt{h}\phi'}\left(\mathcal{H}' + \frac{\mathcal{H}}{r} - \frac{\mathcal{F}}{r}\right),
$$

$$
a_7 = a_3' + \frac{1}{4}\frac{\sqrt{f}r^2(\rho+P)}{\sqrt{h}}\,, \qquad a_8 = -\frac{1}{2}\frac{a_4}{h}\,, \qquad a_9 = a_4' + \left(\frac{1}{r} - \frac{1}{2}\frac{f'}{f}\right)a_4\,, \qquad b_1 = \frac{1}{4}\sqrt{\frac{h}{f}}\mathcal{H}\,,
$$

$$
\begin{aligned}
c_2 = \sqrt{fh}\, \Bigg[& \Bigg\{ \frac{1}{2f}\left(-\frac{1}{2}h(3G_{3,X} - 8G_{4,\phi X})\phi'^2 + \frac{1}{2}h^2(G_{3,XX} - 2G_{4,\phi XX})\phi'^4 - G_{4,\phi} \right) r^2 \\
& - \frac{h\phi'}{f}\left(\frac{1}{2}h^2(2G_{4,XXX} - G_{5,\phi XX})\phi'^4 - \frac{1}{2}h(12G_{4,XX} - 7G_{5,\phi X})\phi'^2 + 3(G_{4,X} - G_{5,\phi}) \right) r \\
& + \frac{h\phi'^2}{4f}\left(G_{5,XXX}h^3\phi'^4 - G_{5,XX}h(10h-1)\phi'^2 + 3G_{5,X}(5h-1) \right) \Bigg\} f' \\
& + \phi' \left\{ \frac{1}{2}G_{2,X} - G_{3,\phi} - \frac{1}{2}h(G_{2,XX} - G_{3,\phi X})\phi'^2 \right\} r^2 \\
& + 2\left\{ -\frac{1}{2}h(3G_{3,X} - 8G_{4,\phi X})\phi'^2 + \frac{1}{2}h^2(G_{3,XX} - 2G_{4,\phi XX})\phi'^4 - G_{4,\phi} \right\} r \\
& - \frac{1}{2}h^3(2G_{4,XXX} - G_{5,\phi XX})\phi'^5 + \frac{1}{2}h\left\{ 2\,(6h-1)\,G_{4,XX} + (1-7h)\,G_{5,\phi X} \right\} \phi'^3 \\
& - (3h-1)(G_{4,X} - G_{5,\phi})\phi' \Bigg] ,
\end{aligned}
$$

$$
c_3 = -\frac{1}{2}\frac{\sqrt{f}r^2}{\sqrt{h}}\frac{\partial \mathcal{E}_{11}}{\partial \phi} ,
$$

$$
\begin{aligned}
c_4 = \frac{1}{4}\frac{\sqrt{f}}{\sqrt{h}} \Bigg[& \frac{h\phi'}{f}\left\{ 2G_{4,X} - 2G_{5,\phi} - h(2G_{4,XX} - G_{5,\phi X})\phi'^2 - \frac{h\phi'(3G_{5,X} - G_{5,XX}\phi'^2 h)}{r} \right\} f' \\
& + 4G_{4,\phi} + 2h(G_{3,X} - 2G_{4,\phi X})\phi'^2 + \frac{4h(G_{4,X} - G_{5,\phi})\phi' - 2h^2(2G_{4,XX} - G_{5,\phi X})\phi'^3}{r} \Bigg] ,
\end{aligned}
$$

$$
c_5 = -h\phi' c_4 - \frac{1}{2}\frac{\sqrt{fh}}{r}\mathcal{G} - \frac{1}{2}\frac{f'}{f}a_4 ,
$$

$$
c_6 = \frac{1}{8}\frac{f'\phi'}{f}a_1 + \frac{1}{2}\frac{f'r}{f}a_4 - \frac{1}{4}\phi' c_2 + \frac{1}{2}h\phi' r c_4 + \frac{1}{4}\sqrt{fh}\,\mathcal{G} , \qquad d_2 = 2hc_4 ,
$$

$$
\begin{aligned}
d_3 = & -\frac{1}{r^2}\left(\frac{2\phi''}{\phi'} + \frac{h'}{h} \right) a_1 + \frac{2f}{(f'r - 2f)\phi'}\left(\frac{2\phi''}{h\phi' r} + \frac{f'^2}{f^2} - \frac{f'h'}{fh} - \frac{2f'}{fr} + \frac{2h'}{hr} + \frac{h'}{h^2 r} \right) a_4 \\
& + \frac{f'r - 2f}{fr}\frac{\partial a_4}{\partial \phi} + \frac{\sqrt{f}}{\phi'\sqrt{h}r^2}\mathcal{F} - \frac{f^{3/2}}{\sqrt{h}(f'r - 2f)\phi'}\left(\frac{f'}{fr} + \frac{2\phi''}{\phi' r} + \frac{h'}{hr} - \frac{2}{r^2} \right)\mathcal{G} - \frac{\sqrt{f}(\rho + P)}{\phi'\sqrt{h}} ,
\end{aligned}
$$

$$
e_2 = -\frac{1}{2\phi'}\left(\frac{f'}{f}a_1 + 2c_2 + 4hrc_4 \right) , \qquad e_3 = \frac{1}{4}\frac{\sqrt{f}r^2}{\sqrt{h}}\frac{\partial \mathcal{E}_\phi}{\partial \phi} ,
$$

$$
\begin{aligned}
e_4 = & \frac{1}{\phi'}c_4' - \frac{1}{2}\frac{f'}{f\phi'^2 h}a_4' - \frac{1}{2}\frac{\sqrt{f}}{\phi'^2\sqrt{h}r}\mathcal{G}' + \frac{1}{h\phi' r^2}\left(\frac{\phi''}{\phi'} + \frac{1}{2}\frac{h'}{h} \right) a_1 \\
& + \frac{1}{4h\phi'^2}\left[\frac{(f'r - 6f)f'}{f^2 r} + \frac{h'(f'r + 4f)}{hrf} - \frac{4f(2\phi'' h + h'\phi')}{\phi' h^2 r(f'r - 2f)} \right] a_4 + \frac{1}{2}\frac{h'}{h\phi'}c_4 - \frac{1}{2}\frac{f'r - 2f}{fhr\phi'}\frac{\partial a_4}{\partial \phi} \\
& + \frac{1}{2}\frac{f'hr - f}{r^2\sqrt{f}\phi'^2 h^{3/2}}\mathcal{F} + \frac{1}{2}\frac{\sqrt{f}}{r\phi'^2 h^{3/2}}\left[\frac{f(2\phi'' h + h'\phi')}{h\phi'(f'r - 2f)} + \frac{1}{2}\frac{2f - f'hr}{fr} \right]\mathcal{G} + \frac{1}{2}\frac{\sqrt{f}(\rho + P)}{h^{3/2}\phi'^2} ,
\end{aligned}
$$

$$
g_2 = -\frac{1}{2}r^2 a_4 , \qquad g_4 = \frac{1}{8}r^2\sqrt{fh}\mathcal{G} , \qquad g_{12} = -hr^2 c_4 , \qquad g_{13} = \frac{1}{4}\frac{r^2 f'}{f}a_4 - \frac{1}{2}r^2 a_4' - \frac{3}{2}ra_4 ,
$$

$$
g_{14} = -\frac{1}{2}r^2 c_5 , \qquad g_{15} = -\frac{1}{2}r^2 d_3 , \qquad g_{16} = -\frac{1}{2}\sqrt{fh}\,\mathcal{G} ,
$$

$$
k_1 = -\frac{1}{4}\frac{\sqrt{f}}{\sqrt{h}}\mathcal{F} , \qquad k_2 = \frac{1}{4}\frac{\sqrt{f}}{\sqrt{h}}\mathcal{G} , \qquad k_3 = \frac{2f\mathcal{G}' + f'(\mathcal{G} - \mathcal{F})}{4\sqrt{fh}\,\phi'} ,
$$

with

$$\begin{aligned}
\mathcal{F} &\equiv 2G_4 + h\phi'^2 G_{5,\phi} - h\phi'^2\left(\frac{1}{2}h'\phi' + h\phi''\right)G_{5,X}\,,\\
\mathcal{G} &\equiv 2G_4 + 2h\phi'^2 G_{4,X} - h\phi'^2\left(G_{5,\phi} + \frac{f'h\phi' G_{5,X}}{2f}\right)\,,\\
\mathcal{H} &\equiv 2G_4 + 2h\phi'^2 G_{4,X} - h\phi'^2 G_{5,\phi} - \frac{h^2\phi'^3 G_{5,X}}{r}\,.
\end{aligned} \tag{5.B.1}$$

Note that $\mathcal{E}_{11}$ and $\mathcal{E}_\phi$ are defined, respectively, by Eqs. (5.1.2b) and (5.1.4).

5.C Asymptotic Expansions

5.C.1 Minimally Coupled Scalar Field

For the model studied in Sec. 5.4, we present the coefficients for the asymptotic expansion of the background fields and then show the coefficients for the perturbation fields.

Background

$$\begin{aligned}
h_0 &= 1\,,\\
h_1 &= -2M\,,\\
h_2 &= \frac{\phi_1^2}{2M_{\rm pl}^2}\,,\\
h_3 &= \frac{M\phi_1^2}{2M_{\rm pl}^2}\,,\\
h_4 &= \frac{2M^2\phi_1^2}{3M_{\rm pl}^2}\,,\\
h_5 &= \frac{M^3\phi_1^2}{M_{\rm pl}^2} - \frac{M\phi_1^4}{48M_{\rm pl}^4}\,,\\
h_6 &= \frac{8M^4\phi_1^2}{5M_{\rm pl}^2} - \frac{M^2\phi_1^4}{10M_{\rm pl}^4}\,,\\
h_7 &= \frac{8M^5\phi_1^2}{3M_{\rm pl}^2} - \frac{59M^3\phi_1^4}{180M_{\rm pl}^4} + \frac{M\phi_1^6}{320M_{\rm pl}^6}\,,\\
h_8 &= \frac{32M^6\phi_1^2}{7M_{\rm pl}^2} - \frac{32M^4\phi_1^4}{35M_{\rm pl}^4} + \frac{8M^2\phi_1^6}{315M_{\rm pl}^6}\,,\\
h_9 &= \frac{8M^7\phi_1^2}{M_{\rm pl}^2} - \frac{327M^5\phi_1^4}{140M_{\rm pl}^4} + \frac{141M^3\phi_1^6}{1120M_{\rm pl}^6} - \frac{5M\phi_1^8}{7168M_{\rm pl}^8}\,,\\
f_0 &= 1\,,\\
f_1 &= -2M\,,\\
f_2 &= 0\,,\\
f_3 &= \frac{M\phi_1^2}{6M_{\rm pl}^2}\,,
\end{aligned}$$

$$f_4 = \frac{M^2\phi_1^2}{3M_{\rm pl}^2}\,,$$

$$f_5 = \frac{3M^3\phi_1^2}{5M_{\rm pl}^2} - \frac{3M\phi_1^4}{80M_{\rm pl}^4}\,,$$

$$f_6 = \frac{16M^4\phi_1^2}{15M_{\rm pl}^2} - \frac{8M^2\phi_1^4}{45M_{\rm pl}^4}\,,$$

$$f_7 = \frac{40M^5\phi_1^2}{21M_{\rm pl}^2} - \frac{145M^3\phi_1^4}{252M_{\rm pl}^4} + \frac{5M\phi_1^6}{448M_{\rm pl}^6}\,,$$

$$f_8 = \frac{24M^6\phi_1^2}{7M_{\rm pl}^2} - \frac{111M^4\phi_1^4}{70M_{\rm pl}^4} + \frac{3M^2\phi_1^6}{35M_{\rm pl}^6}\,,$$

$$f_9 = \frac{56M^7\phi_1^2}{9M_{\rm pl}^2} - \frac{721M^5\phi_1^4}{180M_{\rm pl}^4} + \frac{5257M^3\phi_1^6}{12960M_{\rm pl}^6} - \frac{35M\phi_1^8}{9216M_{\rm pl}^8}\,,$$

$$\phi_0 = 0\,,$$

$$\phi_1 = \phi_1\,,$$

$$\phi_2 = M\phi_1\,,$$

$$\phi_3 = \frac{4M^2\phi_1}{3} - \frac{\phi_1^3}{12M_{\rm pl}^2}\,,$$

$$\phi_4 = 2M^3\phi_1 - \frac{M\phi_1^3}{3M_{\rm pl}^2}\,,$$

$$\phi_5 = \frac{16M^4\phi_1}{5} - \frac{29M^2\phi_1^3}{30M_{\rm pl}^2} + \frac{3\phi_1^5}{160M_{\rm pl}^4}\,,$$

$$\phi_6 = \frac{16M^5\phi_1}{3} - \frac{37M^3\phi_1^3}{15M_{\rm pl}^2} + \frac{2M\phi_1^5}{15M_{\rm pl}^4}\,,$$

$$\phi_7 = \frac{64M^6\phi_1}{7} - \frac{206M^4\phi_1^3}{35M_{\rm pl}^2} + \frac{751M^2\phi_1^5}{1260M_{\rm pl}^4} - \frac{5\phi_1^7}{896M_{\rm pl}^6}\,,$$

$$\phi_8 = 16M^7\phi_1 - \frac{472M^5\phi_1^3}{35M_{\rm pl}^2} + \frac{676M^3\phi_1^5}{315M_{\rm pl}^4} - \frac{2M\phi_1^7}{35M_{\rm pl}^6}\,,$$

$$\phi_9 = \frac{256M^8\phi_1}{9} - \frac{9476M^6\phi_1^3}{315M_{\rm pl}^2} + \frac{5717M^4\phi_1^5}{840M_{\rm pl}^4} - \frac{6959M^2\phi_1^7}{20160M_{\rm pl}^6} + \frac{35\phi_1^9}{18432M_{\rm pl}^8}\,.$$

Perturbations

$$
\begin{aligned}
\delta\phi_{-2} &= \delta\phi_{-2}\,, \\
\delta\phi_{-1} &= -2M\delta\phi_{-2}\,, \\
\delta\phi_0 &= -\frac{H_{0,-2}M\phi_1}{3} + \frac{2M^2\delta\phi_{-2}}{3}\,, \\
\delta\phi_1 &= \frac{M\delta\phi_{-2}\phi_1^2}{6M_{\rm pl}^2}\,, \\
\delta\phi_2 &= \frac{M^2\delta\phi_{-2}\phi_1^2}{3M_{\rm pl}^2}\,, \\
\delta\phi_3 &= \delta\phi_3\,, \\
\delta\phi_4 &= 3M\delta\phi_3 + \delta\phi_{-2}\left(-\frac{11M^4\phi_1^2}{15M_{\rm pl}^2} - \frac{47M^2\phi_1^4}{720M_{\rm pl}^4}\right)\,, \\
\delta\phi_5 &= H_{0,-2}\left(-\frac{3M^4\phi_1^3}{35M_{\rm pl}^2} + \frac{3M^2\phi_1^5}{560M_{\rm pl}^4}\right) + \frac{H_{0,3}M\phi_1}{7} \\
&\quad + \delta\phi_{-2}\left(-\frac{232M^5\phi_1^2}{105M_{\rm pl}^2} - \frac{19M^3\phi_1^4}{90M_{\rm pl}^4} + \frac{M\phi_1^6}{224M_{\rm pl}^6}\right) + \delta\phi_3\left(\frac{48M^2}{7} - \frac{5\phi_1^2}{28M_{\rm pl}^2}\right)\,, \\
\delta\phi_6 &= H_{0,-2}\left(-\frac{3M^5\phi_1^3}{7M_{\rm pl}^2} + \frac{3M^3\phi_1^5}{112M_{\rm pl}^4}\right) + \frac{5H_{0,3}M^2\phi_1}{7} \\
&\quad + \delta\phi_{-2}\left(-\frac{36M^6\phi_1^2}{7M_{\rm pl}^2} - \frac{51M^4\phi_1^4}{140M_{\rm pl}^4} + \frac{3M^2\phi_1^6}{70M_{\rm pl}^6}\right) + \delta\phi_3\left(\frac{100M^3}{7} - \frac{8M\phi_1^2}{7M_{\rm pl}^2}\right)\,, \\
\delta\phi_7 &= H_{0,-2}\left(-\frac{10M^6\phi_1^3}{7M_{\rm pl}^2} + \frac{M^4\phi_1^5}{8M_{\rm pl}^4} - \frac{M^2\phi_1^7}{448M_{\rm pl}^6}\right) + H_{0,3}\left(\frac{50M^3\phi_1}{21} - \frac{5M\phi_1^3}{84M_{\rm pl}^2}\right) \\
&\quad + \delta\phi_{-2}\left(-\frac{688M^7\phi_1^2}{63M_{\rm pl}^2} - \frac{37M^5\phi_1^4}{180M_{\rm pl}^4} + \frac{18493M^3\phi_1^6}{90720M_{\rm pl}^6} - \frac{17M\phi_1^8}{9216M_{\rm pl}^8}\right) \\
&\quad + \delta\phi_3\left(\frac{200M^4}{7} - \frac{191M^2\phi_1^2}{42M_{\rm pl}^2} + \frac{5\phi_1^4}{96M_{\rm pl}^4}\right)\,, \\
\delta\phi_8 &= H_{0,-2}\left(-\frac{4M^7\phi_1^3}{M_{\rm pl}^2} + \frac{15M^5\phi_1^5}{28M_{\rm pl}^4} - \frac{M^3\phi_1^7}{56M_{\rm pl}^6}\right) + H_{0,3}\left(\frac{20M^4\phi_1}{3} - \frac{10M^2\phi_1^3}{21M_{\rm pl}^2}\right) \\
&\quad - \delta\phi_{-2}\left(\frac{200M^8\phi_1^2}{9M_{\rm pl}^2} - \frac{569M^6\phi_1^4}{450M_{\rm pl}^4} - \frac{38657M^4\phi_1^6}{56700M_{\rm pl}^6} + \frac{139M^2\phi_1^8}{6300M_{\rm pl}^8}\right) \\
&\quad + \delta\phi_3\left(56M^5 - \frac{1532M^3\phi_1^2}{105M_{\rm pl}^2} + \frac{52M\phi_1^4}{105M_{\rm pl}^4}\right), \\
H_{0,-2} &= H_{0,-2}\,, \\
H_{0,-1} &= -2H_{0,-2}M\,, \\
H_{0,0} &= \frac{H_{0,-2}\phi_1^2}{3M_{\rm pl}^2} - \frac{2M\delta\phi_{-2}\phi_1}{3M_{\rm pl}^2}\,, \\
H_{0,1} &= \frac{H_{0,-2}M\phi_1^2}{6M_{\rm pl}^2}\,, \\
H_{0,2} &= \frac{H_{0,-2}M^2\phi_1^2}{3M_{\rm pl}^2}\,,
\end{aligned}
$$

$$
\begin{aligned}
H_{0,3} &= H_{0,3}\,,\\
H_{0,4} &= -H_{0,-2}\left(\frac{11M^4\phi_1^2}{15M_{\rm pl}^2}+\frac{47M^2\phi_1^4}{720M_{\rm pl}^4}\right)+3H_{0,3}M\,,\\
H_{0,5} &= H_{0,-2}\left(-\frac{50M^5\phi_1^2}{21M_{\rm pl}^2}-\frac{289M^3\phi_1^4}{2520M_{\rm pl}^4}-\frac{M\phi_1^6}{1120M_{\rm pl}^6}\right)+H_{0,3}\left(\frac{50M^2}{7}-\frac{9\phi_1^2}{28M_{\rm pl}^2}\right)\\
&\quad+\delta\phi_3\frac{2M\phi_1}{7M_{\rm pl}^2}+\delta\phi_{-2}\left(-\frac{6M^4\phi_1^3}{35M_{\rm pl}^4}+\frac{3M^2\phi_1^5}{280M_{\rm pl}^6}\right)\,,\\
H_{0,6} &= H_{0,-2}\left(-\frac{6M^6\phi_1^2}{M_{\rm pl}^2}+\frac{33M^4\phi_1^4}{280M_{\rm pl}^4}+\frac{9M^2\phi_1^6}{560M_{\rm pl}^6}\right)+H_{0,3}\left(\frac{110M^3}{7}-\frac{13M\phi_1^2}{7M_{\rm pl}^2}\right)\\
&\quad+\delta\phi_3\frac{10M^2\phi_1}{7M_{\rm pl}^2}+\delta\phi_{-2}\left(-\frac{6M^5\phi_1^3}{7M_{\rm pl}^4}+\frac{3M^3\phi_1^5}{56M_{\rm pl}^6}\right)\,,\\
H_{0,7} &= H_{0,-2}\left(-\frac{124M^7\phi_1^2}{9M_{\rm pl}^2}+\frac{464M^5\phi_1^4}{315M_{\rm pl}^4}+\frac{241M^3\phi_1^6}{3240M_{\rm pl}^6}+\frac{25M\phi_1^8}{64512M_{\rm pl}^8}\right)\\
&\quad+H_{0,3}\left(\frac{100M^4}{3}-\frac{148M^2\phi_1^2}{21M_{\rm pl}^2}+\frac{25\phi_1^4}{224M_{\rm pl}^4}\right)\\
&\quad+\delta\phi_{-2}\left(-\frac{20M^6\phi_1^3}{7M_{\rm pl}^4}+\frac{M^4\phi_1^5}{4M_{\rm pl}^6}-\frac{M^2\phi_1^7}{224M_{\rm pl}^8}\right)+\delta\phi_3\left(\frac{100M^3\phi_1}{21M_{\rm pl}^2}-\frac{5M\phi_1^3}{42M_{\rm pl}^4}\right)\,,\\
H_{0,8} &= H_{0,-2}\left(-\frac{272M^8\phi_1^2}{9M_{\rm pl}^2}+\frac{9979M^6\phi_1^4}{1575M_{\rm pl}^4}+\frac{6257M^4\phi_1^6}{56700M_{\rm pl}^6}-\frac{53M^2\phi_1^8}{12600M_{\rm pl}^8}\right)\\
&\quad+H_{0,3}\left(\frac{208M^5}{3}-\frac{2332M^3\phi_1^2}{105M_{\rm pl}^2}+\frac{34M\phi_1^4}{35M_{\rm pl}^4}\right)\\
&\quad+\delta\phi_{-2}\left(-\frac{8M^7\phi_1^3}{M_{\rm pl}^4}+\frac{15M^5\phi_1^5}{14M_{\rm pl}^6}-\frac{M^3\phi_1^7}{28M_{\rm pl}^8}\right)+\delta\phi_3\left(\frac{40M^4\phi_1}{3M_{\rm pl}^2}-\frac{20M^2\phi_1^3}{21M_{\rm pl}^4}\right)\,.
\end{aligned}
$$

5.C.2 DEF Model

For the model discussed in Sec. 5.5, we show the coefficients for the asymptotic expansion of the background fields and also present the coefficients for the perturbation fields.

Background

$$
\begin{aligned}
h_0 &= 1\,,\\
h_1 &= -2M\,,\\
h_2 &= \frac{\phi_1^2(1-2\beta)}{2M_{\rm pl}^2}\,,\\
h_3 &= \frac{M\phi_1^2(1-3\beta)}{2M_{\rm pl}^2}\,,\\
h_4 &= \frac{M^2\phi_1^2(2-7\beta)}{3M_{\rm pl}^2}+\frac{\beta\phi_1^4(1-3\beta)}{12M_{\rm pl}^4}\,,\\
h_5 &= \frac{M^3\phi_1^2(6-23\beta)}{6M_{\rm pl}^2}+\frac{M\phi_1^4\left(-51\beta^2+18\beta-1\right)}{48M_{\rm pl}^4}\,,
\end{aligned}
$$

$$
\begin{aligned}
h_6 &= \frac{2M^4\phi_1^2\,(12-49\beta)}{15M_{\rm pl}^2} + \frac{M^2\phi_1^4\left(-195\beta^2+73\beta-6\right)}{60M_{\rm pl}^4} + \frac{\beta\phi_1^6\left(-30\beta^2+15\beta-2\right)}{240M_{\rm pl}^6}\,,\\
h_7 &= \frac{2M^5\phi_1^2\,(60-257\beta)}{45M_{\rm pl}^2} + \frac{M^3\phi_1^4\left(-3135\beta^2+1229\beta-118\right)}{360M_{\rm pl}^4} + \frac{M\phi_1^6\left(-875\beta^3+475\beta^2-79\beta+3\right)}{960M_{\rm pl}^6}\,,\\
h_8 &= \frac{8M^6\phi_1^2\,(20-89\beta)}{35M_{\rm pl}^2} + \frac{2M^4\phi_1^4\left(-1141\beta^2+463\beta-48\right)}{105M_{\rm pl}^4}\\
&\quad + \frac{M^2\phi_1^6\left(-10605\beta^3+6132\beta^2-1152\beta+64\right)}{2520M_{\rm pl}^6} + \frac{\beta\phi_1^8\left(-420\beta^3+315\beta^2-84\beta+8\right)}{5040M_{\rm pl}^8}\,,\\
h_9 &= \frac{M^7\phi_1^2\,(280-1286\beta)}{35M_{\rm pl}^2} - \frac{M^5\phi_1^4\left(87185\beta^2-36300\beta+3924\right)}{1680M_{\rm pl}^4}\\
&\quad - \frac{M^3\phi_1^6\left(105525\beta^3-64036\beta^2+12975\beta-846\right)}{6720M_{\rm pl}^6}\\
&\quad + \frac{M\phi_1^8\left(-93555\beta^4+74340\beta^3-21686\beta^2+2556\beta-75\right)}{107520M_{\rm pl}^8}\,,\\
f_0 &= 1\,,\\
f_1 &= -2M\,,\\
f_2 &= \frac{\beta\phi_1^2}{2M_{\rm pl}^2}\,,\\
f_3 &= \frac{M\phi_1^2\,(1-3\beta)}{6M_{\rm pl}^2}\,,\\
f_4 &= \frac{M^2\phi_1^2\,(2-7\beta)}{6M_{\rm pl}^2} + \frac{\beta\phi_1^4\,(9\beta-2)}{24M_{\rm pl}^4}\,,\\
f_5 &= \frac{M^3\phi_1^2\,(18-65\beta)}{30M_{\rm pl}^2} + \frac{M\phi_1^4\left(105\beta^2+10\beta-9\right)}{240M_{\rm pl}^4}\,,\\
f_6 &= \frac{16M^4\phi_1^2\,(3-11\beta)}{45M_{\rm pl}^2} + \frac{M^2\phi_1^4\left(-15\beta^2+34\beta-8\right)}{45M_{\rm pl}^4} + \frac{\beta\phi_1^6\left(30\beta^2-15\beta+2\right)}{90M_{\rm pl}^6}\,,\\
f_7 &= \frac{2M^5\phi_1^2\,(100-371\beta)}{105M_{\rm pl}^2} + \frac{M^3\phi_1^4\left(-8505\beta^2+7567\beta-1450\right)}{2520M_{\rm pl}^4}\\
&\quad + \frac{M\phi_1^6\left(25515\beta^3-10395\beta^2+259\beta+225\right)}{20160M_{\rm pl}^6}\,,\\
f_8 &= \frac{6M^6\phi_1^2\,(4-15\beta)}{7M_{\rm pl}^2} + \frac{M^4\phi_1^4\left(-10255\beta^2+7572\beta-1332\right)}{840M_{\rm pl}^4}\\
&\quad + \frac{M^2\phi_1^6\left(4375\beta^3-560\beta^2-660\beta+144\right)}{1680M_{\rm pl}^6} + \frac{\beta\phi_1^8\left(4375\beta^3-3500\beta^2+980\beta-96\right)}{13440M_{\rm pl}^8}\,,\\
f_9 &= \frac{2M^7\phi_1^2\,(980-3713\beta)}{315M_{\rm pl}^2} + \frac{M^5\phi_1^4\left(-530145\beta^2+361244\beta-60564\right)}{15120M_{\rm pl}^4}\\
&\quad + \frac{M^3\phi_1^6\left(343035\beta^3+701316\beta^2-473979\beta+73598\right)}{181440M_{\rm pl}^6}\\
&\quad + \frac{M\phi_1^8\left(2096325\beta^4-1575420\beta^3+369138\beta^2-12916\beta-3675\right)}{967680M_{\rm pl}^8}\,,\\
\phi_0 &= 0\,,\\
\phi_1 &= \phi_1\,,
\end{aligned}
$$

$$
\begin{aligned}
\phi_2 &= M\phi_1\,,\\
\phi_3 &= \frac{4M^2\phi_1}{3} + \frac{\phi_1^3\,(3\beta-1)}{12M_{\rm pl}^2}\,,\\
\phi_4 &= 2M^3\phi_1 + \frac{M\phi_1^3\,(3\beta-1)}{3M_{\rm pl}^2}\,,\\
\phi_5 &= \frac{16M^4\phi_1}{5} + \frac{M^2\phi_1^3\,(175\beta-58)}{60M_{\rm pl}^2} + \frac{\phi_1^5\left(75\beta^2-50\beta+9\right)}{480M_{\rm pl}^4}\,,\\
\phi_6 &= \frac{16M^5\phi_1}{3} + \frac{M^3\phi_1^3\,(225\beta-74)}{30M_{\rm pl}^2} + \frac{M\phi_1^5\left(135\beta^2-90\beta+16\right)}{120M_{\rm pl}^4}\,,\\
\phi_7 &= \frac{64M^6\phi_1}{7} + \frac{2M^4\phi_1^3\,(2842\beta-927)}{315M_{\rm pl}^2} + \frac{M^2\phi_1^5\left(25725\beta^2-17101\beta+3004\right)}{5040M_{\rm pl}^4}\\
&\quad + \frac{\phi_1^7\left(5145\beta^3-5145\beta^2+1813\beta-225\right)}{40320M_{\rm pl}^6}\,,\\
\phi_8 &= 16M^7\phi_1 + \frac{4M^5\phi_1^3\,(3283\beta-1062)}{315M_{\rm pl}^2} + \frac{4M^3\phi_1^5\left(1470\beta^2-973\beta+169\right)}{315M_{\rm pl}^4}\\
&\quad + \frac{M\phi_1^7\left(140\beta^3-140\beta^2+49\beta-6\right)}{105M_{\rm pl}^6}\,,\\
\phi_9 &= \frac{256M^8\phi_1}{9} + \frac{M^6\phi_1^3\,(29531\beta-9476)}{315M_{\rm pl}^2} + \frac{M^4\phi_1^5\left(202041\beta^2-133060\beta+22868\right)}{3360M_{\rm pl}^4}\\
&\quad + \frac{M^2\phi_1^7\left(331695\beta^3-331128\beta^2+115077\beta-13918\right)}{40320M_{\rm pl}^6}\\
&\quad + \frac{\phi_1^9\left(76545\beta^4-102060\beta^3+53298\beta^2-12916\beta+1225\right)}{645120M_{\rm pl}^8}\,.
\end{aligned}
$$

Perturbations

$$
\begin{aligned}
\delta\phi_{-2} &= \delta\phi_{-2}\,,\\
\delta\phi_{-1} &= -2M\delta\phi_{-2}\,,\\
\delta\phi_0 &= -\frac{H_{0,-2}M\phi_1}{3} + \delta\phi_{-2}\left(\frac{2M^2}{3} - \frac{\beta\phi_1^2}{2M_{\rm pl}^2}\right)\,,\\
\delta\phi_1 &= \frac{M\delta\phi_{-2}\phi_1^2\,(1-3\beta)}{6M_{\rm pl}^2}\,,\\
\delta\phi_2 &= \delta\phi_{-2}\left[\frac{M^2\phi_1^2\,(2-5\beta)}{6M_{\rm pl}^2} + \frac{\beta\phi_1^4\,(2-3\beta)}{24M_{\rm pl}^4}\right]\,,\\
\delta\phi_3 &= \delta\phi_3\,,\\
\delta\phi_4 &= 3M\delta\phi_3 + \delta\phi_{-2}\left[\frac{M^4\phi_1^2\,(157\beta-66)}{90M_{\rm pl}^2} + \frac{M^2\phi_1^4\left(-105\beta^2+86\beta-47\right)}{720M_{\rm pl}^4}\right.\\
&\qquad\left. + \frac{\beta\phi_1^6\left(-15\beta^2+15\beta-4\right)}{180M_{\rm pl}^6}\right]\,,\\
\delta\phi_5 &= H_{0,-2}\left[\frac{M^4\phi_1^3\,(95\beta-54)}{630M_{\rm pl}^2} + \frac{M^2\phi_1^5\left(345\beta^2-250\beta+27\right)}{5040M_{\rm pl}^4}\right] + \frac{H_{0,3}M\phi_1}{7}\,,
\end{aligned}
$$

$$
\begin{aligned}
&+\delta\phi_{-2}\left[\frac{2M^5\phi_1^2\,(817\beta-348)}{315M_{\rm pl}^2}+\frac{M^3\phi_1^4\left(-450\beta^2+379\beta-266\right)}{1260M_{\rm pl}^4}\right.\\
&\qquad\left.+\frac{M\phi_1^6\left(-815\beta^3+915\beta^2-319\beta+15\right)}{3360M_{\rm pl}^6}\right]\\
&+\delta\phi_3\left[\frac{48M^2}{7}+\frac{\phi_1^2\,(21\beta-5)}{28M_{\rm pl}^2}\right],\\
\delta\phi_6 = {}& H_{0,-2}\left[\frac{M^5\phi_1^3\,(95\beta-54)}{126M_{\rm pl}^2}+\frac{M^3\phi_1^5\left(345\beta^2-250\beta+27\right)}{1008M_{\rm pl}^4}\right]+\frac{5H_{0,3}M^2\phi_1}{7}\\
&+\delta\phi_{-2}\left[\frac{4M^6\phi_1^2\,(941\beta-405)}{315M_{\rm pl}^2}+\frac{M^4\phi_1^4\left(1149\beta^2-712\beta-918\right)}{2520M_{\rm pl}^4}\right.\\
&\qquad+\frac{M^2\phi_1^6\left(-1215\beta^3+1486\beta^2-666\beta+72\right)}{1680M_{\rm pl}^6}\\
&\qquad\left.+\frac{\beta\phi_1^8\left(-315\beta^3+420\beta^2-196\beta+32\right)}{4480M_{\rm pl}^8}\right]\\
&+\delta\phi_3\left[\frac{100M^3}{7}+\frac{M\phi_1^2\,(63\beta-16)}{14M_{\rm pl}^2}\right],\\
\delta\phi_7 = {}& H_{0,-2}\left[\frac{5M^6\phi_1^3\,(95\beta-54)}{189M_{\rm pl}^2}+\frac{M^4\phi_1^5\left(2010\beta^2-1507\beta+189\right)}{1512M_{\rm pl}^4}\right.\\
&\qquad\left.+\frac{M^2\phi_1^7\left(1035\beta^3-1095\beta^2+331\beta-27\right)}{12096M_{\rm pl}^6}\right]\\
&+H_{0,3}\left[\frac{50M^3\phi_1}{21}+\frac{5M\phi_1^3\,(3\beta-1)}{84M_{\rm pl}^2}\right]\\
&+\delta\phi_{-2}\left[\frac{2M^7\phi_1^2\,(11887\beta-5160)}{945M_{\rm pl}^2}+\frac{M^5\phi_1^4\left(29187\beta^2-21556\beta-1036\right)}{5040M_{\rm pl}^4}\right.\\
&\qquad+\frac{M^3\phi_1^6\left(-392715\beta^3+499068\beta^2-258741\beta+36986\right)}{181440M_{\rm pl}^6}\\
&\qquad\left.+\frac{M\phi_1^8\left(-415305\beta^4+589740\beta^3-303066\beta^2+57796\beta-1785\right)}{967680M_{\rm pl}^8}\right]\\
&+\delta\phi_3\left[\frac{200M^4}{7}+\frac{M^2\phi_1^2\,(1455\beta-382)}{84M_{\rm pl}^2}+\frac{\phi_1^4\left(441\beta^2-234\beta+35\right)}{672M_{\rm pl}^4}\right],\\
\delta\phi_8 = {}& H_{0,-2}\left[\frac{M^7\phi_1^3(190\beta-108)}{27M_{\rm pl}^2}+\frac{M^5\phi_1^5\left(1185\beta^2-926\beta+135\right)}{252M_{\rm pl}^4}\right.\\
&\qquad\left.+\frac{M^3\phi_1^7\left(1035\beta^3-1095\beta^2+331\beta-27\right)}{1512M_{\rm pl}^6}\right]\\
&+H_{0,3}\left[\frac{20M^4\phi_1}{3}+\frac{10M^2\phi_1^3\,(3\beta-1)}{21M_{\rm pl}^2}\right]\\
&+\delta\phi_{-2}\left[\frac{4M^8\phi_1^2\,(60037\beta-26250)}{4725M_{\rm pl}^2}+\frac{M^6\phi_1^4\left(240155\beta^2-180038\beta+11949\right)}{9450M_{\rm pl}^4}\right.\\
&\qquad+\frac{M^4\phi_1^6\left(-294480\beta^3+389205\beta^2-232266\beta+38657\right)}{56700M_{\rm pl}^6}
\end{aligned}
$$

$$
\begin{aligned}
&+\frac{M^2\phi_1^8\left(-141375\beta^4+211560\beta^3-119745\beta^2+26914\beta-1668\right)}{75600M_{\rm pl}^8}\\
&\left.+\frac{\beta\phi_1^{10}\left(-1260\beta^4+2100\beta^3-1365\beta^2+410\beta-48\right)}{18900M_{\rm pl}^{10}}\right]\\
&+\delta\phi_3\left[56M^5+\frac{2M^3\phi_1^2\left(2865\beta-766\right)}{105M_{\rm pl}^2}+\frac{M\phi_1^4\left(630\beta^2-345\beta+52\right)}{105M_{\rm pl}^4}\right],
\end{aligned}
$$

$$
\begin{aligned}
H_{0,-2}&=H_{0,-2}\,,\\
H_{0,-1}&=-2H_{0,-2}M-\frac{\beta\delta\phi_{-2}\phi_1}{M_{\rm pl}^2}\,,\\
H_{0,0}&=\frac{H_{0,-2}\phi_1^2\left(2-3\beta\right)}{6M_{\rm pl}^2}+\frac{M\delta\phi_{-2}\phi_1\left(3\beta-2\right)}{3M_{\rm pl}^2}\,,\\
H_{0,1}&=\frac{H_{0,-2}M\phi_1^2\left(1-\beta\right)}{6M_{\rm pl}^2}+\frac{\beta\delta\phi_{-2}\phi_1^3\left(3\beta+1\right)}{12M_{\rm pl}^4}\,,\\
H_{0,2}&=H_{0,-2}\left[\frac{M^2\phi_1^2\left(2-3\beta\right)}{6M_{\rm pl}^2}+\frac{\beta\phi_1^4\left(2-3\beta\right)}{24M_{\rm pl}^4}\right]+\frac{M\beta^2\delta\phi_{-2}\phi_1^3}{2M_{\rm pl}^4}\,,\\
H_{0,3}&=H_{0,3}\,,\\
H_{0,4}&=H_{0,-2}\left[\frac{M^4\phi_1^2\left(97\beta-66\right)}{90M_{\rm pl}^2}+\frac{M^2\phi_1^4\left(-45\beta^2+66\beta-47\right)}{720M_{\rm pl}^4}+\frac{\beta\phi_1^6\left(-15\beta^2+15\beta-4\right)}{180M_{\rm pl}^6}\right]\\
&\quad+3H_{0,3}M-\frac{\beta\delta\phi_3\phi_1}{M_{\rm pl}^2}+\delta\phi_{-2}\left[\frac{M^3\beta\phi_1^3\left(38-155\beta\right)}{60M_{\rm pl}^4}+\frac{M\beta\phi_1^5\left(-495\beta^2+390\beta-37\right)}{1440M_{\rm pl}^6}\right],\\
H_{0,5}&=H_{0,-2}\left[\frac{M^5\phi_1^2\left(367\beta-250\right)}{105M_{\rm pl}^2}+\frac{M^3\phi_1^4\left(-55\beta^2-56\beta-289\right)}{2520M_{\rm pl}^4}\right.\\
&\qquad\left.+\frac{M\phi_1^6\left(-2415\beta^3+2035\beta^2-471\beta-9\right)}{10080M_{\rm pl}^6}\right]\\
&\quad+H_{0,3}\left[\frac{50M^2}{7}+\frac{3\phi_1^2\left(7\beta-3\right)}{28M_{\rm pl}^2}\right]+\frac{2M\delta\phi_3\phi_1\left(1-14\beta\right)}{7M_{\rm pl}^2}\\
&\quad+\delta\phi_{-2}\left[\frac{8M^6\beta\phi_1}{315M_{\rm pl}^2}+\frac{M^4\phi_1^3\left(-5987\beta^2+1880\beta-108\right)}{630M_{\rm pl}^4}\right.\\
&\qquad+\frac{M^2\phi_1^5\left(-9255\beta^3+7434\beta^2-1073\beta+54\right)}{5040M_{\rm pl}^6}\\
&\qquad\left.+\frac{\beta\phi_1^7\left(-105\beta^3+135\beta^2+19\beta-9\right)}{20160M_{\rm pl}^8}\right],\\
H_{0,6}&=H_{0,-2}\left[\frac{M^6\phi_1^2\left(397\beta-270\right)}{45M_{\rm pl}^2}+\frac{M^4\phi_1^4\left(2404\beta^2-3698\beta+297\right)}{2520M_{\rm pl}^4}\right.\\
&\qquad+\frac{M^2\phi_1^6\left(-7305\beta^3+5516\beta^2-1557\beta+162\right)}{10080M_{\rm pl}^6}\\
&\qquad\left.+\frac{\beta\phi_1^8\left(-315\beta^3+420\beta^2-196\beta+32\right)}{4480M_{\rm pl}^8}\right]\\
&\quad+H_{0,3}\left[\frac{110M^3}{7}+\frac{M\phi_1^2\left(61\beta-26\right)}{14M_{\rm pl}^2}\right]
\end{aligned}
$$

$$
\begin{aligned}
&+ \delta\phi_{-2}\left[\frac{8M^7\beta\phi_1}{63M_{\rm pl}^2} + \frac{M^5\phi_1^3\left(-1613\beta^2+589\beta-54\right)}{63M_{\rm pl}^4}\right.\\
&\qquad + \frac{M^3\phi_1^5\left(-20190\beta^3+15503\beta^2-2529\beta+135\right)}{2520M_{\rm pl}^6}\\
&\qquad \left.+ \frac{M\beta\phi_1^7\left(-2745\beta^3+2770\beta^2-623\beta+24\right)}{6720M_{\rm pl}^8}\right]\\
&+ \delta\phi_3\left[\frac{5M^2\phi_1\left(6-47\beta\right)}{21M_{\rm pl}^2} + \frac{\beta\phi_1^3\left(11-42\beta\right)}{42M_{\rm pl}^4}\right],
\end{aligned}
$$

$$
\begin{aligned}
H_{0,7} = H_{0,-2}&\left[\frac{4M^7\phi_1^2\left(4801\beta-3255\right)}{945M_{\rm pl}^2} + \frac{M^5\phi_1^4\left(85385\beta^2-117256\beta+22272\right)}{15120M_{\rm pl}^4}\right.\\
&\qquad + \frac{M^3\phi_1^6\left(-372105\beta^3+234366\beta^2-71415\beta+13496\right)}{181440M_{\rm pl}^6}\\
&\qquad \left.+ \frac{M\phi_1^8\left(-410865\beta^4+502500\beta^3-216562\beta^2+31996\beta+375\right)}{967680M_{\rm pl}^8}\right]\\
&+ H_{0,3}\left[\frac{100M^4}{3} + \frac{M^2\phi_1^2\left(1413\beta-592\right)}{84M_{\rm pl}^2} + \frac{\phi_1^4\left(147\beta^2-118\beta+25\right)}{224M_{\rm pl}^4}\right]\\
&+ \delta\phi_{-2}\left[\frac{80M^8\beta\phi_1}{189M_{\rm pl}^2} + \frac{M^6\phi_1^3\left(-57591\beta^2+23380\beta-2700\right)}{945M_{\rm pl}^4}\right.\\
&\qquad + \frac{M^4\phi_1^5\left(-913563\beta^3+686704\beta^2-125140\beta+7560\right)}{30240M_{\rm pl}^6}\\
&\qquad + \frac{M^2\phi_1^7\left(-384795\beta^4+407238\beta^3-118241\beta^2+11540\beta-540\right)}{120960M_{\rm pl}^8}\\
&\qquad \left.+ \frac{\beta\phi_1^9\left(-11025\beta^4+19140\beta^3-3858\beta^2-1700\beta+375\right)}{1935360M_{\rm pl}^{10}}\right]\\
&+ \delta\phi_3\left[\frac{10M^3\phi_1\left(10-57\beta\right)}{21M_{\rm pl}^2} + \frac{M\phi_1^3\left(-294\beta^2+95\beta-5\right)}{42M_{\rm pl}^4}\right],
\end{aligned}
$$

$$
\begin{aligned}
H_{0,8} = H_{0,-2}&\left[\frac{8M^8\phi_1^2\left(26431\beta-17850\right)}{4725M_{\rm pl}^2} + \frac{M^6\phi_1^4\left(210825\beta^2-272558\beta+59874\right)}{9450M_{\rm pl}^4}\right.\\
&\qquad + \frac{M^4\phi_1^6\left(-1062045\beta^3+306210\beta^2-26379\beta+25028\right)}{226800M_{\rm pl}^6}\\
&\qquad + \frac{M^2\phi_1^8\left(-286425\beta^4+324195\beta^3-134025\beta^2+21683\beta-636\right)}{151200M_{\rm pl}^8}\\
&\qquad \left.+ \frac{\beta\phi_1^{10}\left(-1260\beta^4+2100\beta^3-1365\beta^2+410\beta-48\right)}{18900M_{\rm pl}^{10}}\right]\\
&+ H_{0,3}\left[\frac{208M^5}{3} + \frac{M^3\phi_1^2\left(5685\beta-2332\right)}{105M_{\rm pl}^2} + \frac{M\phi_1^4\left(405\beta^2-325\beta+68\right)}{70M_{\rm pl}^4}\right]\\
&+ \delta\phi_{-2}\left[\frac{32M^9\beta\phi_1}{27M_{\rm pl}^2} + \frac{M^7\phi_1^3\left(-214305\beta^2+94334\beta-12600\right)}{1575M_{\rm pl}^4}\right.\\
&\qquad + \frac{M^5\phi_1^5\left(-760941\beta^3+572334\beta^2-115535\beta+8100\right)}{7560M_{\rm pl}^6}
\end{aligned}
$$

$$
\begin{aligned}
&\qquad + \frac{M^3\phi_1^7\left(-3857625\beta^4+4157325\beta^3-1339725\beta^2+159823\beta-8100\right)}{226800M_{\rm pl}^8} \\
&\qquad \left. + \frac{M\beta\phi_1^9\left(-132525\beta^4+175050\beta^3-69675\beta^2+8980\beta-72\right)}{302400M_{\rm pl}^{10}}\right] \\
&+ \delta\phi_3\left[\frac{2M^4\phi_1\left(100-459\beta\right)}{15M_{\rm pl}^2}+\frac{M^2\phi_1^3\left(-6395\beta^2+2378\beta-200\right)}{210M_{\rm pl}^4}\right. \\
&\qquad \left. + \frac{\beta\phi_1^5\left(-420\beta^2+235\beta-36\right)}{420M_{\rm pl}^6}\right].
\end{aligned}
$$

Chapter 6

Discussion and Outlook

The advent of GW astronomy enables a plethora of new ways to test models that go beyond the standard model of particle physics and GR. In this thesis, we have explored several aspects of how such models impact the GW signal originating from compact binary systems.

In chapter 3, we outlined the details on how Goldberger & Rothstein's EFT approach to the generation of GWs from compact binaries is modified to accommodate an additional massive scalar degree of freedom. During the course of this chapter, we derived the modified conservative dynamics, power loss, and GW phase for binary systems on circular orbits—all at 1PN relative order. While doing so, we kept the Wilsonian coefficients that appear in the PP action model agnostic, and we can thus easily apply the obtained results to various scalar-tensor theories. Most importantly, the presented results extended previously available computations to NLO order.

We continued in chapter 4 by shifting our focus toward NS that are admixed with minimally coupled DM and computed their mass, radius, and tidal deformability for DM masses of order $m_s \sim 10^{-10}\,$eV. In this regime, we were able to describe the DM content as a classical field, so that the resulting objects can be considered to be the combination of a BS with a NS. While the masses and radii of such objects have already been previously computed, we extended these results by investigating the tidal deformability of said objects. We found that even a small amount of DM can significantly enhance the tidal deformability, given that it arranges in a cloud-like configuration, which generally happens for $m_s < 10^{-10}\,$eV.

Chapter 4 continued the exploration of the tidal deformability, but now focusing on scalar-tensor theories, where an additional long-range scalar degree of freedom is present. More specifically, we framed our analysis around Horndeski's theory, which encapsulates all scalar-tensor theories that have at most second-order equations of motion. We leveraged previous results obtained in [166], where the authors derived the general linear perturbation equations for spherical symmetric spacetimes without specifying the gauge. We specialized these perturbation equations for the calculation of static perturbations and complemented it with a detailed analysis from the PP EFT point of view. Doing so we were able to identify and resolve an ambiguity that generically contaminates the Love numbers in scalar-tensor theories. More explicitly, we found that, in contrast to pure GR, there are additional terms in the asymptotic expansion of the metric perturbations at large radii that mimic a tidal response, and we were able to calculate these terms.

There is a multitude of ways on how to expand on the here-presented results. Utilizing the in chapter 3 presented GW phase, one can directly obtain constraints on the worldline coefficients and scalar field parameter without having to specify the full model. Also, it remains to investigate the behavior of, e.g., tail effects in the presence of the finite scalar field mass. Further, while chapter 4 investigates the Love numbers of FBSs by using linear perturbation theory [171] demonstrated that in certain cases linear perturbation theory breaks down due to excessively large perturbations in the scalar field. Investigating under which conditions linear theory breaks down and how to describe higher-order effects via nonlinear perturbation theory seems a critical direction. One of the main results of chapter 5 is the identification of the term that contaminates the quadrupolar even-parity Love numbers, and it remains to investigate the contamination for other multipoles as well as their odd-parity counterparts.

Bibliography

[1] R. F. Diedrichs, N. Becker, C. Jockel, J.-E. Christian, L. Sagunski and J. Schaffner-Bielich, *Tidal deformability of fermion-boson stars: Neutron stars admixed with ultralight dark matter*, *Phys. Rev. D* **108** (2023) 064009, [2303.04089].

[2] R. F. Diedrichs, D. Schmitt and L. Sagunski, *Binary systems in massive scalar-tensor theories: Next-to-leading order gravitational wave phase from effective field theory*, *Phys. Rev. D* **110** (2024) 104073, [2311.04274].

[3] R. F. Diedrichs, S. Tsujikawa and K. Yagi, *Tidal Love numbers of neutron stars in Horndeski theories*, *Phys. Rev. D* **112** (2025) 044023, [2501.07998].

[4] A. Einstein, *Näherungsweise Integration der Feldgleichungen der Gravitation*, *Sitzungsberichte der Königlich Preussischen Akademie der Wissenschaften* (Jan., 1916) 688–696.

[5] LIGO Scientific, Virgo collaboration, B. P. Abbott et al., *Observation of Gravitational Waves from a Binary Black Hole Merger*, *Phys. Rev. Lett.* **116** (2016) 061102, [1602.03837].

[6] LIGO Scientific, Virgo collaboration, B. P. Abbott et al., *Tests of General Relativity with GW170817*, *Phys. Rev. Lett.* **123** (2019) 011102, [1811.00364].

[7] LIGO Scientific, VIRGO, KAGRA collaboration, R. Abbott et al., *Tests of General Relativity with GWTC-3*, 2112.06861.

[8] E. Berti et al., *Testing General Relativity with Present and Future Astrophysical Observations*, *Class. Quant. Grav.* **32** (2015) 243001, [1501.07274].

[9] N. Yunes, K. Yagi and F. Pretorius, *Theoretical Physics Implications of the Binary Black-Hole Mergers GW150914 and GW151226*, *Phys. Rev. D* **94** (2016) 084002, [1603.08955].

[10] L. Barack et al., *Black holes, gravitational waves and fundamental physics: a roadmap*, *Class. Quant. Grav.* **36** (2019) 143001, [1806.05195].

[11] E. Berti, K. Yagi and N. Yunes, *Extreme Gravity Tests with Gravitational Waves from Compact Binary Coalescences: (I) Inspiral-Merger*, *Gen. Rel. Grav.* **50** (2018) 46, [1801.03208].

[12] H. Takeda, S. Tsujikawa and A. Nishizawa, *Gravitational-wave constraints on scalar-tensor gravity from a neutron star and black-hole binary GW200115*, *Phys. Rev. D* **109** (2024) 104072, [2311.09281].

[13] D. Langlois, R. Saito, D. Yamauchi and K. Noui, *Scalar-tensor theories and modified gravity in the wake of GW170817*, *Phys. Rev. D* **97** (2018) 061501, [1711.07403].

[14] S. Jana and S. Mohanty, *Constraints on $f(R)$ theories of gravity from GW170817*, *Phys. Rev. D* **99** (2019) 044056, [1807.04060].

[15] R. Niu, X. Zhang, B. Wang and W. Zhao, *Constraining Scalar-tensor Theories Using Neutron Star–Black Hole Gravitational Wave Events*, *Astrophys. J.* **921** (2021) 149, [2105.13644].

[16] N. Yunes, X. Siemens and K. Yagi, *Gravitational-Wave Tests of General Relativity with Ground-Based Detectors and Pulsar-Timing Arrays*, 2408.05240.

[17] E. J. Copeland, M. Sami and S. Tsujikawa, *Dynamics of dark energy*, *Int. J. Mod. Phys. D* **15** (2006) 1753–1936, [hep-th/0603057].

[18] A. De Felice and S. Tsujikawa, *f(R) theories*, *Living Rev. Rel.* **13** (2010) 3, [1002.4928].

[19] T. Clifton, P. G. Ferreira, A. Padilla and C. Skordis, *Modified Gravity and Cosmology*, *Phys. Rept.* **513** (2012) 1–189, [1106.2476].

[20] A. Joyce, B. Jain, J. Khoury and M. Trodden, *Beyond the Cosmological Standard Model*, *Phys. Rept.* **568** (2015) 1–98, [1407.0059].

[21] K. Koyama, *Cosmological Tests of Modified Gravity*, *Rept. Prog. Phys.* **79** (2016) 046902, [1504.04623].

[22] L. Heisenberg, *A systematic approach to generalisations of General Relativity and their cosmological implications*, *Phys. Rept.* **796** (2019) 1–113, [1807.01725].

[23] M. Ishak, *Testing General Relativity in Cosmology*, *Living Rev. Rel.* **22** (2019) 1, [1806.10122].

[24] V. Cardoso, E. Franzin, A. Maselli, P. Pani and G. Raposo, *Testing strong-field gravity with tidal Love numbers*, *Phys. Rev. D* **95** (2017) 084014, [1701.01116], [Addendum: Phys.Rev.D 95, 089901 (2017)].

[25] A. Saffer and K. Yagi, *Tidal deformabilities of neutron stars in scalar-Gauss-Bonnet gravity and their applications to multimessenger tests of gravity*, *Phys. Rev. D* **104** (2021) 124052, [2110.02997].

[26] T. Katagiri, V. Cardoso, T. Ikeda and K. Yagi, *Tidal response beyond vacuum general relativity with a canonical definition*, *Phys. Rev. D* **111** (2025) 084081, [2410.02531].

[27] G. Creci, I. van Gemeren, T. Hinderer and J. Steinhoff, *Tidal effects in gravitational waves from neutron stars in scalar-tensor theories of gravity*, *SciPost Phys. Core* **8** (2025) 042, [2412.06620].

[28] R. Cayuso, A. Kuntz, M. Bezares and E. Barausse, *Scalar emission from neutron star-black hole binaries in scalar-tensor theories with kinetic screening*, *Phys. Rev. D* **110** (2024) 104071, [2410.16367].

[29] M. Quartin, S. Tsujikawa, L. Amendola and R. Sturani, *Constraining Horndeski theory with gravitational waves from coalescing binaries*, *JCAP* **08** (2023) 049, [2304.02535].

[30] M. Motaharfar and P. Singh, *Loop quantum gravitational signatures via Love numbers*, *Phys. Rev. D* **111** (2025) 106018, [2501.09151].

[31] T. Kobayashi, *Gravitomagnetic tidal response of relativistic stars in partially screened scalar-tensor theories*, *Phys. Rev. D* **111** (2025) 084053, [2501.10659].

[32] P. A. Cano, *Love numbers beyond GR from the modified Teukolsky equation*, *JHEP* **07** (2025) 152, [2502.20185].

[33] M. Motaharfar and P. Singh, *Love Numbers of Covariant Loop Quantum Black Holes*, 2505.14784.

[34] T. Damour and G. Esposito-Farese, *Nonperturbative strong field effects in tensor - scalar theories of gravitation*, *Phys. Rev. Lett.* **70** (1993) 2220–2223.

[35] T. Damour and G. Esposito-Farese, *Tensor - scalar gravity and binary pulsar experiments*, *Phys. Rev. D* **54** (1996) 1474–1491, [gr-qc/9602056].

[36] P. Kanti, N. E. Mavromatos, J. Rizos, K. Tamvakis and E. Winstanley, *Dilatonic black holes in higher curvature string gravity*, *Phys. Rev. D* **54** (1996) 5049–5058, [hep-th/9511071].

[37] P. Kanti, N. E. Mavromatos, J. Rizos, K. Tamvakis and E. Winstanley, *Dilatonic black holes in higher curvature string gravity. 2: Linear stability*, *Phys. Rev. D* **57** (1998) 6255–6264, [hep-th/9703192].

[38] T. Torii, H. Yajima and K.-i. Maeda, *Dilatonic black holes with Gauss-Bonnet term*, *Phys. Rev. D* **55** (1997) 739–753, [gr-qc/9606034].

[39] L. Blanchet, *Gravitational Radiation from Post-Newtonian Sources and Inspiralling Compact Binaries*, *Living Rev. Rel.* **17** (2014) 2, [1310.1528].

[40] C. R. Galley and M. Tiglio, *Radiation reaction and gravitational waves in the effective field theory approach*, *Phys. Rev. D* **79** (2009) 124027, [0903.1122].

[41] R. A. Porto, *The effective field theorist's approach to gravitational dynamics*, *Phys. Rept.* **633** (2016) 1–104, [1601.04914].

[42] S. Foffa, R. A. Porto, I. Rothstein and R. Sturani, *Conservative dynamics of binary systems to fourth Post-Newtonian order in the EFT approach II: Renormalized Lagrangian*, *Phys. Rev. D* **100** (2019) 024048, [1903.05118].

[43] G. Kälin, Z. Liu and R. A. Porto, *Conservative Dynamics of Binary Systems to Third Post-Minkowskian Order from the Effective Field Theory Approach*, *Phys. Rev. Lett.* **125** (2020) 261103, [2007.04977].

[44] C. Dlapa, G. Kälin, Z. Liu and R. A. Porto, *Dynamics of binary systems to fourth Post-Minkowskian order from the effective field theory approach*, *Phys. Lett. B* **831** (2022) 137203, [2106.08276].

[45] W. D. Goldberger and A. Ross, *Gravitational radiative corrections from effective field theory*, *Phys. Rev. D* **81** (2010) 124015, [0912.4254].

[46] W. D. Goldberger, A. Ross and I. Z. Rothstein, *Black hole mass dynamics and renormalization group evolution*, *Phys. Rev. D* **89** (2014) 124033, [1211.6095].

[47] W. D. Goldberger, *Effective field theories of gravity and compact binary dynamics: A Snowmass 2021 whitepaper*, in *Snowmass 2021*, 6, 2022. 2206.14249.

[48] W. D. Goldberger, *Effective Field Theory for Compact Binary Dynamics*, 12, 2022.

[49] V. Cardoso, O. J. C. Dias and P. Figueras, *Gravitational radiation in d>4 from effective field theory*, *Phys. Rev. D* **78** (2008) 105010, [0807.2261].

[50] A. Kuntz, F. Piazza and F. Vernizzi, *Effective field theory for gravitational radiation in scalar-tensor gravity*, *JCAP* **05** (2019) 052, [1902.04941].

[51] T. Liu, W. Zhao and Y. Wang, *Gravitational waveforms from the quasicircular inspiral of compact binaries in massive Brans-Dicke theory*, *Phys. Rev. D* **102** (2020) 124035, [2007.10068].

[52] T. K. Poddar, S. Mohanty and S. Jana, *Gravitational radiation from binary systems in massive graviton theories*, *JCAP* **03** (2022) 019, [2105.13335].

[53] Y. Higashino and S. Tsujikawa, *Inspiral gravitational waveforms from compact binary systems in Horndeski gravity*, *Phys. Rev. D* **107** (2023) 044003, [2209.13749].

[54] W. D. Goldberger and I. Z. Rothstein, *An Effective field theory of gravity for extended objects*, *Phys. Rev. D* **73** (2006) 104029, [hep-th/0409156].

[55] J. Huang, M. C. Johnson, L. Sagunski, M. Sakellariadou and J. Zhang, *Prospects for axion searches with Advanced LIGO through binary mergers*, *Phys. Rev. D* **99** (2019) 063013, [1807.02133].

[56] J. Zhang, Z. Lyu, J. Huang, M. C. Johnson, L. Sagunski, M. Sakellariadou et al., *First Constraints on Nuclear Coupling of Axionlike Particles from the Binary Neutron Star Gravitational Wave Event GW170817*, *Phys. Rev. Lett.* **127** (2021) 161101, [2105.13963].

[57] M. Khlopov, B. A. Malomed and I. B. Zeldovich, *Gravitational instability of scalar fields and formation of primordial black holes*, *Mon. Not. Roy. Astron. Soc.* **215** (1985) 575–589.

[58] E. G. M. Ferreira, *Ultra-light dark matter*, *Astron. Astrophys. Rev.* **29** (2021) 7, [2005.03254].

[59] M. Colpi, S. L. Shapiro and I. Wasserman, *Boson Stars: Gravitational Equilibria of Selfinteracting Scalar Fields*, *Phys. Rev. Lett.* **57** (1986) 2485–2488.

[60] R. Ruffini and S. Bonazzola, *Systems of selfgravitating particles in general relativity and the concept of an equation of state*, *Phys. Rev.* **187** (1969) 1767–1783.

[61] T. Hinderer, *Tidal Love numbers of neutron stars*, *Astrophys. J.* **677** (2008) 1216–1220, [0711.2420], [Erratum: Astrophys.J. 697, 964 (2009)].

[62] G. W. Horndeski, *Second-order scalar-tensor field equations in a four-dimensional space*, *Int. J. Theor. Phys.* **10** (1974) 363–384.

[63] A. Abac et al., *The Science of the Einstein Telescope*, 2503.12263.

[64] K. Thorne, "Ligo and the discovery of gravitational waves." Nobel Lecture, 2017.

[65] I. Goldman and S. Nussinov, *Weakly Interacting Massive Particles and Neutron Stars*, *Phys. Rev. D* **40** (1989) 3221–3230.

[66] C. Kouvaris, *WIMP Annihilation and Cooling of Neutron Stars*, *Phys. Rev. D* **77** (2008) 023006, [0708.2362].

[67] C. Kouvaris and P. Tinyakov, *Can Neutron stars constrain Dark Matter?*, *Phys. Rev. D* **82** (2010) 063531, [1004.0586].

[68] F. Sandin and P. Ciarcelluti, *Effects of mirror dark matter on neutron stars*, *Astropart. Phys.* **32** (2009) 278–284, [0809.2942].

[69] P. Ciarcelluti and F. Sandin, *Have neutron stars a dark matter core?*, *Phys. Lett. B* **695** (2011) 19–21, [1005.0857].

[70] S. C. Leung, M. C. Chu and L. M. Lin, *Dark-matter admixed neutron stars*, *Phys. Rev. D* **84** (2011) 107301, [1111.1787].

[71] T. Güver, A. E. Erkoca, M. Hall Reno and I. Sarcevic, *On the capture of dark matter by neutron stars*, *JCAP* **05** (2014) 013, [1201.2400].

[72] A. Li, F. Huang and R.-X. Xu, *Too massive neutron stars: The role of dark matter?*, *Astropart. Phys.* **37** (2012) 70–74, [1208.3722].

[73] Q.-F. Xiang, W.-Z. Jiang, D.-R. Zhang and R.-Y. Yang, *Effects of fermionic dark matter on properties of neutron stars*, *Phys. Rev. C* **89** (2014) 025803, [1305.7354].

[74] L. Tolos, J. Schaffner-Bielich and Y. Dengler, *Dark Compact Planets*, *Phys. Rev. D* **92** (2015) 123002, [1507.08197], [Erratum: Phys.Rev.D 103, 109901 (2021)].

[75] S. Mukhopadhyay, D. Atta, K. Imam, D. N. Basu and C. Samanta, *Compact bifluid hybrid stars: Hadronic Matter mixed with self-interacting fermionic Asymmetric Dark Matter*, *Eur. Phys. J. C* **77** (2017) 440, [1612.07093], [Erratum: Eur.Phys.J.C 77, 553 (2017)].

[76] J. Ellis, G. Hütsi, K. Kannike, L. Marzola, M. Raidal and V. Vaskonen, *Dark Matter Effects On Neutron Star Properties*, *Phys. Rev. D* **97** (2018) 123007, [1804.01418].

[77] D. McKeen, A. E. Nelson, S. Reddy and D. Zhou, *Neutron stars exclude light dark baryons*, *Phys. Rev. Lett.* **121** (2018) 061802, [1802.08244].

[78] G. Baym, D. H. Beck, P. Geltenbort and J. Shelton, *Testing dark decays of baryons in neutron stars*, *Phys. Rev. Lett.* **121** (2018) 061801, [1802.08282].

[79] T. F. Motta, P. A. M. Guichon and A. W. Thomas, *Implications of Neutron Star Properties for the Existence of Light Dark Matter*, *J. Phys. G* **45** (2018) 05LT01, [1802.08427].

[80] T. F. Motta, P. A. M. Guichon and A. W. Thomas, *Neutron to Dark Matter Decay in Neutron Stars*, *Int. J. Mod. Phys. A* **33** (2018) 1844020, [1806.00903].

[81] O. Ivanytskyi, V. Sagun and I. Lopes, *Neutron stars: New constraints on asymmetric dark matter*, *Phys. Rev. D* **102** (2020) 063028, [1910.09925].

[82] N. F. Bell, G. Busoni, T. F. Motta, S. Robles, A. W. Thomas and M. Virgato, *Nucleon Structure and Strong Interactions in Dark Matter Capture in Neutron Stars*, *Phys. Rev. Lett.* **127** (2021) 111803, [2012.08918].

[83] W. Husain, T. F. Motta and A. W. Thomas, *Consequences of neutron decay inside neutron stars*, *JCAP* **10** (2022) 028, [2203.02758].

[84] J. M. Berryman, S. Gardner and M. Zakeri, *Neutron Stars with Baryon Number Violation, Probing Dark Sectors*, *Symmetry* **14** (2022) 518, [2201.02637].

[85] M. Cassing, A. Brisebois, M. Azeem and J. Schaffner-Bielich, *Exotic Compact Objects with Two Dark Matter Fluids*, 2210.13697.

[86] F. Di Giovanni, N. Sanchis-Gual, P. Cerdá-Durán and J. A. Font, *Can fermion-boson stars reconcile multimessenger observations of compact stars?*, *Phys. Rev. D* **105** (2022) 063005, [2110.11997].

[87] V. Sagun, E. Giangrandi, O. Ivanytskyi, I. Lopes and K. A. Bugaev, *Constraints on the fermionic dark matter from observations of neutron stars*, *PoS* **PANIC2021** (2022) 313, [2111.13289].

[88] E. Giangrandi, V. Sagun, O. Ivanytskyi, C. Providência and T. Dietrich, *The effects of self-interacting bosonic dark matter on neutron star properties*, 2209.10905.

[89] D. J. Kaup, *Klein-Gordon Geon*, *Phys. Rev.* **172** (1968) 1331–1342.

[90] A. B. Henriques, A. R. Liddle and R. G. Moorhouse, *Combined boson-fermion stars*, *Phys. Lett. B* **233** (1989) 99.

[91] A. B. Henriques, A. R. Liddle and R. G. Moorhouse, *Stability of boson-fermion stars*, *Phys. Lett. B* **251** (1990) 511–516.

[92] S. Valdez-Alvarado, C. Palenzuela, D. Alic and L. A. Ureña-López, *Dynamical evolution of fermion-boson stars*, *Physical Review D* **87** (apr, 2013) .

[93] S. Valdez-Alvarado, R. Becerril and L. A. Ureña-López, *Fermion-boson stars with a quartic self-interaction in the boson sector*, *Physical Review D* **102** (sep, 2020) .

[94] F. D. Giovanni, S. Fakhry, N. Sanchis-Gual, J. C. Degollado and J. A. Font, *Dynamical formation and stability of fermion-boson stars*, *Physical Review D* **102** (oct, 2020) .

[95] F. D. Giovanni, S. Fakhry, N. Sanchis-Gual, J. C. Degollado and J. A. Font, *A stabilization mechanism for excited fermion–boson stars*, *Classical and Quantum Gravity* **38** (aug, 2021) 194001.

[96] A. Einstein, L. Infeld and B. Hoffmann, *The Gravitational equations and the problem of motion*, *Annals Math.* **39** (1938) 65–100.

[97] L. Bernard, *Dynamics of compact binary systems in scalar-tensor theories: Equations of motion to the third post-Newtonian order*, *Phys. Rev. D* **98** (2018) 044004, [1802.10201].

[98] L. Bernard, *Dynamics of compact binary systems in scalar-tensor theories: II. Center-of-mass and conserved quantities to 3PN order*, *Phys. Rev. D* **99** (2019) 044047, [1812.04169].

[99] L. Bernard, L. Bernard and L. Bernard, *Dipolar tidal effects in scalar-tensor theories*, *Phys. Rev. D* **101** (2020) 021501, [1906.10735], [Erratum: Phys.Rev.D 107, 069901 (2023)].

[100] L. Bernard, L. Blanchet and D. Trestini, *Gravitational waves in scalar-tensor theory to one-and-a-half post-Newtonian order*, *JCAP* **08** (2022) 008, [2201.10924].

[101] F.-L. Julié and E. Berti, *Post-Newtonian dynamics and black hole thermodynamics in Einstein-scalar-Gauss-Bonnet gravity*, *Phys. Rev. D* **100** (2019) 104061, [1909.05258].

[102] B. Shiralilou, T. Hinderer, S. Nissanke, N. Ortiz and H. Witek, *Nonlinear curvature effects in gravitational waves from inspiralling black hole binaries*, *Phys. Rev. D* **103** (2021) L121503, [2012.09162].

[103] B. Shiralilou, T. Hinderer, S. M. Nissanke, N. Ortiz and H. Witek, *Post-Newtonian gravitational and scalar waves in scalar-Gauss–Bonnet gravity*, *Class. Quant. Grav.* **39** (2022) 035002, [2105.13972].

[104] F.-L. Julié, V. Baibhav, E. Berti and A. Buonanno, *Third post-Newtonian effective-one-body Hamiltonian in scalar-tensor and Einstein-scalar-Gauss-Bonnet gravity*, *Phys. Rev. D* **107** (2023) 104044, [2212.13802].

[105] L. Bernard, E. Dones and S. Mougiakakos, *Tidal effects up to next-to-next-to leading post-Newtonian order in massless scalar-tensor theories*, 10, 2023.

[106] S. Mirshekari and C. M. Will, *Compact binary systems in scalar-tensor gravity: Equations of motion to 2.5 post-Newtonian order*, *Phys. Rev. D* **87** (2013) 084070, [1301.4680].

[107] R. N. Lang, *Compact binary systems in scalar-tensor gravity. II. Tensor gravitational waves to second post-Newtonian order*, *Phys. Rev. D* **89** (2014) 084014, [1310.3320].

[108] R. N. Lang, *Compact binary systems in scalar-tensor gravity. III. Scalar waves and energy flux*, *Phys. Rev. D* **91** (2015) 084027, [1411.3073].

[109] N. Sennett, S. Marsat and A. Buonanno, *Gravitational waveforms in scalar-tensor gravity at 2PN relative order*, *Phys. Rev. D* **94** (2016) 084003, [1607.01420].

[110] J. Alsing, E. Berti, C. M. Will and H. Zaglauer, *Gravitational radiation from compact binary systems in the massive Brans-Dicke theory of gravity*, *Phys. Rev. D* **85** (2012) 064041, [1112.4903].

[111] E. Berti, L. Gualtieri, M. Horbatsch and J. Alsing, *Light scalar field constraints from gravitational-wave observations of compact binaries*, *Phys. Rev. D* **85** (2012) 122005, [1204.4340].

[112] A. Hook and J. Huang, *Probing axions with neutron star inspirals and other stellar processes*, *JHEP* **06** (2018) 036, [1708.08464].

[113] L. Sagunski, J. Zhang, M. C. Johnson, L. Lehner, M. Sakellariadou, S. L. Liebling et al., *Neutron star mergers as a probe of modifications of general relativity with finite-range scalar forces*, *Phys. Rev. D* **97** (2018) 064016, [1709.06634].

[114] A. Bhattacharyya, S. Ghosh and S. Pal, *Worldline effective field theory of inspiralling black hole binaries in presence of dark photon and axionic dark matter*, *JHEP* **08** (2023) 207, [2305.15473].

[115] F. Zwicky, *Die Rotverschiebung von extragalaktischen Nebeln*, *Helvetica Physica Acta* **6** (Jan., 1933) 110–127.

[116] V. C. Rubin and W. K. Ford, Jr., *Rotation of the Andromeda Nebula from a Spectroscopic Survey of Emission Regions*, *Astrophysical Journal* **159** (Feb., 1970) 379.

[117] K. C. Freeman, *On the Disks of Spiral and S0 Galaxies*, *Astrophysical Journal* **160** (June, 1970) 811.

[118] F. Lelli, S. S. McGaugh and J. M. Schombert, *SPARC: Mass Models for 175 Disk Galaxies with Spitzer Photometry and Accurate Rotation Curves*, *Astron. J.* **152** (2016) 157, [1606.09251].

[119] D. Clowe, M. Bradac, A. H. Gonzalez, M. Markevitch, S. W. Randall, C. Jones et al., *A direct empirical proof of the existence of dark matter*, *Astrophys. J. Lett.* **648** (2006) L109–L113, [astro-ph/0608407].

[120] Planck collaboration, N. Aghanim et al., *Planck 2018 results. VI. Cosmological parameters*, *Astron. Astrophys.* **641** (2020) A6, [1807.06209], [Erratum: Astron.Astrophys. 652, C4 (2021)].

[121] B. Carr and F. Kuhnel, *Primordial black holes as dark matter candidates*, *SciPost Phys. Lect. Notes* **48** (2022) 1, [2110.02821].

[122] D. M. Jacobs, G. D. Starkman and B. W. Lynn, *Macro Dark Matter*, *Mon. Not. Roy. Astron. Soc.* **450** (2015) 3418–3430, [1410.2236].

[123] L. Roszkowski, E. M. Sessolo and S. Trojanowski, *WIMP dark matter candidates and searches—current status and future prospects*, *Rept. Prog. Phys.* **81** (2018) 066201, [1707.06277].

[124] A. Einstein, *Erklärung der Perihelionbewegung des Merkur aus der allgemeinen Relativitatstheorie*, *Sitzungsberichte der Königlich Preussischen Akademie der Wissenschaften* **47** (Jan., 1915) 831–839.

[125] T. Kaluza, *Zum Unitätsproblem der Physik*, *Sitzungsber. Preuss. Akad. Wiss. Berlin (Math. Phys.)* **1921** (1921) 966–972, [1803.08616].

[126] O. Klein, *Quantum Theory and Five-Dimensional Theory of Relativity*, *Z. Phys.* **37** (1926) 895–906.

[127] S. Weinberg, *The Cosmological Constant Problem*, *Rev. Mod. Phys.* **61** (1989) 1–23.

[128] S. Deser, *Selfinteraction and gauge invariance*, *Gen. Rel. Grav.* **1** (1970) 9–18, [gr-qc/0411023].

[129] D. Lovelock, *Divergence-free tensorial concomitants*, *Aequat. Math.* **4** (1970) 127–138.

[130] D. Lovelock, *The Einstein tensor and its generalizations*, *J. Math. Phys.* **12** (1971) 498–501.

[131] C. Brans and R. H. Dicke, *Mach's principle and a relativistic theory of gravitation*, *Phys. Rev.* **124** (1961) 925–935.

[132] K. Schwarzschild, *Über das Gravitationsfeld eines Massenpunktes nach der Einsteinschen Theorie*, *Sitzungsberichte der Königlich Preussischen Akademie der Wissenschaften* (Jan., 1916) 189–196.

[133] A. Einstein, *On a stationary system with spherical symmetry consisting of many gravitating masses*, *Annals Math.* **40** (1939) 922–936.

[134] J. R. Oppenheimer and H. Snyder, *On Continued gravitational contraction*, *Phys. Rev.* **56** (1939) 455–459.

[135] T. Regge and J. A. Wheeler, *Stability of a Schwarzschild singularity*, *Phys. Rev.* **108** (1957) 1063–1069.

[136] R. Penrose, *Gravitational collapse and space-time singularities*, *Phys. Rev. Lett.* **14** (1965) 57–59.

[137] T. Damour and A. Nagar, *Relativistic tidal properties of neutron stars*, *Phys. Rev. D* **80** (2009) 084035, [0906.0096].

[138] T. Binnington and E. Poisson, *Relativistic theory of tidal Love numbers*, *Phys. Rev. D* **80** (2009) 084018, [0906.1366].

[139] R. C. Tolman, *Static solutions of einstein's field equations for spheres of fluid*, *Phys. Rev.* **55** (Feb, 1939) 364–373.

[140] J. R. Oppenheimer and G. M. Volkoff, *On massive neutron cores*, *Phys. Rev.* **55** (Feb, 1939) 374–381.

[141] J. Schaffner-Bielich, *Compact Star Physics*. Cambridge University Press, 8, 2020, 10.1017/9781316848357.

[142] A. Hewish, S. J. Bell, J. D. H. Pilkington, P. F. Scott and R. A. Collins, *Observation of a rapidly pulsating radio source*, *Nature* **217** (1968) 709–713.

[143] R. A. Hulse and J. H. Taylor, *Discovery of a pulsar in a binary system*, *Astrophys. J. Lett.* **195** (1975) L51–L53.

[144] J. H. Taylor and J. M. Weisberg, *Further experimental tests of relativistic gravity using the binary pulsar PSR 1913+16*, *Astrophys. J.* **345** (1989) 434–450.

[145] O. Heaviside, *Electromagnetic Theory*. Cambridge Library Collection - Technology. Cambridge University Press, 2011.

[146] M. Maggiore, *Gravitational Waves. Vol. 1: Theory and Experiments*. Oxford University Press, 2007, 10.1093/acprof:oso/9780198570745.001.0001.

[147] J. M. Antelis and C. Moreno, *Obtaining gravitational waves from inspiral binary systems using LIGO data*, *Eur. Phys. J. Plus* **132** (2017) 10, [1610.03567], [Erratum: Eur.Phys.J.Plus 132, 103 (2017)].

[148] LIGO-Virgo-Kagra | Aaron Geller | Northwestern, "Masses in the stellar graveyard." https://media.ligo.northwestern.edu/gallery/mass-plot.

[149] C. P. Burgess, *Introduction to Effective Field Theory*, *Ann. Rev. Nucl. Part. Sci.* **57** (2007) 329–362, [hep-th/0701053].

[150] A. Einstein, *Über Gravitationswellen*, *Sitzungsberichte der Königlich Preussischen Akademie der Wissenschaften* (Jan., 1918) 154–167.

[151] R. A. Porto and R. Sturani, *Scalar gravity: Post-Newtonian corrections via an effective field theory approach*, in *Les Houches Summer School - Session 86: Particle Physics and Cosmology: The Fabric of Spacetime*, 1, 2007. gr-qc/0701105.

[152] A. Ross, *Multipole expansion at the level of the action*, *Phys. Rev. D* **85** (2012) 125033, [1202.4750].

[153] D. Schmitt and R. F. Diedrichs, "NLO Gravitational Waveform in Massive Scalar-Tensor Theory." https://github.com/DMGW-Goethe/ScalarTensorWaveform, 2023.

[154] A. B. Henriques, A. R. Liddle and R. G. Moorhouse, *Combined Boson-Fermion Stars: Configurations and Stability*, *Nucl. Phys. B* **337** (1990) 737–761.

[155] S. Valdez-Alvarado, C. Palenzuela, D. Alic and L. A. Ureña-López, *Dynamical evolution of fermion-boson stars*, *Phys. Rev. D* **87** (2013) 084040, [1210.2299].

[156] K. S. Thorne, *Tidal stabilization of rigidly rotating, fully relativistic neutron stars*, *Phys. Rev. D* **58** (1998) 124031, [gr-qc/9706057].

[157] J. Eby, C. Kouvaris, N. G. Nielsen and L. C. R. Wijewardhana, *Boson Stars from Self-Interacting Dark Matter*, *JHEP* **02** (2016) 028, [1511.04474].

[158] L. Sagunski, S. Gad-Nasr, B. Colquhoun, A. Robertson and S. Tulin, *Velocity-dependent Self-interacting Dark Matter from Groups and Clusters of Galaxies*, *JCAP* **01** (2021) 024, [2006.12515].

[159] V. Doroshenko, V. Suleimanov, G. Pühlhofer and A. Santangelo, *A strangely light neutron star within a supernova remnant*, *Nature Astronomy* **6** (03, 2022) 14441451.

[160] T. E. Riley, A. L. Watts, S. Bogdanov et al., *A NICER View of PSR J0030+0451: Millisecond Pulsar Parameter Estimation*, *Astrophys. J. Lett.* **887** (2019) L21, [1912.05702].

[161] T. E. Riley et al., *A NICER View of the Massive Pulsar PSR J0740+6620 Informed by Radio Timing and XMM-Newton Spectroscopy*, *Astrophys. J. Lett.* **918** (2021) L27, [2105.06980].

[162] D. Kandel and R. W. Romani, *An Optical Study of the Black Widow Population*, *Astrophys. J.* **942** (2023) 6, [2211.16990].

[163] R. W. Romani, D. Kandel, A. V. Filippenko, T. G. Brink and W. Zheng, *PSR J0952−0607: The Fastest and Heaviest Known Galactic Neutron Star*, *Astrophys. J. Lett.* **934** (2022) L18, [2207.05124].

[164] LIGO Scientific, Virgo collaboration, B. P. Abbott, R. Abbott, T. D. Abbott et al., *Properties of the binary neutron star merger GW170817*, *Phys. Rev.* **X9** (2019) 011001, [1805.11579].

[165] K.-L. Leung, M.-c. Chu and L.-M. Lin, *Tidal deformability of dark matter admixed neutron stars*, *Phys. Rev. D* **105** (2022) 123010, [2207.02433].

[166] R. Kase and S. Tsujikawa, *Relativistic star perturbations in Horndeski theories with a gauge-ready formulation*, *Phys. Rev. D* **105** (2022) 024059, [2110.12728].

[167] B. Kol and M. Smolkin, *Black hole stereotyping: Induced gravito-static polarization*, *JHEP* **02** (2012) 010, [1110.3764].

[168] K. S. Thorne, *Multipole Expansions of Gravitational Radiation*, *Rev. Mod. Phys.* **52** (1980) 299–339.

[169] D. D. Doneva, F. M. Ramazanoğlu, H. O. Silva, T. P. Sotiriou and S. S. Yazadjiev, *Spontaneous scalarization*, *Rev. Mod. Phys.* **96** (2024) 015004, [2211.01766].

[170] M. Minamitsuji and S. Tsujikawa, *Stability of neutron stars in Horndeski theories with Gauss-Bonnet couplings*, *Phys. Rev. D* **106** (2022) 064008, [2207.04461].

[171] E. Giangrandi, H. R. Rüter, N. Kunert, M. Emma, A. Abac, A. Adhikari et al., *Numerical Relativity Simulations of Dark Matter Admixed Binary Neutron Stars*, 2504.20825.